

# **An Evaluation of Alumina Supported Platinum Catalysts for the Oxidative Dehydrogenation of *n*-Butane**

*A Thesis Presented to  
the University of Glasgow  
for the Degree of  
Doctor of Philosophy*

*by*

John Martin McNamara

*September 2000*

ProQuest Number: 13833968

All rights reserved

INFORMATION TO ALL USERS

The quality of this reproduction is dependent upon the quality of the copy submitted.

In the unlikely event that the author did not send a complete manuscript and there are missing pages, these will be noted. Also, if material had to be removed, a note will indicate the deletion.



ProQuest 13833968

Published by ProQuest LLC (2019). Copyright of the Dissertation is held by the Author.

All rights reserved.

This work is protected against unauthorized copying under Title 17, United States Code  
Microform Edition © ProQuest LLC.

ProQuest LLC.  
789 East Eisenhower Parkway  
P.O. Box 1346  
Ann Arbor, MI 48106 – 1346



Copy 1 - 12056

## Abstract

The oxidative dehydrogenation of *n*-butane has been studied as a potential alternative to conventional catalytic straight dehydrogenation for the production of butene olefin species. This work was inspired by recent advances in catalytic oxidative dehydrogenation studies utilising short contact times and surface science measurements highlighting the importance of ‘hot oxygen’ surface chemistry. Two low loading Pt/Al<sub>2</sub>O<sub>3</sub> catalysts have been extensively characterised and used throughout this work. Experimental parameters such as temperature, flow-rate, catalyst mass and hydrocarbon:oxygen ratio were manipulated in an attempt to build a greater understanding of the influential factors responsible for the activity and selectivity of system.

The results have shown that catalytic oxidative dehydrogenation is not feasible under the conditions used and that combustion reactions forming carbon dioxide dominate. In contrast, in the absence of the catalyst, relatively high olefin selectivity was observed as a result of homogeneous radical processes. The results from catalytic straight dehydrogenation reactions were dependent on the substrate used. With the 0.65wt% Pt/Al<sub>2</sub>O<sub>3</sub>, known from CO chemisorption data to consist of very small platinum crystallites, high dehydrogenation selectivity was observed at modest conversion. Further studies also demonstrated this to be the case regardless of the depth of the catalyst bed. On the contrary, the 0.5wt% Pt/Al<sub>2</sub>O<sub>3</sub> catalyst displayed very poor dehydrogenation selectivity as well as low activity. This was due to the larger platinum crystallites contained in this catalyst, yielding unwanted isomerisation, cracking and hydrogenolysis products, which are known to be structure sensitive favouring larger particle sizes. The low activity observed in the straight dehydrogenation reactions on both catalysts occurred as a result of a combination of carbonaceous blocking of the active sites and pore blocking, restricting access to the active sites.

Flow-rate studies demonstrated that the dehydrogenation selectivity could be controlled by manipulation of reactant contact time with the catalyst. Again, the trends were dependent on the substrate used. With the small particles of the 0.65wt% catalyst extended contact times were found to be more favourable for high olefin selectivity, whereas short contact times were found to give the best results for the larger particles

of the 0.5wt% catalyst. These observations are consistent with the proposed reaction sequence and the contrasting surface chemistry of the two catalysts, with respect to their particle sizes.

On the basis of ‘hot oxygen’ chemistry, where it was demonstrated that very low concentrations of oxygen could have a profound effect on oxidation reactions involving  $\beta$ -hydrogen abstraction on single crystal surfaces, a study was carried out to see if the dehydrogenation selectivity could be enhanced by manipulation of the hydrocarbon:oxygen ratio. It was found that increasing the oxygen concentration from zero to 1:2 resulted in a dramatic decrease in olefin selectivity with a subsequent increase in butane conversion. It was concluded that the maintenance of a ‘hot oxygen’ concentration was not possible on the supported catalyst systems studied in a plug flow reactor and that combustion processes were dominant. These combustion reactions being responsible for the increased conversion and decreased selectivity.

Pulse-flow measurements were used in order to investigate the initial conditioning of the catalyst surface in an attempt to identify the processes responsible for the effects seen in the continuous-flow (steady state) experiments. A direct correlation was found between the deposition of carbonaceous material on the catalyst surface and the dehydrogenation selectivity. It is observed that the selectivity towards the olefin products increased as carbonaceous material was deposited. It was proposed from this that the presence of the carbonaceous material invoked a change in the electronic nature of the metal surface in a similar manner to that for platinum/tin alloys. The presence of oxygen was found to remove some of the carbonaceous material necessary for olefin formation.

In conclusion, the presence of oxygen in the catalytic dehydrogenation of butane using supported platinum catalyst is detrimental to the production of the favoured butene species and that the particle size of the platinum crystallites contained in the catalyst is crucial to obtaining high olefin yields. Dehydrogenation being favoured by small platinum crystals. We also conclude that bridging the gap between single crystal surface science studies and supported catalyst chemistry is not feasible in a microreactor environment operating in steady and non-steady state regimes to achieve the clean, controlled environment compatible with a UHV study.

## Acknowledgments

Grateful thanks are made to my supervisor Dr. D. Lennon (Dave) for his guidance, patience and sound advice throughout this project. The opportunity to work as part of his research group during its first days has been both educational and a privilege and has provided me with a sound training in the field of heterogeneous catalysis. Thanks also goes to Dr. S. D. Jackson at ICI Synetix for the helpful advice supplied during the quarterly meetings (try not to spill your coffee on this report!).

Many thanks go to various members of the Chemistry Department, in particular Mr. W. McCormick for his expertise in glass blowing, Mr. S. Mackay and Dr. K. Tyler for their help and support in all computing matters and Dr. G. Noble for running surface area measurements. Much appreciation also goes to fellow Tetris king Dave Kennedy for his help and friendship during my first year as a research student as well as to all the souls of the inorganic research office for their good humour and endless conversation (arguments) on the rights and wrongs of world wide current affairs. Apologies are made to anyone I have missed, their contribution is also appreciated.

Thanks also go to my girlfriend Susan for keeping me sane over the past few years and for putting up with the occasional moan. Maybe she will finally realise that my visits at the weekend were not just to pick up my weekly food parcels from my mum. I am also grateful to my Aunt Kathleen and Uncle Tommy for showing a genuine interest in my progress over the years and for funding the binding and printing of this thesis.

The greatest thanks however, go to my mum and dad for their unending support and kindness in every way possible (including food parcels) without which I would certainly not have had the opportunities I have now. For this reason my thesis is dedicated to them. Their help will never be forgotten - Thanks.

*To Mum and Dad*

# Contents

## Abstract

## Acknowledgements

## Contents

<b>1.</b>	<b>Introduction</b>	<b>1</b>
<i>1.1</i>	<i>Economic Importance</i>	2
<i>1.2</i>	<i>Catalytic Dehydrogenation with and without Promotion</i>	3
<i>1.3</i>	<i>Industrial Processes using Catalytic Dehydrogenation Technology</i>	12
1.3.1	UOP Oleflex Process	13
1.3.2	Phillips STAR (Steam Active Reforming) Process	14
1.3.3	Catofin Process (UCI-ABB Lummus Crest)	16
1.3.4	FBD Process (Snamprogetti-Yarsintez)	17
1.3.5	Linde-BASF Process	18
<i>1.4</i>	<i>Catalyst Deactivation</i>	18
1.4.1	Carbonaceous deposits	19
1.4.2	Catalyst Sintering and Poisoning	26
<i>1.5</i>	<i>Catalytic Oxidative Dehydrogenation</i>	30
<i>1.6</i>	<i>Isomerisation, Hydrogenolysis and Combustion Reactions</i>	38
<i>1.7</i>	<i>Surface Science Studies of the Role of Oxygen</i>	42
<i>1.8</i>	<i>Summary of Introduction Section</i>	44

<b>2. Characterisation and Testing Facility</b>	<b>46</b>
<i>2.1 Construction and Capabilities of Catalyst Testing and Characterisation Facility</i>	46
2.1.1 Gas Cylinders and Mixing Section	46
2.1.2 Vacuum Line	48
2.1.3 The Reactor	49
2.1.4 The Gas Chromatograph (GC)	50
2.1.5 The Infrared Spectrophotometer (IRS)	54
2.1.6 The Mass Spectrometer (MS)	55
<b>3. Materials</b>	<b>57</b>
<i>3.1 Catalysts Used</i>	57
3.1.1 Catalyst Preparation	57
3.1.1.1 Pt/Al <sub>2</sub> O <sub>3</sub> (JM code-64268, batch-97099)	57
3.1.1.2 Pt/Al <sub>2</sub> O <sub>3</sub> (ICI - P5211)	58
3.1.2 Choice of Support Material	58
3.2 Gases Used	59
3.3 Abbreviations used throughout this Thesis	63
<b>4. Experimental</b>	<b>64</b>
<i>4.1 Continuous-flow Experiments</i>	64
4.1.1 Catalyst Preparation	64
4.1.2 Catalyst Reduction	64
4.1.3 Continuous-flow Procedure	65

<b>4.2</b>	<i>Pulse-flow Experiments</i>	<b>67</b>
4.2.1	Pulse-flow Procedure	67
4.2.2	Preparation of the Reaction Mixture Bulbs	70
4.2.3	GC Calibration	71
<b>4.3</b>	<i>Characterisation Techniques</i>	<b>72</b>
4.3.1	Temperature Programmed Reduction (TPR)	72
4.3.2	Volumetric Adsorption Isotherms	73
4.3.3	Transmission Electron Microscopy (TEM)	76
4.3.4	Transmission Infrared Spectroscopy of Carbon Monoxide Chemisorption	77
4.3.5	Carbon Monoxide Temperature Programmed Desorption (TPD)	79
4.3.6	Temperature Programmed Oxidation (TPO)	79
4.3.7	Total Surface Area and Pore Size Measurements	80
<b>5.</b>	<b>Results and Discussion</b>	<b>81</b>
<b>5.1</b>	<i>Equilibrium Considerations for Straight and Oxidative Dehydrogenation</i>	<b>81</b>
5.1.1	Straight Dehydrogenation	81
5.1.2	Oxidative Dehydrogenation	87
<b>5.2</b>	<i>Characterisation of 0.5% and 0.65% Pt/Al<sub>2</sub>O<sub>3</sub> Catalysts</i>	<b>89</b>
5.2.1	Temperature Programmed Reduction (TPR)	89
5.2.2	Volumetric Adsorption Isotherms	90
5.2.3	Transmission Electron Microscopy (TEM)	93
5.2.4	Transmission Infrared of Carbon Monoxide Chemisorption	94
5.2.5	Carbon Monoxide TPD	99

5.2.6	<i>Total Surface Area and Pore Size Measurements</i>	102
5.3	<i>The Straight and Oxidative Dehydrogenation of Butane using an Empty Reactor Vessel</i>	103
5.3.1	Straight Dehydrogenation	103
5.3.2	Oxidative Dehydrogenation	104
5.4	<i>The Straight and Oxidative Dehydrogenation of Butane using the <math>\gamma\text{-Al}_2\text{O}_3</math> Support Material from the 0.5% Pt/<math>\text{Al}_2\text{O}_3</math> Catalyst</i>	111
5.4.1	Straight Dehydrogenation using the 0.5% Pt/ $\text{Al}_2\text{O}_3$ Support material	111
5.4.2	Oxidative Dehydrogenation using the 0.5% Pt/ $\text{Al}_2\text{O}_3$ Support material	112
5.5	<i>The Straight and Oxidative Dehydrogenation of Butane using 0.5% Pt/<math>\text{Al}_2\text{O}_3</math></i>	126
5.5.1	The Straight Dehydrogenation of Butane as a function of Temperature under Continuous-flow conditions using 0.5% Pt/ $\text{Al}_2\text{O}_3$	126
5.5.2	The Oxidative Dehydrogenation of Butane as a function of Temperature under Continuous-flow conditions using 0.5% Pt/ $\text{Al}_2\text{O}_3$	135
5.5.3	The Straight Dehydrogenation of Butane as a function of Flow-rate under Continuous-flow conditions using 0.5% Pt/ $\text{Al}_2\text{O}_3$	143
5.5.4	The Oxidative Dehydrogenation of Butane as a function of Flow-rate under Continuous-flow conditions using 0.5% Pt/ $\text{Al}_2\text{O}_3$	150
5.5.5	Summary of the Testing Reactions of the 0.5% Pt/ $\text{Al}_2\text{O}_3$ Catalyst under Continuous-flow conditions	156

5.5.6	<i>Post-reaction Analysis of the 0.65% Pt/Al<sub>2</sub>O<sub>3</sub> Catalyst after Continuous-flow Experiments</i>	159
5.6	<i>The Straight and Oxidative Dehydrogenation of Butane using 0.65% Pt/Al<sub>2</sub>O<sub>3</sub></i>	163
5.6.1	The Straight Dehydrogenation of Butane as a function of Temperature under Continuous-flow conditions using 0.65% Pt/Al <sub>2</sub> O <sub>3</sub>	163
5.6.2	The Oxidative Dehydrogenation of Butane as a function of Temperature under Continuous-flow conditions using 0.65% Pt/Al <sub>2</sub> O <sub>3</sub>	170
5.6.3	The Straight Dehydrogenation of Butane as a function of Flow-rate under Continuous-flow conditions using 0.65% Pt/Al <sub>2</sub> O <sub>3</sub>	177
5.6.4	The Oxidative Dehydrogenation of Butane as a function of Flow-rate under Continuous-flow conditions using 0.65% Pt/Al <sub>2</sub> O <sub>3</sub>	183
5.6.5	The Straight Dehydrogenation of Butane as a function of Catalyst Mass under Continuous-flow conditions using 0.65% Pt/Al <sub>2</sub> O <sub>3</sub>	189
5.6.6	The Oxidative Dehydrogenation of Butane as a function of Catalyst Mass under Continuous-flow conditions using 0.65% Pt/Al <sub>2</sub> O <sub>3</sub>	195
5.6.7	The Oxidative Dehydrogenation of Butane as a function of Hydrocarbon:Oxygen Ratio under Continuous-flow conditions using 0.65% Pt/Al <sub>2</sub> O <sub>3</sub>	201
5.6.8	Summary of the Testing Reactions of the 0.65% Pt/Al <sub>2</sub> O <sub>3</sub> Catalyst under Continuous-flow conditions	209
5.6.9	Post-reaction Analysis of the 0.65% Pt/Al <sub>2</sub> O <sub>3</sub> Catalyst after Continuous-flow Experiments	213
5.7	<i>The Straight and Oxidative Dehydrogenation of Butane using 0.65% Pt/Al<sub>2</sub>O<sub>3</sub> under Pulse-flow Conditions</i>	216

**References**

**Future Work**

*Chapter 1*

**Introduction**

The production of valuable products from light hydrocarbons is presently one of the major challenges of the petroleum and petrochemical industry. In particular olefins continue to be a fundamental building block and favoured feedstock for many of the largest industrial processes [1]. Traditionally, production of olefins such as ethene, propene and butenes have been obtained from the thermal pyrolysis of longer chain alkanes and straight-run gasoline. This process also uses a catalyst and is subsequently known as catalytic cracking.

The high temperatures required (800-900°C) to overcome the thermodynamic equilibrium constraints creates many problems. These include limitations on conversion and selectivity as a result of the thermodynamics, unwanted side-reactions, reducing selectivity and resulting in difficulties with respect to separation of the olefins from the paraffins and other by-products. The formation of coke on the catalyst, as a result of the high temperatures, requires frequent regeneration by steam and ultimately leads to irreversible catalyst deactivation reducing the overall catalyst lifetime [2]. All this results in a process which is inefficient and capital-intensive.

As the global demand for olefins and downstream products, such as IPA (*iso*-propylalcohol), MTBE (methyl tertiary butyl ether) and TBA (tertiary butyl alcohol), is increasing, and with the existing capacity insufficient to meet future demands, the investigation of new processes is highly justified [3].

Catalytic dehydrogenation, in addition to requiring relatively low capital outlay, allows for the production of specific olefins such as propene, *iso*-butene and *n*-butenes either individually or mixed with one another, thus avoiding the large capital and operating expenses associated with the recovery and processing of the many by-products from pyrolysis units [4]. However, catalytic dehydrogenation still requires high temperatures to overcome the equilibrium constraints and still requires that the catalyst undergo frequent regeneration. This project investigates the feasibility of using oxidative dehydrogenation as an alternative route to olefin formation.

The concept of oxidative dehydrogenation provides a cheap and easy route to the production of olefins as it offers the advantage of faster and exothermic oxidation reactions. Another benefit is that the presence of molecular oxygen in the feed-gas potentially has the effect of quenching deactivation of the catalyst from the deposition of coke thus increasing its lifetime [5].

This chapter attempts to review the important and influential literature, past and present, of dehydrogenation and oxidative dehydrogenation. Various issues are considered such as the economic importance of olefins in general, the catalysts used in dehydrogenation and oxidative dehydrogenation and the industrial processes that currently exist. Parallel processes such as combustion, cracking or hydrogenolysis reactions, isomerisation and deactivation are highlighted as well as the effect of promoters and poisons. Issues such as structure sensitivity and the role of the support material are also discussed. The section is summarised in section 1.8.

### 1.1 *Economic Importance*

The demand for butene species has been substantial, for many years. Historically, butenes were required in the late 1930's/early 1940's for the manufacture of high grade alkylate gasoline for fighter planes during World War two [4]. More recently environmental concerns have established a dramatic increase in demand for oxygenates such as gasoline blending components MTBE/ETBE with the increased restriction on the aromatic content [6], which are included to improve the octane number in fuel. These species contain *iso*-butene, generating a demand well beyond its availability from traditional sources [1]. Indeed from 1991 to 1992 the fastest growing chemicals in the top 50 chemicals were *iso*-butene and ethyl benzene [3]. This rapid growth emphasises the importance of dehydrogenation technology to the oil and chemicals industry towards the formation of olefins. Table 1.1.1 lists the US production rates for the above chemicals and selected others that are produced as a result of dehydrogenation processes.

In particular, an important petrochemical use of n-butenes is oxidative dehydrogenation to give 1,3-butadiene, which is the precursor for the production of polybutadiene rubbers. Mixtures of n-butenes may also be hydrated to give 2-butanol, which can be further dehydrogenated to produce methyl ethyl ketone (MEK). But-1-ene may also be separated and used as part of the co-monomer feed for use in polyethene production [7], as well as being used to form the highly sought after *iso*-butene for uses as mentioned above, from direct isomerisation. The supply in this case comes from the hydrogenation of 1,3-butadiene [8]. The world production of butenes

**Table 1.1.1** The US Production Rates of Chemicals Relevant to Dehydrogenation [3].

Chemical	Production		Rank	Rank	Annual		Annual		Annual	
	(billion lb)	(billion lb)			1992	1991	1991-1992	1990-1991	1987-1992	1982-1992
Ethene	40.41	39.96	4	3	1.1	1.1	9.6	2.9	2.9	5.1
Propene	22.60	21.55	9	10	4.8	-1.4	4.1	4.1	4.1	6.1
Ethylbenzene	10.99	8.87	18	20	23.9	6.0	3.2	3.2	3.2	5.1
MTBE	10.86	9.57	19	19	13.5	7.7	26.4	26.4	26.4	29.4
Styrene	8.94	8.12	21	22	10.2	1.2	2.0	2.0	2.0	4.2
Iso-butene	1.29	0.97	50	n/a	32.4	-19.8	4.5	4.5	4.5	5.7

in 1992 stood at approximately  $2.5 \times 10^6$  tonnes [9] and an economically sustainable performance requires a yield of greater than 20% [10].

## 1.2 Catalytic Dehydrogenation with and without Promotion

Catalytic dehydrogenation involves the removal of hydrogen using a suitable catalyst. Equation 1.1 shows the basic process that takes place using butane as an example. The thermodynamics of the system are covered in detail in chapter 5. However, the reaction is endothermic with  $\Delta H = +126 \text{ kJ mol}^{-1}$ . As a result catalytic dehydrogenation requires high temperatures of approximately  $600^\circ\text{C}$  in order to achieve reasonable conversion [11]. Consequently, other products are formed as well making this an inefficient process. Figure 1.2.1 is a diagram of hydrocarbon conversion over platinum catalysts showing the approximate range of temperatures where various reactions take place.



It is clear from this diagram that at the high temperatures required for dehydrogenation, various other reactions take place simultaneously. Figure 1.2.2 shows the possible reaction pathways achievable under normal dehydrogenation conditions [1].

This section highlights some of the current literature dealing with the catalytic dehydrogenation of alkanes, mainly *n*-butane, *iso*-butane and propane. Due to industrial influence, the majority of the work reported in the literature involving alkane dehydrogenation using noble metal catalysts concerns their performance relative to the performance of similar catalysts containing additional promoters. The effect of the promoter is currently a contentious issue in the field of catalytic dehydrogenation and at present there are three main theories used to explain why the addition of a second or third metal to the catalyst has a positive effect on catalyst activity, dehydrogenation selectivity and in some cases catalyst lifetime. These three theories are:

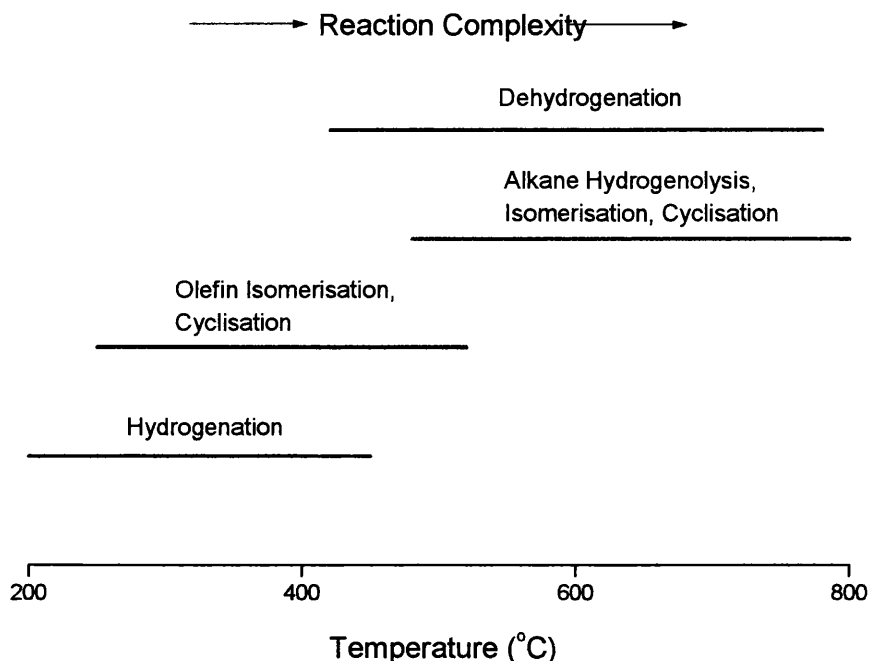


**Fig. 1.2.1** Hydrocarbon Conversion over Platinum Catalysts.

- an electronic effect
- an ensemble effect
- and a selective poisoning effect.

The **electronic effect** involves a metal, commonly tin, in solid solution form, as small metallic clusters or alloyed with the noble metal, giving electrons to the holes of the Pt 5d band, in the case of platinum-tin systems. This has the effect of weakening the adsorptive properties of the platinum, therefore reducing the amount of reactions taking place that require strong adsorption such as hydrogenolysis and cracking reactions which ultimately lead to coke formation. It is also possible to explain the promotion effect of tin by assuming that coke precursors are not adsorbed on the surface of the doped platinum crystals, but rather they move to the support material thus avoiding deactivation [12].

The addition of tin to platinum can also give rise to the dilution of platinum atoms, with the formation of smaller ensembles of atoms. This can be achieved when

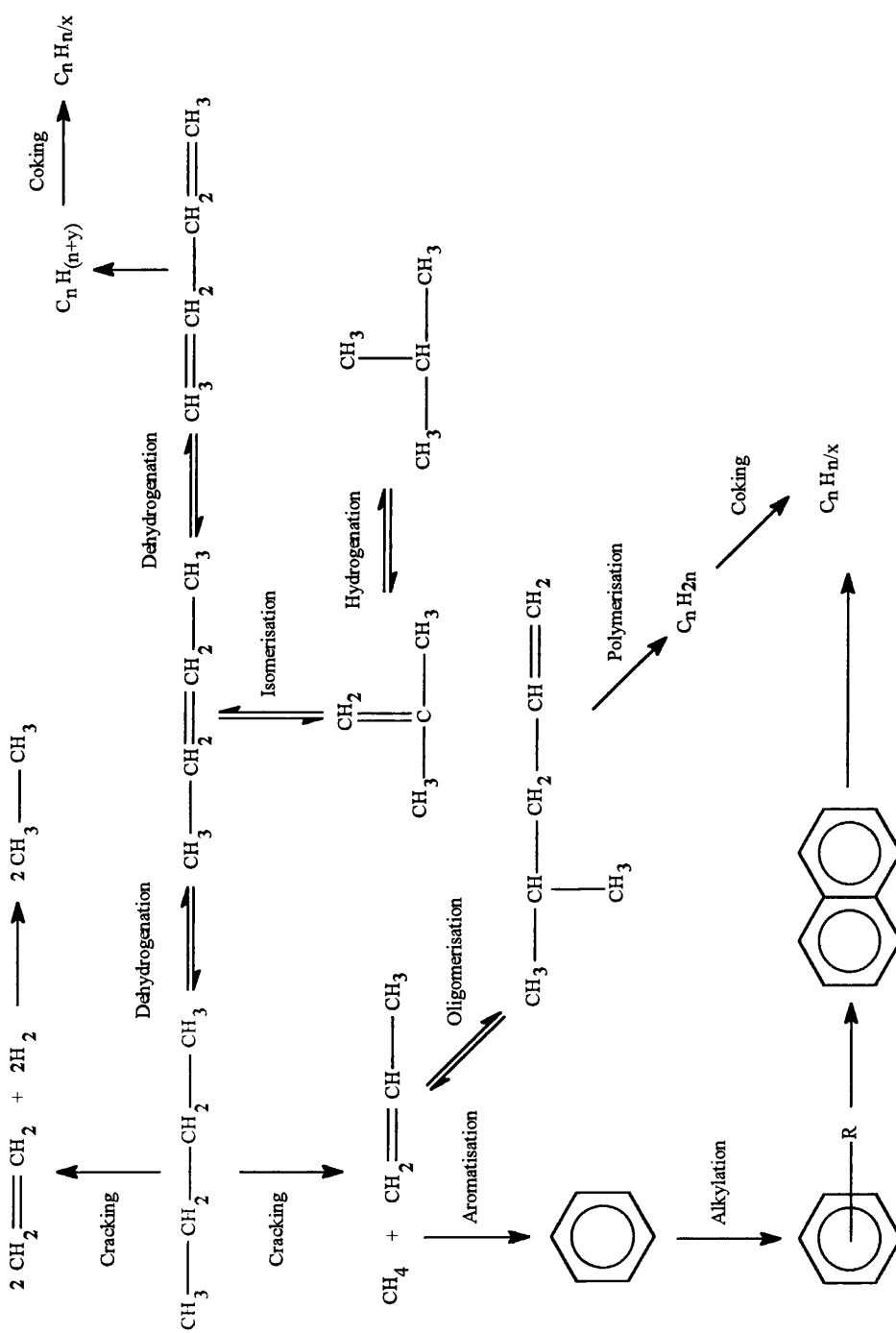


Fig. 1.2.2 Possible Reaction Pathways under Dehydrogenation Conditions [1].

large amounts of tin are used, forming an alloy, or small amounts of tin in platinum crystallites, where surface enrichment in tin is expected. The formation of these small ensembles has a big effect with regard to the control of which reactions take place. Structure-sensitive reactions *i.e.* those where the turnover frequency (TOF) is dependent on the size of the metal crystallites [13], can be influenced greatly by changing the size of the metal ensembles. Reactions such as hydrogenolysis and cracking, which lead to deactivation and loss of dehydrogenation selectivity, are said to be structure-sensitive reactions requiring large ensembles where many active sites are found. On the other hand dehydrogenation and hydrogenation reactions are structure-insensitive requiring only single metal atoms as the active site [14] and so by diluting the platinum crystallites using tin, small ensembles are formed and the reaction pathway can be limited to only dehydrogenation reactions, thus increasing the dehydrogenation selectivity and reducing deactivation caused by coking. This is known as the **ensemble effect** [1].

**Selective poisoning** occurs when small amounts of promoter adsorb on the principle metal surface, predominantly on sites of low coordination, subsequently inhibiting the reactivity of these sites. This effect is not limited to using metals such as tin but can occur by the addition of small amounts of sulphur or phosphorous atoms [15].

The observation that dehydrogenation requires only one metal atom was made by Schactler *et al* when studying the dehydrogenation of propane using Pt-Au catalysts [14]. In this work, the effect of diluting the platinum with catalytically inert gold was investigated. It was found that the rate of propene formation per unit surface area of alloy powders varied linearly with the bulk platinum concentration of the alloys. From this it was concluded that only one platinum metal atom was required for the conversion of one molecule of propane to one molecule of propene and one molecule of hydrogen. The resultant proposed mechanism is initiated with the dissociative chemisorption of propane on a single platinum atom to which two adsorption sites are associated, one for the adsorbed propyl and one for the left over hydrogen atom. The subsequent conversion of the propyl radical into the  $\pi$ -bonded propene via  $\beta$ -hydrogen elimination is the rate limiting step, with the desorption of the  $\pi$ -bonded propene having a relatively low activation energy. With reactions such as hydrogenolysis and

cracking requiring a larger number of metal atoms per active site [1], this result is very important towards the justification and understanding of theories such as the ensemble effect.

Further investigation of the ensemble effect was reported by Somorjai *et al* using the dehydrogenation of *n*-pentane, *n*-hexane and cyclohexane as probe reactions [16]. The catalysts used in this work were platinum based and the effect of added rhenium and sulphur was assessed. Rhenium is known to be a very good hydrogenolysis catalyst [17], especially when alloyed with platinum. By adding sulphur it was found that rhenium's affinity for hydrogenolysis could be capped and that dilution of the platinum by the rhenium-sulphur could be achieved. Once again, as a result of dilution and subsequent reduction in ensemble size, it was found that the selectivity towards the dehydrogenation products increased as the hydrogenolysis, dehydrocyclisation, isomerisation and cyclisation reactions were inhibited. It was also concluded that the small ensembles were highly resistant towards the formation of carbonaceous layers, thereby enhancing the catalysts durability. It was thought that this might be due to the small ensembles having no space on which to grow the large polymeric carbon structures. This stability was only maintained as long as the sulphur was in contact with the rhenium. Loss of sulphur resulted in growth of the particles and subsequent deactivation [16].

Work on the *n*-butane dehydrogenation process using platinum/silica based catalysts was carried out by Chen *et al* [18]. It was found, using 1% Pt/SiO<sub>2</sub>, that initial conversion of 100% could be achieved at temperatures of 450°C. However, only cracking products were formed and no dehydrogenation was observed as well as rapid deactivation from coking. Nevertheless, a correlation was made where an increase in dehydrogenation selectivity (up to 40% total olefin) was accompanied by the formation of carbonaceous deposits on the Pt surface. However, it was concluded that the extent of carbon laydown was uncontrollable and therefore of no real use. It was also observed, again, that the addition of small amounts of sulphur to Pt and Pd metal catalysts enhanced the dehydrogenation selectivity and that the unwanted cracking reactions could be poisoned.

The effect of small amounts of lead on the palladium based catalyst was also investigated. It was concluded that changes to the surface structure and charge

distribution were responsible for the increase in dehydrogenation selectivity observed [18].

A comparison of Pt/Al<sub>2</sub>O<sub>3</sub> and Pt-Sn/Al<sub>2</sub>O<sub>3</sub> catalysts for the dehydrogenation of propane was made during the investigation of the influence of tin on coking by Bariås *et al* [12]. It was observed that the platinum dispersion increased on addition of tin, as measured by hydrogen chemisorption. It was proposed that this observation could be due to an increase in the rate of hydrogen spillover to the support [12], or possibly platinum assisted hydrogen adsorption on tin sites close to the platinum atoms. In terms of activity, the TOF for the Pt and Pt-Sn catalysts were very similar initially (~1.0 s<sup>-1</sup> and 1.2 s<sup>-1</sup> respectively) but almost instantaneous deactivation of the Pt catalyst occurred while the Pt-Sn catalyst maintained a TOF of ~1.0 s<sup>-1</sup> over a 2000 minute period. Again, it was pointed out that carbonaceous overlayer formation is structure-sensitive and requires large ensembles of platinum atoms and that the addition of tin, forming an alloy, resulted in the isolation of platinum atoms and therefore the prevention of large ensemble formation.

It was also proposed that the addition of tin changed the nature and location of the coke, making it less toxic to the catalyst. It was suggested that a higher degree of coke was found on the Pt/Sn catalyst but that it was located on the support material and not on the metal. It was therefore concluded that the tin facilitates the transportation of the coke precursors to the support thus keeping the active metal surface clean [12].

These concepts were developed further by the same author in a later publication [19]. Comparison of alumina and silica supported catalysts found that tin was reduced to metallic tin and formed an alloy with the silica based platinum catalysts whereas with the platinum-tin alumina systems alloy formation was not observed to any great extent. Instead it was suggested that the effect of tin in this case was as a promoter of the support properties, particularly of the ability to transport chemisorbed species from the active metal surface. It was also found that tin acts as a poison to the acidic sites of the alumina support leading to the suppression of cracking reactions.

Extensive work was carried out by Kiperman and co-workers in the late 1980's and early 1990's on the kinetics of *iso*-butane, propane and *n*-butane dehydrogenation, with promotion using a variety of different species [20-25]. The effect of copper, selenium, germanium, lead, indium and tin were compared to 0.6% Pt-K/Al<sub>2</sub>O<sub>3</sub>

catalysts (potassium was added to reduce the acidic properties of the alumina) and it was observed that indium and tin were the most effective promoters for the formation of olefins due to the retardation of the isomerisation and cracking reactions, inducing an increase in the rate of the rate limiting step of the dehydrogenation pathway.

In the case of *n*-butane dehydrogenation [22] it was concluded that the production of *n*-butenes and 1,3-butadiene proceed across different active sites on the catalyst surface. It was suggested that butadiene forms on the sites where *n*-butenes adsorption is strongest. In all cases it was proposed that the addition of indium does not change the kinetic equation for the dehydrogenation reactions but affects the coefficients in the equations, decreasing the strength of adsorption of the resultant olefins allowing desorption of the favoured product instead of further reaction to form the unwanted cracking and isomerisation products. This action could be interpreted as an electronic effect. In all cases it was proposed that the rate limiting step involved the formation of the adsorbed alkyl species. Figure 1.2.3 shows the reaction pathway for the dehydrogenation of propane with \* indicating an active site on the catalyst surface and with the blue highlighting the rate limiting step. Work carried out by Fiaty *et al* re-emphasised the kinetic and mechanistic work carried out on the *iso*-butane system also using Pt-In catalysts [26].

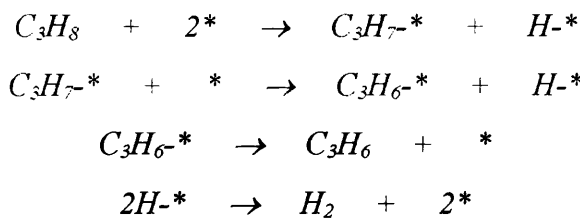


**Fig. 1.2.3** The mechanism for the dehydrogenation of propane [20-26].

Follow-up studies by Kiperman *et al* [24, 25] were carried out where the effect of water in the feedgas was also considered during the dehydrogenation of *iso*-butane, propane and *n*-butane. Again, adsorption of the produced olefin on the Pt-K catalyst without Sn or In promotion was found to be so strong that the water vapour was mainly adsorbed on alumina or on the boundary sites between the metal and support. On promotion an increase in dehydrogenation selectivity was observed due to a weakening in strength of the adsorbed olefin species. As well as this, the introduction

of water vapour resulted in the suppression of isomerisation reactions as the water adsorbed on the sites active towards this reaction pathway. It was also shown that the water vapour decreased the amount of coke formed during the dehydrogenation reactions.

The kinetics of alkane dehydrogenation has also been carried out by Jackson *et al*. In this study propane dehydrogenation was carried out using chromia and chromia/potassium catalysts supported on alumina. Using deuterium labeled compounds under steady state and transient conditions it was determined that the rate limiting step was the removal of the second hydrogen atom forming the adsorbed olefin species, as indicated in red on figure 1.2.3 [27]. These results agree with the earlier work reported by Schactler *et al* [14].

Further support to the electronic effect theory was provided by Liwu *et al* during a microcalorimetric study of dehydrogenation activity using Pt/Al<sub>2</sub>O<sub>3</sub> and Pt-Sn/Al<sub>2</sub>O<sub>3</sub> catalysts [28]. Table 1.2.1 shows the conversion and selectivity figures for the dehydrogenation of a mixture consisting of 81.36% *iso*-butane and 18.64% *n*-butane using the promoted and un-promoted catalysts. Adsorption microcalorimetry was used to measure the solid acid-base properties thereby providing information on the nature of the gas-solid interaction and the properties of the adsorbent surface on the catalysts. Using CO as adsorbate, it was shown that with the inclusion of tin the strength of adsorption decreased on the strongest adsorption site, from 100 kJmol<sup>-1</sup> to 40 kJmol<sup>-1</sup>. It was concluded that an increase in dehydrogenation activity and selectivity was achieved as a result of an increase in the number of these lower heats of adsorption sites indicating that the strongly adsorbing sites are not suitable for dehydrogenation and ultimately lead to break-up of the butane molecule.

**Table 1.2.1** The Dehydrogenation Activity and Selectivity for mixed C<sub>4</sub> Alkanes on 0.4% Pt/Al<sub>2</sub>O<sub>3</sub> Catalysts (Alloys containing 1.9% Sn) [28].

Catalyst	Conv. (%)	Conv. (%)	Sel. (%)	Sel. (%)
	Initial	180mins	Initial	180mins
Pt	30.66	14.49	77.14	91.44
Pt-Sn (co-impregnation)	49.00	42.93	98.47	98.79
Pt-Sn (Sequential-impregnation)	48.30	35.32	96.98	95.72

It was also shown here that as the reaction time increased on the un-promoted catalyst, the conversion decreased as a result of carbonaceous deposits, and the dehydrogenation selectivity increased. This indicates that carbonaceous deposits are beneficial to dehydrogenation reactions and suggests that a possible link exists between the changes in the electronic properties brought about by tin and those brought about by carbonaceous deposits.

Further substance was added to the electronic effect theory by Szabo *et al* during the correlation between hydrogen chemisorption, state of metal and the activity of Pt/Al<sub>2</sub>O<sub>3</sub> and Pt-Sn/Al<sub>2</sub>O<sub>3</sub> catalysts in propane dehydrogenation [29]. Table 1.2.2 lists the activity and selectivity measurements observed during the experimental work which was carried out at 560°C. The results show that both catalysts show high stability over an 80 minute period. Overall though, it was shown that the promoted catalyst was better in terms of dehydrogenation selectivity, the un-promoted catalyst experiencing processes of destructive decomposition of propane forming methane and ethane and ultimately leading to deactivation.

**Table 1.2.2** Conversion and Selectivity of Pt and Pt-Sn/Al<sub>2</sub>O<sub>3</sub> Catalysts in Propane Dehydrogenation at 560°C [29].

Catalyst	Conv. (%)	Sel. 20mins	Conv. (%)	Sel. 50mins	Conv. (%)	Sel. 80mins	ΔConv. (20- 80mins)
		20mins	50mins	50mins	80mins	80mins	
Pt	9.8	91.3	8.4	93.2	8.1	92.9	-1.7
Pt-Sn	8.7	99.2	8.3	99.3	9.4	98.2	+0.7

X-ray photoelectron spectroscopy (XPS) and hydrogen chemisorption data were collected for the promoted and un-promoted catalysts. From these measurements it was concluded that the Pt in the modified catalyst was more reduced than the Pt in the un-modified case, characterised by the lower bond strength of the main portion of chemisorbed hydrogen. The dispersion, as measured by the hydrogen chemisorption, increased on promotion of the catalyst by tin. It was proposed that the increase in dehydrogenation selectivity with the promoted catalyst could be due to the weakening of propene adsorption sites resulting in a reduction in C-C bond cleavage and resulting

in the dehydrogenation pathway being the most favourable. It was also concluded that the effect of tin addition on the selectivity of propene could be effected through an increase in the degree of Pt reduction, causing an increase in coverage by hydrogen to the formation of weakly bound hydrogen chemisorption sites, thus preventing the destruction of propane, shifting the process in the direction of dehydrogenation.

The effect of phosphine ligated precursors on alkane dehydrogenation using Pt/SiO<sub>2</sub> and Pt-Au/SiO<sub>2</sub> was studied by Pignolet and co-workers [30]. It was observed that both catalysts exhibited conversion of around 35%. However, the phosphorous containing catalyst displayed dehydrogenation selectivity of typically 80% during the dehydrogenation of propane at 550°C compared to around 50% without promotion. It was concluded from these results that the triphenylphosphine containing precursor for this catalyst resulted in the formation of much smaller particle sizes and that the phosphine residues, in a similar way to sulphur addition, act as selective poisons for the un-wanted cracking, isomerisation and cyclisation reactions. It was suggested that the rate of olefin formation in the cases where the catalysts contained no phosphorous component was far lower than the rate of the competing reactions mentioned above, resulting in poor selectivity towards the alkene products.

A weakening of the platinum's adsorptive properties was demonstrated using CO TPD. In the non-phosphorous containing case the CO desorption was observed at 240-270°C while in the promoted catalyst the desorption of CO peaked at 140°C. This implied an electronic effect on promotion with the phosphine residues. It should be noted that this work only adds to the confusion which surround this issue in terms of whether the effect is ensemble, electronic or selective poisoning in nature.

Finally, an interesting body of work was carried out by Scelza and co-workers [31] where the effect of gallium addition to Pt/Al<sub>2</sub>O<sub>3</sub> on the activity, selectivity and deactivation in propane dehydrogenation was investigated. Again, it was found that the selectivity towards propene was enhanced by the addition of a promoter, in this case gallium, while catalyst deactivation from carbonaceous deposits were reduced. It was mentioned that the gallium appears to have a low effect on the acidity of the catalyst and that it is the structure of the metallic phase that is modified, depending on the activation temperature. Low temperature activation (300°C) led to geometric effects, whereas at high activation temperature (500°C), additional effects such as blocking and electronic modifications to the platinum metal took place.

Pulse-flow reactions were carried out during this study to investigate the behaviour of the fresh catalyst during the initial reaction stages of the dehydrogenation of propane, in terms of initial carbon deposition and its relationship with the conversion and selectivity. It was observed that the platinum catalysts was susceptible to a high degree of deactivation initially over the first few pulses decreasing towards the final few pulses. This was correlated with the high initial deposition of carbon during the first few pulses. It was also shown that the selectivity to propene increased with increasing pulse number, while the selectivity to cracking products was reduced. These observations were explained by suggesting that the acidic sites responsible for the hydrogenolysis reactions are quickly poisoned by coke with resultant catalyst deactivation, thus decreasing the catalyst's hydrogenolenic capacity and increasing dehydrogenation selectivity. It was pointed out that similar Pt ensembles are involved both in coke formation and in hydrogenolysis reactions.

It was concluded that Ga enhanced the initial propene selectivity and reduced carbon retention. Previous results showed that the effect of Ga on the acidic sites of the support were minor with respect to the enhancement of propene selectivity compared to the modifications to the metallic phase brought about by promotion. Overall, the effect of Ga was to block un-favoured reaction sites and dilute the platinum metallic phase, and possibly to impose an electronic effect which in turn decreased the strength of adsorption of the olefin products allowing desorption without further reaction.

### *1.3 Industrial Processes using Catalytic Dehydrogenation Technology*

Currently there are four or five processes existing within industry for the production of olefins from their parent alkanes on a commercial scale. These are the UOP Oleflex process, the Catofin process (UCI-ABB Lummus Crest), the FBD process (Snamprogetti-Yarsintez), the Phillips STAR process and to a lesser extent the Linde BASF process. These processes will now be briefly described.

### 1.3.1 UOP Oleflex Process

The oleflex process is used to produce a variety of olefins from a variety of starting materials, mainly propene and *iso*-butene from propane and *iso*-butane respectively. The catalyst used in this process consists of 0.1-1wt% Pt, 0.1-4wt% Sn and 0.1-4wt% alkali metals (used to suppress the acidic effect of the support material [32]) supported on spherical pellets containing  $120\text{m}^2\text{g}^{-1}$   $\gamma\text{-Al}_2\text{O}_3$  [1]. The temperatures used are between 550-620°C, the pressure is typically 2-5atm and the LHSV (liquid hourly space velocity - feed rate) is 4hr<sup>-1</sup>.

As explained previously, at these temperatures and long residence times, competition with cracking reactions take place and coke formation occurs. Hydrogen is therefore used to maintain the catalyst activity by preventing the deposition of carbon. Care has to be taken though to ensure that the amount of hydrogen is minimal enough to prevent the reaction being driven in the direction of the alkane starting material. The hydrogen:hydrocarbon ratio used is typically 1:10. With this continuous catalyst regeneration system the catalyst lifetime tends to be 1-3 years. Table 1.3.1 lists the activity and selectivity obtained using Oleflex dehydrogenation technology [1].

**Table 1.3.1** Activity and Selectivity achieved using the UOP Oleflex Process.

Reaction	Conversion (%)	Dehydrogenation Selectivity (%)
Propane $\rightarrow$ propene	25	89-91
<i>iso</i> -Butane $\rightarrow$ <i>iso</i> -Butene	35	91-93

By optimisation of the residence time (*i.e.* minimisation of the non-catalytic residence time), space velocity, temperature and other process variables, it has been possible to increase the selectivity while maintaining a similar conversion. The coke deposited on the catalyst was found to be about 0.01wt % of hydrocarbon feed which is much less than the 2-5wt % coke yield found on the more traditional chromia-alumina catalyst systems. The platinum based catalysts allows plant operation for up to 10-12 days without regeneration with virtually full activity restored after a regeneration cycle [4]. These catalysts also have the added advantage of being non-

toxic, unlike the chromia-alumina system and that the fines from the reactor can be collected and reprocessed for platinum recovery thus increasing the economic efficiency of the process.

The process of regeneration is one of the distinctive features of the Oleflex process. On the plant the regeneration section is completely independent of the dehydrogenation reactor. This means that the regenerator can be stopped, for several days in succession, without detriment to the dehydrogenation process flow. Unless the regenerator is stopped for long periods of time, the activity profile of the catalyst remains uniform at all times so that there is no need to modify operating conditions. This procedure also ensures safe operation of the plant. Another advantage of the system as a result of its design is that catalyst beds can be added or removed from the system without interrupting the main function of the dehydrogenation reactor. Due to the success of this design towards the production of dehydrogenation products the technology has been implemented in over 100 units world-wide, such as in reforming and in aromatic production [4, 33].

Product separation has also been considered when designing the process. First of all the products are compressed and then subjected to a heat exchanger and expansion train, where the non-condensable gases consisting of hydrogen and methane, obtained from cracking reactions and the reaction of hydrogen with the carbonaceous material on the catalyst surface, are removed from the system or recycled for another use. It has been reported that 85-90mol % purity of hydrogen can be recovered and used in other plants or burned as fuel. In addition, a small quantity is also recycled and used throughout the process to stabilise the catalyst and also as an extra heat carrier for the energy intensive dehydrogenation reactions [33]. The light hydrocarbons can also be used as fuel, either in the gas turbine or for the production of steam to drive the steam turbine, which powers the reactant effluent compressor used in the product separation process [4].

### **1.3.2 Phillips STAR (Steam Active Reforming) Process**

The Phillips STAR process involves the dehydrogenation of C<sub>2</sub>-C<sub>4</sub> and the dehydrocyclisation of C<sub>6</sub>-C<sub>7</sub> alkanes [1]. It uses an arrangement of fixed-bed multitubes of 2 inch diameter, made of 27% chromium steel, located within a fired furnace

[34]. The catalyst consists of 0.01-5wt % Pt, 0.1-5wt % Sn supported on zinc aluminate or magnesium aluminate (used due to their high temperature stability and durability in the presence of water [35]). Calcium aluminate and alkali metals are also included as a binding material and to reduce the acidic nature of the support material respectively. Catalyst life is limited to 1-2 years as a result of the gradual loss in activity after each regeneration cycle.

The conditions used during the process include temperatures of 480-620°C, pressures in the region of 3-8atm, LHSV in the range 0.5-10hr<sup>-1</sup> and a steam:hydrocarbon ratio of 4-5. The reported activity and selectivity are listed on table 1.3.2 [3].

**Table 1.3.2** Activity and Selectivity achieved using the Phillips STAR Process.

Reaction	Conversion (%)	Dehydrogenation Selectivity (%)
Propane → propene	30-40	80-90
iso-Butane → iso-Butene	40-55	92-98
Butane → Butenes	45-55	85-95

The presence of steam not only increases the thermodynamic conversion, by acting as a diluent reducing the partial pressure of the hydrocarbon (see later in section 5.1), but its presence also allows the reactor to be operated under a positive pressure, avoiding potential hazards brought about by leakages. The addition of steam can also act as a heat sink therefore maximising energy efficiency as well as removing any coke products which would ultimately lead to catalyst deactivation and reduced lifetime [3]. The advantage claimed of this technology and reactor design is that the fired reactor avoids high temperature pre-heating sections and therefore limits the formation of coke. The positive pressure operation also has the advantage that it requires a lower compression ratio than a typical vacuum operation thus making the plant safer to operate.

### 1.3.3 Catofin Process (UCI-ABB Lummus Crest)

The Catofin process again involves the dehydrogenation of C<sub>3</sub>-C<sub>4</sub> hydrocarbons and was derived from the earlier Catadiene process for the production of butadiene from butenes [1]. The catalyst used is the more traditional 18-20wt % Cr<sub>2</sub>O<sub>3</sub> and 1-2wt % alkali metals supported on θ-alumina in the form of 3-4mm pellets, to which inert material is added to provide extra heat capacity [99]. The catalyst lifetime is reported to be to be 1-2 years.

The conditions used during the process involve temperatures of 590-650°C, pressures in the range 0.33-0.50atm (vacuum) and a LHSV of 0.4-2.0hr<sup>-1</sup>. The results reported in the literature for this process are listed in table 1.3.3.

**Table 1.3.3** Activity and Selectivity achieved using the Catofin Process.

Reaction	Conversion (%)	Dehydrogenation Selectivity (%)
Propane → propene	48-65	82-87
iso-Butane → iso-Butene	60	93

The coke deposited on the catalyst at the end of each reaction cycle is approximately 0.02wt %. The exotherm produced from its combustion is used to reheat the catalyst bed in preparation for the following reaction cycle. The catalyst is also subject to gradual irreversible deactivation over a period of time, as a result the temperature is gradually increased to compensate, with a subsequent reduction in selectivity of approximately 5% over a 500 day period. After use the catalyst can be collected and used to recover chromium metal used in the production of stainless steel.

In terms of advantages over other process, the Catofin process incorporates a cyclic operation *i.e.* reaction-regeneration-reaction *etc.*, which results in a high degree of safety for the operator. It has been mentioned that over a 25 year period no major accidents have been reported. It is also suggested that due to the high selectivity towards the olefin products, the consumption of feedstock is low, increasing the economic efficiency of the process. The reactor also operates under energy efficient conditions (nearly adiabatic operation), with the heat for the reaction being provided

by the catalyst reduction procedure and coke oxidation and is maintained by burning additional fuel. The catalysts tolerance towards oxygenates, high thermal stability, resistance to attrition and breakage and tolerance of poisons such as water and heavy metals makes this process very economic and efficient [3].

### 1.3.4 FBD Process (Snamprogetti-Yarsintez)

The FBD process involves the catalytic dehydrogenation of low molecular weight paraffins to their respective olefins using technology involving a fluidised bed reactor under non-dilute conditions [1]. The catalyst used consists of 12-20wt % Cr<sub>2</sub>O<sub>3</sub>, 1-2wt % K<sub>2</sub>O and 1-2wt % SiO<sub>2</sub> supported on a mixture of high transition aluminas *i.e.* δ, θ and α. Microspheroidal catalyst particles, typically <0.1mm diameter, are used to provide a high resistance against attrition, which is required to cope with fluidised bed conditions. The main process parameters used are 550-600°C, 1.1-1.5atm and a LHSV of 0.4-2.0hr<sup>-1</sup>. Table 1.3.4 lists the activity and selectivity achieved when using this type of reactor configuration.

**Table 1.3.4** Activity and Selectivity achieved using the FBD Process.

Reaction	Conversion (%)	Dehydrogenation Selectivity (%)
Propane → propene	40	89
iso-Butane → iso-Butene	50	91

The following advantages are proposed for this process:

- Continuous or periodical catalyst replenishment results in steady operating conditions and a high on-stream factor.
- Safe operation as a consequence of the slight positive pressure conditions, which results in less leaks, and the separation of the dehydrogenation and oxidation processes.
- Good temperature control, with the highest value of temperature at the reactor outlet where the highest conversion is ideally required.

- The absence of fired heaters and the introduction of highly efficient dust filters result in good environmental compatibility.

### **1.3.5 Linde-BASF Process**

Currently this technology has not been commercialised. Again, it involves alkane dehydrogenation under isothermal conditions, without diluent and at pressures above ambient [1]. Again, the catalyst involves the more traditional chromia supported on alumina subjected to operating conditions such as a maximum temperature of 590°C for butanes and 620°C for propane. The conversion and selectivity in the reaction of propane to propene is 30% and 90% respectively and the catalyst, as with the other processes, is required to undergo periodic regeneration which is carried out in the temperature range 500-640°C. Regeneration takes place for 3 hours after just 6 hours operation during which the initial activity is restored. Minimal irreversible deactivation occurs from the numerous regeneration cycles.

The advantages gained by using this technology include maximised selectivity and minimised cracking reactions and diolefin formation through the use of isothermal operating conditions, positive pressures which result in operator safety, undiluted feed-gas which enables the use of small compact reactors and that cyclic processing (reaction-regeneration) enables continuous operation and a high on-stream factor.

### *1.4 Catalyst Deactivation*

It is clear from the preceding section that one of the major problems affecting reactions involving hydrocarbon conversion, in particular alkane dehydrogenation, is loss of the catalyst activity with time-on-stream, *i.e.* catalyst deactivation. Indeed from an industrial point of view catalyst deactivation is very important as it ultimately determines the lifetime of the catalyst and therefore effects the economics of the reaction. A few days down-time can have a detrimental effect on plant economy [32].

Deactivation can be both physical and chemical in nature and can occur simultaneously or separately from the main reaction (*e.g.* it can take place during the regeneration of the catalyst). There are various ways in which the catalyst can be

deactivated, these are coking (or the formation of carbonaceous material on the catalyst surface), sintering (the agglomeration of the catalyst particles to form larger particles) and poisoning which involves blocking of the active sites by another material hindering the progress of the reaction of interest [15].

This section of the introduction deals mainly with the formation of carbonaceous deposits as these present the main route to deactivation during alkane dehydrogenation reactions. Sintering and poisoning are also very important, but less so than the formation of carbonaceous deposits, and are so dealt with to a lesser extent.

#### 1.4.1 Carbonaceous deposits

The difficulties mentioned above provide a challenge to both the catalytic chemist and the chemical engineer. It is the job of the chemist to develop a catalyst that is more resistant to the formation of carbonaceous deposits thus maximising the lifetime of the catalyst, while the optimisation of reactor design and equipment together with procedures for catalyst regeneration are the domain of the chemical engineering. Figure 1.4.1 shows the relationship between the formation of carbonaceous deposits and catalyst lifetime for various processes. It is clearly shown that dehydrogenation is a reaction that suffers very badly from this type of deactivation with lifetimes in the region of minutes expected.

In general the mechanism involved in the deposition of carbonaceous material is complex and varied, depending on such things as available active sites, catalyst type, the reaction under investigation and process parameters, in particular temperature. In most cases where hydrocarbons are involved, coking (also described as the deposition of carbonaceous material) of the catalyst starts from catalytic cracking reactions on the acid sites. These become blocked by the carbonaceous deposits formed via chain reactions from olefin intermediates, in the case of saturated and unsaturated straight chain alkanes, or from poly-alkylation and condensation in the case of cyclic hydrocarbons and aromatics. Another route commonly found in industry, especially when using nickel, cobalt and iron, is the formation of whiskers. These tend not to deactivate the catalyst immediately but can result in the break-down of catalyst particles [32].

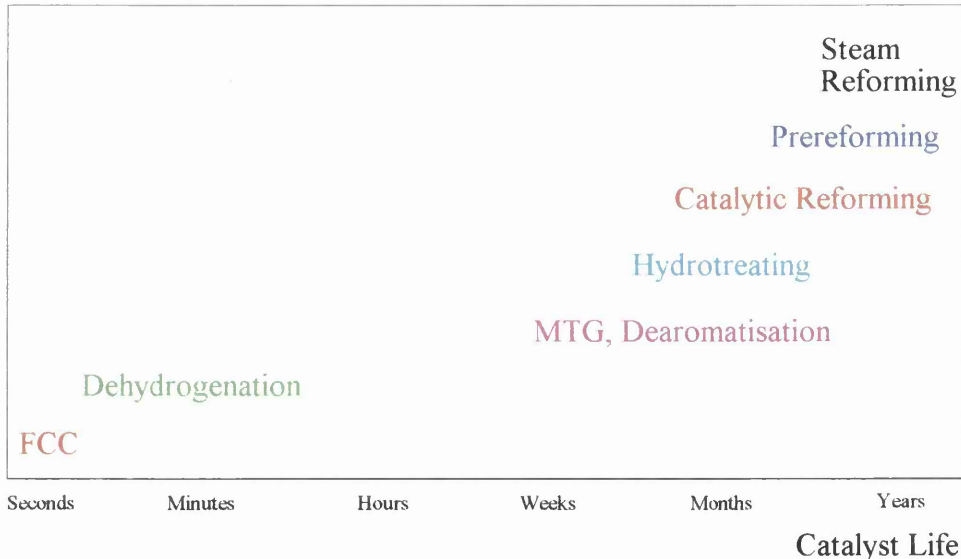


**Fig. 1.4.1** Catalyst Lifetimes Resulting from the formation of Carbonaceous Deposits [32].

Historically, nickel catalysts, used mainly for reforming reactions [36], were amongst the first to be identified as suffering deactivation from the deposition of carbonaceous material. It was found that carbon oxides and hydrocarbons could be split apart, on large ensembles of metal atoms, forming coke. Indeed, from single crystal work it was identified that the rate of deposition was greatest on the (111) surface compared to the (110) and (100) surfaces, hence the requirement of the large ensembles. It was discovered that carbon formed on the catalyst surface and then migrated into the bulk of the particle forming 3-dimensional columns and resulting in the segregation of the nickel surface [37].

Trimm and co-workers also studied the effect on platinum based catalysts [38]. Parameters such as temperature, reactant hydrocarbon and active sites were investigated in order to determine any trends. Using 0.3% Pt/Al<sub>2</sub>O<sub>3</sub> the rates of coking were compared for reactions involving n-hexane, hex-1-ene and cyclohexane. It was found that the rate at which carbonaceous material was deposited increased in the order:



It was also observed that the rate of coking for n-hexane doubled with the addition of Cl<sup>-</sup>, which increases the acidity of the catalyst thus promoting the cracking reactions. For n-hexane the rate of coking increased dramatically on increasing the temperature from 450°C to 500°C then to 550°C. It was suggested that the high rate of coking for n-hexane and hex-1-ene is associated with the polymerisation reactions which become more important as the temperature is increased.

In contrast, the cyclohexane coking was found to take place through a mechanism involving a bimolecular condensation and was largely unaffected by the acidity of the catalyst but did require the presence of large metal particles.

Extensive work was carried out to investigate the reactivity and composition of the strongly adsorbed carbonaceous deposits on platinum surfaces, in particular single crystal surfaces, by Somorjai [39]. Various hydrocarbon transformation reactions such as isomerisation, hydrogenolysis, hydrogenation and dehydrogenation were studied. It was found when comparing hydrogenolysis with isomerisation on clean surfaces and surfaces pre-treated with n-pentane and n-hexane, that the activity towards isomerisation was more strongly suppressed on the pre-treated surfaces, where irreversible carbon deposits were formed, than hydrogenolysis reactions.

Again, the significance of temperature towards the deactivation was stressed and it was demonstrated that alkanes with higher carbon number generally displayed less deactivation at given carbon coverages. For example, with a C:Pt ratio of greater than 2 the activity of *iso*-butane and n-pentane transformations approached 0, whereas n-hexane continued to display appreciable activity at carbon coverages equivalent to C:Pt ratios of 4 or more. It was thought that this could be due to the different site requirements of light alkane and n-hexane reactions.

It was also suggested that the reactions may indeed be taking place on bare metal surface and that the carbonaceous material deposited form into large three dimensional structures, the growth mechanism being sensitive to both surface structure and the structure of the reacting hydrocarbon, and that areas of bare metal remained present. In fact evidence was presented to suggest that at very high carbon coverages, uncovered sites tended to be isolated areas consisting of 1-10 adjacent atoms, whereas at lower carbon coverages the uncovered platinum sites appeared to exist in the form of patches which contain upwards of 10-20 atoms. This was confirmed by carbon monoxide chemisorption studies. These latter experiments also highlighted a difference

in desorption temperature between clean surfaces and those covered with carbonaceous material. A significantly lower desorption temperature was observed for those surfaces covered with carbonaceous deposits. From this it was concluded that the graphitic-like surface carbon reduced both the binding energy and saturation coverage of the carbon monoxide molecules.

As mentioned above, the effect of surface carbonaceous material on hydrogenation/dehydrogenation reactions was also investigated. It was shown that the strongly adsorbed carbonaceous species which formed at temperatures of 200-250°C acted as a non-selective poisons for simple hydrogenation reactions. It was suggested that the surface carbonaceous material in this case essentially blocked the sites required for hydrogenation (in this case cyclohexene). However, at lower temperatures of 100-200°C, on Pt(111), it was shown that although the catalyst activity was lowered with the depositions of carbonaceous material, the reaction rates were still exceedingly high. It was suggested that this might be due to the ability of the carbonaceous layer to act as a hydrogen transfer agent. This was reinforced by hydrogen TPD studies [39].

Bond has also carried out extensive work in this area [40]. Again, it was emphasised that crystal faces such as the Pt(111) facilitate hydrocarbon break-up and cause the formation of surface coke. The use of alloys were highlighted as a way of breaking up the surface preventing the formation of larger ensembles. It was mentioned that metals in high coordination sites, like those on (111) planes tend to decompose hydrocarbon reactant molecules and retain the residues on the surface. However, atoms on steps and edges, which are of lower coordination, allow hydrogen atoms access to the carbonaceous material and therefore its removal from the surface. In terms of alkane dehydrogenation, the use of high temperatures is required to achieve useful conversions, and the absence of hydrogen encourages carbon formation. It is for this reason, as mentioned in previous sections, that the use of alloys is essential for the segregation of platinum with the maintenance of small ensembles.

In terms of the hydrocarbon structure, it was suggested again that the more unsaturated the molecule, the more willing it is to form strongly held surface species. The greater the degree of unsaturation, the more carbon-metal bonds that can be formed as soon as chemisorption takes place. As a result reactions which involve aromatics or olefin species, which act as coke precursors, tend to form amorphous carbon or graphite, which deactivates the catalyst. The likelihood of formation of toxic

multiply-bonded species increases with temperature, carbon chain length and decreasing hydrogen/carbon ratio. From this evidence it is clear why dehydrogenation is a very difficult reaction to catalyse.

As well as single crystal work there has been many investigations carried out to characterise the structure and reactivity of carbonaceous deposits on supported metal catalysts. Barbier *et al* conducted an investigation into the effect of metal dispersion (and therefore particle size) on the formation of coke deposits for various hydrogenation and hydrogenolysis reactions [41]. The Pt/Al<sub>2</sub>O<sub>3</sub> catalysts with metal loadings of between 0.1-16% were subject to pre-coking by injecting cyclohexane at 450°C in a fluidised bed reactor. TPO of the coke showed the presence of two distinct peaks, at 200°C and 380°C. It was observed that the coke corresponding to the peak at lower temperature altered the metallic activity whereas the higher temperature peak did not, and that all the activity was recovered upon removal of the carbon at 200°C. The reason suggested for this was that the first peak was due to carbon deposited on the metallic surface and the second peak corresponded to carbonaceous deposits on the support material. It was also concluded from their results that less coke was deposited on catalysts with high dispersions and lower metal loading.

Finally, it was also suggested that the deposition of carbonaceous material induced an electronic effect on the metal. Evidence supporting this idea was supplied in the form of the activity measurements [41]. It was demonstrated that the coke hindered the structure sensitive hydrogenolysis of cyclopentane by poisoning the sites required, while the structure insensitive benzene hydrogenation was unaffected. These ideas agree with those proposed by Somorjai, detailed above [39].

The use of temperature programmed techniques in the characterisation of coke deposits was further investigated by Querini *et al* [42]. Pt, Pt-Re and Pt-Re-S catalysts supported on alumina were compared with respect to their accumulation and removal abilities of surface carbonaceous material. TPO showed that after 213 hrs at 500°C the Pt-Re and Pt-Re-S catalysts contained 4.11 and 13.0wt% carbon respectively, while the Pt only catalyst contained only 1.24wt% carbon after exposure to n-heptane for 290 hrs at 482°C. However, in terms of removal, the sulphur containing catalyst was cleaned quicker, with the Pt-Re and the Pt only catalyst falling behind in that order. The explanation for these observations was that the Pt-Re-S catalyst facilitates the transportation of the carbonaceous material from the metal to the support and so can

go on accumulating carbon for longer, whereas when the metal surface is deactivated on the Pt only catalyst coke accumulation stops.

It was also found that some of the carbonaceous material could be removed at very high temperatures (730-920°C) by passing inert helium over the catalyst. From this result it appears that steam gasification takes place, where water molecules, formed by dehydroxylation of the alumina support, react with the surface carbon forming carbon monoxide and hydrogen. However, this was limited to the number of surface hydroxyl groups available.

Similar theories were developed by Anderssen while investigating the effect of time-on-stream (TOS) for the dehydrogenation of propane using Pt/Al<sub>2</sub>O<sub>3</sub> and Pt-Sn/Al<sub>2</sub>O<sub>3</sub> catalysts[43]. It was found that more coke was deposited on the Pt-Sn catalyst compared to the monometallic catalyst. TPO highlighted the presence of two distinct peaks for the monometallic catalyst after 5hrs deactivation, whereas on the Pt-Sn TPO profile only a shoulder was observed on the larger peak. From these results it is believed that the first peak is associated with coke on or near the platinum metal, whereas the second peak represents the coke deposited on the alumina support material. It is suggested that part of the coke belonging to the lower temperature peak is responsible for the deactivation of the active sites on the metal and that it hinders the transportation of coke precursors to the support, thus increasing the coke accumulation on the platinum. The addition of tin reduces the metal-carbon bond strength leaving a larger metal surface free, while promoting the migration of coke precursors to the alumina support. Again, it was suggested that the precursors to carbon deposition were the olefinic species formed during dehydrogenation and that the rate of coke formation could be perturbed by the addition of hydrogen, which also reduces the rate of formation of the olefin products and coke precursors. It was emphasised that the presence of hydrogen prevents the deposition of coke and not its removal.

An isotope labeling study on propane dehydrogenation was carried out by Webb *et al* in order to identify the activity/selectivity relationship associated with the formation of carbonaceous over-layers [44]. Using 0.66wt% Pt/Al<sub>2</sub>O<sub>3</sub> it was found that the activity decreased from 40.8% to 10% after a 48 minute period. Consequently, the propene selectivity increased from 70 to ~90% over the same time period. By calculation of carbon mass balance it was established that the increase in selectivity

was accompanied by extensive carbon deposition and was therefore deemed to be critical to the efficiency of the dehydrogenation reaction. Using 13-carbon and 2-hydrogen isotopes in conjunction with pulse-flow methodology, it was established that the deposited carbonaceous material consisted of  $C_xH_y$ , and that considerable mixing between  $^{13}C$  and  $^{12}C$  and  $^2H$  and  $^1H$  was evident in the methane product at 500 and 600°C.

Again, it was emphasised that the majority of the carbon was found on the support material and that the nature of the coke was dependent on the source *i.e.* coke from CO and toluene pre-treatment were both different from the coke deposited during the propane dehydrogenation in terms of ease of removal.

Pulse-flow and continuous-flow techniques were also applied to the derivation of a kinetics based deactivation model of an isothermal propane dehydrogenation reactor using a chromia/alumina based catalyst [45]. The expression used to model the deactivation resulting from the formation of carbonaceous deposits was:-

$$\phi = \exp(-\alpha \cdot C_c) \quad \text{eq. 1.2}$$

where  $\phi$  is the activity relative to the fresh catalyst,  $C_c$  is the coke concentration and  $\alpha$  is a constant. By fitting the data obtained from the experiments to the above expression it was concluded that different types of active site were responsible for the dehydrogenation and non-selective reactions and that deactivation occurs preferentially. This is consistent with the observation that dehydrogenation selectivity increases with deactivation and that the sites responsible for catalyst deactivation become fouled, as mentioned in several papers above [44].

Coke formation during catalytic dehydrogenation was also studied for but-1-ene using a 19wt%  $Cr_2O_3/Al_2O_3$  catalyst and temperatures between 525-600°C by Mandani and Hughes [46]. It was discovered that at 525°C a parallel deactivation mechanism was observed to be taking place where coking occurred simultaneously with dehydrogenation reactions. When the temperature was increased to 600°C, a series mechanism was adopted where coking took place after the formation of butadiene species. It was suggested by correlation of coke formation with deactivation

that coking reactions and dehydrogenation reactions take place at the same sites. This is contrary to the conclusions made by Jackson *et al* [45].

In the same study, using mercury porosimetry measurements before and after dehydrogenation, it was found that a significant amount of pore blocking by coke deposits occurred reducing the accessibility of the mercury in some cases by ~50% and that a considerable reduction of over 60% in the corresponding pore surface area was also observed. It was therefore concluded that the deactivation of the catalyst resulted from pore blocking, reducing the accessibility of the active metal, as well as site blocking induced by the deposition of carbonaceous material onto the metal surface.

This latter argument was supported by work carried out by Froment, who also emphasised that pore blocking plays a big part in the deactivation of supported metal catalysts. It was also emphasised that the sites covered with coke, and therefore inactive for dehydrogenation, were still active for continued coke growth [47].

#### 1.4.2 Catalyst Sintering and Poisoning

Sintering of a supported metal catalyst usually refers to the loss of active surface area as a result of a structural modification of the catalyst. This loss of surface area takes place due to a mechanism involving agglomeration and coalescence of small metal crystallites into larger ones with lower surface-to-volume ratios. Two models have been proposed in general for sintering of supported metal catalysts, *i.e.* the atomic migration model and the crystallite migration model. The first process involves the release of metal particles from a crystallite, transportation of these across the surface of the support and subsequent capture of the migrating atoms on collision with another metal crystallite. Due to the higher stability of the larger particles, as a result of the metal-metal bond energies being greater than the metal-support interaction, the small crystallites diminish and the larger ones increase. The second model visualises sintering to occur via migration of the metal crystallites along the surface of the support, followed by collision and coalescence of two crystallites [15].

Temperature probably has the greatest effect on sintering. However, various species and atmospheres can induce or reduce sintering also. Zhang *et al* have studied the effect of chlorine on the agglomeration of platinum particles [48]. The comparison was made using clean 0.3wt% Pt/Al<sub>2</sub>O<sub>3</sub> and the same catalyst pre-treated with

ammonium chloride at ambient temperature for 0.5hrs. It was shown that Pt crystallites of less than 1.5nm on  $\gamma$ -alumina were stable against thermal ageing in hydrogen at temperatures as high as 500°C. It was stated that the reason for this was due to the strong interaction between the particles and Lewis acid sites on the support material, giving rise to an anchoring effect of Pt by the support. Techniques such as XPS, TEM and CO IR were used to characterise the catalyst in terms of size and comparison could be made between the untreated and treated samples for differences in binding energy, particle size, number of active sites and their availability. After pre-treatment the small particles sintered at 320°C under the hydrogen atmosphere. It was thought this process took place as a result of de-anchoring effect of the chloride, weakening the interaction of the Pt with the acid sites. On heating further it was suggested that the formed Pt-chloride complexes begin to melt increasing their mobility leading to agglomeration. Particles in the order of 5-8nm were found.

An opposite argument was constructed by Bournonville *et al* who investigated the effect of chlorine under both oxidising and reducing atmospheres [49]. It was suggested that under oxidising conditions and in the presence of chlorine, chloroplatinum aluminate species form which appear to be strongly bound to the support material and so the rate of sintering appeared to be slow. Under a hydrogen atmosphere, it was found that the surface atoms on the crystallites were covered with adsorbed hydrogen. It was suggested that the interaction between the platinum moiety and the support was enhanced by increasing the acidity of the support material by the addition of chlorine atoms, withdrawing electrons from the support thereby increasing the acidic nature of the acid sites.

The effect of working in atmosphere where water is present was also emphasised by Forzatti *et al* [15]. It was stated that water vapour accelerates crystallisation together with changes in the structure of the oxide supports. In order to reduce this effect it is necessary when using high surface area catalysts to minimise the water vapour concentration at high temperatures during both operation and activation procedures, as well as where water is produced as a result of the reducing hydrogen interacting with the surface oxygen [50].

Efforts to overcome sintering of Pt particles when working under demanding conditions, such as those found in dehydrogenation reactions, was studied by Rennard

and Freel [35]. The use of magnesium aluminate support materials was investigated in an effort to increase the stability of the platinum crystallites. Small amounts of sulphur in the feed were shown to suppress reactions such as hydrogenolysis and cracking reactions, which ultimately lead to coke formation. Selectivity for propane dehydrogenation was found to be as high as 92-94% at conversions of 28% over six 24hr reaction/regeneration cycles at 600°C, after which the activity fell steeply due to metal sintering. Platinum dispersion was even more stable on magnesium aluminate than on alumina in the presence of oxygen at high temperature. With Pt/Al<sub>2</sub>O<sub>3</sub> significant growth in Pt crystallites size was observed after cycles of reduction in hydrogen (600°C) followed by oxidation in air (500°C). More extensive Pt sintering occurred during regeneration of Pt/Al<sub>2</sub>O<sub>3</sub> in air after use in the dehydrogenation experiments. This sintering grew progressively worse after each coke burn-off, and occurred whether hydrogen sulphide was present or not. Pt/MgAl<sub>2</sub>O<sub>4</sub>, on the other hand, was stable in all experiments except those where coke was burned off a catalyst which had been previously exposed to hydrogen sulphide during propane dehydrogenation. It was proposed that the reason for the given sulphur effect was due to reconstruction of the support material forming magnesium and aluminium sulphates, weakening the metal support interaction.

The final deactivating mechanism to be discussed here is catalyst poisoning. Poisoning is the loss of activity due to the strong chemisorption on the active sites of impurities present in the feed-gas. The poison may impose a geometric effect on the catalyst by blocking the active sites required for reaction or may alter the adsorptivity of other species, essentially by an electronic effect. Poisons can also cause surface reconstruction through the formation of new compounds or by changing the chemical nature of the active sites so that the performance of the catalyst is altered [15].

The poisoning effect of sulphur on platinum based catalyst was studied by Jackson *et al* [51]. It was found that adsorbed sulphur poisons the sites on which it is adsorbed, and it may also poison a larger number of sites by removing a geometrical degree of freedom from the surface. In addition it was shown that the formation of a bond between a metal atom in an array and a sulphur atom may effect the ability of neighboring metal atoms to form bonds of the correct strength to allow catalytic reactions to occur, by inducing an electronic effect. This has been used in a positive sense in many circumstances *e.g.* in propane dehydrogenation, the addition of S to a

Pt/Al<sub>2</sub>O<sub>3</sub> catalyst has been shown to decrease the propensity of the catalyst to produce methane in a non-steady state period by blocking the sites required for hydrogenolysis [52]. In terms of CO adsorption, it was found that the sulphur containing species completely blocked the sites available after pre-adsorption. The capacity was reduced to 2% of the total possible sites on 0.88% Pt/Al<sub>2</sub>O<sub>3</sub> and it was also shown that sulphur could displace a small amount of adsorbed CO.

The sulphurisation and regeneration was also studied in depth by Mathieu and Primet [52]. Using a 5% Pt/Al<sub>2</sub>O<sub>3</sub> catalyst it was shown that chemisorption of H<sub>2</sub>S is a dissociative process resulting in the total coverage of the active metal surface of sulphur atoms at temperatures in excess of 100°C. Titration with hydrogen at 400°C partly removes some of the sulphur, restoring the catalyst activity towards reactions such as benzene hydrogenation and linear CO chemisorption (*i.e.* processes requiring only 1 metal atom). However, processes in need of poly-atomic sites, such as n-butane hydrogenolysis and chemisorption of bridged CO, remained inhibited. Full regeneration of the poisoned catalyst was achieved by treatment in oxygen followed by reduction under mild conditions. In this case adsorbed sulphate groups were formed which were subsequently removed during reduction. Under more severe conditions, however, the formation of sulphate groups resulted, again, in the poisoning of the metal surface.

Chlorine has also been shown to act as a poison to platinum based catalysts in a study of the oxidation of propane and propene by Marecot *et al* for the automotive industry [53]. It was shown that supported Pt and Pd catalysts, prepared using chlorinated salts, display a significant loss in activity as shown by an increase in the light-off temperature by about 80°C. It is suggested that the halogen atoms poison the sites needed for activation of the oxygen. This blocking of the reactant gas was also demonstrated by Simone *et al* [54]. It was also shown that the chloride could be removed from the catalyst surface by water produced during the combustion reaction, however, excess water (10%) inhibited the oxidation process. This latter observation was probably due to a loss of surface area and an increase in particle size brought about by sintering.

## 1.5 Catalytic Oxidative Dehydrogenation

In an attempt to overcome the thermodynamic limitations of catalytic straight dehydrogenation oxidative dehydrogenation presents an exothermic alternative to olefin formation from the corresponding alkane molecules. There currently exists two main methods of carrying out catalytic oxidative dehydrogenation. It can be done using metal oxide based catalysts where the source of oxygen appears to be in the catalyst itself and by using noble metal based catalysts where the source of oxygen comes from the gas phase.

The most widely studied metallic oxide based substrate used in oxidative dehydrogenation to date is the metal vanadate catalysts. These exist mainly as supported orthovanadates ( $M_3(VO_4)_2$ ) and metavanadates ( $MV_2O_6$ ) where M can be Mg, Zn, Ca or Pb [55]. One of the early groups to work on these catalysts was Kung *et al.* The ODH (oxidative dehydrogenation) of alkanes, in particular butane, was studied in great detail with the purpose of finding a catalyst giving high yield and the elucidation of a mechanism that would aide in the further improvement and development of these materials in the production of olefins. Reactions were carried out in the presence of molecular oxygen with the surface becoming active towards dehydrogenation at roughly 500°C. At this temperature combustion products, such as CO and CO<sub>2</sub>, were formed as well as the dehydrogenation products of but-1-ene, *cis* but-2-ene, *trans* but-2-ene and 1,3-butadiene when using the V-Mg-O catalysts. Oxygenate by-product formation was found to be suppressed [56]. The optimum vanadium loading was found to be 19% which, when compared to the MgO support which promotes cracking reactions, resulted in a decrease in conversion from 60% to 34%. Consequently, the selectivity to dehydrogenation products increased from 43 to 56% and CO and CO<sub>2</sub> decreased from 16.5 to 12.4% and 36.8 to 24.3% respectively. The effect of temperature was also measured. As expected an increase in temperature resulted in an increase in conversion. This was achieved with only a small penalty in the dehydrogenation selectivity. Butadiene selectivity increased as that of the mono-olefin products decreased. A slight increase in combustion products was also observed while the cracking products remained minimal.

Based on the work carried out on propane and butane, Kung proposed a mechanism for the process (Mars Van Krevelen mechanism) [56, 57]. It was suggested

that the alkane molecule was activated by the catalyst by H atom abstraction forming an adsorbed butyl radical and a surface OH group. This however, required the availability of a reactive surface oxygen species such as O<sup>-</sup>. It was explained that this species could form by the charge transfer as shown below.



The butyl radical is very reactive and goes on to form butene species by losing another hydrogen from the carbon atoms adjacent to the first carbon site. This can lead to a variety of product distributions depending on which carbon atom the initial hydrogen was lost from.

Loss of any one of the three hydrogen atoms at position A on figure 1.5.1 leads to but-1-ene formation. Loss of one of the hydrogen at position B leads to *cis* but-2-ene, loss of the other leads to *trans* but-2-ene. If this step is fast and the loss of hydrogen statistical, the observed ratio becomes 3:1:1, which is different from the equilibrium ratio of 1:1:1.1. Further dehydrogenation to 1,3-butadiene can also take place either primary or secondary, which requires desorption-adsorption of the produced mono-olefin. The observed ratio in this study was found to be 3:1:1 but-1-ene:*cis* but-2-ene:*trans* but-2-ene.

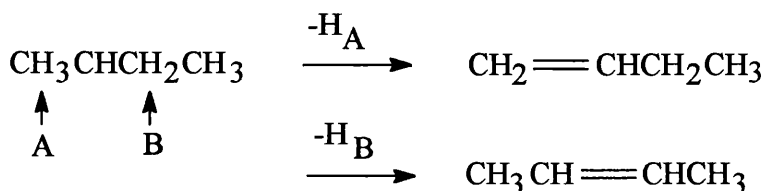


**Fig. 1.5.1** Possible sites for hydrogen elimination.

Further studies of the vanadium based catalysts by Burch and Crabb led to some important conclusions in this particular area [58]. In their study a comparison between the catalytic reaction and the non-catalytic reaction was carried out. The results of the thermal pyrolysis and the non-catalytic ODH of propane show that it was possible to obtain good yields of propene and ethene in the glass reactor vessel used. In the absence of oxygen, temperatures in excess of 700°C were required to achieve high conversions, which is consistent with the calculations described in the

thermodynamics section. However, at 600°C and propane:air ratio of 1:2 the ODH reaction can give propane conversions close to 50% at olefin selectivity of 70% compared to the catalytic reaction using 30wt% V/MgO at 500°C and propane:air ratio of 1:4, which results in conversion of 33% and 44% olefin selectivity over a period of 70 minutes.

The activity/selectivity observed in these reactions were compared to other examples found across the literature to see if there was any correlation. It was concluded that “*even the best catalysts are only as good as no catalyst at all?*” [58]. In fact, given that the catalysed reaction produced CO and CO<sub>2</sub> rather than ethene, as produced in the non-catalytic reaction, it could be said that the homogeneous reaction is more efficient than the purely heterogeneously catalysed reaction. It was suggested on this basis that purely catalytic reactions have an upper limit on selectivity for a specific conversion which is similar to that obtained without any catalyst. It was finally concluded therefore, that contributions from both homogeneous and heterogeneous processes were necessary to achieve the best commercially acceptable yields of propene.

Many other groups have made a variety of in-depth studies using vanadium based oxides. Although these investigations were carried out with the purpose of finding a new, efficient process to the formation of olefin species from the parent alkanes, using oxidative dehydrogenation, the inclusion of the detail in this overview is not necessary. A detailed review of this work was carried out by Mamedov and Corberan [59]. It was however, concluded in this report that there was no firm basis from which to define a specific reaction mechanism and that further studies at a molecular level would be necessary in order to be more definitive about the overall reaction pathway.

The conclusions made by Burch and Crabb were also accepted by Delmon *et al* within the range of catalysts under comparison [60]. The possibility of various processes taking place to allow the reaction mechanism proposed above (Mars Van Krevelen) to occur were also explained as well as other possible reaction mechanisms using various catalytic substrates. One such possibility described was oxygen spillover. This phenomenon is due to the action exerted by surface mobile oxygen on the surface of one phase (acceptor). Spillover oxygen reacts with the surface of the acceptor maintaining the active sites. The other phase, which does not need to possess any

catalytic activity, acts as an oxygen donor to the acceptor phase. Again, the need for further studies in the quest for the definitive reaction mechanism was highlighted.

In an attempt to elucidate the reason for the apparent upper limit, in terms of selectivity/conversion, in the literature for the ODH reactions, a study was carried out by Hodnett and Batiot to investigate the role of reactant and product bond energies in determining limitations to selective catalytic oxidation reactions [61]. The investigation was to determine if there was any relationship between the structure of the reactants and products of ODH reactions and the ability of oxide catalysts to achieve specific alkane transformations. Also the extent to which oxide catalysts and their active sites are selective was addressed. It was shown, from the data taken from the literature, that the upper limit for *n*-butane oxidation remains stable at around 50-60% selectivity at conversions above 20% (using oxide based catalysts). The selective dehydrogenation product tends to be metastable and given sufficient time in contact with the catalyst will fully oxidise to carbon dioxide and water. The reactions proceed through the pathway shown on figure 1.5.2, where k are the rate constants for the various reaction steps.

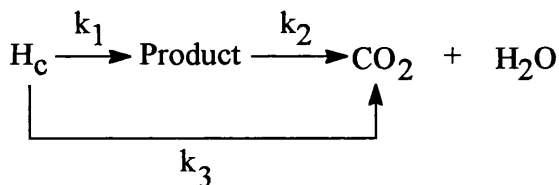


**Fig. 1.5.2** Alkane oxidation reaction pathway.

The idea is that oxidative dehydrogenation involves the activation of a C-H bond in the hydrocarbon starting material as described in many of the papers discussed above and below. The lower the bond dissociation enthalpy the easier the activation process, hence the greater the value of  $k_1$ . The value of  $k_2$  is determined by the bond dissociation enthalpy of the weakest C-H or C-C bond in the dehydrogenation product, and the value of  $k_3$  depends on the bond dissociation enthalpy of the weakest C-C bond in the starting material. Selectivity is therefore dependent on the oxide catalyst distinguishing C-H bonds in the reactant from those in the products. Using the equation:

$$\Delta^{\circ}H_{C-H(\text{reactant})} - \Delta^{\circ}H_{C-H \text{ or } C-C(\text{product})} \quad \text{eq. 1.4}$$

where  $\Delta^{\circ}H_{C-H(\text{reactant})}$  is the bond dissociation enthalpy of the weakest C-H bond in the reactant species and  $\Delta^{\circ}H_{C-H \text{ or } C-C(\text{product})}$  is the bond dissociation enthalpy of the weakest bond in the dehydrogenation product, there was a very clear linear correlation between the limiting selectivity and bond dissociation enthalpies. This suggests that there is a crucial role for the weakest bonds in the starting material and in the dehydrogenation product in determining selectivity. It was shown that if the difference is less than 30 kJ mol<sup>-1</sup> a very high selectivity could be achievable at all conversions, whereas for differences greater than 70 kJ mol<sup>-1</sup> poor selectivity can be expected.

As well as the oxide based catalyst mentioned above, pioneering work carried out on noble metal catalysts supported on ceramic monoliths and using platinum alumina catalysts in conjunction with fluidised bed technology has been investigated with tremendous success by Schmidt *et al* [5, 62]. Using this technology, manipulation of various reaction parameters, including contact time, hydrocarbon:oxygen ratio and the effect of inert diluent has been possible in order to optimise the ODH of propane and *n*-butane to obtain high selectivity without any loss of conversion.

Using monolith supported catalysts, reaction temperatures in the region of 1000°C were achieved by the light-off of the reactant gases while set at stoichiometry (which favours the production of CO and H<sub>2</sub>) generating the necessary exotherm. Once the desired temperature was reached the reactant composition was set to the appropriate ratio for optimum olefin formation. The results showed that the ODH of propane and *n*-butane produced similar olefin products, *i.e.* propene and ethene, no butene products were observed. It was found that for *n*-butane:oxygen ratios of less than 0.5 the main products were CO and H<sub>2</sub>, while for ratios greater than 0.5 the olefin products were dominant. In fact at the value of 0.65, 32% selectivity towards ethene was observed while at 0.85 40% propene was achieved. Overall, as the ratio increased total olefin production was found to be optimal at a *n*-butane:oxygen ratio of 0.7. Conversion and selectivity could also be manipulated by varying the amount of nitrogen diluent. A reduction in nitrogen in the feed-gas resulted in an increase in reaction temperature which resulted in an increase in conversion which ultimately led to a decrease in the production of olefins.

A crucial aspect of this work was the utilisation of monolith supports and fluidised beds, which permitted the employment of high space velocities and short contact times. As the flow-rate was increased the conversion of *n*-butane decreased (as it was allowed less time exposed to the catalyst surface) and the ethene selectivity also decreased. However, the production of the longer chain propene increased dramatically while using flow-rates in the region 7000 SLPM (standard litres per minute). Consideration of all these conditions resulted in an ultimate total olefin selectivity of 65% at 100% conversion for monoliths and 65-70% selectivity with 90% conversion for the fluidised bed reactors. It should also be mentioned that no deactivation or gas phase reaction could be detected in either case. Deactivation was prevented by the sufficiently high partial pressures of CO<sub>2</sub> and H<sub>2</sub>O continuously removing any coke from the surface by either reverse Boudouard (CO<sub>2</sub> reforming) or steam reforming.

In both cases the mechanism proposed was similar to that suggested for the metal oxide based catalysts. Reaction of the *n*-butane with surface oxygen (it was believed that the adsorption of oxygen from the gas-phase resulted in the formation of an adsorbed layer of oxygen on the surface of the platinum) led to hydrogen abstraction and the formation of adsorbed alkyl and hydroxyl groups. However, unlike at the lower temperatures, β-alkyl elimination was preferred to β-hydrogen elimination (C-C bond is easier to break than the C-H bonds) to form propene. Secondary cracking reactions to form ethene, steam reforming to CO and H<sub>2</sub> and hydrogenolysis of the surface adsorbed methyl groups to methane also occurred [5, 62].

A similar study was carried out by Forazatti *et al* to investigate the role of a 5wt% Pt/Al<sub>2</sub>O<sub>3</sub> catalyst in the ODH of propane in an annular reactor system [10]. In an annular reactor the catalyst is deposited in the form of a thin, short layer onto a tubular ceramic support inserted into a quartz tube. The apparent advantage of this type of configuration is that it allows the use of high temperatures together with isothermal stability and the attainment of high space velocities (contact times of 10<sup>-6</sup>-10<sup>-3</sup> seconds) which would not be possible in a packed bed arrangement. This allows the use of a wide range of reaction conditions.

Using this reactor configuration over a temperature range of 200-500°C and propane:oxygen ratio of 1:1, only combustion products were present in the product

mixture. In comparison with similar empty tube reactions, it was concluded that this combustion was thoroughly catalytic. In fact it was found that the reaction rate on the Pt surface was so fast that the process underwent interphase diffusion control at temperatures as low as 200°C. This was suggested from the result which showed an almost flat temperature dependence of propane and oxygen conversion up to 500-550°C. Above this temperature olefins were formed in quite large amounts. However, it was shown from the empty reactor studies that gas-phase oxidative pyrolysis was active and could produce similar amounts of olefin *i.e.* 55% total olefin selectivity at 60% conversion, which could be enhanced by decreasing the contact time through the reactor. The effect of increasing the bed depth was also investigated. It was found that longer reactor beds increased the amount of combustion products produced.

It was concluded that little evidence was found to suggest heterogeneous formation of olefins in the ODH, contrary to the surface mechanism previously presented in Schmidt's work. These findings also agree with those of Burch and Crabb on the oxide based catalysts. It was therefore concluded that the Pt/Al<sub>2</sub>O<sub>3</sub> catalyst was extremely active in the non-selective oxidation of propane in the range 200-600°C and that combustion was the only active route at low temperature compared to the gas-phase reactions which were much more selective in the production of olefins [10].

Following on from the above study, an investigation of the role of the catalyst in autothermal conditions was carried out [63]. This time the 5wt% Pt/Al<sub>2</sub>O<sub>3</sub> catalyst was deposited onto a high void fraction (to reduce potential back pressure) metallic support. It was determined that low contact times and propane:oxygen ratios greater than 2 were optimal for the selective production of olefins. The best yields obtained for total olefin were 50%, at 90% conversion of propane and 100% conversion of oxygen. Increased conversion and decreased olefin formation was also observed with an increase in oxygen content. The formation of CO and CO<sub>2</sub> was also observed during these changes.

Comparison of the experimental results obtained from the catalytic tests and the data collected from homogeneous model simulations suggested, again, that the catalyst is very efficient for propane oxidation and is merely used as an ignitor to the gas-phase reactions when operating the dehydrogenation process. The role of the catalyst was therefore small. The observed olefin yields in the presence of the platinum

catalyst were in fact comparable with the maximum values obtainable in a purely homogeneous process.

Noble metal gauzes have also been used by Lodeng *et al* as catalysts in an attempt to carry out ODH of alkanes [64]. Catalytic gauzes, again, allow contact times in the order of  $10^{-5}$  seconds to be achieved, although significant bypass is also observed. The catalyst consisted of a single 15mm diameter circular layer piece of gauze (made of platinum or 10% rhodium/platinum) positioned between two cylindrical pieces of corderite monolith, added for its thermal insulation properties. The results were similar to those obtained by Forzatti *et al* [10, 63] in that the catalyst acted as a very effective source of ignition of the homogeneous reactions thus enabling increased reaction rates compared to the empty reactor. Again, at temperatures below 500-600°C, combustion reactions were dominant. Other by-products, such as ethyne and benzene, were also observed. Benzene was regarded as a precursor to coke formation on the internal walls of the process equipment. These deposits were also observed to form on the exit part of the quartz reactor. These by-products could be minimised by avoiding excessive residence times.

The use of coals as catalysts for the ODH of *n*-butane was investigated by Portela *et al* [65]. Coals are one of the cheapest sources of carbonaceous materials. They are also members of the sedimentary rock family, composed of inorganic materials such as sulphur, nitrogen and oxygen containing compounds, which can be present as independent species or in trace amounts associated with the organic phase. These latter species could also display some catalytic activity. The coals used are ranked from lignite B to 1v bituminous. Low rank coals tend to be more porous than the bituminous ones, decreasing in mainly the meso and macropore volume as the rank is increased. Low rank coals have a large amount of oxygenated compounds whereas the bituminous coals tend to have a higher carbonaceous content.

Portela showed that coals were catalytically active for ODH of *n*-butane, but gaseous oxygen is required in the reactor feed. Two processes take place *i.e.* dehydrogenation and coal combustion forming CO and CO<sub>2</sub>. Lower butane conversion and greater coal stability was obtained with feeds rich in butane, but C<sub>4</sub> selectivity was found to be similar to that found in an oxygen rich feed. Conversion is also favoured with increasing temperature, however, beyond 500°C C<sub>4</sub> selectivity decreased while isomerisation and cracking reactions became prevalent. The optimised yield was 8% at

400°C, obtained by increasing the contact time, which resulted in a large increase in C<sub>4</sub> initial selectivity, showing values as high as 70%, but decreasing with time-on-stream. The increase in coal rank also favoured butane conversion and longer run times (8 hrs compared to 2-3 hrs for the lower ranked coals). The highest selectivity for dehydrogenation products was found to be in the middle of the range coals.

The final piece of work to be summarised was carried out a by Golunski *et al* [66]. In this study the ODH of *iso*-butane to *iso*-butene using platinum deposited on a support consisting of tin oxide and zirconium oxide, where the presence of the Sn was said to stabilised the small platinum ensembles (as described in a previous section). At 500°C, dehydrogenation yields of approximately 20% at time-on-stream of 5-7 hrs were observed. Deactivation was found to be steady at 3-4% over a 2 hr period. Decreasing the GHSV from 3000 hr<sup>-1</sup> to 1500 hr<sup>-1</sup> resulted in an increase in yield of approximately 5-10%. Combustion products were found to be minimal, just above the detection limit.

In conclusion, it was claimed that the benefits gained from using oxygen in the feed-gas were:

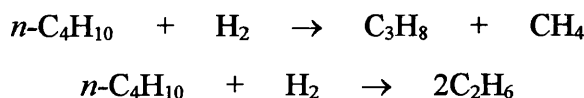
1. the exothermic reaction with the hydrogen produced provided heat within the catalyst bed;
2. the consumption of hydrogen shifted the equilibrium in favour of the olefin products; and
3. the presence of oxygen quenches the two main causes of catalyst deactivation *i.e.* carbon deposition and sintering caused by the oxidation of the carbonaceous deposits.

### 1.6 Isomerisation, Hydrogenolysis and Combustion Reactions

As well as the dehydrogenation reactions mentioned above, various other primary and secondary reactions can take place when carrying out *n*-butane dehydrogenation with or without the presence of oxygen. These reactions are isomerisation (butane or butene), hydrogenolysis or cracking (depending on the conditions) and combustion of the hydrocarbon in the gas-phase or of the carbonaceous material deposited on the catalyst surface, all of which can be effectively catalysed by both platinum and alumina when using the same conditions of temperature.

It was reported by Somorjai *et al* that among the group VIII metals, platinum is a uniquely selective catalyst for both isomerisation and hydrogenolysis (cracking in the presence of hydrogen)[67]. It was observed that these reactions were sensitive to the structure of the surface on which they were exposed. It was found that hydrogenolysis reactions were best suited to kinked platinum surfaces of (111) orientation and that isomerisation displayed its highest activity on the stepped (100) face (13,1,1). It has also been observed that strongly retained carbonaceous species block the sites required for hydrogenolysis reactions [68, 69].

Jackson *et al* also acknowledged the surface sensitivity of these processes, in particular hydrogenolysis, and defined it as “the breakage of carbon-carbon bonds with the uptake of hydrogen”[70]. It was also reported that platinum possesses a high selectivity towards single hydrogenolysis (where only one C-C bond is broken), unlike metals such as tungsten, tantalum and iron which have a high tendency towards total degradation to methane. The following reactions are possible in the hydrogenolysis of *n*-butane.



Jackson and co-workers have shown that hydrogenolysis and isomerisation display very similar activation energies, when using the tested Pt/Al<sub>2</sub>O<sub>3</sub> catalyst. The mechanism agreed for hydrogenolysis was:

1. dissociative chemisorption of molecular hydrogen,
2. chemisorption of the alkane by the loss of a hydrogen atom,
3. fragmentation of the resultant alkyl species, and
4. rehydrogenation and desorption of the smaller chain product alkanes.

For the bond-shift isomerisation reactions involving *n*-butane and *iso*-butane, the following mechanisms are possible on Pt-based catalysts:

1. a bifunctional mechanism, involving acid sites on both the metal and the support material,
2. isomerisation involving the metal-only, and
3. isomerisation involving the support material only.

On platinum-alumina catalysts, all the above mechanisms are possible, whereas on platinum-silica systems only mechanism 2 is possible, since the silica support has no available acid sites strong enough to allow the reactions to take place. The metal only mechanism involves:

1. carbon-carbon bond fission,
2. carbon backbone rearrangement, and
3. carbon-carbon bond recombination.

The silica supported catalysts show greatest efficiency towards isomerisation compared to the alumina supported catalyst which display a greater affinity towards the hydrogenolysis/cracking type reactions. It is thought that this might be due to the  $\delta^+$  polarisation of the platinum sites on the Pt/Al<sub>2</sub>O<sub>3</sub> catalyst inhibiting steps 2 and 3 in the latter suggested mechanism, compared to the silica based catalyst [70].

It has also been suggested that the easiest route towards isomerisation was by firstly forming the dehydrogenation product, which could then be more easily isomerised, and then rehydrogenation to alkane product [71]. In *n*-butane isomerisation to *iso*-butane, the platinum phase would initially dehydrogenate the *n*-butane to an *n*-olefin, the alumina support would then isomerise this to *iso*-butene with rehydrogenation, again, taking place on the platinum metal. It was found that Pt-Cu systems were particularly effective for this reaction.

With alumina only induced isomerisation reactions, again, it was found to be desirable to firstly form the olefin, which could be isomerised more easily at lower temperatures to *iso*-butane, compared with *n*-butane. It was observed that olefin isomerisation reactions occur readily on the acid sites and become increasingly difficult in the order: cis-trans < double-bond << skeletal isomerisation. It was concluded that cis-trans and double bond isomerisation could take place on weakly acidic catalysts such as unpromoted alumina at low temperature, whereas skeletal reactions require more strongly acidic conditions associated with the use of promoted aluminas at higher temperatures [72].

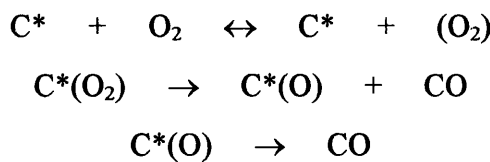
In addition to this an in-depth study of alumina materials was carried out by Morterra [73]. It was found that transitional aluminas only became active at temperatures greater than 400°C, *i.e.* after the elimination of over 60-70% of the

surface hydrated layer and the onset of the formation of defect sites in which multiple anion vacancies were present.

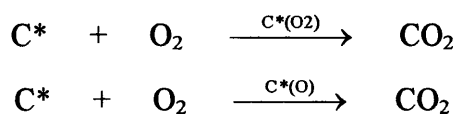
Finally, it was also found by Ponec *et al* that Bronsted acids, Lewis acids and redox active oxides all catalysed isomerisation [74]. Reactions found that double bond and skeletal transformations could take place on alumina substrates at temperatures of 350–400°C, and at slightly lower temperatures with aluminas modified with halogens, which increase the acidic nature of the acid sites.

As mentioned above, when oxygen is present oxidation reactions can also take place. In fact, catalytic fuel combustion is a process that is used within the automotive industry to remove one of the three main gaseous pollutants. Platinum is the most common component of three way catalysts fitted to cars today. The combustion of *n*-butane, using platinum catalysts, to form CO<sub>2</sub>, CO and water has already been mentioned in section 1.5 above [63, 65]. Due to its exothermicity this reaction can take place at temperatures as low as 200°C. Schmidt also observed oxidation reactions when using precious metal gauzes for oxygenate formation from *n*-butane [75]. In the aforementioned work it was found that the formation of oxygenates and olefins decreased sharply and the combustion products increased sharply at H<sub>c</sub>:O<sub>2</sub> ratios  $\geq 3$  (at 80–90% selectivity). It was also found that combustion products dominate in high dilution conditions. At H<sub>c</sub>:O<sub>2</sub> ratios of 2.6, olefin and oxygenates were dominant below 20% dilution, whereas combustion products were dominant above this figure. Longer contact times also favoured combustion products.

As well as combustion of the gaseous hydrocarbons either in the gas-phase or with the use of a catalyst, removal of carbonaceous deposits can also be achieved using oxygen, again, with the resultant products of carbon oxides and water. The kinetics of CO and CO<sub>2</sub> evolution during TPO of coke deposits on cracking catalysts was carried out by Brown *et al* [76]. It was found that the removal efficiency was affected by i) combustion within the catalyst pores which can, under certain circumstances be diffusion limited; and ii) oxidation of the hydrogen component of coke, which precedes the carbon combustion resulting in significant temperature fluctuations. Three elementary steps represent the heterogeneous elimination of CO during carbon oxidation:



where  $C^*$  is a free carbon site (a carbon in the carbonaceous deposits),  $C^*(O_2)$  is a dioxygen surface complex and  $C^*(O)$  is a stable oxygen surface species. The formation of  $CO_2$  could proceed through the following mechanism:

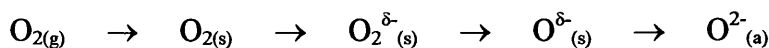


The ability of the acid sites on the activated alumina towards cracking reactions and the formation of carbonaceous deposits and catalyst deactivation was also re-emphasised.

### 1.7 *Surface Science Studies of the Role of Oxygen*

It is accepted, from the supported catalyst literature, that one of the key conditions responsible for the resultant activity and selectivity in the oxidative dehydrogenation of alkanes, forming olefins, is the relative concentration of the hydrocarbon and the oxygen in the feed-gas. In fact, H-abstraction by a surface oxygen species of some description seems to be an important step in the mechanism.

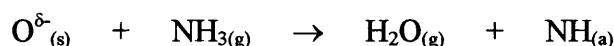
The formation of reactive oxygen species capable of this behaviour, on a catalyst surface, was studied in great detail by two authors in particular. Using surface science techniques and metal single crystals, the reaction of ammonia with oxygen was investigated by Roberts and co-workers [77]. Using XPS and STM it was established that surface oxygen could play a dual role, *i.e.* it could give an unreactive atomically clean metal surface very specific chemical reactivity while the thermodynamically stable perfect oxide overlayer was comparatively unreactive. It was suggested that dissociative chemisorption of molecular oxygen involved the following steps.



where  $O^{2-}_{(a)}$  is the adsorbed thermodynamically stable oxide and  $O^{\delta}_{(s)}$  is the short lived metastable oxygen species commonly known as ‘hot oxygen’ [77], which displays some translational energy and can be used in H-abstraction type reactions.

It was discovered that the residence time of this surface oxygen species before reaction or the formation of the stable oxide was in the region of  $10^{-5}$ s [77]. It was also discovered that the  $O^{\delta}_{(s)}$  concentration decreased dramatically as the oxygen coverage increased. These observations would vary depending on metal, surface structure, temperature and pressure of the reactions.

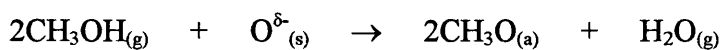
The activation of ammonia by preadsorbed oxygen on Cu(111) surfaces was one of the test reactions investigated [77].



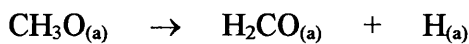
It was found that the reaction rate was sensitive to oxygen coverage and became unmeasurably slow as the preadsorbed oxygen coverage approached unity. Using STM it was observed that as the oxygen concentration increased, the single reactive oxygen adatoms became associated with Cu-O-Cu-O chains that were also observed to be active in the H-abstraction process. With further addition of oxygen these chains became islands with unreactive (at temperatures below 127°C) cores, where only the edges of the islands were active towards H-abstraction. This led to the general proposition that the activity of oxygen in H-abstraction reactions decreased as oxygen clusters developed, and became close to zero for the ultimately formed oxide overlayer. This is the origin of the oxygen concentration dependency. These observations were also observed by Madix *et al* who studied the same reaction using Cu(110) surfaces [78]. It was also observed that at 127°C reactions even occurred inside the oxygen islands.

A similar study was also carried out by Roberts *et al* on the oxidation of methanol to formate [79]. Again, the reaction rate was highly dependent on the formation of the active oxygen species and the prevention of oxide islands. The mechanism for this reaction is shown below.

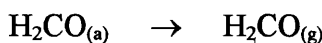
1. H-abstraction from the methanol by the reactive oxygen species forming adsorbed methoxy species and water.



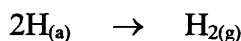
2. Formation of the adsorbed formate species and a hydrogen atom.



3. Desorption of the previously formed formate species.



4. The association and desorption of hydrogen gas.



It is intriguing to wonder if knowledge attained from these surface science experiments can be applied to understand the processes responsible for the favourable yields reported by Schmidt and co-workers.

### 1.8 *Summary of Introduction Section*

The aim of the introduction was to provide a background into the area of chemistry associated with the dehydrogenation of alkanes to their corresponding olefins. It is evident that many issues are involved as well as a variety of problems which have to be overcome. Issues such as equilibrium restrictions, deactivation and the separation of unwanted products are real problems which exist and have to be overcome in order to make the process economically viable in terms of olefin production and energy input. In doing so, great effort is needed, from a chemical and engineering perspective, to build suitable, cost effective and safe facilities in which to carry out the reactions.

Oxidative dehydrogenation, being exothermic, potentially allows the production of olefins from the parent alkane molecules at lower temperature and higher yield than could ever be achieved under conventional dehydrogenation conditions. As a result, many researchers have studied a wide variety of substrates, mainly oxide based catalysts, in pursuit of an answer to the problem. However, as yet

no catalysts have been developed providing enough benefits, in terms of activity and lifetime, to convince industry to convert from using conventional dehydrogenation processes. However, recent pioneering work carried out using monolith supported noble metal catalysts and supported metal catalysts in fluidised bed type reactors by Schmidt *et al* has demonstrated that with a combination of oxidative dehydrogenation and supported catalysts high conversion and high selectivity can be achieved.

The postulated mechanism is that of the Mars Van Krevelen mechanism, which involves the ODH of the alkane species by the adsorbed oxygen to form a surface alkyl.  $\beta$ -Hydrogen abstraction followed by  $\beta$ -alkyl elimination of the adsorbed alkyl leads to olefin production rather than cracking reactions producing surface carbon. It is also assumed that all the reactions which took place were metal surface related and that no homogeneous gas phase reactions occurred. This mechanism was also supported by most of the ODH work carried out in the metal oxide studies.

Surface science studies carried out by Roberts *et al* and Madix *et al* have emphasised the role of oxygen in terms of activating reactant molecules, such as alkanes, by the process of hydrogen abstraction and concluded by highlighting the importance of the oxygen concentration to reactivity of the surface oxygen species formed and the prevention of stable oxide formation with the resultant loss in activity. The lifetime of the active oxygen species was also found to be crucial to its activity.

On the basis of these studies, our aim was to develop these ideas using conventional supported platinum catalysts at more moderate temperatures, as well as investigating the observations made in the surface science work in an attempt to improve, by lowering the reaction temperature and eliminating deactivation, the current catalytic dehydrogenation processes used in industry.

## *Chapter 2*

### Characterisation and Testing Facility

This section describes the catalyst testing and characterisation facility built in order to carry out dehydrogenation work as well as to find out information about the physical and chemical properties of the catalysts used during the investigation. Outlined below is a summary of the capabilities of the unit in terms of its main features, as well as its integrated analytical abilities.

## *2.1 Construction and Capabilities of Catalyst Testing and Characterisation Facility*

The catalyst testing and characterisation facility has been constructed in order to be as flexible and self-contained as possible. It enables catalyst characterisation to be carried out using a number of different techniques, as well as enabling catalyst testing under pulse-flow and continuous-flow conditions to be conducted, all using the same apparatus. Figure 2.1.1 is a schematic diagram of the facility. The rig can be broken up into six individual sections. These are - the gas cylinders and mixing section, vacuum line, reactor, and the analysis systems comprising a Gas Chromatograph (GC), Infrared Spectrophotometer (IRS) and Mass Spectrometer (MS). All of which are connected together to allow specific gas mixtures to be tested with a characterised catalyst under pre-set, controlled conditions; with the resultant products being separated and analysed in various ways. Photograph 1 shows the apparatus in its entirety. It should be emphasised that a great deal of work was put into the construction, development and optimisation of this piece of apparatus over the period of approximately 1.5-2 years.

### **2.1.1 Gas Cylinders and Mixing Section**

Figure 2.1.2 is a schematic diagram of the main features involved in this section. As well as the reactant gases, this section provides the carrier gas for pulse-flow reactions (helium), reducing gas mixture for catalyst activation purposes (6% hydrogen/nitrogen) and the sample and reference flow system (helium) for the operation of the gas chromatograph (GC). Photograph 2 illustrates the configuration of the apparatus as it was constructed.

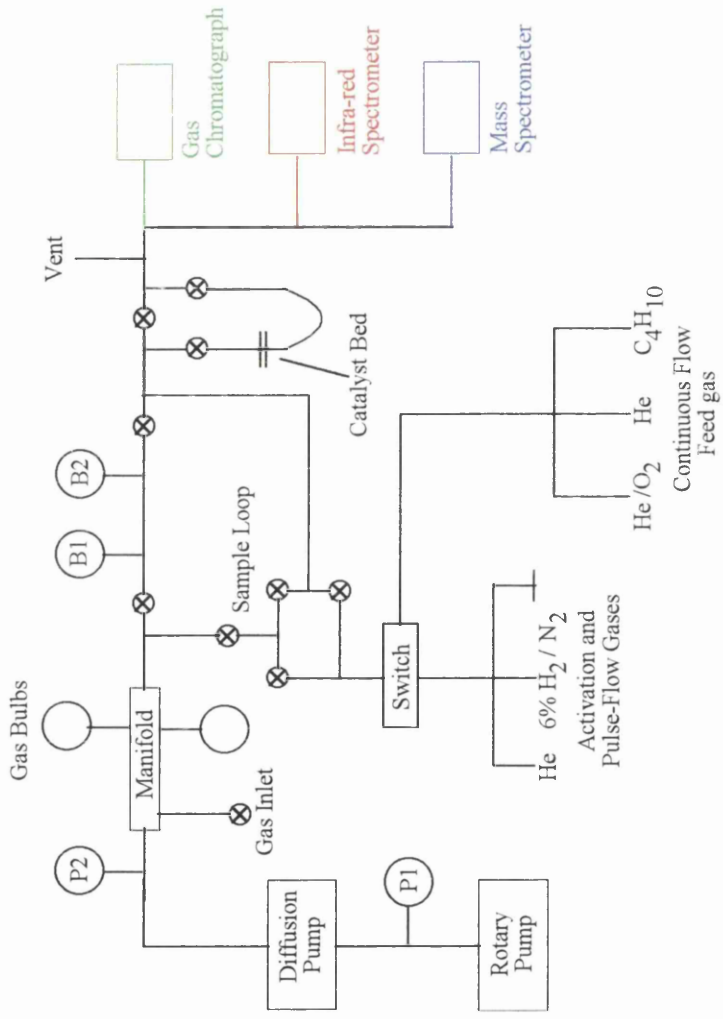


**Fig. 2.1.1** Schematic Diagram of the Catalyst Testing and Characterisation Facility.

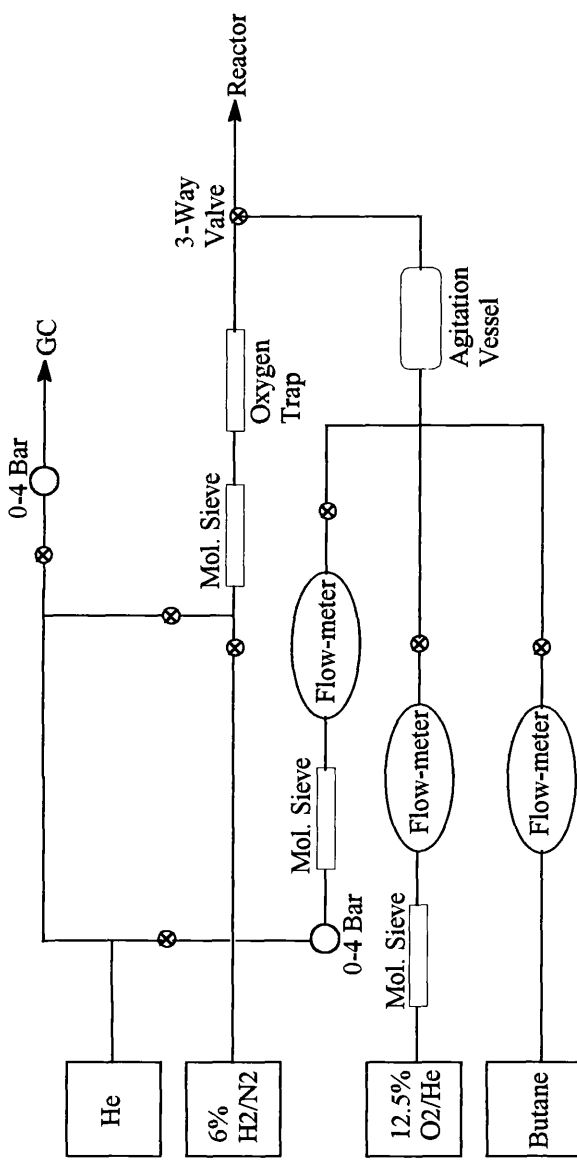


**Fig. 2.1.2** Schematic Diagram of the Gas Cylinders and Mixing Section.

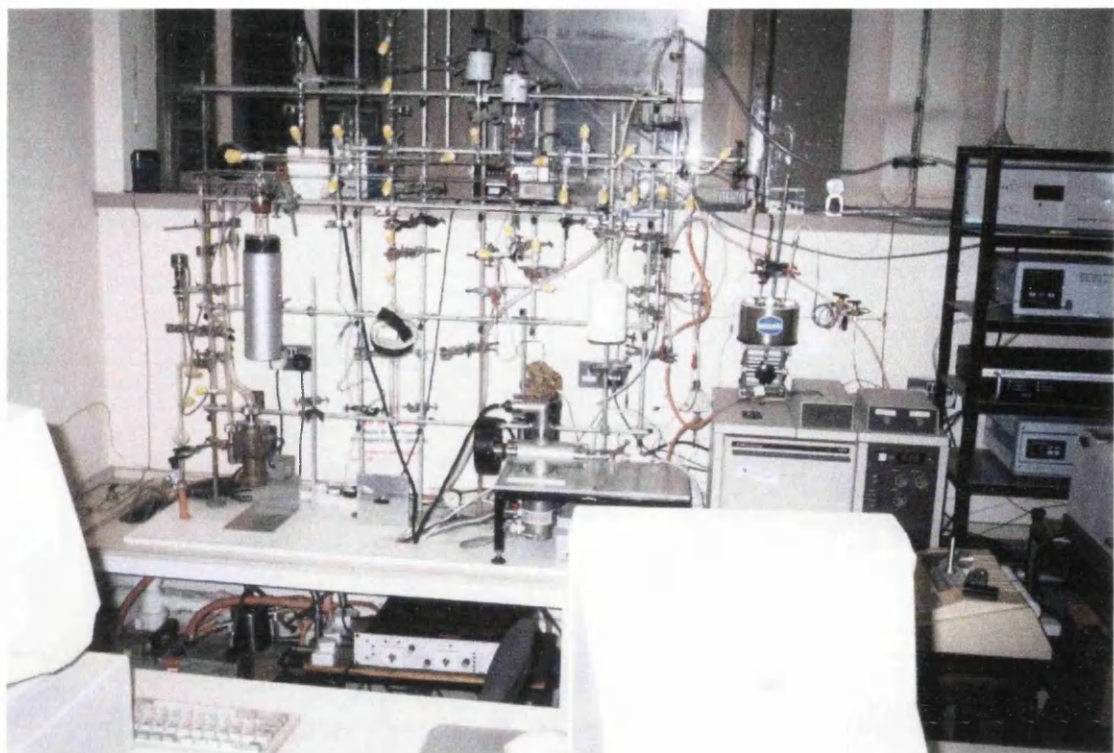


**Photo. 1** The Catalyst Testing and Characterisation Facility.

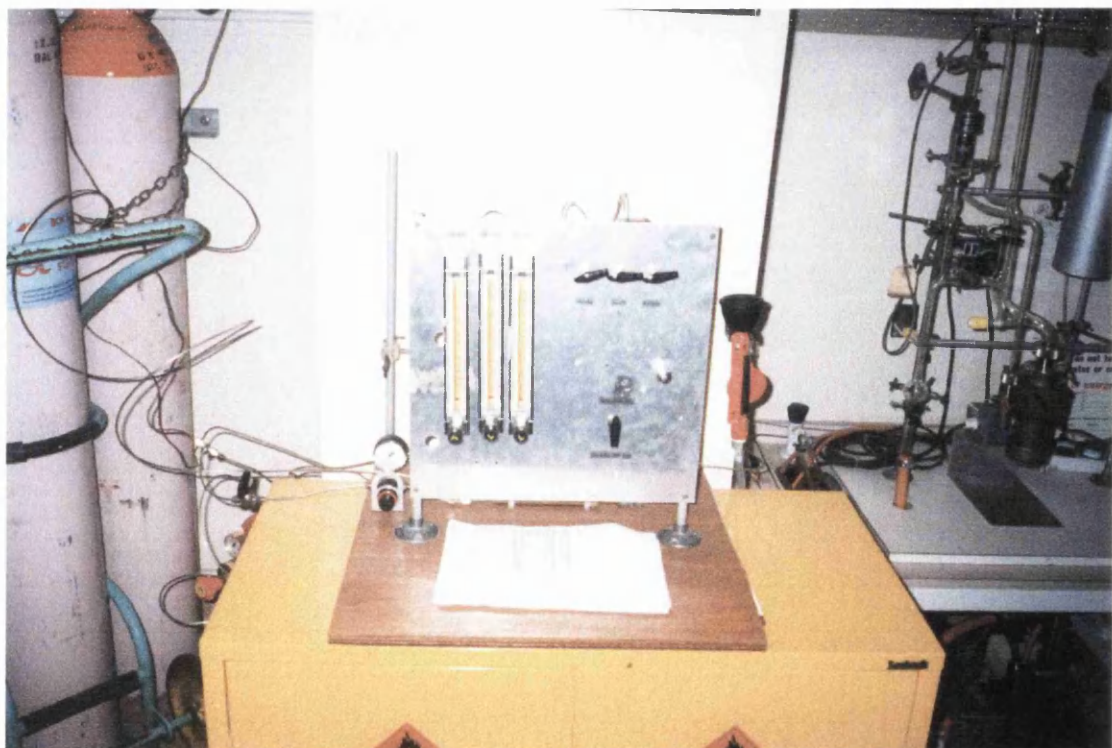


**Photo. 2** The Gas Cylinders and Mixing Section.

When using the continuous-flow section the gases (butane, oxygen and helium) were mixed at the required ratios for a particular reaction with respect to flow-rate. This operation was carried out using a suitable combination of Cole-Palmer flow meters. From the flow meters the gases were combined at a Swagelok union cross from which the mixture entered a metal vessel filled with glass beads to ensure thorough mixing. The helium from the cylinder could be used to feed the reactor gas mixing section as well as providing the flow system for the GC simultaneously.

To operate the pulse-flow section, the helium could be directed towards the catalyst and the GC at the desired flow-rates and pressures without running through the gas mixing apparatus. The system was designed to allow the activating gas mixture to follow the same route (without using the GC) as the pulse-flow gases.

Various traps have been incorporated to remove any unwanted impurities within the gases. Oxygen traps made from a glass tube filled with a palladium tungstate catalyst, prepared by impregnation, were inserted in order to remove unwanted oxygen from the helium carrier gas and activating gas mixture. Molecular Sieves (5A) were introduced to remove any trace water from the gases used. These were regenerated regularly.

### **2.1.2 Vacuum Line**

The vacuum line was constructed mainly from Pyrex glass and employed not only to handle reactant gases and gas mixtures used during pulse-flow reactions and other characterisation techniques requiring pulses of gas, but it has also been used to carry out volumetric adsorption isotherm measurements. It has been constructed without the need for mercury (for pumps and manometers) and vacuum grease thus making it a clean system and ensuring that reactant gases, such as hydrocarbons, are not affected by interaction with the grease in any way. Figure 2.1.1 and photo 1 also highlight this section of the testing rig (section constructed from glass).

The vacuum in the line has been obtained by a combination of a rotary pump and an oil diffusion pump. The two stage Edwards E2M5 rotary pump creates a vacuum of approximately  $5 \times 10^{-2}$  torr, measured by a Genevac Pirani gauge, and an Edwards EO 40/55 oil diffusion pump reducing this further to approximately  $1.5 \times 10^{-5}$

torr. The ultimate vacuum in the manifold is measured by an ion gauge (ITL gauge and VG controller), and its integrity tested to ensure that the vacuum is maintained when isolated. It was also thought necessary to include a fore-line trap above the rotary pump to prevent any rotary pump oil entering the vacuum manifold.

Figure 2.1.1 also shows an inlet for introducing gases into the vacuum manifold. These gases can come from a number of sources ranging from large cylinders to small aluminium canisters. The pressure introduced can be monitored using two MKS pressure transducers (baratron capacitance manometer), working in the ranges  $1 \times 10^{-3}$  torr to 1 torr (B1 on figure 2.1.1) and 1 torr to 1000 torr (B2) thus; allowing a wide range of pressures to be accessed. Provision has also been made to store the various gases, or gas mixtures, by the inclusion of two bulbs (volume approximately 1 litre) attached via Youngs ball and socket joints, where the seal is made by a nupro ‘O’ ring.

The determination of the volume of certain sections of the vacuum line was calculated to allow the introduction of predetermined amounts of reactant gas or adsorbent gas to the catalyst surface. This was done using Boyle’s Law as written in equation 2.1 where P is pressure and V is volume.

$$P_1V_1 = P_2V_2 \quad \text{eq. 2.1}$$

A bulb of known volume, determined from its weight when filled with distilled water, containing a known pressure of nitrogen gas was used in the measurements. The bulb was opened and its contents allowed to expand into the appropriate sections of the vacuum line. Using equation 2.1 the volume of the sample loop was calculated several times, taking the average as the final volume. These volumes are listed in table 2.1.1.

### 2.1.3 The Reactor

A down-flow micro reactor was used throughout this work for all of the catalyst testing experiments (continuous and pulse-flow) as well as for TPD and TPO measurements. This reactor consisted of a u-tube made from quartz glass with a sintered glass platform on which the catalyst bed was placed, and was connected to the

glass line via Youngs ball and socket joints. The reactor also included a thermocouple pocket attached adjacent to the catalyst bed so that the temperature could be monitored accurately. The temperature was controlled using a Watlo furnace connected to a Eurotherm temperature programmer. Figure 2.1.3 is a schematic representation of the quartz microcatalytic reactor.

The reactor used for the chemisorption measurements was a glass tube connected to the vacuum line via a Youngs ball and socket joint with a nupro 'O' ring providing a vacuum tight seal. In the IR experiments the reactor was place in the FTIR spectrometer used allowing *in-situ* experiments to be carried out (section 2.1.5).

**Table 2.1.1** Sample Loop Volume Calculations.

Calculation	Loop Volume (ml)
1	5.06
2	5.06
3	5.06
4	5.06
5	4.79
Average Value	5.01

#### **2.1.4 The Gas Chromatograph (GC)**

In order to be totally quantitative in terms of reaction products it was necessary to construct a two stage separation system with the GC. This involved having two columns arranged in series. The first column, a 5A molecular sieve, was operated at room temperature outside the GC and was used to separate oxygen, methane and carbon monoxide. The second column, mounted inside the Philips PU chromatograph, was made from 33% dimethyl sulfulone (DMS) on Chromsorb-p and was also operated at room temperature. This column was used to separate the remaining products. Figure 2.1.4 is a schematic diagram of the equipment set up to carry out this task while photograph 3 depicts the arrangement after construction.

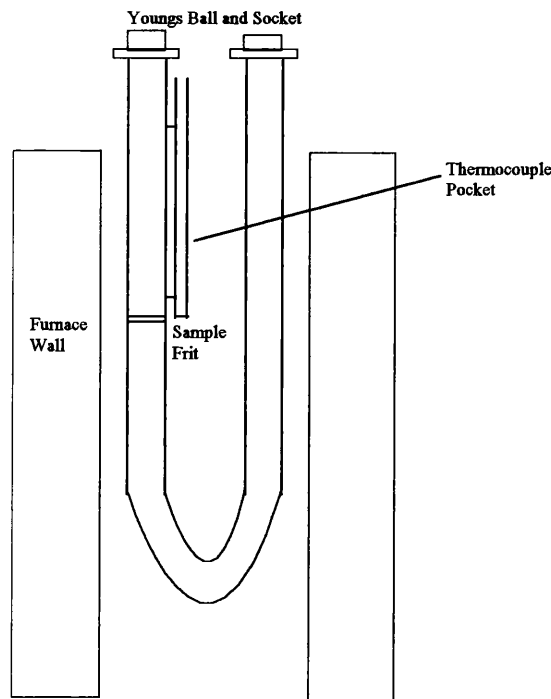


**Fig. 2.1.3** The Quartz Microcatalytic Reactor.

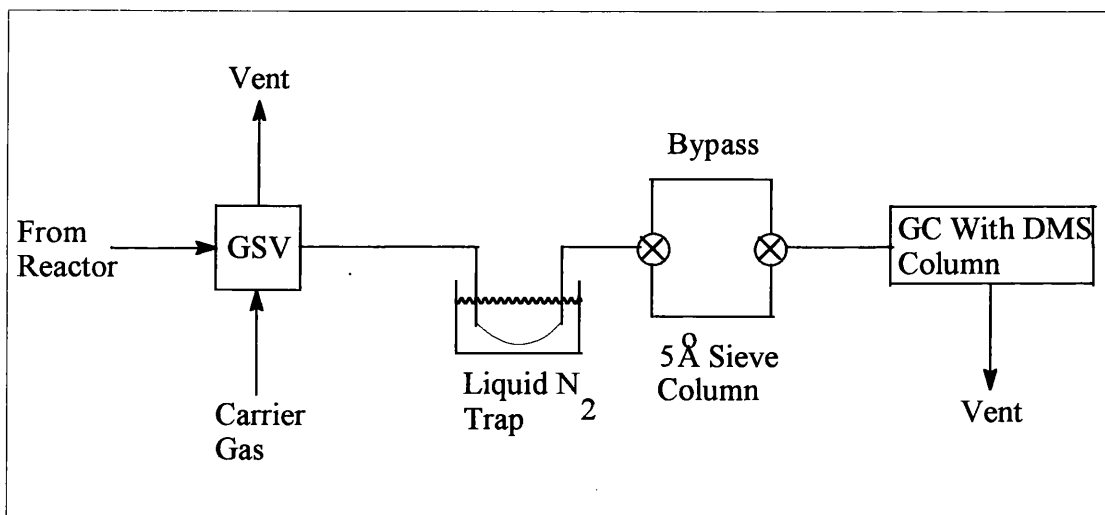


**Fig. 2.1.4** Schematic Diagram of the Chromatographic Analysis System.

The system operates in the following manner. Firstly, a sample of the effluent from the reactor is injected into the system via the six-way gas sample valve. The sample then passes through the trap, which is filled with liquid nitrogen, withholding all products with the exception of methane, oxygen and carbon monoxide. These three gases are then directed through the 5A molecular sieve, separated, and their amounts

measured. Once these have eluted completely from the column the remaining products are expelled from the trap by heating with a hot air gun. These are directed across the bypass and straight into the GC which houses the 33% DMS on Chromsorb-p column which separates these into their individual components. The separations are shown on figure 2.1.5 and retention times are listed on table 2.1.2. The same procedure was used in the pulse-flow experiments with the only difference being that the GC was on-line, straight from the reactor, and therefore the six-way gas sample valve was not required.

Unfortunately, the signals for carbon dioxide and propane have similar retention times and therefore judgment has been used in certain areas, where appropriate, to identify which species has been detected.

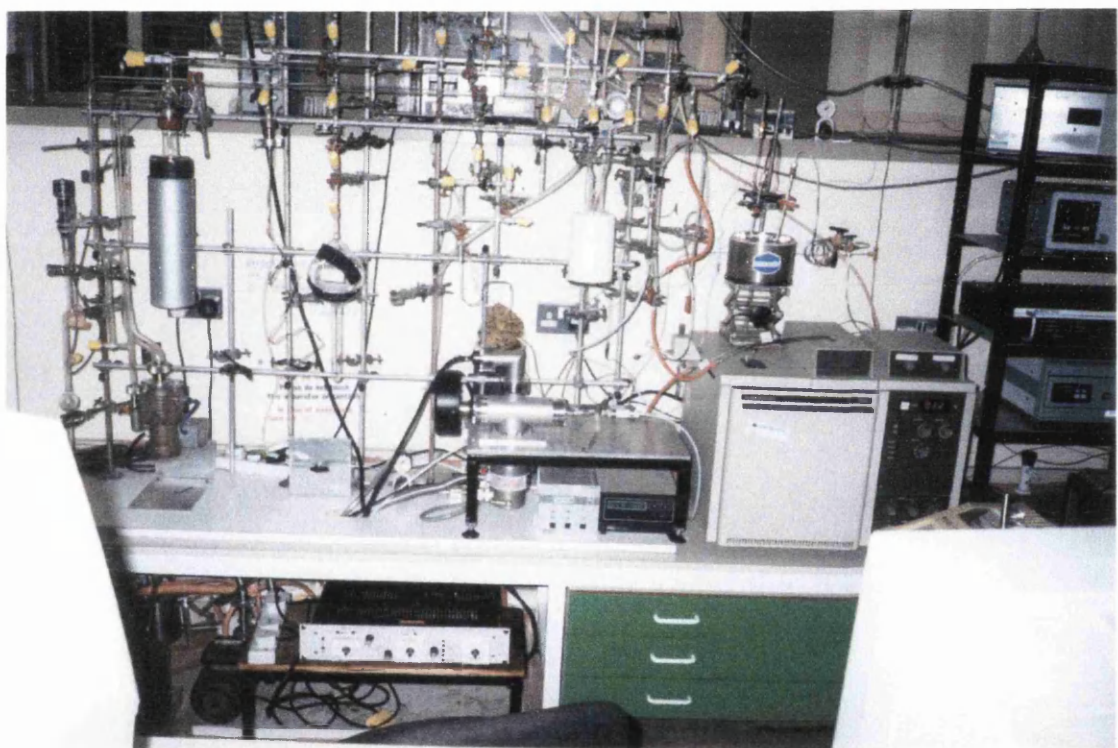


**Photo. 3**      The GC and MS sections.

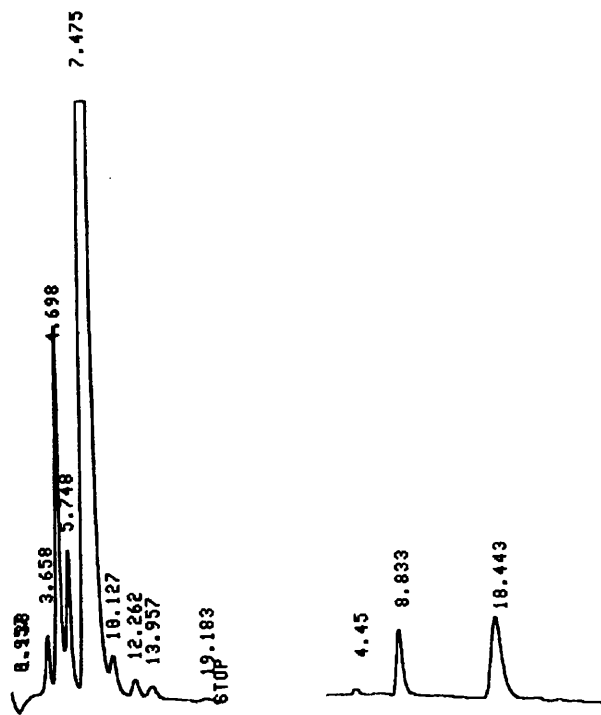


**Fig. 2.1.5** An Example GC Trace showing all the Reaction Products.

**Table 2.1.2** The Retention Times of all the Reaction Products.

Compound	Retention Time (mins)
Oxygen	4.45
Methane	8.833
Carbon Monoxide	18.443
Ethane	3.658
CO <sub>2</sub> /Propane	4.698
iso-Butane	5.748
n-Butane	7.475
But-1-ene	10.127
trans But-2-ene	12.262
cis But-2-ene	13.957
1,3-Butadiene	19.183

### 2.1.5 The Infrared Spectrophotometer (IRS)

The IRS is an important tool in catalysis, finding its role in characterisation and *in situ* reaction testing, leading to mechanism elucidation. Within the characterisation and testing facility under discussion, the Nicolet Magna 550 with an auxiliary experiment module has been arranged with suitable cells and plumbing to allow Transmission (TIR) and Diffuse Reflectance (DRIFTS) techniques to be carried out. Figures 2.1.6 show the configurations for both these techniques. The environmental cell can either be the TIR (shown on photograph 4) cell or the DRIFTS cell, both of which are temperature controlled.

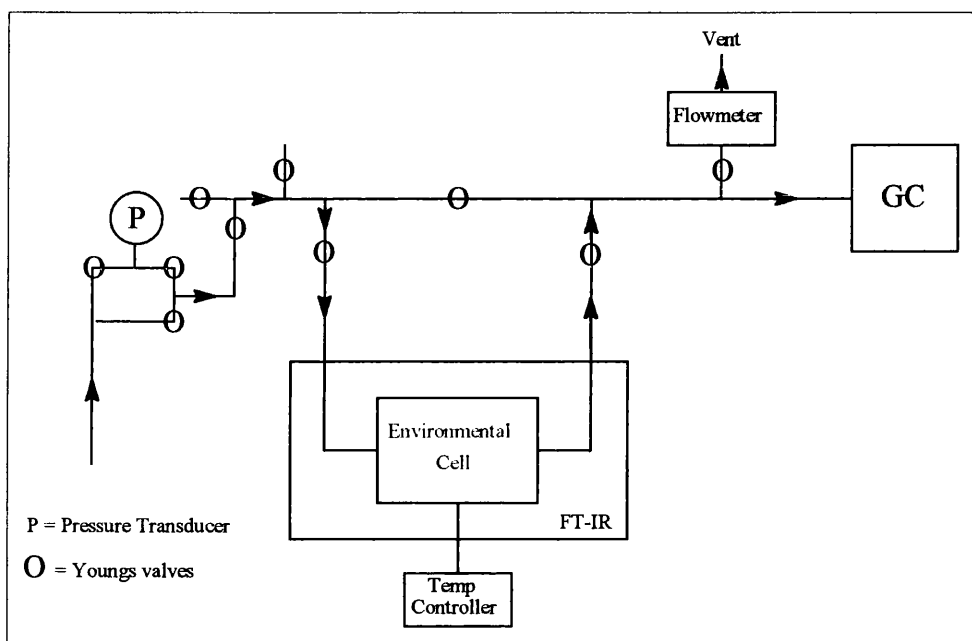


**Fig. 2.1.6** Schematic Diagram of *In Situ* IRS System

*In Situ* measurements can be carried out by connecting the inlet and outlet pipes from the two cells to the main line, in place of the conventional quartz micro reactor. The connections are made using Young's ball and socket joints which are connected via Kovar glass to metal seals to stainless steel tubing, which is then connected to the cells via the appropriate Swagelok fittings.

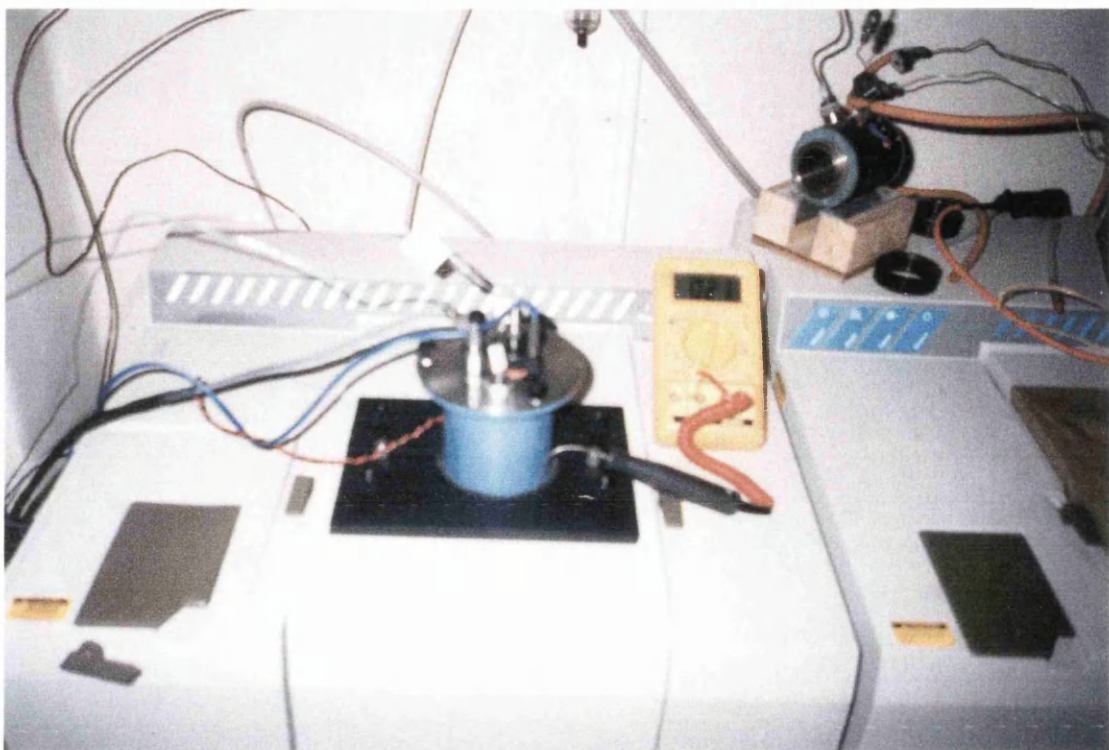


**Photo. 4**      The Transmission Infrared Environmental Cell.

### 2.1.6 The Mass Spectrometer (MS)

Like the IRS the MS is an extremely important tool in the discipline of heterogeneous catalysis. Its can be used very effectively as a tool to measure and detect effluent species exiting the exhaust during reaction testing, providing activity and selectivity data. In this project, however, its main function has been in characterisation, utilising the technique of Temperature Programmed Desorption (TPD) and post reaction analysis in the form of Temperature Programmed Oxidation (TPO). The main asset of the MS for these techniques is its ability to record data as a function of time and temperature. The MS used during this work was a Leda Mass Quadrapole spectrometer.

Four main components make up a quadrupole mass spectrometer. These are the gas inlet, the ion source, the quadrupoles and the detector. After the sample gas passes through the gas inlet it is ionised by interacting with an electron beam produced by heating two filaments either side of the ion source. The quadrapole consists of four parallel metal rods of circular cross-section through which a combination of DC and

RF voltages are passed. If balanced correctly a potential ‘valley’ is produced through which the positively charged ion pass towards the detector. The detector can either be the Faraday Cup or the Secondary Electron Multiplier depending on the signal to noise requirements. During this project the Faraday Cup type detector was used.

The sampling system used in this apparatus involved reducing the pressure of the sample gas from atmospheric to less than approximately  $1 \times 10^{-6}$  torr. This was achieved using both capillary tubing and various vacuum pumps. The gas was introduced to the MS system via a one metre length of capillary tubing at atmospheric pressure. In combination with a rotary pump attached to the inlet side of the main chamber, the pressure was reduced to approximately  $1 \times 10^{-3}$  torr. The remaining sample gas was then introduced to the main MS chamber through a small orifice on a platinum disc. The pressure in the chamber was then held below  $1 \times 10^{-6}$  torr using a turbo pump backed by another rotary pump. Figure 2.1.7 schematically represents the apparatus while photograph 3 shows the configuration of the equipment with respect to the overall facility.

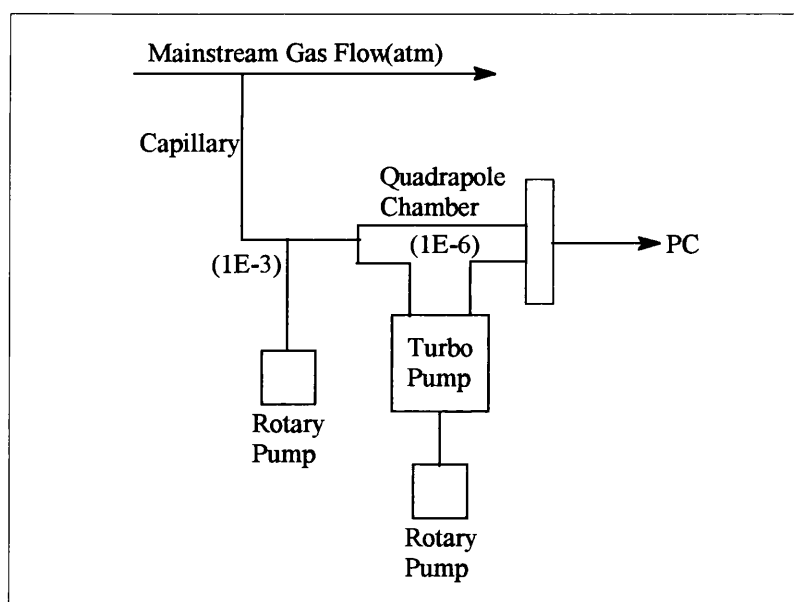


**Fig. 2.1.7** Schematic Representation of MS System.

## *Chapter 3*

### Materials

### **3.1      Catalysts Used**

The catalysts used during this study were not prepared in house. Instead they were supplied as extrudates from ICI Synetex and Johnson Matthey. Table 3.1.1 lists the catalysts together with the metal content as measured by atomic absorption and the place of origin. From extrudate form, the catalysts were ground using a mortar and pestle and sieved to a grain size of 250-500 $\mu\text{m}$ , at which particle size distribution reaction testing was carried out. A broad distribution of catalyst particles could lead to varying pressure gradients across the bed which would affect reactant residence times. Adopting a specific range of catalyst grain sizes ensures homogeneous residence times throughout the catalyst bed. Due to the non-uniformity of metal distribution throughout the ICI sample it was necessary to grind the pellet up until fines were obtained. Using an infrared press and dye assembly the fines were compressed into a disc before grinding and sieving to 250-500 $\mu\text{m}$ . It was found that more uniform grains and thus more reproducible tests and characterisation results were obtained using this method.

**Table 3.1.1    The Catalysts used and their Metal Content.**

Catalyst	Metal Content from Atomic Absorption
Pt/Al <sub>2</sub> O <sub>3</sub> (JM)	0.5%
Pt/Al <sub>2</sub> O <sub>3</sub> (ICI)	0.65%

#### **3.1.1    Catalyst Preparation**

##### **3.1.1.1 Pt/Al<sub>2</sub>O<sub>3</sub> (JM code-64268, batch-97099)**

This catalyst was prepared and supplied by Johnson Matthey as part of the EPSRC Innovative Manufacturing Initiative (IMI). It is meant to represent a generic 0.5% Pt/Al<sub>2</sub>O<sub>3</sub> ( $\gamma$ -Al<sub>2</sub>O<sub>3</sub>) catalyst. No information is available on the precise method of preparation.

### 3.1.1.2 Pt/Al<sub>2</sub>O<sub>3</sub> (ICI - P5211)

A known weight (1000g) of  $\gamma$ -alumina was placed in a pascall rotatory tumbler and H<sub>2</sub>PtCl<sub>6</sub> (21g), dissolved in de-ionised water (1000ml), was added. The container was purged with nitrogen and a water vacuum pump connected. The [PtCl<sub>6</sub>]<sup>2-</sup>/ $\gamma$ -alumina was dried in a rotatory vacuum at room temperature for 2 days and in an oven at 313K for 16 hours and calcined at 823K for 3 hours. The preparation and characterisation of this catalyst is described elsewhere [87].

### 3.1.2 Choice of Support Material

Support materials used in heterogeneous catalysis provide many advantages and have various roles. In general they provide a means of dispersing the metal, such as Pt, for its most effective and cost effective use, or as a means of improving the mechanical strength of an inherently weak catalyst. They can, however, be involved in the reaction chemistry which takes place, *e.g.* under the appropriate conditions the acidic sites on alumina can induce cracking reactions [70, 76] or be involved in isomerisation processes [70, 72].

In platinum based catalyst the main properties of the support that determine the catalytic behaviour are the following:

- (a) surface acidity;
- (b) stability during reaction and regeneration and stabilisation of the metal dispersion during all the stages of catalyst treatment;
- (c) chemical interaction with promoters;
- (d) pore-size distribution.

Alumina was chosen for this project as it is representative of catalysts used in this environment in industry, as it is ‘tough’ - *i.e.* can tolerate high temperatures and resist sintering. It is known that additives can be used to suppress acidity and increase further resistance towards sintering. ZnAl<sub>2</sub>O<sub>4</sub> and MgAl<sub>2</sub>O<sub>4</sub> are slightly basic or neutral and do not need any alkali promoters. On the other hand, alumina-based catalyst require additional promoters such as Cs, Li and K in order to suppress the acidity [32]. The main role of the support is to stabilise the dispersion of the metal, especially during

coke burn-off, in the case of dehydrogenation. When silica is used sintering occurs during the oxidation treatment, whereas virtually no sintering is observed for platinum on alumina, and no sintering at all occurs for platinum supported over  $MgAl_2O_4$ , even after several regeneration cycles [35]. Nevertheless, additives were not used during this project as it was our wish to use a support that did not have additional contributions from the presence of additives, the concentration and effect of which could vary during the course of the reaction sequence.

### 3.2 *Gases Used*

Compatibility is a major concern when working with gas mixtures of hydrocarbons and air or oxygen as explosive limits exist within which ignition can occur. It is important to ensure that any mixture of these materials remains outwith either the lower explosive limit (LEL) or the upper explosive limit (UEL). Table 3.2.1 shows the explosive limits for propane and butane in air and in oxygen.

**Table 3.2.1** Explosive mixtures of propane and butane in air and oxygen [80].

Hydrocarbon	LEL (Air) %Vol.	UEL (Air) %Vol.	LEL (Oxygen) %Vol.	UEL (Oxygen) %Vol.
Propane	2.2	9.5	2.3	55
Butane	1.9	8.5	1.8	49

In oxidative dehydrogenation using oxide based catalysts it is necessary to work in an oxygen rich environment in order that the oxygen used during the reaction can be restored, thereby maintaining the oxide nature of the catalyst [81, 82]. It is obvious from this that safe mixtures in this regime must remain below the LEL. When using supported metal catalysts, however, it is important that just enough oxygen is used to remove the hydrogen produced (in the form of water) as a result of dehydrogenation, as an excess would result in the formation of an oxide layer similar to that of the pre-reduced catalyst which would result in a loss of activity or excessive combustion. As a consequence of this the oxidative dehydrogenation of butane is carried out in an oxygen lean environment. It has been shown by Schmidt *et al* [62]

that the best results were obtained using hydrocarbon:oxygen ratios of *e.g.* 2:1, 1:1 and 1:2. The stoichiometric ratio of hydrocarbon:oxygen in this reaction is 2:1, as shown by equation 1, and was used as a starting point for this work.



Figure 3.2.1 and 3.2.2 show the plots of propane and butane mixtures with oxygen as a function of inert diluent added, respectively. The blue line illustrates the border inside which the composition is potentially explosive, the black dotted line is the zero oxygen line and the full black line indicates the percentage when the ratio of air is used. The oxygen content at any position can be determined using the equation shown on the graph [80].

It was discussed previously that a set mixture of oxygen and inert gas (in this case helium) was obtained ( $\text{He}:\text{O}_2 = 7:1$ , BOC) and used to ensure control of the hydrocarbon:oxygen ratio over a range of flow-rates while keeping outwith the explosive area. The full red line on the butane plot indicates a mixture of oxygen:helium in a 1:7 ratio while the dotted red line indicates an oxygen:helium ratio of 1:1. Tables 3.2.2 and 3.2.3 contain the figures used to construct these lines.

In order to derive an oxygen:helium ratio of 1:7, it was necessary to draw a line at a tangent to the explosive region with the gradient equal to that of the zero oxygen line. This is called the minimum constant oxidant line [80] which corresponds to the minimum oxidant concentration needed to support combustion of a particular combustible material at a specified temperature and pressure. The oxygen:helium ratio of 1:7 is the closest mixture composition to this line allowing the favourable hydrocarbon:oxygen ratios to be obtained without ever entering into the explosive region. It was therefore decided that this would be the ideal composition to use. The importance of the choice of oxygen:helium ratio can be illustrated by looking at the 1:1 composition (dotted red line on figure 3.2.2). In this case there is less flexibility with respect to lower hydrocarbon:oxygen ratios. As the ratio is decreased it can be observed that the line falls into the explosive area, therefore placing a restriction on the mixtures that can be used safely. The effects of pressure and temperature have also been considered but these have a minimal contribution.

With the set oxygen:helium ratio of 1:7 it is possible to control the reaction conditions in terms of contact time and hydrocarbon:oxygen ratio. As shown by previous workers [62] it is important, with regard to selectivity, to minimise the contact times of the reactants through the catalyst bed. This can be done by increasing the helium flow-rate (from the helium only cylinder, see figure 2.1.2) which has no effect on the overall hydrocarbon:oxygen ratio. It is clear from figure 3.2.2 (full red line) that there is no risk of falling inside the explosive range as a result of this action. It is also important that there is some degree of flexibility within the system in terms of hydrocarbon:oxygen ratio. Lower ratios can be obtained simply by increasing the amount of diluent (from the helium only cylinder) while decreasing the amount of hydrocarbon thus maintaining constant flow-rates (see table 3.2.2). It is also possible to access much higher ratios by increasing the amount of hydrocarbon while decreasing the amount of the helium:oxygen mixture used. This procedure ensures that there is no danger of entering into the explosive region.

**Table 3.2.2** Figures used to construct the 1:7 line.

Amount of Hydrocarbon (%)	He:O <sub>2</sub> Mixture		Extra He (%)	Hydrocarbon:O <sub>2</sub> Ratio
	He(%)	O(%)		
20	70	10	0	2 : 1
10	70	10	10	1 : 1
5	70	10	15	1 : 2

**Table 3.2.3** Figures used to construct the 1:1 line.

Amount of Hydrocarbon (%)	He:O <sub>2</sub> Mixture		Extra He (%)	Hydrocarbon:O <sub>2</sub> Ratio
	He(%)	O(%)		
50	25	25	0	2 : 1
40	25	25	10	8 : 5
25	25	25	25	1 : 1

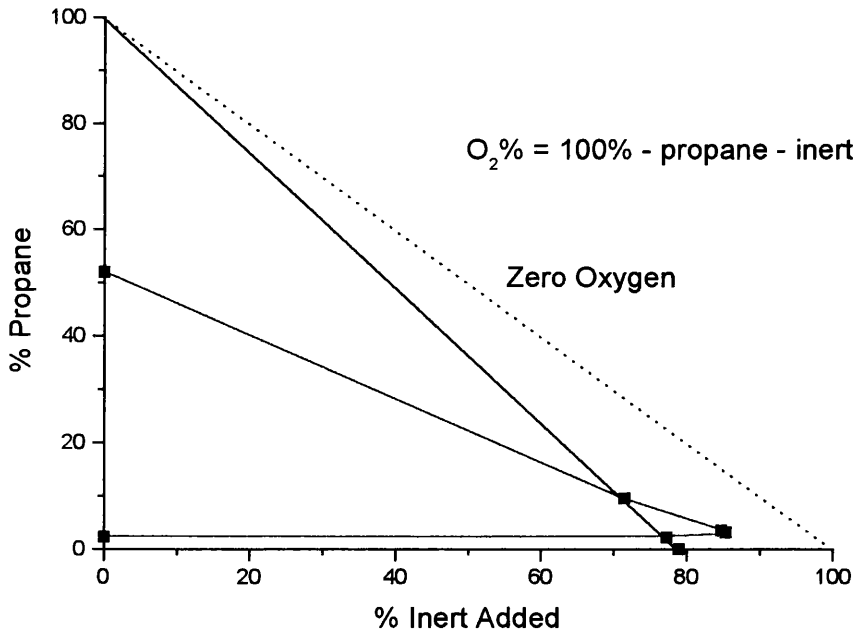


**Fig. 3.2.1** The explosion limits for mixtures of propane and oxygen as a function of inert diluent.

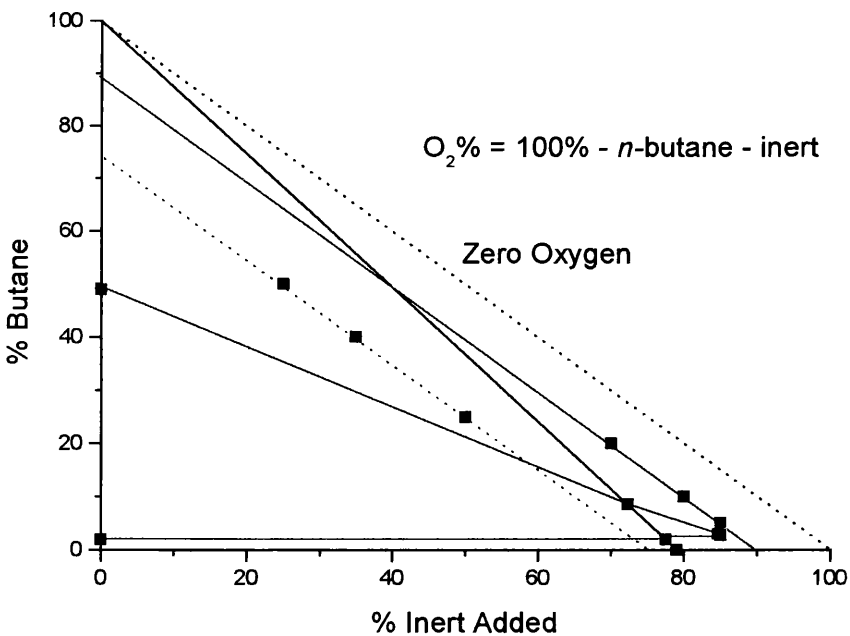


**Fig. 3.2.2** The explosion limits for mixtures of butane and oxygen as a function of inert diluent.

### 3.3 Abbreviations used throughout this Thesis

Various abbreviations have been used throughout the results and discussion section. These abbreviations are listed on table 3.3.1.

**Table 3.3.1** The Abbreviations used throughout the Results and Discussion section.

Full Word	Abbreviation
Temperature	Temp.
Minutes	Mins.
Conversion	Conv.
Selectivity	Sel.
Propane	Pr.
Methane	Met.
Ethane	Eth.
Iso Butane	Iso.
But-1-ene	B-1
Trans But-2-ene	Trans B-2
Cis But-2-ene	Cis B-2
1,3-Butadiene	Diene
Dehydrogenation	Dehydro.
Equilibrium	Eq.

$$\text{Weight Hourly Space Velocity (WHSV)}[\text{ref}] = \frac{\text{weight of butane (g per hour)}}{\text{weight of catalyst (g)}} \quad \text{eq. 3.2}$$

$$\text{Gas Hourly Space Velocity (GHSV)}[\text{ref}] = \frac{\text{flow - rate of butane (ml per hour)}}{\text{volume of catalyst (ml)}} \quad \text{eq. 3.3}$$

*Chapter 4*

**Experimental**

This chapter details how the experiments were performed that generated the results described in chapter 5. The operational modes of continuous-flow and pulse-flow are described, while the actual reaction parameters for each specific reaction are listed in tabular form. The characterisation techniques used to gather information on the catalyst are also described, as well as the calculations used to convert the collected data into more conventional plots. Details such as preparation of the catalyst and filling of glass bulbs with reactant mixtures are also described.

#### **4.1     *Continuous-flow Experiments***

##### **4.1.1   Catalyst Preparation**

The catalysts were received as extrudates and were prepared according to the processes described in chapter 3. Before use it was necessary to crush the pellets and sieve to a grain size of 250-500 $\mu\text{m}$  in order to prevent the build-up of back-pressure behind the catalyst bed. This grain size resulted in the catalyst density of  $\rho=1.24\text{ml g}^{-1}$ . It was found with the ICI supplied catalyst extrudates (0.65% Pt/Al<sub>2</sub>O<sub>3</sub>) that only the outside of the pellet was coated with catalyst (shell catalyst) and so preparation by the above method resulted in a mixture of grains, some densely populated with platinum metal and some consisting totally of support material. In order to overcome this and ensure a more homogeneous distribution of the metal throughout the catalyst bed, the pellets were firstly crushed into a fine powder. This was then followed by compression in 15mm diameter dye assembly (as used in infrared spectroscopy) at a pressure of 10 tons for 5 minutes, forming a disc, which was then crushed to the grain size mentioned above. The appropriate amount of catalyst was then weighed out and placed into the reactor described in section 2.1.3.

##### **4.1.2   Catalyst Reduction**

Before carrying out any of the catalyst studies (except temperature programmed reduction (TPR)) the catalyst required activation in the reactor mentioned above. To achieve this the required sample was placed onto the sinter in the reactor vessel and

treated with 6% hydrogen in nitrogen balance at  $30\text{ml min}^{-1}$ . The temperature of the reactor bed was increased to  $300^\circ\text{C}$  at  $5^\circ\text{C min}^{-1}$ , using a Eurotherm temperature programmer, and held isothermally at this temperature for a period of 180 mins. After this period, the gas was switched to helium for 120 mins maintaining the temperature above. At this point the catalyst bed was allowed to cool to ambient temperature before subsequent use.

If the sample had been left to cool in a hydrogen flow there would have been a possibility of dissociative chemisorption of the hydrogen molecules on the platinum surface resulting in blockage of the sites required for the subsequent reactions. As mentioned above the temperature was controlled using a Eurotherm temperature programmer, however, the temperature of the catalyst bed was also monitored using a separate chromel/alumel thermocouple positioned in the thermocouple pocket as shown on the schematic diagram of the reactor vessel, figure 2.1.3 in section 2.1.3. The gas flow-rate was monitored using a bubble flow-meter attached to the effluent gas stream and could be adjusted using a Whitey needle valve.

#### 4.1.3 Continuous-flow Procedure

Straight and oxidative dehydrogenation of *n*-butane was carried out under continuous-flow conditions enabling steady-state data to be obtained. A variety of different reaction conditions were used in order to attempt to optimise the process and observe any changes that might provide evidence towards an explanation of the results. With both catalysts the effect of temperature and flow-rate was determined for the straight and oxidative dehydrogenation ( $\text{H}_c:\text{O}_2$  ratio of 2:1). The effect of the  $\text{H}_c:\text{O}_2$  ratio and the depth of the catalyst bed were also studied in addition to the above for the 0.65% Pt/ $\text{Al}_2\text{O}_3$  catalyst.

After catalyst reduction, as described in section 4.1.2, the reactor was isolated under an atmosphere of helium (approximately 1atm above atmospheric pressure). At this point the temperature of the catalyst bed was increased from room temperature to the reaction temperature using the Eurotherm temperature programmer mentioned previously, at a ramp rate of  $5^\circ\text{C min}^{-1}$ . Simultaneously, the feed-gas composition was prepared using the gas mixing arrangement described in section 2.1.1. When the gas flows and reaction temperature were stable the bypass was closed and the reactor

opened allowing the reactant gas mixture to flow over the catalyst bed. The initial sample was taken after 30 seconds, allowing the product effluent to completely pass through the system, filling the 0.5ml six-way sample loop, before leaving the system through the vent. Subsequent samples were taken at intervals determined by the analysis time, which amounted to approximately 20mins for the straight dehydrogenation and 38mins minutes for the oxidative dehydrogenation reactions, the latter requiring a two stage separation process, as described in section 2.1.4. Parameters such as temperature, total linear velocity and individual linear velocities of the reactant components, gas hourly space velocity (GHSV), weight hourly space velocity with respect to butane (WHSV), sample weights and H<sub>c</sub>:O<sub>2</sub> ratio for each reaction carried out are listed in tables 4.1.1-4.1.5, for both catalysts used. Empty vessel reactions and those using the support material only were carried out in a similar fashion to those in the tables mentioned above, except that no catalyst was used and support material only (250mg) was used, respectively. These experiments were conducted to distinguish homogeneous gas-phase reactions and reactions taking place on the support from those taking place on the metal surface.

It was decided to keep the WHSV with respect to butane constant where possible to enable meaningful comparisons between the various reactions carried out in terms of carbon exposure. This value was changed only during varied weight and H<sub>c</sub>:O<sub>2</sub> ratio experiments. The GHSV was varied in the reactions where the linear velocity was changed in order to change the contact time. The samples were retained after reactor cooling for post-reaction analysis.

The areas obtained on the GC from the products detected during reaction testing were converted to molar quantities as described in section 4.2.3. This enabled conversion, product selectivity and yield data to be determined allowing the performance of the catalyst during a specific reaction to be assessed. The definitions for the terms above are given by the following equations [83]. The other terms used in the results and discussion section, dehydrogenation selectivity and dehydrogenation yield, are found by addition of the values of but-1-ene, *trans* but-2-ene, *cis* but-2-ene and 1,3-butadiene selectivity and yield, respectively.

$$\text{Conversion(%)} = \frac{\text{No. of Moles Butane In} - \text{No. of Moles Butane Out}}{\text{No. of Moles Butane In}} \times 100 \quad \text{eq. 4.1}$$

**Table 4.1.1 Reaction Conditions for Straight Dehydrogenation as a function of Temperature and Flow-rate.**

Temperature (°C)	Sample Weight (mg)	Helium Linear Velocity (ml min <sup>-1</sup> )	Butane Linear Velocity (ml min <sup>-1</sup> )	Total Linear Velocity (ml min <sup>-1</sup> )	GHSV (hr <sup>-1</sup> )	WHSV (g <sub>out</sub> g <sub>cat</sub> <sup>-1</sup> hr <sup>-1</sup> )
200	250	40	10	50	9677.4	6.2
300	250	40	10	50	9677.4	6.2
400	250	40	10	50	9677.4	6.2
500	250	40	10	50	9677.4	6.2
600	250	40	10	50	9677.4	6.2
700	250	40	10	50	9677.4	6.2
400/500	250	20	10	30	5806.4	6.2
400/500	250	40	10	50	9.677.4	6.2
400/500	250	90	10	100	19354.8	6.2
400/500	250	120	10	130	25161.3	6.2

**Table 4.1.2** Reaction Conditions for Oxidative Dehydrogenation as a function of Temperature and Flow-rate.

Temperature (°C)	Sample Weight (mg)	H <sub>c</sub> :O <sub>2</sub> Ratio	Helium Linear Velocity (ml min <sup>-1</sup> )	Butane Linear		GHSV (hr <sup>-1</sup> ) (g <sub>but</sub> g <sub>cat</sub> <sup>-1</sup> hr <sup>-1</sup> )
				Oxygen Linear Velocity (ml min <sup>-1</sup> )	Total Linear Velocity (ml min <sup>-1</sup> )	
200	250	2:1	35	10	5	50
300	250	2:1	35	10	5	50
400	250	2:1	35	10	5	50
500	250	2:1	35	10	5	50
600	250	2:1	35	10	5	50
400/500	250	2:1	35	10	5	50
400/500	250	2:1	85	10	5	100
400/500	250	2:1	115	10	5	130
						9677.4
						9677.4
						9677.4
						9677.4
						19354.8
						25161.3
						6.2
						6.2
						6.2
						6.2

**Table 4.1.3** Reaction Conditions for Straight Dehydrogenation as a function of Catalyst Mass for the 0.65% Pt/Al<sub>2</sub>O<sub>3</sub>.

Temperature (°C)	Sample Weight (mg)	Helium Linear Velocity (ml min <sup>-1</sup> )	Butane Linear Velocity (ml min <sup>-1</sup> )	Total Linear Velocity (ml min <sup>-1</sup> )	GHSV (hr <sup>-1</sup> )	WHSV (g <sub>but</sub> g <sub>cat</sub> <sup>-1</sup> hr <sup>-1</sup> )
400	250	40	10	50	9677.4	6.2
400	375	40	10	50	6451.6	4.1
400	753	40	10	50	3213.0	2.1

**Table 4.1.4** Reaction Conditions for Oxidative Dehydrogenation as a function of Catalyst Mass for the 0.65% Pt/Al<sub>2</sub>O<sub>3</sub> Catalyst.

Temperature (°C)	Sample Weight (mg)	H <sub>c</sub> :O <sub>2</sub> Ratio	Helium Linear Velocity (ml min <sup>-1</sup> )	Butane Linear Velocity (ml min <sup>-1</sup> )	Oxygen Linear Velocity (ml min <sup>-1</sup> )	Total Linear Velocity (ml min <sup>-1</sup> )	GHSV (hr <sup>-1</sup> )	WHSV (g <sub>but</sub> g <sub>cat</sub> <sup>-1</sup> hr <sup>-1</sup> )
400	250	2:1	35	10	5	50	9677.4	6.2
400	375	2:1	35	10	5	50	6451.6	4.1
400	752	2:1	35	10	5	50	3217.2	2.1

**Table 4.1.5** Reaction Conditions for Oxidative Dehydrogenation as a function of H<sub>c</sub>:O<sub>2</sub> Ratio for the 0.65% Pt/Al<sub>2</sub>O<sub>3</sub> Catalyst.

Temperature (°C)	Sample Weight (mg)	H <sub>c</sub> :O <sub>2</sub> Ratio	Helium Linear Velocity (ml min <sup>-1</sup> )	Butane Linear Velocity (ml min <sup>-1</sup> )	Oxygen Linear Velocity (ml min <sup>-1</sup> )	Total Linear Velocity (ml min <sup>-1</sup> )	GHSV (hr <sup>-1</sup> )	WHSV (g <sub>but</sub> g <sub>cat</sub> hr <sup>-1</sup> )
400	250	25:1	39.6	10	0.4	50	9677.4	6.2
400	250	13.3:1	39.25	10	0.75	50	9677.4	6.2
400	250	4:1	37.5	10	2.5	50	9677.4	6.2
400	250	2:1	35	10	5	50	9677.4	6.2
400	250	1:1	40	5	5	50	9677.4	3.1
400	250	1:2	42.5	2.5	5	50	9677.4	1.6

$$\text{Product Selectivity}(\%) = \frac{\text{No. of Moles of Specific Product}}{\text{No. of Moles Butane In} - \text{No. of Moles Butane Out}} \times 100$$

eq. 4.2

$$\text{Yield}(\%) = \frac{(\text{Conversion}(\%)) \times (\text{Product Selectivity}(\%))}{100}$$

eq. 4.3

In some plots the average value of conversion, selectivity and yield are plotted against another variable, such as temperature. Equation 4.4 describes how the mean was obtained, using conversion as an example, where n is the number of points at steady state during a reaction [84].

$$\text{Mean Conversion at Steady State} = \frac{\sum_{i=1}^n \text{Conversion}_{(i)}}{n}$$

eq. 4.4

As well as the mean value, error bars were also included so that the accuracy and reproducibility of the steady state measurements could be evaluated. The error bars represent the standard deviation of the mean value. The equation used to calculate these values is shown below, again using conversion as an example [84].

$$\text{Standard Deviation of the Mean Conversion} = \sqrt{\frac{\sum_{i=1}^n (\text{Conversion}_{(i)} - \text{mean})^2}{n}}$$

eq. 4.5

## 4.2 Pulse-flow Experiments

### 4.2.1 Pulse-flow Procedure

Before embarking on the pulse-flow experiments, the catalyst required reduction for the same reasons as before with the continuous-flow. This was done in an identical manner to that described above in section 4.1.2. The grain size of the catalysts was also the same as above, *i.e.* 250-500μm. Pulse-flow is very different to continuous-

flow in that it is a non-steady state experiment where controlled amounts of the reactants are pulsed over the catalyst bed using an inert carrier gas, whereas in continuous-flow the reactant gases are constantly flowing over the catalyst bed in the pre-set composition. However, these two techniques can be complimentary when used in the same study with pulse-flow allowing the approach to steady state to be observed, thus providing important information on how the catalyst behaves during this period, with continuous-flow leading directly to the steady-state conditions. All of which is carried out in the same reactor and apparatus.

The reactions carried out during this work all used 250mg of the 0.65% Pt/Al<sub>2</sub>O<sub>3</sub> catalyst. After reduction the catalyst bed was left under flowing helium (carrier gas) at 50ml min<sup>-1</sup>, while the catalyst bed temperature was increased to 400°C. Upon reaching reaction temperature, the catalyst was ready for pulses of the reactant mixture. Three types of reaction were carried out: (i) straight dehydrogenation, where only *n*-butane pulses were used; (ii) co-adsorption studies, where gas mixtures consisting of *n*-butane and oxygen in a pre-prepared mixture (see below) were pulsed over the catalyst; and (iii) sequential studies where oxygen and *n*-butane were sequentially pulsed over the catalyst bed from separate bulbs. Table 4.2.1 lists the concentrations of reactants used in these reactions. Again analysis was carried out using the two stage chromatographic process described in section 2.1.4, except that the GC in this case was on-line and there was therefore no requirement for the six-way sample valve used in the continuous-flow experiments. In the sequential studies the oxygen pulse was always passed over the catalyst first, in an attempt to form the active oxygen species, as described in section 1.7, which would potentially enhance conversion and dehydrogenation selectivity. After this pulse the products were analysed. This was then followed by an *n*-butane pulse and again the products were analysed. This sequential pulsing procedure was continued until the end of the experiment.

The sample loop and the mechanism of pulsing is schematically represented on figure 4.2.1. The green arrows represents the configuration used when only helium carrier gas was flowing over the catalyst bed. The sample loop could be simultaneously prepared by evacuation and then filling with the desired amount of reactant. The blue arrows depicts the direction of flow when a pulse of reactant gases is injected over the

**Table 4.2.1** The Reactants and there Concentrations used during the Pulse-flow experiments.

Reaction	H <sub>2</sub> :O <sub>2</sub> Ratio	n-Butane Pressure (torr)	Oxygen Pressure (torr)	Total Pulse Pressure (torr)
Straight Dehydrogenation	-	100	-	-
Un-reduced	-	100	-	100
Co-Adsorbed	20:1	100	5	105
Co-Adsorbed	2:1	100	50	150
Sequential Adsorption	20:1	100	5	No mixture used
Sequential Adsorption	2:1	100	50	No mixture used

catalyst bed and on towards the GC for analysis. Figure 2.1.1 in section 2.1 shows the location of the sample loop with respect to the rest of the testing facility.

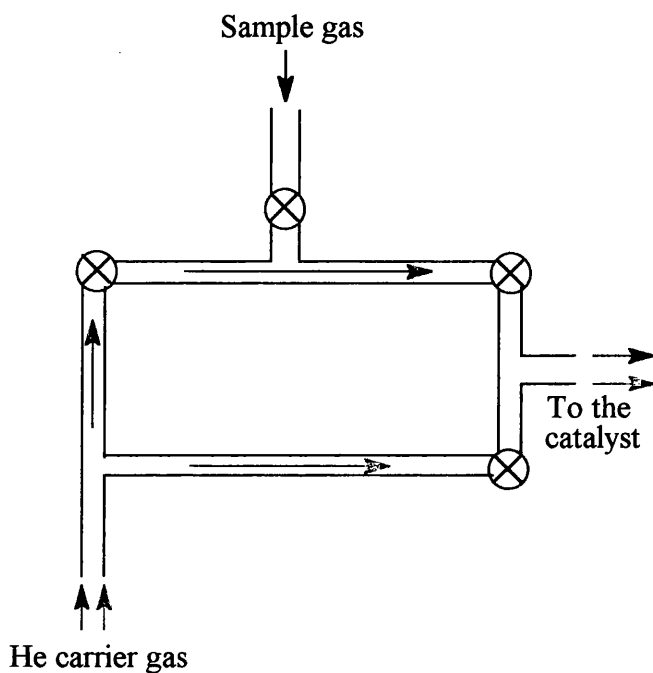


**Fig. 4.2.1** Schematic diagram of the Sample Loop used in Pulse-flow experiments.

The desired amount of reactant gases admitted to the sample loop for pulsing can be calculated using the ideal gas equation (equation 4.6), where n is the number of moles of gas, P is the pressure in the sample loop, V is the volume of the sample loop (in this case 5.0ml), R is the gas constant and T is the temperature. Pulse-flow thus allows precise control of the number of reactant molecules exposed to the catalyst surface. A similar technique using the sample loop and equation 4.6 was adopted for the GC calibrations. This is described in more detail below in section 4.2.3.

$$PV = nRT \quad \text{eq. 4.6}$$

A common feature of catalytic reactions using alkane reactants is the deactivation of the catalyst by the deposition of carbonaceous material. This carbonaceous material consists of a layer (or layers) of hydrocarbon fragments which

are adsorbed onto the surface of the active sites of the catalyst, therefore reducing the influence of the catalyst towards the reaction under study.

It is possible under pulse-flow conditions, to determine the amount of material retained by the catalyst. The following equation describes how this is carried out using carbon as the element of choice. The number of atoms in and out are determined using the GC.

$$\text{No. of Retained Carbon Atoms} = (\text{No. of Carbons In}) - (\text{No. of Carbons Out}) \quad \text{eq. 4.7}$$

As well as carbon, the mass balance calculation can also be applied to quantify the amount of hydrogen and oxygen retained by the catalyst, thus allowing any changes to the catalyst surface to be determined as a function of its exposure to the reactant materials. However, in this study, due to the formation of water, it was not possible to quantify accurately the amount of hydrogen and oxygen retained.

#### 4.2.2 Preparation of the Reaction Mixture Bulbs

The gas mixtures were prepared and handled using the vacuum line described in section 2.1.2. The position of the bulbs used to store the reactant gases and the gas inlet allowing the introduction of the various gases for bulb filling is shown on figure 2.1.3. Firstly, the bulbs were pumped down to the base vacuum of approximately  $1.5 \times 10^{-5}$  torr and heated with a hot air gun while pumping to remove any water from the surface of the glass.

In order to fill the bulbs, a gas cylinder was attached to the gas inlet mentioned above. The connection between the cylinder and the vacuum line was purged before admitting any gases to the bulbs, to ensure no contaminant air got into the gas mixture. Purging involved opening the cylinder three times with subsequent pumping. After this process the bulbs could be filled. The pressure admitted to the bulb was monitored using the MKS pressure transducers mentioned in section 2.1.2.

This method was suitable for filling bulbs with one gas. However, in order to carry out the experiments where *n*-butane and oxygen mixtures were used an additional process was required when filling the bulbs. Firstly, the required amount of *n*-butane was admitted to the bulb and then the bulb was closed off to the vacuum line.

At this point the vacuum manifold was pumped down to the base pressure and the gas inlet prepared for oxygen introduction. At the same time the *n*-butane in the bulb was frozen into a cold finger (built onto the base of the spherical bulb) which resulted in the vacuum in the bulb being restored. While maintaining the frozen *n*-butane (which took up a very small and insignificant volume in the bulb) the bulb was again opened to the manifold and pumped down to ensure maximum vacuum. At this point the desired amount of oxygen was introduced to the bulb and again isolated from the main manifold. After this was complete the *n*-butane was allowed to heat up and expand into the bulb together with the oxygen and therefore the mixture was produced.

Freezing of the *n*-butane (boiling point -0.5°C) was accomplished using a slush produced by adding liquid nitrogen to acetone which lowered the temperature to -94.6°C. Liquid nitrogen alone was not used as it has a boiling point of -195.8°C which would also result in the condensation of oxygen (boiling point -183.0°C), which is potentially explosive on exposure to organic material. The explosive limit plots were used to ensure that the mixtures of oxygen and *n*-butane remained outside the potentially explosive region.

#### 4.2.3 GC Calibration

In order to relate the areas of the peaks obtained on the gas chromatograms, resulting from the various reactions, to the number of moles of the various products produced, it was necessary to calibrate the GC with known quantities of all the possible products and starting materials. This was done using a pulse-flow technique similar to that used in the pulse-flow experiments. The retention times of each product were also determined during these calibrations allowing the products to be identified during reaction (see section 2.1.3). To do this, known amounts of each of the species were pulsed over the catalysts, as described above, producing a peak with a measured area. Equation 4.6 above was used to convert the pressures used to fill the sample loop to a number of moles, therefore allowing a plot of number of moles against area to be produced. Figure 4.2.3 shows an example of the type of plot obtainable, using *n*-butane as an example. Section 2.1.3 shows an example chromatogram with the retention times for all the products measured during an experiment.

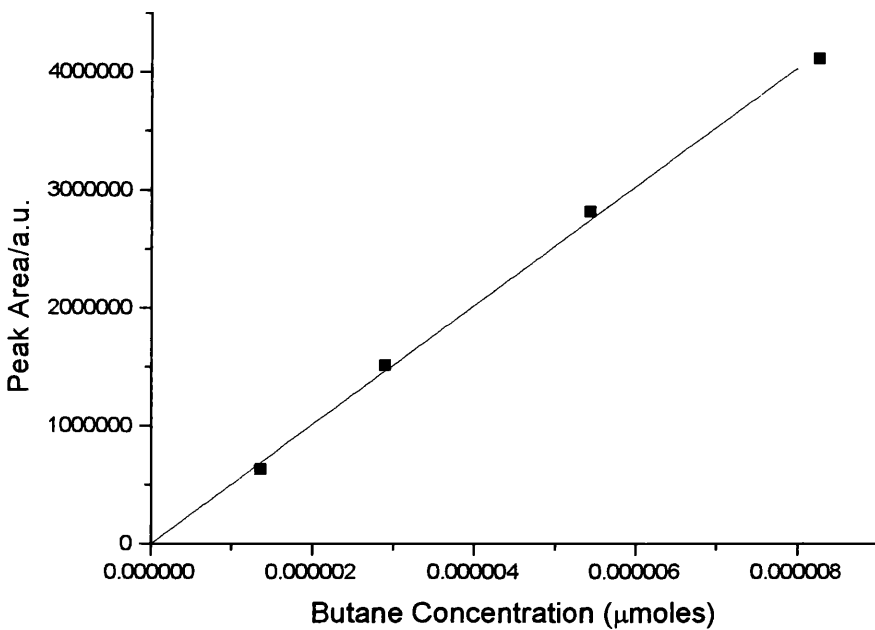


**Fig. 4.2.3** GC Calibration for *n*-Butane.

#### 4.3 Characterisation Techniques

##### 4.3.1 Temperature Programmed Reduction (TPR)

Before reduction, the metal component of a catalyst, such as Pt/ $\text{Al}_2\text{O}_3$ , exists as an oxide. When subjected to a programmed temperature rise and exposure to a reducing gas mixture, such as 6%  $\text{H}_2/\text{N}_2$ , the hydrogen is adsorbed as a function of the temperature-reactivity relationship of the oxidised species. The rate of reaction is continuously measured by monitoring the composition of the reducing gas at the outlet side of the reactor. TPR is a highly sensitive technique which does not depend on any specific property of the catalyst other than that the species under study is in a reducible condition.

The experiments were carried out in a closed system, with a flow through a fixed-bed reactor vessel similar to that used during the testing reactions (see figure 2.1.4). Approximately 250mg of catalyst with a grain-size of 250-500 $\mu\text{m}$  was used during these experiments. The reactant gas, 6% $\text{H}_2/\text{N}_2$ , was passed over the catalyst bed at 50ml  $\text{min}^{-1}$ , controlled by a Brooks mass-flow controller, at room temperature to

allow the thermal conductivity detector (TCD), which was used to detect the change in effluent gas composition, to stabilise. When this was complete the temperature was increased to 500°C at 5 and 10°C min<sup>-1</sup>. As the reduction temperature was approached the hydrogen in the feed-gas was taken up by the catalyst, reacting with the oxide layer to produce water, as well as other products, such as hydrochloric acid. This up-take was measured by the difference in thermal conductivity of the gas before and after reaction. The signal was measured by a Hewlett-Packard integrator coupled to the TCD. Initially the signal was measured against time, which was later correlated directly with temperature, which was increased linearly and controlled by a Eurotherm temperature controller.

A cold trap (dry ice/acetone) was incorporated after the reactor vessel and before the TCD to remove any reduction products from the gas stream which may have been harmful to the tungsten/rhodium filaments of the TCD.

#### 4.3.2 Volumetric Adsorption Isotherms

Volumetric adsorption isotherms are used in catalysis mainly as a technique to estimate the dispersion of the metal. The dispersion of a catalyst, such as Pt/Al<sub>2</sub>O<sub>3</sub>, is the ratio of the surface Pt to the total amount of platinum. The technique involves the gradual exposure of adsorbate molecules, such as carbon monoxide, to the catalyst, covering all the possible sites until no more sites are available. This point is called saturation. From the saturation curve produced, a value for the number of moles of gas adsorbed on the active metal surface can be obtained, thus the number of active metal sites available for adsorption can be calculated.

$$\% \text{ Dispersion} = \frac{\text{No. of Surface Metal Atoms}}{\text{Total No. of Metal Atoms}} \times 100 \quad \text{eq. 4.8}$$

In terms of conducting the experiments, figure 4.3.1 shows the section of the apparatus that was used. In a similar way to the testing reactions, the catalyst firstly required reduction to clean its surface of mainly oxygen, exposing all the possible reaction/adsorption sites on the metal. However, unlike in the testing reactions where the reduction was carried out under flowing conditions, these adsorption isotherms

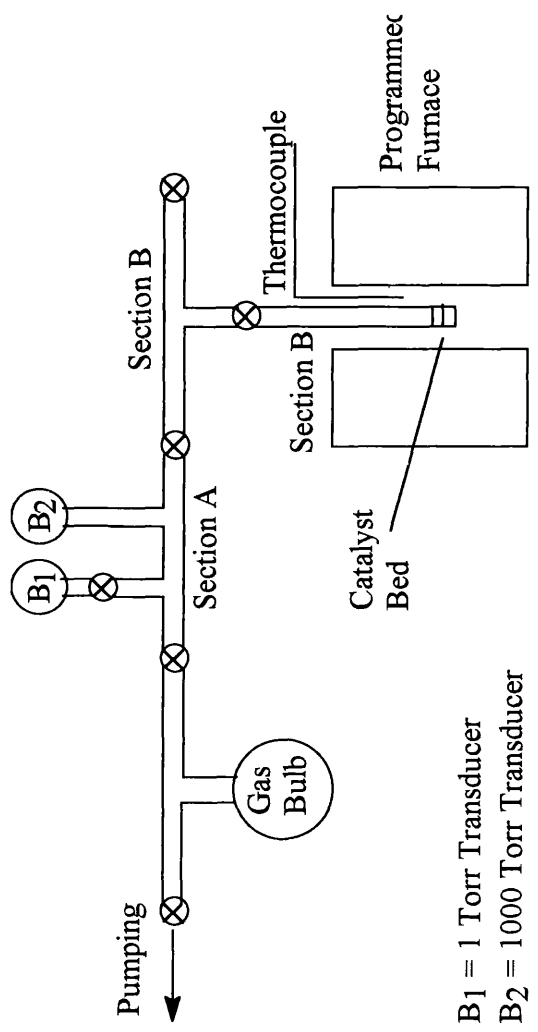


**Fig. 4.3.1** A Schematic Representation of the Apparatus used for the Adsorption Isotherm Measurements.

were conducted under static conditions and so a reduction procedure also under static conditions was developed.

To do this, approximately 200 mg of catalyst (the exact amount noted for each experiment) was deposited into the isotherm tube and attached to the vacuum line using a Youngs ball and socket connection, with a nupro 'O' ring making the vacuum tight seal. The sample was then degassed by pumping down to the base vacuum of approximately  $1.5 \times 10^{-5}$  torr. After this was complete, the temperature of the catalyst bed was increased at  $5^\circ\text{C min}^{-1}$  to  $350^\circ\text{C}$  for 60mins while maintaining pumping. At the end of this period the temperature was reduced to  $300^\circ\text{C}$  and the vacuum isolated. The catalyst was then exposed to 200 torr of high purity hydrogen and left for 60 mins, after which time the hydrogen was pumped away and then replenished with a fresh 200 torr batch. Again, this was left for a further 60 mins. After this period the hydrogen was again removed and the temperature increased to  $350^\circ\text{C}$  for 120 mins while pumping. This period ensured the removal of any materials adsorbed on the surface of the catalyst, leaving behind a bare metal surface ready for adsorption.

The following procedure was developed for the measurement of the volumetric adsorption isotherm. The notation corresponds to the labels on figure 4.3.1. After completion of the activation process the catalyst bed was allowed to cool to room temperature at which temperature the measurements were made. The vacuum manifold was then isolated from the vacuum pumps. The valve connecting section B and therefore the catalyst was also closed. Section A was then filled from the bulb with the required amount of adsorbate gas (in this case hydrogen or carbon monoxide) and then isolated. The pressure in this section was then recorded using the MKS transducers (both at the high (B2) and the low pressure (B1) ends). At this point section B was then opened to section A allowing exposure of the contents to the catalyst. When the pressure stabilised and the catalyst was at equilibrium, the pressure again (in section AB, which is the combined sections of A and B) was recorded. After this was accomplished section B was again isolated and section A filled with the required amount of adsorbate and the above procedure was repeated. This process was continued until the catalyst became saturated, *i.e.* the point at which the surface was covered with approximately one monolayer of adsorbate. The data obtained was in the form of equilibrium pressures of the adsorbate gas over the catalyst sample.

**Table 4.3.1** Equations used in the calculation of Adsorption Isotherms.

Equation	Use	Terms of Equation
$P_{AB} = \frac{1}{V_{AB}}(P_A V_A + P_B V_B)$	To determination the predicted equilibrium pressure.	$P_{A,B,AB}$ = pressure in section A, B and AB of apparatus. $V_{A,B,AB}$ = volume of section A, B, and AB of apparatus.
$Q_o = \frac{P_{AB} V_{AB}}{RT}$	To convert the predicted equilibrium pressure to number of moles in section AB of the apparatus.	$R$ = gas constant. $T$ = temperature (K). $Q_o$ = predicted number of moles in AB.
$Q_{diff} = Q_o - Q$	To determine the difference between predicted number of moles and measured number of moles in section AB ( <i>i.e.</i> number of moles adsorbed).	$Q_{diff}$ = number of moles adsorbed. $Q_o$ = predicted number of moles in section AB. $Q$ = measured number of moles in section AB.
$Total Q_{diff(i)} = Q_{diff(i)} + Q_{diff(i-1)}$	To determine the summed number of moles adsorbed after each individual dose.	Total $Q_{diff(i)}$ = summed number of moles adsorbed for dose $i$ . $i$ = dose number. $i-1$ = previous dose number.
$N_i = \frac{\text{Total } Q_{diff(i)}}{\text{weight of catalyst}}$	To determine the summed number of moles adsorbed per gram of catalyst for each individual dose.	$N_i$ = summed number of moles adsorbed as a function of catalyst weight for dose $i$ .

Equilibrium pressures were converted to the parameters in equation 4.8. The method of calculation applies Boyle's law and is based on the difference between the theoretical value for the equilibrium pressure and the actual observed value. Table 4.3.1 contains the equations needed and a description of their use in the calculation. Again the notation refers to figure 4.3.1.

The resultant adsorption isotherm consists of a plot of the measured equilibrium pressure (x-axis) against the summed number of moles adsorbed as a

function of catalyst weight (y-axis). By extrapolation of the point of saturation to the y-axis, the number of surface metal atoms available for adsorption was determined.

The value of dispersion of the metal component can also be used to estimate the size of the metal crystallites. To obtain particle sizes from dispersion data, assumptions have to be made concerning particle shape. It is assumed that the supported metal particles are spheres of equal diameter. The average metal crystallite particle size is calculated using equation 4.9 [85].

$$\text{Average Particle Diameter} = \frac{6 \cdot \frac{V_m}{A_m}}{D_m} \quad \text{eq. 4.9}$$

where  $D_m$  is the fractional metal dispersion,  $A_m$  is the average surface area occupied by a metal atom on the surface ( $\text{nm}^2$ ) and  $V_m$  is the volume of metal atoms in the bulk ( $\text{nm}^3$ ). Table 4.3.2 lists the values used in the equation for platinum.

**Table 4.3.2** Values used in the Particle Size Estimation Equation.

Symbol	Value
$V_m$	$0.0151 \text{ nm}^3$
$A_m$	$0.08 \text{ nm}^2$
$D_m$	%Dispersion/100

### 4.3.3 Transmission Electron Microscopy (TEM)

TEM was used as another technique to provide information on the particle size and the metal dispersion of each of the catalysts used during this study, thus providing confirmation to the results gathered by the adsorption isotherm described above. The difference between the two techniques is that TEM is a direct physical measurement of the metal particles on the support, whereas the dispersion measured from adsorption isotherms is an indirect chemical technique.

Finely ground catalyst, having been previously reduced, was suspended in dry ethanol at room temperature in a small glass tube. This was then suspended in an

ultrasonic bath for approximately 10 mins in order to disperse the powder homogeneously throughout the liquid. A drop of the fine suspension was then placed on a carbon coated copper grid and placed in a 40°C oven overnight to allow the ethanol to evaporate leaving behind the fine powder on the grid. The impregnated grid was then placed in the microscope and TEM measurements were conducted using a Joel 1200EX and a Topcon 002 electron microscope with high resolution capability.

Measurements were also made on catalysts which had been previously used in both straight and oxidative dehydrogenation reactions, in an attempt to observe any changes to the particle size as a result of the reactions. The samples in this case were taken directly from the reactor and prepared by placing on a carbon coated grid in a similar way to the fresh samples described previously.

#### **4.3.4 Transmission Infrared Spectroscopy of Carbon Monoxide Chemisorption**

Catalyst surfaces generally offer a variety of reactive site available for adsorption. These adsorption sites can be different in nature and can vary depending on characteristics such as the metal and particle size of the metallic crystallites. The chemisorption techniques described above in section 4.3.2 allows a quantitative estimate of the total number of active sites on a particular catalyst, however, it does not allow the nature of these sites to be determined. Using the combination of surface infrared spectroscopy and adsorption/desorption experiments, the specific nature of these sites and their relative distribution can be observed. Different sites, involving different numbers of metal atoms (*e.g.* three-fold hollow or on a single metal atom) have different strengths of adsorption. Using carbon monoxide the population and strength of adsorption of these sites can be probed.

Figure 2.1.6 in section 2.1.5 describes the apparatus that was used during this work. Although the system was set up to enable the use of DRIFTS and transmission IR, the technique of choice for this study was the latter. Unlike DRIFTS, where the neat powder could be used, transmission required the sample to be pressed into a small disc. After trial and error using different compositions of catalyst and KBr as well as neat catalyst, the best disc, taking into consideration light transmission, mechanical integrity and catalyst concentration, was found to consist of 50 mg of KBr and 20 mg

of catalyst. With this composition the sample was pressed under 10 tons using a 1.5 mm diameter dye assembly.

The experiments were carried out in a similar fashion to the pulse-flow experiments described in section 4.2.1, where the quartz microreactor was replaced by the transmission infrared cell described in section 2.1.4 (Graesby Specac heated gas cell fitted with a glass ‘spider’ sample holder). Again, helium was used as carrier gas and pulses of carbon monoxide were injected over the catalyst disc. The following method was adopted in order to obtain the most data from each reactant. Firstly the catalyst was reduced *in situ*. To do this 6% H<sub>2</sub>/N<sub>2</sub> was passed through the cell and disc at 30ml min<sup>-1</sup> while the temperature was ramped at 5°C min<sup>-1</sup> to 250°C (maximum operating temperature of the cell). This temperature was held for a period of 120 mins before the reducing mixture was switched to helium for a further 60 mins at the same temperature. After this was complete the cell was allowed to cool to ambient at which temperature the adsorption of CO was carried out.

The procedure for recording spectra involved the following steps. Firstly, a background spectrum was recorded with the clean, reduced catalyst disc in place. This was followed by a sample spectrum which gave the baseline to enable the following changes to be observed on adsorption of CO (100 scans with the 0.65% Pt/Al<sub>2</sub>O<sub>3</sub> and 400 scans with the 0.5% Pt/Al<sub>2</sub>O<sub>3</sub> catalyst at a resolution of 4 cm<sup>-1</sup>). After this was complete 50 torr pulses were injected onto the catalyst and spectra recorded after 1-1.5 mins. This time lapse was to allow the adsorbate gas to reach the catalyst and the gas-phase to be removed from the cell, thus reducing its contribution to the end results. Such large pulses of incident gas were required to overcome the large amount of gas by-pass inherent with this IR cell.

After the series of adsorption spectra were recorded, another background spectrum of the saturated catalyst was obtained to produce another baseline against which the desorption spectra could be compared. At this point the temperature was increased in 25°C increments by the Eurotherm temperature controller under a flow of 50 ml min<sup>-1</sup> helium, taking spectra at each temperature. This was continued up to 175°C at which point all the carbon monoxide was removed and the experiment was complete.

#### **4.3.5 Carbon Monoxide Temperature Programmed Desorption (TPD)**

Like the IR technique described above, TPD also allows the nature and relative amounts of the various adsorption sites to be determined. This technique uses the difference in heats of adsorption of an adsorbate molecule, in this case carbon monoxide, on different metal sites of the catalyst surface. The method involves the gradual increase in temperature of the catalyst bed, which had previously been exposed to an adsorbate, and detection of the resultant effluent gas. In this work the detection system used was an on-line mass spectrometer, as described in section 2.1.6. Figure 4.3.2 is a schematic diagram of the whole system used to make these measurements.

Before carrying out the experiments the catalyst was reduced in the same way as before with the pulse-flow and continuous-flow studies (see section 4.1.2) and then allowed to cool to room temperature in the inert helium flow at  $50 \text{ ml min}^{-1}$  before exposure to carbon monoxide. The mass spectrometer was set to ‘multiple ion mass mode’ which allowed the partial pressures of various species to be monitored and recorded as a function of time, which could be correlated to temperature at a later time. This arrangement permitted estimates of the relative population of the various sites to be made.

The pulsing technique used during the pulse-flow experiments was also used here in order to dose a series of  $5 \times 50$  torr pulses of carbon monoxide onto the catalyst at ambient temperature. This ensured that the adsorption sites available on the catalyst surface were saturated. After this was complete, the system was given approximately 10 mins to stabilise, after which the temperature was increased at  $30^\circ\text{C min}^{-1}$  to  $600^\circ\text{C}$ , monitoring the effluent gas as discussed above. This ramp-rate was found to be appropriate as it was fast enough to desorb the carbon monoxide preventing re-adsorption, while being slow enough to ensure reasonable separation between the various peaks. Again the temperature was controlled using a Eurotherm temperature programmer.

#### **4.3.6 Temperature Programmed Oxidation (TPO)**

TPO studies were carried out on used sample specimens to observe the temperature at which the carbonaceous material deposited during the hydrocarbon conversion

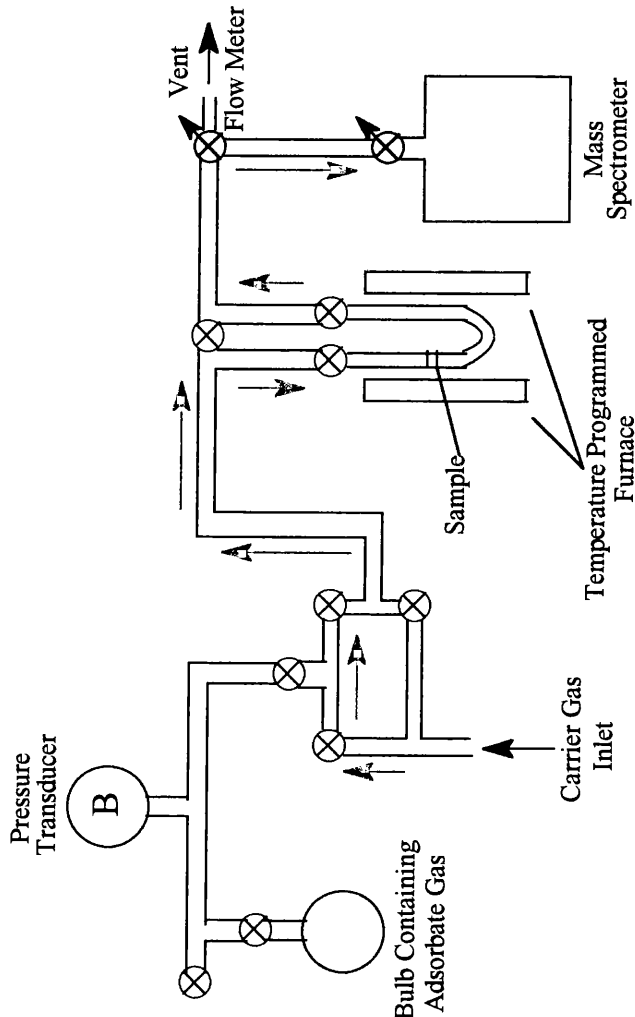


**Fig. 4.3.2** Schematic Representation of the Apparatus used for the TPD Measurements.

reactions could be oxidised. The method was developed according to the procedure adopted by Querini *et al* [42]. The used catalyst samples were loaded into the reactor vessel described in section 2.1.3. The reactor was then purged with helium at  $50\text{ ml min}^{-1}$  at ambient temperature for a period of approximately 10 mins. After this was completed the reactor was isolated and the gas allowed to flow through the bypass. At this point the oxidising gas mixture was set to 5% oxygen and 95% helium using the gas mixing section described in section 2.1.1. After stabilisation of this flow and the mass spectrometer, which was set up in a similar way to the TPD experiments described above, the bypass was opened and the reactant mixture exposed to the used catalyst sample. Again, this configuration was given time to stabilise before the temperature was increased at a rate of  $10^\circ\text{C min}^{-1}$  to the ultimate temperature of  $600^\circ\text{C}$ .

#### 4.3.7 Total Surface Area and Pore Size Measurements

BET surface area measurements and pore size and volume measurements were carried out to further characterise the two catalysts used. Unlike adsorption isotherm measurements, which determines the metal surface area, BET measures the total area of the catalyst, including the metal and the support material. The adsorption in this case was carried out at liquid nitrogen temperatures and used nitrogen itself as the adsorbate. At this temperature condensation of the exposed nitrogen occurs covering the total surface of the catalyst. The uptake of nitrogen by the un-reduced catalyst samples was measured using a Micromeritics Gemini machine. The same piece of equipment was also used in the measurement of pore volume and pore diameter.

## *Chapter 5*

### **Results and Discussion**

The Results and Discussion chapter describes and attempts to explain the results obtained for the straight and oxidative dehydrogenation of butane. Different studies were carried out with many variables changed in order to influence the conversion of butane and increase the selectivity towards the olefin products. These variables include temperature, linear velocity of the reactant gas flow through the reactor vessel, hydrocarbon:oxygen ratio, catalyst mass and the use of two catalysts with different physical properties.

The preparation and origin of the 0.5% Pt/Al<sub>2</sub>O<sub>3</sub> and 0.65% Pt/Al<sub>2</sub>O<sub>3</sub> catalysts were described in section 3.1. When using two different substrates it is important, in terms of being able to interpret the results, to characterise the catalysts as fully as possible in order to determine the difference between them. Before the results from the catalyst testing are illustrated, the outcome of the characterisation experiments are detailed and summarised. These experiments include TPR, adsorption isotherm measurements using carbon monoxide and hydrogen as adsorbates, carbon monoxide TPD, IR using carbon monoxide as a probe, TEM, surface area and pore size measurements; all of which are described in more detail in chapter 4.

As well as the results from the various experiments mentioned above the Results and Discussion chapter begins with a presentation of butane dehydrogenation thermodynamics. This section describes and explains the limits enforced on this work by the thermodynamic constraints of the system. Throughout the remainder of the chapter the theoretical results are displayed next to the experimental results, where appropriate, so that the performance of the catalyst can be fully appreciated. At the end of each sub-section presenting results for the catalysts under a range of conditions, the data is summarised.

## *5.1 Equilibrium Considerations for Straight and Oxidative Dehydrogenation*

### **5.1.1 Straight Dehydrogenation**

The breaking of reactant bonds in the formation of products requires a supply of energy in order to overcome activation barriers. As a result catalytic dehydrogenation of butane is an endothermic process, with its conversion limited by thermodynamic equilibrium [2]. Therefore in order to achieve high conversion of butane it is necessary

to implement high temperatures. However, increasing the process temperature only increases the complexity of the reactions taking place. As well as dehydrogenation processes, isomerisation to *iso*-butane and cracking reactions leading to the formation of smaller chain alkanes and alkenes, aromatization products and condensed ring aromatic structures, can also take place. Formation of carbonaceous deposits on the surface of the catalyst is also important at high temperatures and leads to the deactivation of the catalyst [15].

When assessing the performance of the catalyst in terms of conversion and yield, the thermodynamic equilibrium of the system needs to be considered, as an improvement on equilibrium can never be achieved [34]. As the reactions of interest involve the dehydrogenation of butane to form butene species and subsequently to 1,3-butadiene, only the reactions below are considered (equation 5.1 and 5.2).



The reaction of butane in the formation of butene species and 1,3-butadiene proceeds through a complex reaction pathway in which dehydrogenation and isomerisation (between *cis* and *trans* but-2-ene and but-1-ene) processes occur. Figure 5.1.1 illustrates the possible products formed during the conditions required for dehydrogenation. Due to the absence of isotopic studies the assumption that 1,3-butadiene can be formed from each of the mono-olefins is made, as it is not possible to be more specific about its origin.

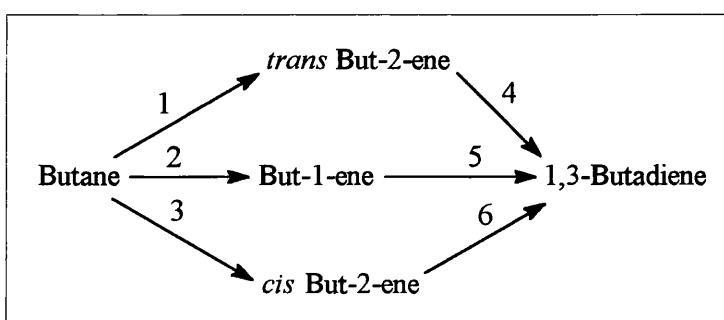


**Fig. 5.1.1** Reaction Scheme during the Catalytic Dehydrogenation of Butane.

When carrying out reactions it is useful to know, at any temperature, what the conversion and product composition should be, assuming that everything taking place is the dehydrogenation of butane without isomerisation to *iso*-butane or cracking processes. Knowing this, the catalyst can be quantitatively and qualitatively assessed. In order to calculate the predicted conversion (and yield) and product composition as a function of temperature, it is necessary to know the equilibrium constants ( $K_{eq}$ ). These can be obtained for each of the products at various temperatures from equation 5.3 [2].

$$\Delta G^\circ_T = -RT \ln K_{eq} \quad \text{eq. 5.3}$$

The values of  $\Delta G^\circ$  at various temperatures can be calculated from the enthalpy of dehydrogenation ( $\Delta H^\circ$ ) and the entropy of dehydrogenation ( $\Delta S^\circ$ ) according to equation 5.4[ref].

$$\Delta G^\circ = \Delta H^\circ - T \cdot \Delta S^\circ \quad \text{eq. 5.4}$$

The  $\Delta H^\circ$  values can be calculated from the heats of formation of the entities in equations 5.1 and 5.2, while the  $\Delta S^\circ$  values are obtained from the entropy values of the same entities[88]. Table 5.1.1 lists the values of  $\Delta G^\circ$  for each product as a function of temperature (the numbers relate to the pathways shown on figure 5.1.1) and table 5.1.2 contains the  $K_{eq}$  values obtained from the  $\Delta G^\circ$  values, again as a function of temperature.

In line with the above discussion, it is important from a quantitative and qualitative point of view, to know how the reactions carried out in the laboratory compare (in terms of conversion, yield and product composition) with the thermodynamic equilibrium limits. Equation 5.5 describes how the overall equilibrium constant  $K_{eq}$  is used to establish the equilibrium conversion ( $P$  = partial pressure of butane in the diluted reactant gas mixture)[34].

$$\text{Equilibrium Conversion (\%)} = \sqrt{\frac{K_{eq}}{P + K_{eq}}} \times 100 \quad \text{eq. 5.5}$$

Table 5.1.3 displays the thermodynamic conversions as a function of temperature and is presented for all the butane partial pressures used during the reactions, while figure 5.1.2 presents the same material in graphical form for the dehydrogenation of butane to all butene species. As expected the conversion increases as the temperature is increased and also as the amount of dilution is increased, which explains why in industry diluted butane reactant mixtures are used [3]. The equilibrium yield value can be worked out according to equation 4.3 in section 4.1.3 assuming, as described above, that all processes taking place are dehydrogenation of butane to the corresponding C<sub>4</sub> alkenes, *i.e.* 100% selectivity. As a result of this assumption, the values of yield when the system is at equilibrium are equivalent to the conversion values at equilibrium.

**Table 5.1.1** The ΔG° values for the Straight Dehydrogenation of Butane to form butenes as a function of Temperature (kJ mol<sup>-1</sup>).

Temp. (°C)	B-1 (2)	Trans B-2 (1)	Cis B-2 (3)	Diene (from B-1) (5)	Diene (from Trans B- 2) (4)	Diene (from Cis B-2) (6)
200	65.656	59.559	61.594	62.081	68.178	66.143
300	52.856	47.859	49.394	51.781	56.778	55.243
400	40.056	36.159	37.194	41.481	45.378	44.343
500	27.256	24.459	24.994	31.181	33.978	33.443
600	14.456	12.759	12.794	20.881	22.578	22.543
700	1.656	1.059	0.594	10.581	11.178	11.643

The relative distribution of the butene products as a function of temperature are listed in table 5.1.4, and displayed in graphical form in figure 5.1.3. It is clear that at the low temperature end the dominant product should be *trans* but-2-ene according to the calculations. It can also be predicted that 1,3-butadiene is not produced until temperatures of approximately 500°C are reached. These observation and numbers are in agreement with the general literature available [2, 34].

**Table 5.1.2** The  $K_{eq}$  values for the Straight Dehydrogenation of Butane to form Butenes as a function of Temperature.

Temperature (°C)	B-1	Trans B-2	Cis B-2	Diene (overall)	Overall $K_{eq}$ value
200	5.6127E-8	2.6455E-7	1.5768E-7	2.3457E-14	4.7835E-7
300	1.5187E-5	4.3353E-5	3.1411E-5	8.6711E-10	8.9952E-5
400	7.7796E-4	0.0016	0.0013	1.4074E-6	0.0036
500	0.0144	0.0222	0.0205	3.3741E-4	0.0574
600	0.1365	0.1724	0.1716	0.0230	0.5035
700	0.8149	0.8773	0.9292	0.6609	3.2823

**Table 5.1.3** Equilibrium Conversion as a function of Temperature and Butane Partial Pressure for the Straight Dehydrogenation of Butane to Butenes.

Temp. (°C)	Conv. (%) 1 atm	Conv. (%) 0.3333 atm	Conv. (%) 0.2000 atm	Conv. (%) 0.1000 atm	Conv. (%) 0.0769 atm
200	0.06	0.12	0.15	0.22	0.25
300	0.95	1.64	2.12	3.00	3.42
400	6.02	10.39	13.37	18.74	21.25
500	23.30	38.34	47.23	60.40	65.38
600	57.87	77.57	84.60	91.34	93.14
700	87.55	95.28	97.08	98.51	98.85

**Table 5.1.4** Equilibrium Product Composition as a function of Temperature during the Straight Dehydrogenation of Butane.

Temp. (°C)	B-1 (%)	Trans B-2 (%)	Cis B-2 (%)	Diene (%)
200	11.73	55.30	32.96	4.90E-6
300	16.88	48.20	34.92	9.64E-4
400	21.38	42.86	35.72	0.04
500	25.06	38.73	35.63	0.59
600	27.10	34.24	34.08	4.58
700	24.83	26.73	28.31	20.14

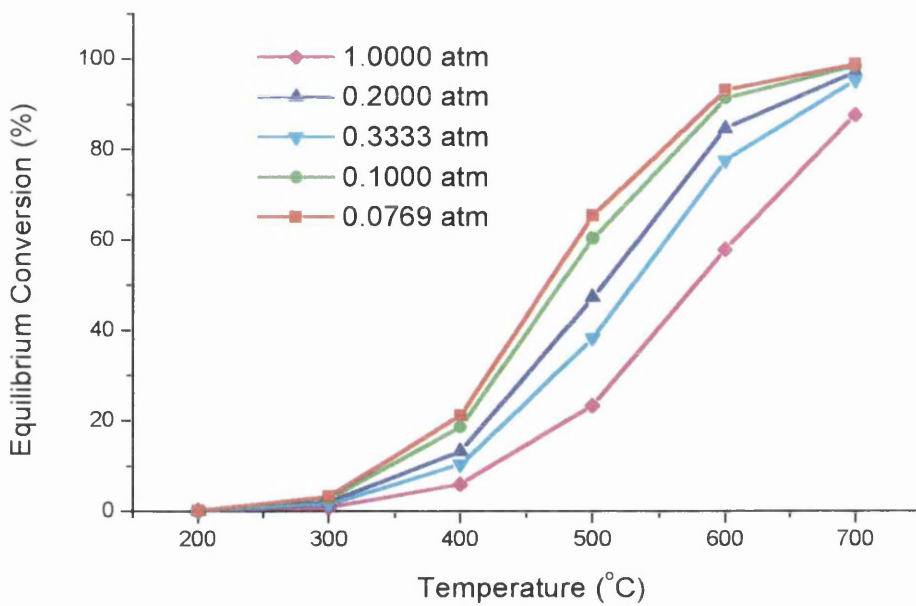


**Fig. 5.1.2** Equilibrium Conversion during the Straight Dehydrogenation of Butane to Butenes as a function of Temperature and Butane Partial Pressure.

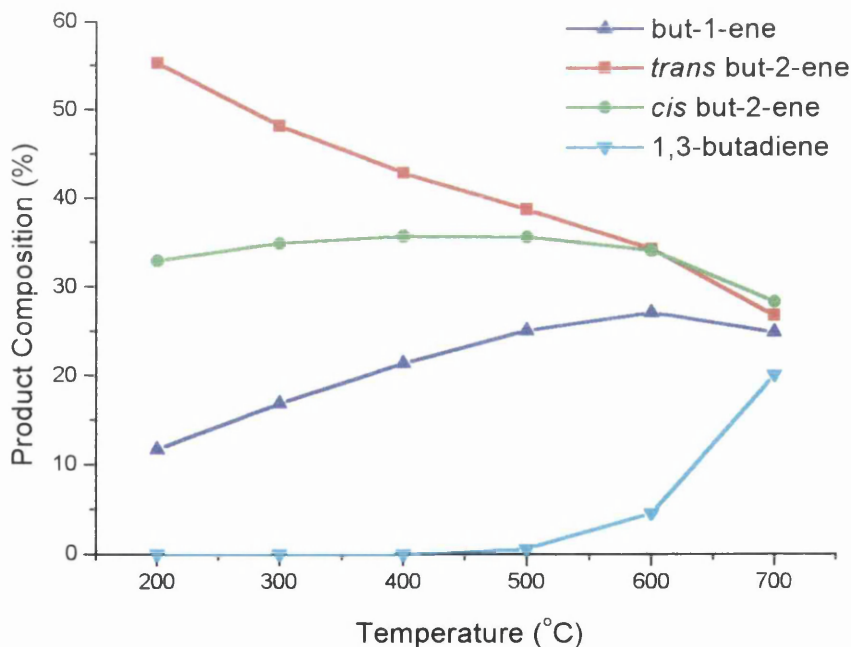
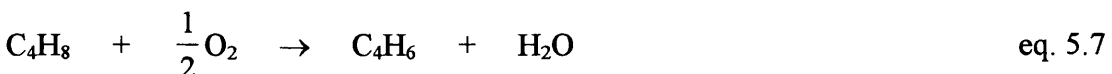
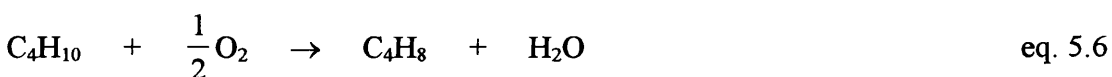


**Fig. 5.1.3** Equilibrium Composition of the Product Mixture during the Straight Dehydrogenation of Butane to Butenes as a function of Temperature.

The diagrams and tables presented above contain the important theoretical statistics for the dehydrogenation of butane in the production of butene species and 1,3-butadiene. During the course of the remaining results and discussion chapter these values will be displayed along with the experimental results obtained in the laboratory, where appropriate, so that easy analysis of the reaction behaviour can be deduced.

### 5.1.2 Oxidative Dehydrogenation

In a similar way to straight dehydrogenation, during the production of butene species from butane, bonds have to be broken under oxidative dehydrogenation conditions. However, as oxidative dehydrogenation involves molecular oxygen in the reactant gas mixture and with the resultant product mixture including water (equations 5.6 and 5.7), which is highly desirable in thermodynamic terms, the oxidative dehydrogenation is an exothermic process. The possible dehydrogenation products expected from this type of reaction are the same as those depicted in figure 5.1.1. So only these processes are considered here.



Similar calculations to those above have been carried out. As the reaction is highly exothermic the thermodynamics are relatively straight forward in comparison to the straight dehydrogenation. Table 5.1.5 lists the  $\Delta G^\circ$  values for the oxidative dehydrogenation of butane in the production of butene species. It is apparent on observation of these values that the dominant product should be 1,3-butadiene. The reason for this is that in its production, two moles of water are produced and so the reaction is more favourable than in the case where only one of the bonds in the butane molecule is dehydrogenated to an olefin.

Table 5.1.6 contains the  $K_{eq}$  values for the oxidative dehydrogenation. It can be concluded from these values, using equation 5.5, that 100% conversion should be

observed at all temperatures with 100% selectivity towards 1,3-butadiene. From these observations it would appear that this method of olefin production is highly efficient. However, another more dominant reaction is possible with butane and oxygen at these temperatures. This process is combustion, forming carbon dioxide and water (equation 5.8) [63, 65]. The thermodynamic calculations, in terms of  $\Delta G$  and  $K_{eq}$  are presented in table 5.1.7 for this process.

**Table 5.1.5** The  $\Delta G^\circ$  values for the Oxidative Dehydrogenation of Butane to form butenes as a function of Temperature (kJ mol<sup>-1</sup>).

Temp. (°C)	B-1 (2)	Trans B-2 (1)	Cis B-2 (3)	Diene (from B-1) (5)	Diene (from Trans B-2) (4)	Diene (from Cis B-2) (6)
200	-405.296	-411.392	-409.358	-158.870	-152.774	-166.208
300	-413.646	-418.642	-417.108	-164.720	-159.724	-172.658
400	-421.996	-425.892	-424.858	-170.570	-166.674	-179.108
500	-430.346	-433.142	-432.608	-176.420	-173.624	-185.558
600	-438.696	-440.392	-440.358	-182.270	-180.574	-192.008
700	-447.046	-447.642	-448.108	-188.120	-187.524	-198.458

**Table 5.1.6** The  $K_{eq}$  values for the Oxidative Dehydrogenation of Butane to form Butenes as a function of Temperature.

Temperature (°C)	B-1	Trans B-2	Cis B-2	Diene (overall)
200	1.4136E17	6.6626E17	3.9710E17	9.9954E35
300	8.2880E14	2.3659E15	1.7142E15	1.1144E31
400	2.2379E13	4.4908E13	3.7324E13	3.7545E27
500	1.5385E12	2.3774E12	2.1875E12	1.0144E25
600	1.9531E11	2.4675E11	2.4556E11	1.0718E23
700	3.7896E10	4.0799E10	4.3212E10	2.9031E21

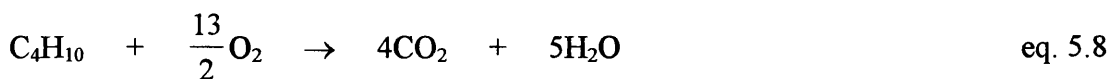


**Table 5.1.7** The  $\Delta G^\circ$  and  $K_{eq}$  values for the Combustion of Butane forming Carbon Dioxide and Water as a function of Temperature.

Temp. (°C)	$\Delta G^\circ$ (kJ mol <sup>-1</sup> )	$K_{eq}$
200	-2.736E6	--
300	-2.752E6	7.3253E250
400	-2.768E6	6.5987E214
500	-2.784E6	1.2595E188
600	-2.799E6	3.1781E167
700	-2.8152E6	1.3743E151

It is shown from these calculations that the combustion reaction is much more favourable than the oxidative dehydrogenation. This outcome is of major importance when trying to interpret the results from the reactions carried out in the laboratory.

## 5.2 Characterisation of 0.5% and 0.65% Pt/Al<sub>2</sub>O<sub>3</sub> Catalysts

### 5.2.1 Temperature Programmed Reduction (TPR)

The TPR experiments were carried out as described in section 4.3.1. Figure 5.2.1 contains the reduction profile for the 0.65% catalyst. It can be seen that the maximum rate of hydrogen consumption takes place at approximately 230-240°C. At this temperature the hydrogen interacts with the oxygen covering the surface of the platinum particles resulting in the formation of water. This temperature is slightly higher than expected, but is in the region expected for platinum supported alumina catalysts [87]. There is also a second, broader, peak centered at approximately 275°C which can be attributed to the reduction of the bulk platinum oxide. As a consequence of this result it was agreed that reduction temperatures of 300°C would be used when activating the catalyst in preparation for testing.

Similar experiments were carried out using the 0.5% Pt/Al<sub>2</sub>O<sub>3</sub>. However, this catalyst did not produce a reduction profile. In order to remain consistent, it was decided to activate this catalyst also at 300°C before commencing catalyst testing.

### 5.2.2 Volumetric Adsorption Isotherms

Chemisorption experiments were conducted as described in section 4.3.2 with the resultant isotherms calculated as outlined in the same section. Carbon monoxide and hydrogen were used as adsorbates as they can be used to work out the dispersion and metal surface area as explained in section 4.3.2. Because the equipment was built specifically for this project it was thought it would be necessary to standardise the section built for isotherm measurements. To do this the isotherm for a sample of Europt-1 ( $\text{Pt}/\text{SiO}_2$ ) was measured and the result compared to the literature result. Figure 5.2.2 shows the curve produced for the adsorption of hydrogen on Europt-1 at room temperature.

Comparison with the literature shows that the curve below is almost identical to that produced by other groups [89]. Benchmarking in this manner confirms the validity of chemisorption results on the catalysts under examination in this study.

Having standardised the system, the adsorption of hydrogen and carbon monoxide on the 0.5wt% and 0.65wt%  $\text{Pt}/\text{Al}_2\text{O}_3$  was carried out. Figure 5.2.3 shows the results obtained when the activated catalysts were exposed to CO. It is obvious that the 0.65wt% catalysts is much better dispersed than the 0.5wt% catalyst. The dispersion values were worked out as described in section 4.3.2. A value of 78.0% was calculated for the 0.65wt% catalyst, while the 0.5wt% catalyst was only 31.6% dispersed.

The above experiments were also conducted using hydrogen as the adsorbate. This time the dispersion calculated for the 0.65wt% catalyst was 111.0%, while the value for the 0.5wt% catalyst was 44.4%. The isotherms for these experiments are illustrated on figure 5.2.4. The dispersion value of 111.0% looks to be impossibly high, however there are well known problems with the adsorption of hydrogen on noble metals [89, 90]. These include reversibly adsorbed hydrogen at room temperature, spillover of hydrogen from the metal to the support material, reduction of surface metal oxides at the metal-support interface and adsorption of more than one hydrogen atom per metal surface atom at sites of low metal coordination.

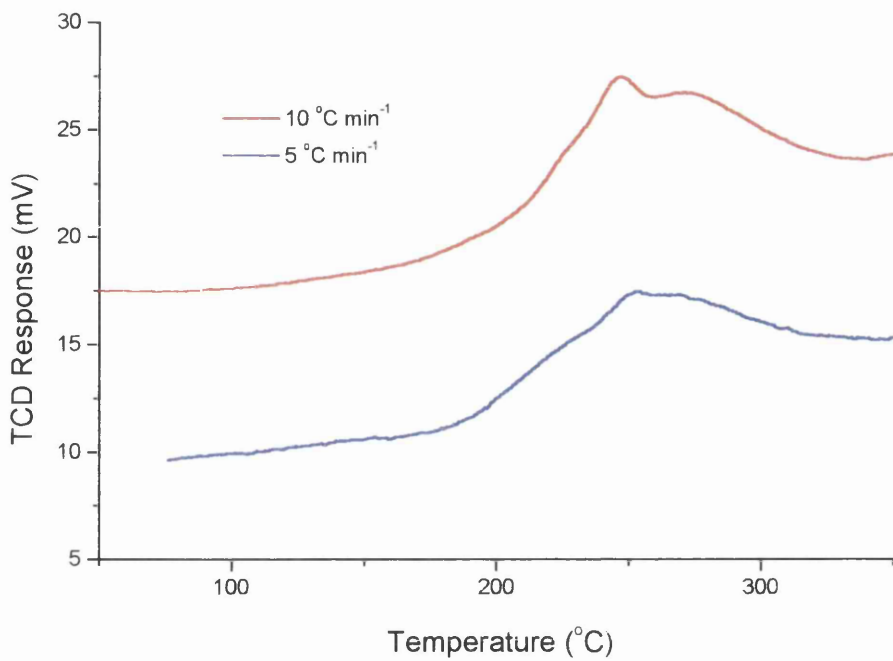


**Fig. 5.2.1** TPR profile for the 0.65% Pt/Al<sub>2</sub>O<sub>3</sub> Catalyst.

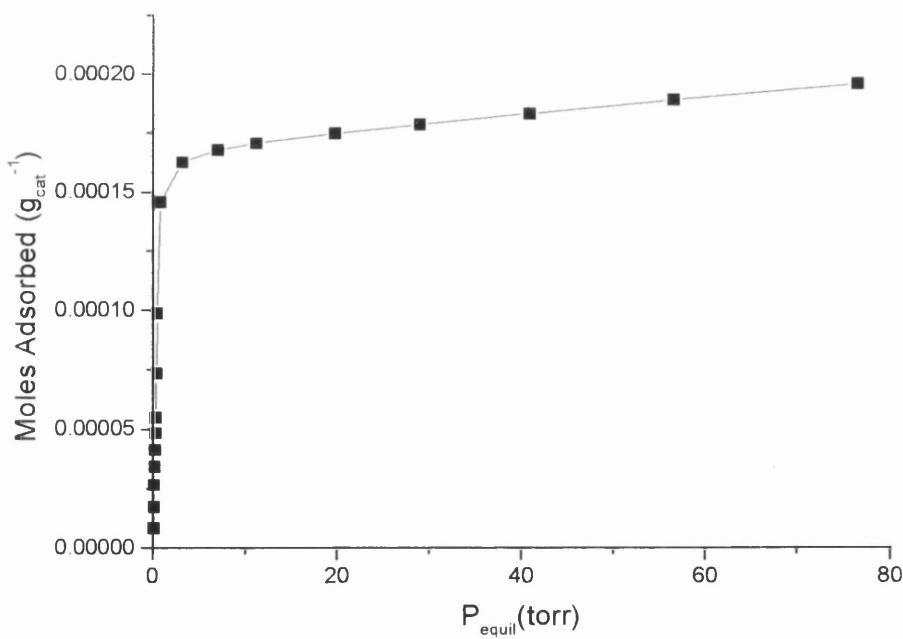


**Fig. 5.2.2** Adsorption Isotherm for Hydrogen Adsorbed on Europt-1.

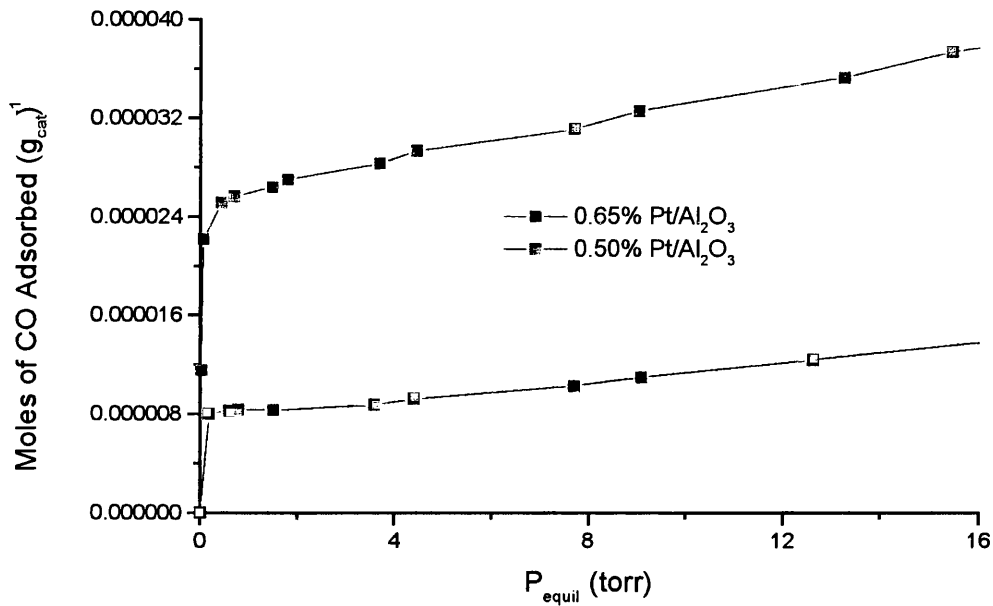


**Fig. 5.2.3** Adsorption Isotherms of CO Adsorbed on 0.5% and 0.65% Pt/Al<sub>2</sub>O<sub>3</sub>.

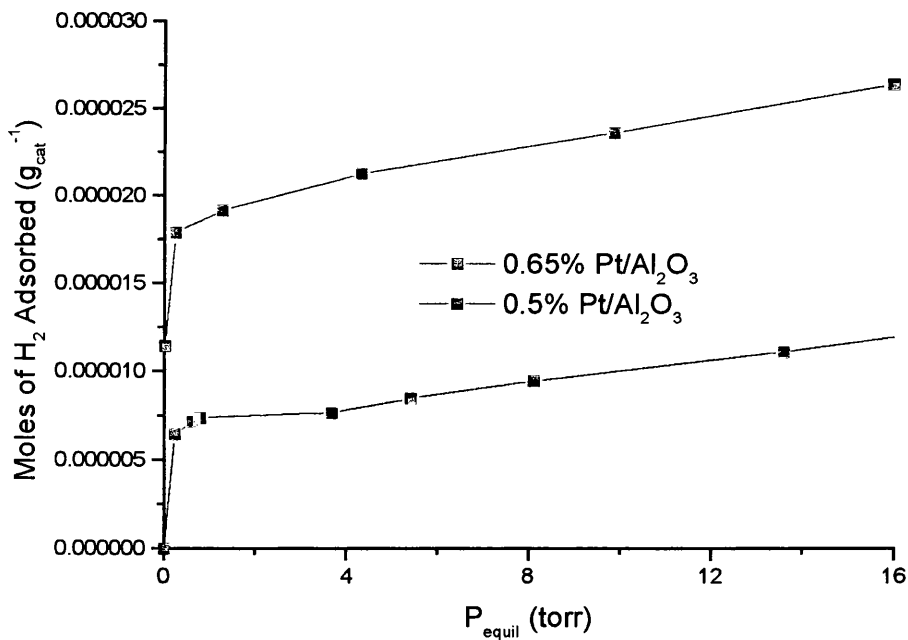


**Fig. 5.2.4** Adsorption Isotherms of H<sub>2</sub> Adsorbed on 0.5% and 0.65% Pt/Al<sub>2</sub>O<sub>3</sub>.

All of these things may lead to overly high values of dispersion[90]. The latter problem could well be taking place on the 0.65% Pt/Al<sub>2</sub>O<sub>3</sub> catalyst as it is clear that it consists of very small metal particles. The estimated size of these particles is calculated below and measured using TEM (section 4.3.3).

Section 4.3.2 describes the method used for calculating the average size of the metal particles using the measured dispersion values.

### 5.2.3 Transmission Electron Microscopy (TEM)

Section 4.3.3 describes some of the theory behind the technique of TEM. Its use within this study is to measure the particle size of the metal crystallites and calculate the particle size distribution on the Pt/Al<sub>2</sub>O<sub>3</sub> catalysts. The value obtained can be compared to that estimated using chemisorption (described in section 4.3.2).

Figures 5.2.6 and 5.2.7 are examples of TEM micrographs for the 0.5% and 0.65% Pt/Al<sub>2</sub>O<sub>3</sub> catalysts respectively. For the 0.5% catalyst the particles were easily seen and were counted in order to obtain a distribution plot. This plot is shown on figure 5.2.5 and the mean particle size was calculated to be 4.6±1.7 nm. This compares quite well to the value of 3.6 nm obtained from CO chemisorption. However, the particles for the 0.65% catalyst could not be distinguished in the electron micrographs and so it was concluded that the particle size was less than 2nm, the lower limit of detection for the electron microscope used. Again comparison with the chemisorption results highlight that in fact it could have been predicted that TEM would have shown no particles. The estimated particle size from the chemisorption experiment was 1.4 nm. Table 5.2.1 summarises the dispersion values and the particle metal sizes measured from TEM and estimated from the CO chemisorption results.

**Table 5.2.1** Summary of the Metal Dispersion and Particle Size.

Catalyst	Dispersion (CO chemisorption)	Particle Size (TEM)	Particle Size (CO chemisorption)
0.5wt% Pt/Al <sub>2</sub> O <sub>3</sub>	31.6%	4.6 nm	3.6 nm
0.65wt% Pt/Al <sub>2</sub> O <sub>3</sub>	78.0%	<2 nm	1.4 nm

#### 5.2.4 Transmission Infrared of Carbon Monoxide Chemisorption

In order to probe the surface morphology of the platinum metal particles, transmission infrared spectroscopy was used. Using CO chemisorption it is possible to identify different adsorption sites such as bridged and linear species. Figure 5.2.8 contains the results from the chemisorption of CO on the 0.5% Pt/Al<sub>2</sub>O<sub>3</sub> catalyst using the method previously described in section 4.3.4. Two features are clearly visible, a band indicating the presence of linear ‘on top’ adsorbed species at 2026 cm<sup>-1</sup> and one at 1800 cm<sup>-1</sup> indicating the bridged species (possibly in a 3-fold hollow site) [91]. The difference in the wavenumber of adsorption between the two species can be explained in terms of synergic bonding. The basic concept involves the back-donation of electrons from the metal surface into the  $\pi^*$  antibonding orbital of the CO molecule, thus increasing the bondlength and decreasing the bond order, subsequently weakening the C-O bond. If the CO molecule was attached directly to two or three metal atoms, in a bridged site, this effect would be more significant than the case of the linearly adsorbed species where the CO molecule is only attached to one metal atom. Therefore, it is expected that the bridged species will have a lower wavenumber than the linear species. If the bridged species in the 3-fold hollow was detected it is likely it would have a smaller wavenumber than the bridged species in the 2-fold site [91, 92].

Another observation that can be seen on the spectra is the small shift in wavenumber of the bands to higher energy as the amount of adsorbed CO is increased. The linear species shows a shift from 2026 cm<sup>-1</sup> to 2030 cm<sup>-1</sup>, while the bridged species increases from 1800 cm<sup>-1</sup> to 1811 cm<sup>-1</sup>. This effect occurs when species of the same chemical type are parallel to each other thus allowing their vibrational dipole moments to couple together with the overall enhancement of the band position. This is termed dipolar coupling.[91]

The final observation to be made from figure 5.2.8 is the presence of a band centered at 2143 cm<sup>-1</sup> indicating the presence of gas phase CO in the IR cell. This is easily assigned as it is well resolved allowing the P and R branches, which results from transitions between rotational-vibrational energy levels, to be observed. It is also possible to see the rotational fine structure on the low frequency R branch.[93]

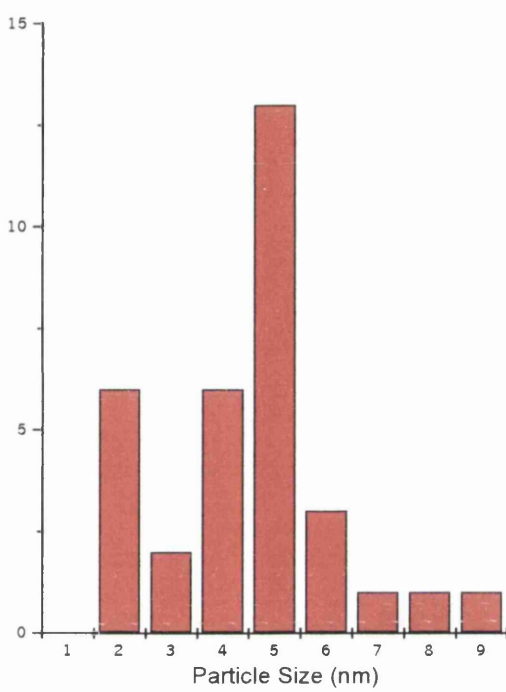


**Fig. 5.2.5**      Particle Size Distribution for the 0.5% Pt/Al<sub>2</sub>O<sub>3</sub>.

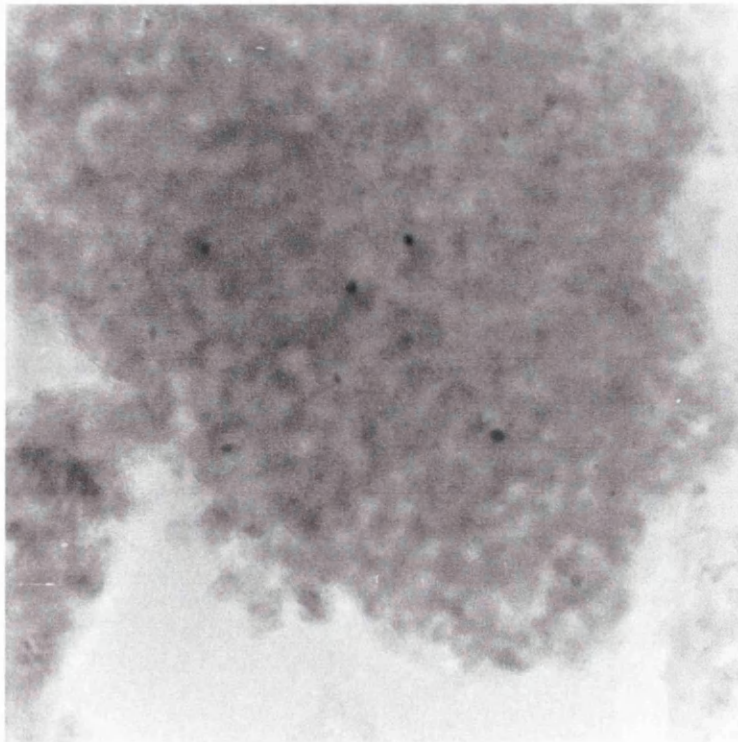


**Fig. 5.2.6**      TEM Micrograph of the 0.5% Pt/Al<sub>2</sub>O<sub>3</sub> Catalyst.

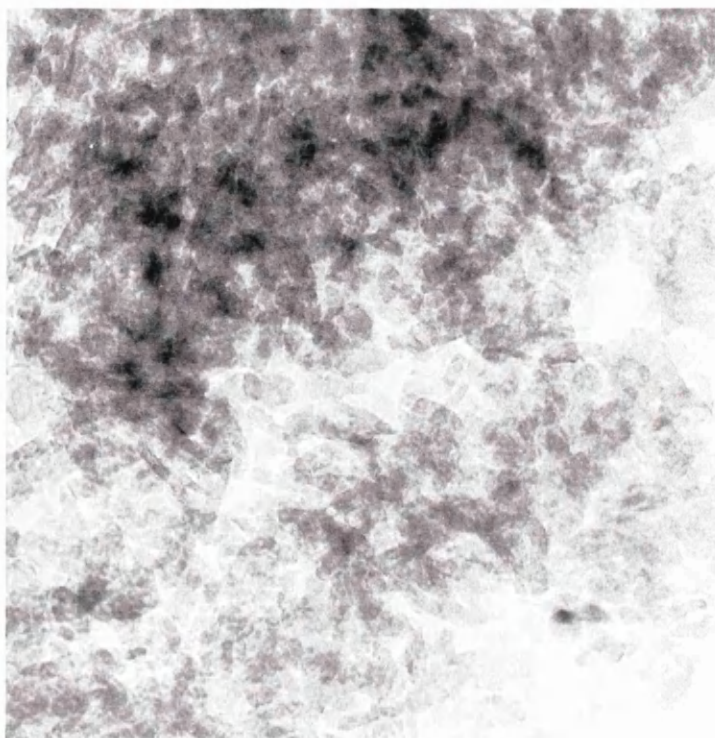


**Fig. 5.2.7** TEM Micrograph of the 0.65% Pt/Al<sub>2</sub>O<sub>3</sub> Catalyst.

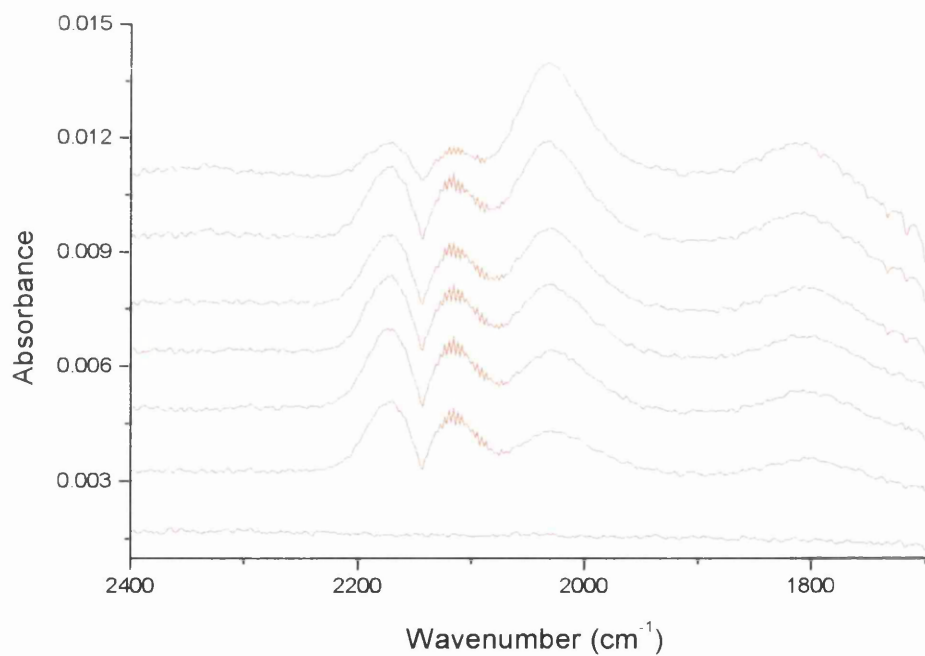


**Fig. 5.2.8** Infrared of CO Chemisorbed on 0.5% Pt/Al<sub>2</sub>O<sub>3</sub> (50 torr pulses).

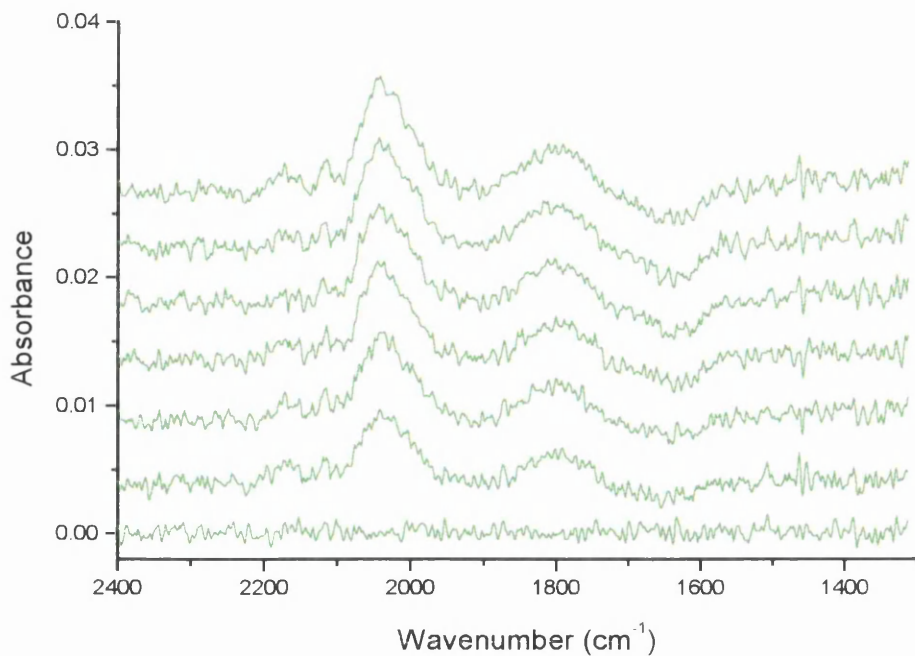


**Fig. 5.2.9** Infrared of CO Chemisorbed on 0.65% Pt/Al<sub>2</sub>O<sub>3</sub> (50 torr pulses).

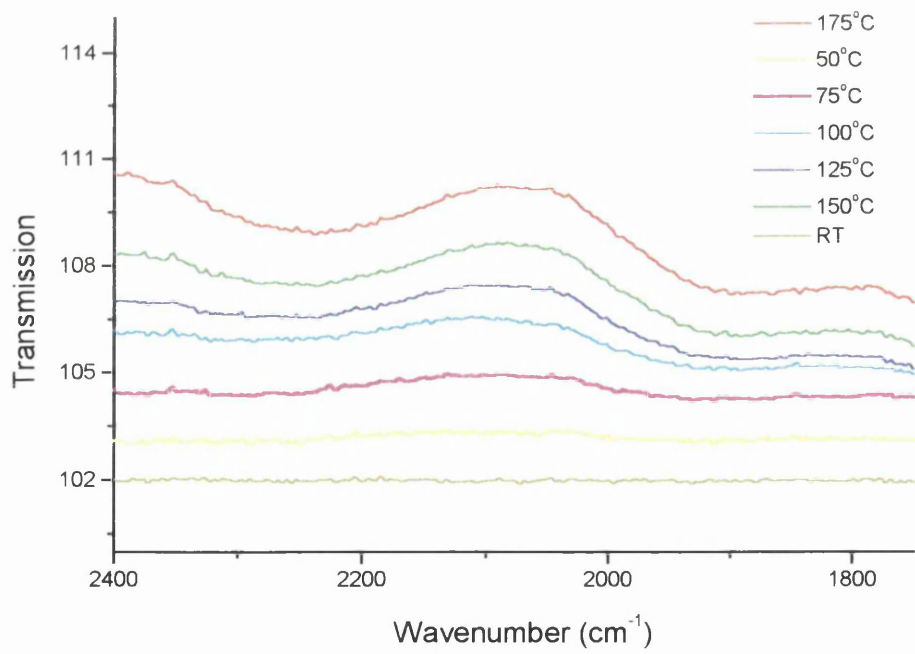


**Fig. 5.2.10** Desorption Spectra of CO from 0.5% Pt/Al<sub>2</sub>O<sub>3</sub>.

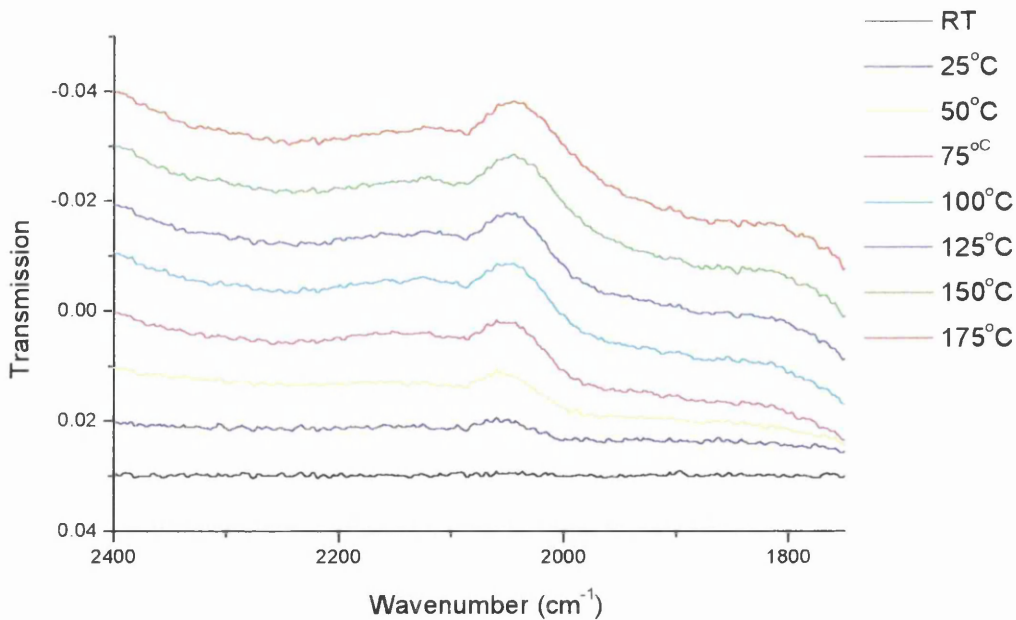


**Fig. 5.2.11** Desorption Spectra of CO from 0.65% Pt/Al<sub>2</sub>O<sub>3</sub>.

Figure 5.2.9 shows the infrared spectra of CO adsorbed on the 0.65% Pt/Al<sub>2</sub>O<sub>3</sub> catalyst. Again, bridged and linear species are detected. The bridged in this case are more likely to be 2-fold as the particle size is very small in this case. The linear species are observed at 2034 cm<sup>-1</sup> increasing to 2040 cm<sup>-1</sup> as the coverage is increased and the effect of dipolar coupling becomes more apparent, while the bridged species is found at 1794 cm<sup>-1</sup> increasing to 1800 cm<sup>-1</sup>. The noise is much greater in this set of spectra compared to the data from the previous catalyst as the number of scans for each spectrum was greater in the latter case resulting in improved signal to noise. A hint of gas phase CO can be observed around the 2143 cm<sup>-1</sup> region.

Figures 5.2.10 and 5.2.11 show the spectra for the desorption of CO from the surface of the 0.5% and 0.65% Pt/Al<sub>2</sub>O<sub>3</sub> respectively. Here the room temperature CO saturation spectra is taken as the background which was then subtracted from the subsequent desorption runs. In this form a positive inflection implies loss of adsorbent. The bridged and linear species can be observed desorbing from the catalyst surface as the temperature is increased. It is also possible to see a reverse dipolar coupling effect as the CO is removed from the platinum metal crystallites. In the 0.5% Pt/Al<sub>2</sub>O<sub>3</sub> case it is possible to see the wavenumber decrease from 2092 cm<sup>-1</sup> to 2071 cm<sup>-1</sup> for the linear

species and from  $1805\text{ cm}^{-1}$  to  $1798\text{ cm}^{-1}$  for the bridged species as this takes effect. The same can be seen for the 0.65% catalyst. For the linear ‘on top’ CO species the wavenumber decreases from  $2054\text{ cm}^{-1}$  to  $2042\text{ cm}^{-1}$  and for the bridged species from  $1818\text{ cm}^{-1}$  to  $1793\text{ cm}^{-1}$  as the CO is removed stepwise.

Although distinctions can be made between bridged and linear adsorbed species on each catalyst it is very difficult to interpret the spectra in order to determine the nature of the bridged species in each case. As the 0.65% catalyst has very small particles it was hoped that 2-fold bridged species would be observed, in contrast to the 0.5% catalyst, which is expected to contain a higher degree of (111) planes (due to it containing larger particles), on which 3-fold bridged species might be detected. The 3-fold species displaying lower wavenumber than the 2-fold species. However, the wavenumber of these species is highly dependent on coverage (which was unknown in these experiments) and particle size and as a consequence the information can not be obtained from this set of spectra.

### 5.2.5 Carbon Monoxide TPD

TPD is used as a technique that can probe the surface morphology of the platinum particles, complementing the results from the IR study detailed above [94]. As discussed previously, different modes of adsorption have different heats of adsorption. Consequently, when the temperature is increased each mode of adsorption should produce desorption peaks at different temperatures. Section 4.3.5 explains the method used during these experiments and the information that can be abstracted from the data.

Figure 5.2.12 shows the CO profiles of both the 0.5% and 0.65% Pt/ $\text{Al}_2\text{O}_3$  catalysts. It is evident that the area of peak for the 0.65% catalyst is considerably larger than that for the 0.5% catalyst. Indeed, determination of the areas, by integration of the overall curve for each catalyst sample has shown that the 0.65% Pt/ $\text{Al}_2\text{O}_3$  held 2.0 times more CO than the 0.5% catalysts. This figure correlates well with that obtained from the chemisorption of the two catalysts (figure 5.2.3). As highlighted above the 0.65% catalyst was found to have an adsorption capacity of approximately  $25\text{ }\mu\text{mol g}^{-1}$  of CO while the 0.5% catalyst adsorbs  $8\text{ }\mu\text{mol g}^{-1}$ , giving a ratio of

approximately 3. The other distinct feature of these plots is the appearance of two modes of adsorption, the linear species and the bridged species. The presence of a species adsorbed in 3-fold hollow sites may also be observed. Evidence for the existence of this species was presented in the literature by Haaland using IR spectroscopy [92]

**Table 5.2.1** Characteristics of the TPD Spectra for the 0.5% and 0.65% Pt/Al<sub>2</sub>O<sub>3</sub> Catalysts.

Catalyst	Temperature (°C)	Adsorbed Species	Requirements	Relative Unit Area
0.5%	123	linear	all sites (typically low coordination)	3.6
	246	bridged	2-fold hollow site	3.9
	369	3-fold bridged	3-fold hollow site (typically found on 111 surfaces)	1.0
0.65%	172	linear	all sites (typically low coordination)	12.1
	247	bridged	2-fold hollow site	28.9
	372	3-fold bridged	3-fold hollow site (typically found on 111 surfaces)	1.0

The three modes of adsorption for each catalyst have been studied more closely providing a good comparison between the two catalyst samples in terms of surface morphology. In order to compare the amounts of each of the modes of adsorption

found for one catalyst with the other it was necessary to fit gaussian curves to the plots, this was carried out using the Origin data handling package. Table 5.2.1 lists the characteristics of each catalyst.

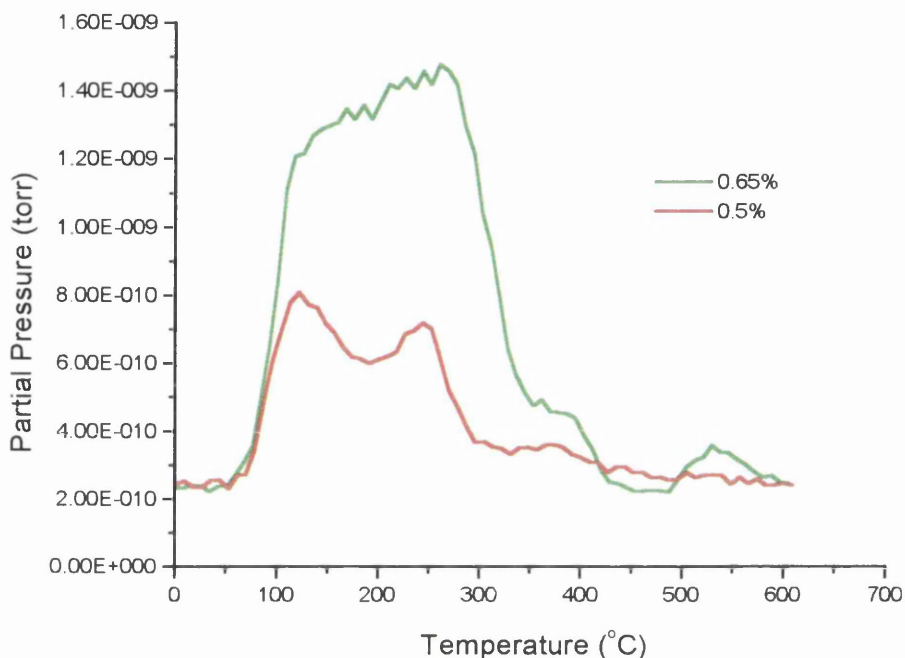


**Fig. 5.2.12** Desorption Spectra of CO from the Pt/Al<sub>2</sub>O<sub>3</sub> Catalysts.

Conclusions can be drawn from this information with respect to the structure and morphology of the metal crystallites. It is shown that the 0.65% catalyst has more linear species compared to the 0.5% catalysts but less 3-fold bridged species. As the 3-fold species requires Pt(111) planes and the number of faces of this symmetry increases with particle size [91, 92], it is therefore clear from this information that the 0.5% Pt/Al<sub>2</sub>O<sub>3</sub> consists of metal particles of larger size. This correlates well with the adsorption isotherm measurements and the particle size data obtained from the TEM.

The position of the peaks, in particular the linear adsorption, also provide evidence to suggest that the metal crystallites are larger on the 0.5% catalyst compared to the 0.65%. The desorption temperature found for the linear species on the former is 123°C compared to 172°C for the latter. This suggests that the CO is bound to low coordination platinum atoms, which would be found with smaller particles, on the 0.65% catalyst compared to the 0.5% case. These results are consistent with those

found in the literature and reinforce the results collected from the other characterisation techniques used in this study, thus emphasising the importance of TPD as a powerful tool in catalytic chemistry.

### 5.2.6 Total Surface Area and Pore Size Measurements

The total surface area and pore size measurements were carried out as described in section 4.3.7, providing more information about the physical structure of the catalysts and how they differ from each other. Table 5.2.2 contains the results obtained during these measurements.

**Table 5.2.2** The Results from the Surface Area and Pore Volume Measurements.

Measurement	0.5% Pt/Al <sub>2</sub> O <sub>3</sub>	0.65% Pt/Al <sub>2</sub> O <sub>3</sub>
BET Surface Area (m <sup>2</sup> g <sup>-1</sup> )	95.0825	179.9537
Average Pore Diameter (A)	100.0156	85.2258
Single Point Total Pore Volume (pores less than 1000 A) (cm <sup>3</sup> g <sup>-1</sup> )	0.237743	0.383417
Micropore Volume (cm <sup>3</sup> g <sup>-1</sup> )	0.000860	-
BJH Desorption Cumulative Pore Volume (pores between 17 and 3000 A) (cm <sup>3</sup> g <sup>-1</sup> )	0.236203	0.390166

### 5.3 The Straight and Oxidative Dehydrogenation of Butane using an Empty Reactor Vessel

During the dehydrogenation of butane in the pursuit of butene species, many types of reaction take place. As a consequence of the high temperatures required in accordance with the thermodynamics, cracking reactions to form C<sub>3</sub>, C<sub>2</sub> and C<sub>1</sub> species, isomerisation to form *iso*-butane and aromatisation reactions forming condensed ring structures on the catalyst surface also take place in addition to dehydrogenation reactions[2, 34]. As a result of this it is necessary to perform the experiments using an empty reactor vessel under identical conditions to those with the catalyst, in order to determine which processes are taking place due to the active metal component and which can be attributed to homogeneous reactions taking place in the gas phase. The support material also contributes products, under certain conditions, to the overall product mixture. These processes are considered in section 5.4.

#### 5.3.1 Straight Dehydrogenation

Tables 5.3.1, 5.3.2 and 5.3.2 contain the conversion and product molar quantities, the product selectivity and the product yield values respectively for the straight dehydrogenation of butane using an empty reactor vessel. It is apparent that under the conditions described in section 4.1.3 and using the equipment specified in chapter 2 that no reactions take place until temperatures above 500°C have been reached. At this point no dehydrogenation is observed and only cracking reactions forming methane and ethane together with isomerisation processes producing *iso*-butane take place. These observations have been seen in similar work carried out for the propane system and highlight the difficulties involved in trying to produce alkenes from alkanes at high temperatures [18, 58, 95].

Figure 5.3.1 contains a graphical representation of the experimental conversion observed, as a function of temperature, under these conditions using an empty reactor vessel. Also shown on the figure is the equilibrium curve for conversion obtained as explained in section 5.1. It is clear that the experimental value is significantly less than it should be in theory. Because the empty vessel contains no catalyst or support material on the glass sinter, the reactant gas experiences a relatively un-obstructed

passage through the vessel resulting in short residence times inside the reactor. As a consequence, it is possible that the reactant gas does not reach the reaction temperature, resulting in lower than expected conversion figures. In hindsight, the use of a preheating coil could have been employed allowing the temperature of the reactant gas flow to reach that set on the programmer. However, as the conversion obtained was higher than the literature values (10% compared to 1% [58]), the initial experimental arrangement was retained [18, 58, 95].

The products formed at these temperatures, using the empty reactor vessel, represent homogeneous gas phase reactions. The results shown above can be used when analysing the catalyst test results so that contributions to the product mixture that do not belong to surface reaction pathways can be determined.

### 5.3.2 Oxidative Dehydrogenation

The above study carried out under straight dehydrogenation conditions was repeated using a mixture of butane and oxygen in a 2:1 butane:oxygen ratio in order to simulate oxidative dehydrogenation reactions. Section 4.1.3 describes how the reaction was carried out. Again the purpose of this study was to determine which processes occurred due to gas phase homogeneous reactions and at what temperature they were initiated. Tables 5.3.4, 5.3.5 and 5.3.6 contain the conversion and product molar quantities, the product selectivity and the product yield values respectively for the oxidative dehydrogenation of butane using an empty reactor vessel. The conversion and dehydrogenation selectivity plots are shown on figure 5.3.3 with a more detailed breakdown of the olefin species formed illustrated on figure 5.3.4. It is shown that as the temperature increases the conversion of butane increases as expected. In comparison to the straight dehydrogenation shown above, the homogeneous reactions occur at lower temperatures. Indeed, conversions of approximately 10% are observed at 200°C while at 400°C almost 20% of the butane in the reactant mixture has reacted. This is the main reason for pursuing oxidative dehydrogenation as an alternative route in the production of olefins.

It is also interesting to see that without the presence of a catalyst there is dehydrogenation taking place. In fact, 25-30% selectivity towards dehydrogenation is observed between 400-500°C. Figure 5.3.4 shows that the most favoured species

formed is but-1-ene (15-17%) with *trans* and *cis* but-2-ene also formed to a lesser extent (5-7%). It can also be observed that above temperatures of 500°C 1,3-butadiene is also formed. These processes are due to radical reactions between the oxygen and the butyl radicals formed during thermal pyrolysis, possibly following the pathways described in the equations below [58]. Initiation by an the oxygen atom abstracting a hydrogen atom, forming a butyl radical could also be possible. Water is also formed as a result of these radical processes. This was confirmed by visual inspection of the exhaust side of the reactor, where water condensation was clearly seen.

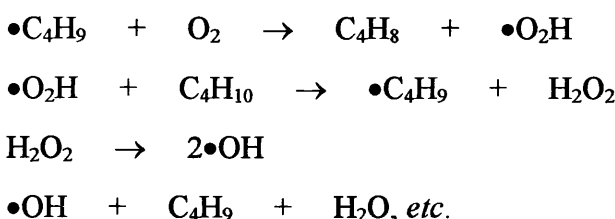


Figure 5.3.5 illustrates the dehydrogenation yield, which plots the dehydrogenation selectivity in association with conversion. It is shown that the maximum yield of dehydrogenation products is at 500°C and therefore this is the optimum temperature at which this reaction operates when production of olefins is the reaction of interest. In a similar way to the dehydrogenation selectivity, the dehydrogenation yield decreases above this temperature. This happens as a result of cracking reactions taking place, forming smaller chain alkanes in the same way as in the straight dehydrogenation, which reduces the selectivity resulting in decreasing yield.

The higher temperature processes such as cracking reactions and isomerisation of butane to *iso*-butane are illustrated in figure 5.3.6. It is shown that these reactions do not occur until temperatures of approximately 400°C are reached. At this temperature the most abundant product formed is *iso*-butane with ethane/ethene and methane produced as a result of C-C bond fission. Ethane and ethene were not separable in the GC columns used. It is important to observe that only very small amounts, if any, of propane are formed. It could be that the initial cracking reaction takes place between C<sub>2</sub> and C<sub>3</sub> to form two moles of ethane, then methane forms from the cracking reaction of ethane. This would result in no propane formation.

Two other products are also formed during this reaction. Partial oxidation takes place, when the oxygen reacts with the hydrocarbons molecules, with the resultant formation of carbon monoxide at temperatures in excess of 300°C. The selectivity is highest at 400°C and starts to decrease as a result of the cracking reaction taking place. Carbon dioxide also forms but at a lesser extent. This again is as a consequence of the short residence time within the reactor vessel. If the residence time was longer, total oxidation would occur and carbon dioxide would be the expected dominant product.

**Table 5.3.1** Conversion and Product Molar Quantities for the Straight Dehydrogenation of Butane without the presence of a Catalyst.

Temp. (°C)	Moles Bypass (x10 <sup>-7</sup> )	Moles Reacted (x10 <sup>-7</sup> )	Conv. (%)	Met. (x10 <sup>-7</sup> )	Eth. (x10 <sup>-7</sup> )	Iso (x10 <sup>-7</sup> )	B-1 (x10 <sup>-7</sup> )	Trans B-2 (x10 <sup>-7</sup> )	Cis B-2 (x10 <sup>-7</sup> )	Diene (x10 <sup>-7</sup> )
200	38.74	0	0	0	0	0	0	0	0	0
300	38.74	0	0	0	0	0	0	0	0	0
400	38.74	0	0	0	0	0	0	0	0	0
500	38.74	0	0	0	0	0	0	0	0	0
600	38.74	3.92	10.1	1.05	1.38	1.03	0	0	0	0

**Table 5.3.2** Product Selectivity for the Straight Dehydrogenation of Butane without the presence of a Catalyst.

Temp. (°C)	Met. Sel. (%)	Eth. Sel. (%)	Iso Sel. (%)	B-1 Sel. (%)	Trans B-2 Sel. (%)	Cis B-2 Sel. (%)	Diene Sel. (%)	Dehydro. Sel. (%)
200	0	0	0	0	0	0	0	0
300	0	0	0	0	0	0	0	0
400	0	0	0	0	0	0	0	0
500	0	0	0	0	0	0	0	0
600	6.7	17.6	26.4	0	0	0	0	0

**Table 5.3.3** Product Yields for the Straight Dehydrogenation of Butane without the presence of a Catalyst.

Temp. (°C)	Met. Yield (%)	Eth. Yield (%)	Iso Yield (%)	B-1 Yield (%)	Trans B-2 Yield (%)	Cis B-2 Yield (%)	Diene Yield (%)	Dehydro. Yield (%)
200	0	0	0	0	0	0	0	0
300	0	0	0	0	0	0	0	0
400	0	0	0	0	0	0	0	0
500	0	0	0	0	0	0	0	0
600	0.68	1.78	2.67	0	0	0	0	0

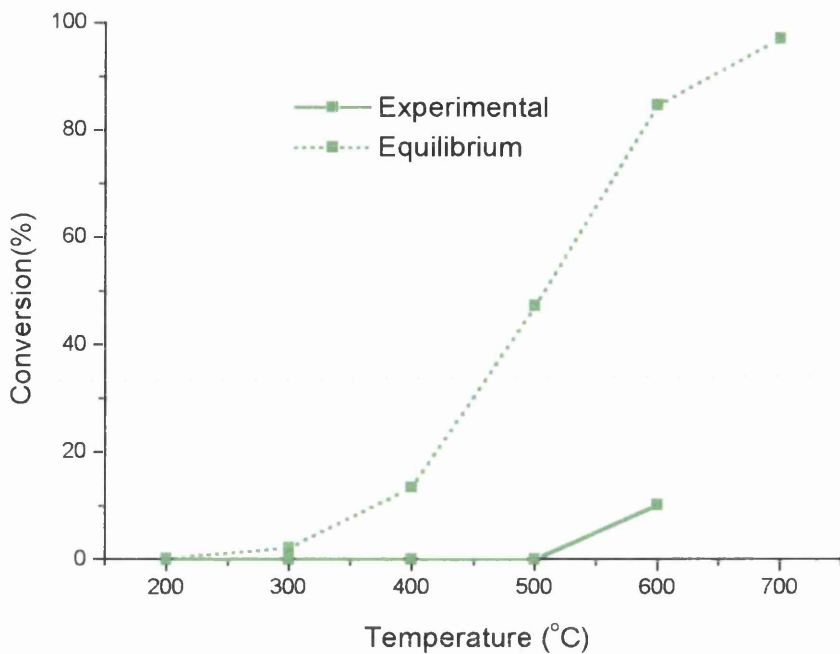


**Fig. 5.3.1** The Experimental and Equilibrium Conversion during the Straight Dehydrogenation of Butane using an Empty Reactor Vessel.

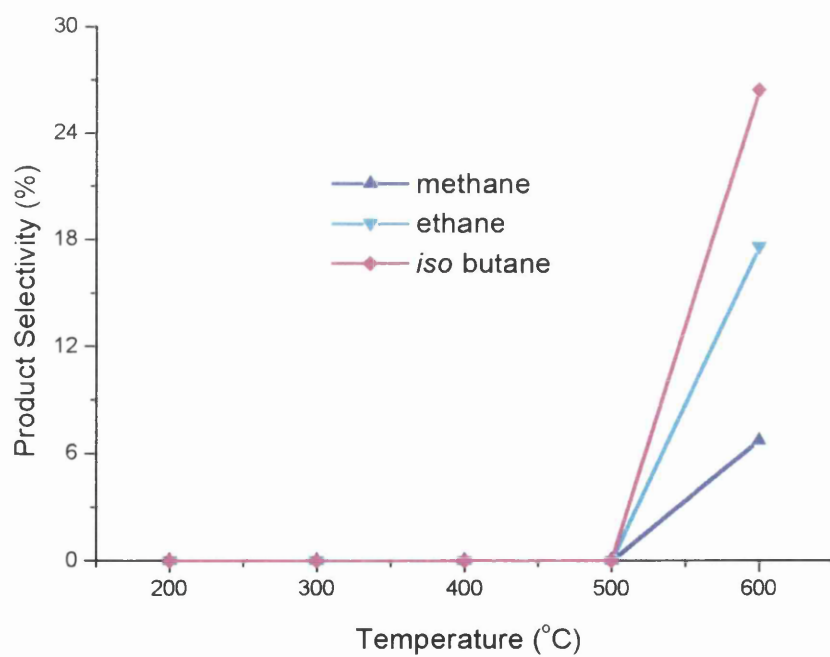


**Fig. 5.3.2** Product Selectivity as a function of Temperature during the Straight Dehydrogenation of Butane using an Empty Vessel.

**Table 5.3.4** Conversion and Product Molar Quantities for the Oxidative Dehydrogenation of Butane without the presence of a Catalyst.

Temp. (°C)	Moles Bypass (x10 <sup>-7</sup> )	Moles Reacted (x10 <sup>-7</sup> )	Conv. (%)	CO <sub>2</sub> /Pr (x10 <sup>-7</sup> )	CO (x10 <sup>-7</sup> )	Met. (x10 <sup>-7</sup> )	Eth. (x10 <sup>-7</sup> )	Iso (x10 <sup>-7</sup> )	B-1 (x10 <sup>-7</sup> )	Trans B-2 (x10 <sup>-7</sup> )	Cis B-2 (x10 <sup>-7</sup> )	Diene (x10 <sup>-7</sup> )
200	46.93	4.41	9.4	0	0	0	0	0	0	0	0	0
200	46.93	3.86	8.2	0	0	0	0	0	0	0	0	0
300	46.93	0.19	0.4	0	0	0	0	0	0	0	0	0
300	46.93	0	0	0	0	0	0	0	0	0	0	0
400	46.93	7.84	16.7	0.36	2.65	0.57	0.61	0.33	1.19	0.62	0.44	0
400	46.93	9.83	20.9	0.36	2.27	0.51	0.57	0.28	1.17	0.59	0.44	0
500	46.93	11.99	25.5	0.37	0.76	1.49	2.32	1.58	2.04	0.80	0.63	0
600	46.93	29.87	63.6	0.74	3.95	8.94	10.02	6.50	0.98	0.31	0.21	0.20
600	46.93	27.98	59.6	0.09	3.49	9.21	10.54	6.94	0.77	0.26	0.17	0.18

**Table 5.3.5** Product Selectivity for the Oxidative Dehydrogenation of Butane without the presence of a Catalyst.

Temp. (°C)	CO <sub>2</sub> /Pr Sel. (%)	CO Sel. (%)	Met. Sel. (%)	Eth. Sel. (%)	Iso Sel. (%)	B-1 Sel. (%)	Trans B-2 Sel. (%)	Cis B-2 Sel. (%)	Diene Sel. (%)	Dehydro. Sel. (%)
200	0	0	0	0	0	0	0	0	0	0
200	0	0	0	0	0	0	0	0	0	0
300	0	0	0	0	0	0	0	0	0	0
300	0	0	0	0	0	0	0	0	0	0
400	1.1	8.4	1.8	3.9	4.2	15.2	7.9	5.6	0	28.7
400	0.9	5.8	1.3	2.9	2.8	11.9	6.0	4.5	0	22.4
500	0.8	1.6	3.1	9.7	13.2	17.0	6.7	5.2	0	28.9
600	0.1	3.3	7.5	16.8	21.8	3.3	1.0	0.7	0.7	5.7
600	0.1	3.1	8.2	18.8	24.8	2.8	0.9	0.6	0.6	4.9

**Table 5.3.5** Product Yields for the Oxidative Dehydrogenation of Butane without the presence of a Catalyst.

Temp. (°C)	CO <sub>2</sub> /Pr Yield (%)	CO Yield (%)	Met. Yield (%)	Eth. Yield (%)	Iso Yield (%)	B-1 Yield (%)	Trans B-2 Yield (%)	Cis B-2 Yield (%)	Diene Yield (%)	Dehydro. Yield (%)
200	0	0	0	0	0	0	0	0	0	0
200	0	0	0	0	0	0	0	0	0	0
300	0	0	0	0	0	0	0	0	0	0
300	0	0	0	0	0	0	0	0	0	0
400	0.18	1.40	0.30	0.65	0.70	2.54	1.32	0.94	0	4.79
400	0.19	1.21	0.27	0.61	0.58	2.49	1.25	0.94	0	4.68
500	0.20	0.41	0.79	2.47	3.37	4.34	1.71	1.33	0	7.37
600	0.06	2.40	4.77	10.68	13.86	2.10	0.64	0.44	0.44	3.62
600	0.06	1.85	4.89	11.2	14.78	1.67	0.54	0.36	0.36	2.92

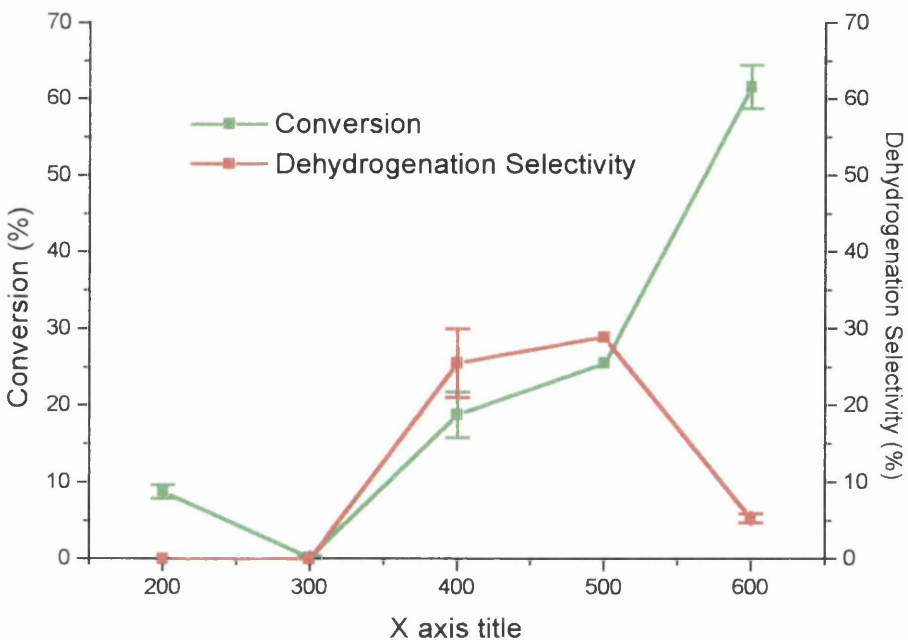


**Fig. 5.3.3** The Conversion and Dehydrogenation Selectivity during the Oxidative Dehydrogenation of Butane using an Empty Reactor Vessel.

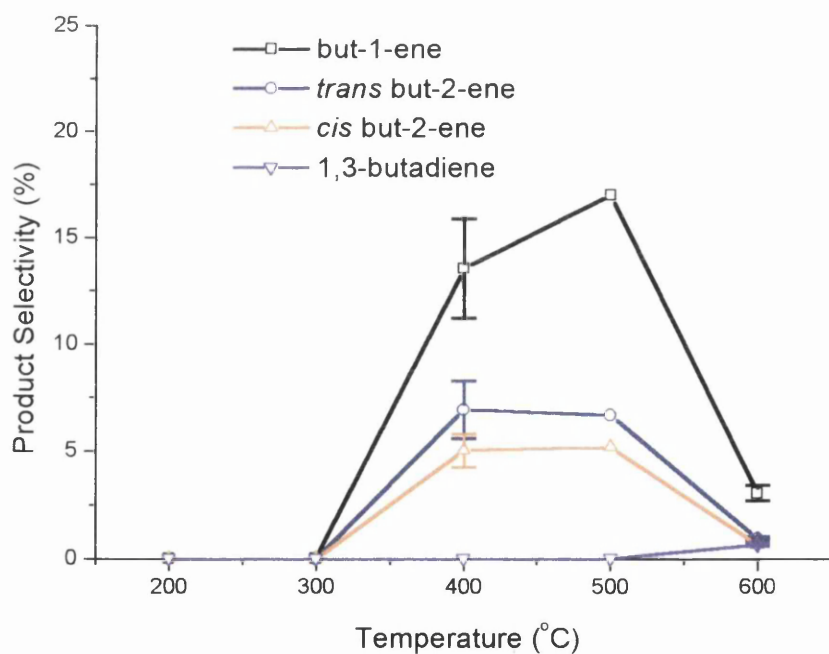


**Fig. 5.3.4** Selectivity to the Olefin species during the Oxidative Dehydrogenation of Butane using an Empty Reactor Vessel.

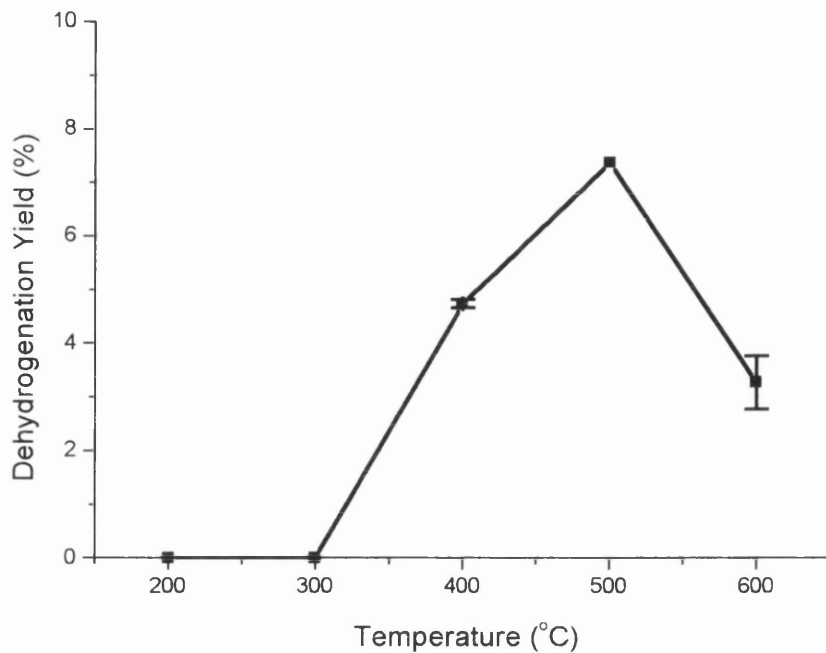


**Fig. 5.3.5** Dehydrogenation Yield during the Oxidative Dehydrogenation of Butane using an Empty Reactor Vessel.

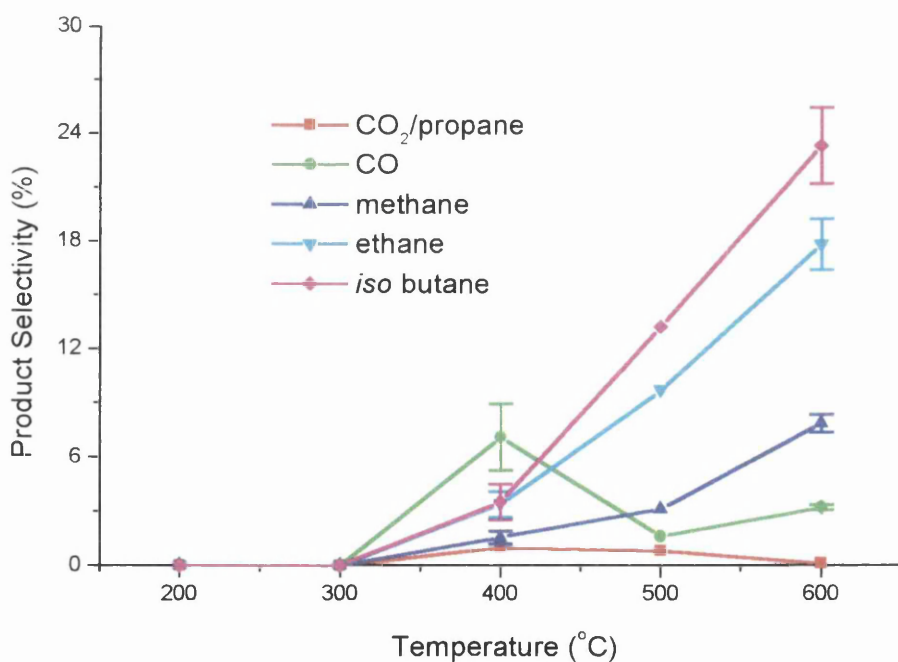


**Fig. 5.3.6** Product Selectivity during the Oxidative Dehydrogenation using an Empty Reactor Vessel.

## *5.4 The Straight and Oxidative Dehydrogenation of Butane using the $\gamma$ -Al<sub>2</sub>O<sub>3</sub> Support Material from the 0.5% Pt/Al<sub>2</sub>O<sub>3</sub> Catalyst*

In the section above the reactions were carried out using an empty reactor vessel in order that when the results from the catalyst testing are discussed the homogeneous gas phase reactions can be distinguished from catalytic processes. The catalysts under discussion throughout this work are supported metal catalysts. As well as distinguishing homogeneous processes it is also important to be able to assign reactions to those taking place on the support material. Knowing which reactions take place on the support and which take place in the gas phase allows the reactions which take place on the metal particles to be specifically identified.

A study has been conducted where the straight and oxidative dehydrogenation reactions have been carried out at various temperatures on the support material from the 0.5% Pt/Al<sub>2</sub>O<sub>3</sub> catalyst. Due to time restrictions placed on the project it was not possible to carry out similar work on the alumina support of the 0.65% catalyst. This was also  $\gamma$ -alumina and is expected to yield similar results to the support used for the 0.5% catalyst. Nevertheless, the results given below should provide some information on the reactions which take place as a result of the alumina component. Section 3.1.2 in the materials chapter outlines the need for support materials and describes some of the properties of alumina substrates.

### **5.4.1 Straight Dehydrogenation using the 0.5% Pt/Al<sub>2</sub>O<sub>3</sub> Support material**

Section 4.1.3 describes the methods used to carry out this body of work. Tables 5.4.1, 5.4.2 and 5.4.3 contain the conversion and product molar quantities, the product selectivity and the product yield values respectively for the straight dehydrogenation of butane using the support material. Figures 5.4.1 - 5.4.8 graphically represent these results with respect to the conversion, individual product selectivity, dehydrogenation selectivity and dehydrogenation yield as a function of time and temperature, showing the equilibrium results, where appropriate, for comparison.

The results show that virtually no conversion occurred at 500°C (<1%) with subsequently no product formation apart from a small amount of *iso*-butane which

could result from the acidic sites on the support material [73]. At 600 and 700°C significant conversions are reached, approximately 20 and 65% respectively. This is due partly to homogeneous reactions, as a consequence of the high temperatures, and the acidic site processes which induce cracking reactions and butane isomerisation. In both cases the resultant products are mainly methane and ethane formed as discussed above and *iso*-butane (figures 5.4.5 - 5.4.6).

The selectivity towards dehydrogenation products is minimal especially at 600°C, where only *trans* but-2-ene is formed at a selectivity of <1%. On comparison with the equilibrium value (34.24%) this is a very low amount indeed (see figure 5.4.5). At 700°C the dehydrogenation selectivity is higher at approximately 4%, with all the C<sub>4</sub> olefin species formed. However, when compared to the equilibrium amounts it is clear, again, that the reaction is under-performing with respect to dehydrogenation. This also, as explained above, stems from the escalation of the cracking products and butane isomerisation which take place at this high temperature.

When the dehydrogenation selectivity and conversion are used to calculate the yield, figure 5.4.8 shows that as the temperature is increased the dehydrogenation yield also increases, as expected. Again, when the experimental results are plotted along with the equilibrium yield it is clear that the reaction is under performing in terms of dehydrogenation and that a range of other processes are occurring, other than that described by the dehydrogenation reactions.

#### 5.4.2 Oxidative Dehydrogenation using the 0.5% Pt/Al<sub>2</sub>O<sub>3</sub> Support material

The above study carried out under straight dehydrogenation conditions was repeated using a mixture of butane and oxygen in a 2:1 butane:oxygen ratio in order to simulate the oxidative dehydrogenation reactions. Section 4.1.3 describes how these reactions were carried out. Tables 5.4.4, 5.4.5 and 5.4.6 list the conversion and product molar quantities, the product selectivity and the product yield values respectively for the oxidative dehydrogenation of butane using the support material.

The results are very similar to those for the empty vessel reactions indicating that the processes taking place are due almost exclusively to homogeneous processes. Figures 5.4.9 - 5.4.17 illustrate these results with respect to the conversion, individual product selectivity, dehydrogenation selectivity and dehydrogenation yield as a

function of time and temperature. It is shown again that the conversion increases as the temperature is increased. At 400 and 500°C approximately 20% of the butane is converted while at 600°C this figure rises to 60%.

The selectivity to the dehydrogenation products proceeds through a maximum in the same way as it did in the case of the empty vessel (compare figures 5.4.15 and 5.3.3). The highest dehydrogenation selectivity occurred at 400 and 500°C where values of 30% and 20% were obtained respectively. Thereafter there was a decrease to <10% at 600°C as the cracking and isomerisation processes dominate.

Figures 5.4.12 - 5.4.14 contain the specific product selectivity at each of the temperatures studied. At 400°C the most dominant product formed was but-1-ene with *trans* and *cis* but-2-ene also formed. Cracking and isomerisation reactions products were also formed in small amounts (<6%). At 500°C the most notable change is the large increase in the amount of isomerisation that is taking place with selectivity as high as approximately 25% compared to 3% at 400°C. Again, for the reasons explained above, this could be due to the effect of the support material at high temperatures, as well as homogeneous reactions. There is also an increase in the cracking products with methane and ethane being formed in greater quantities.

At 600°C dehydrogenation is reduced as discussed previously and there is a significant increase in the amount of *iso*-butane and ethane produced. Again, these results are due to a combination of the support material and to homogeneous reactions [58, 73].

In a similar way to the empty vessel reactions there is C<sub>1</sub> oxygenate formation. Figure 5.4.17 shows that selectivity towards CO and CO<sub>2</sub> is minimal with a maximum of approximately 7% for both at 500°C. Again, these products form as a result of combustion processes between the hydrocarbon(s) and the oxygen.

**Table 5.4.1** Conversion and Product Molar Quantities for the Straight Dehydrogenation of Butane using 0.5% Pt/Al<sub>2</sub>O<sub>3</sub> Support Material.

Temp. (°C)	Time (mins)	Moles Bypass (x10 <sup>-7</sup> )	Moles Reacted (x10 <sup>-7</sup> )	Conv. (%)	Met. (x10 <sup>-7</sup> )	Eth. (x10 <sup>-7</sup> )	Iso (x10 <sup>-7</sup> )	B-1 (x10 <sup>-7</sup> )	Trans B-2 (x10 <sup>-7</sup> )	Cis B-2 (x10 <sup>-7</sup> )	Diene (x10 <sup>-7</sup> )
500	0	41.56	0.22	0.5	0	0	0.04	0	0	0	0
500	23	41.56	0	0	0	0	0	0	0	0	0
500	49	41.56	0.33	0.8	0	0	0.04	0	0	0	0
500	71	41.56	0	0	0	0	0	0	0	0	0
500	101	41.56	0.53	1.3	0	0	0	0	0	0	0
600	0	51.00	14.26	28.0	0.77	0.93	0.72	0	0.05	0	0
600	21	51.00	10.73	21.0	0.79	0.98	0.75	0	0.04	0	0
600	46	51.00	10.88	21.3	0.78	0.97	0.74	0	0	0	0
600	73	51.00	8.82	17.3	0.80	1.02	0.81	0	0.05	0	0
600	112	51.00	10.56	20.1	0.74	0.96	0.74	0	0.05	0	0
600	162	51.00	10.18	20.0	0.72	0.88	0.77	0	0.08	0	0
700	0	45.30	33.90	74.8	7.98	11.31	5.62	0.39	0.22	0.17	0.67
700	23	45.30	30.52	67.4	9.95	14.91	7.25	0.39	0.21	0.17	0.72
700	53	45.30	28.60	63.1	11.09	16.71	8.24	0.44	0.21	0.17	0.64
700	77	45.30	30.37	67.0	9.97	15.12	7.41	0.39	0.16	0.18	0.42
700	99	45.30	30.62	66.3	10.34	15.53	7.67	0.40	0.14	0.15	0.43
700	122	45.30	29.83	65.8	10.57	16.00	7.86	0.42	0.16	0.12	0.40

**Table 5.4.2** Product Selectivity for the Straight Dehydrogenation of Butane using 0.5% Pt/Al<sub>2</sub>O<sub>3</sub> Support Material.

Temp. (°C)	Time (mins)	Met. Sel. (%)	Eth. Sel. (%)	Iso Sel. (%)	B-1 Sel. (%)	Trans B-2 Sel. (%)	Cis B-2 Sel. (%)	Diene Sel. (%)	Dehydro. Sel. (%)
500	0	0	0	18.2	0	0	0	0	0
500	23	0	0	0	0	0	0	0	0
500	49	0	0	12.1	0	0	0	0	0
500	71	0	0	0	0	0	0	0	0
500	101	0	0	0	0	0	0	0	0
600	0	1.3	3.3	5.0	0	0.4	0	0	0.4
600	21	1.8	4.6	7.0	0	0.4	0	0	0.4
600	46	1.8	4.4	6.8	0	0	0	0	0
600	73	2.3	5.8	9.2	0	0.6	0	0	0.6
600	112	1.8	4.5	7.0	0	0.5	0	0	0.5
600	162	1.8	4.3	7.6	0	0.8	0	0	0.8
700	0	5.9	16.7	16.6	1.2	0.6	0.5	2.0	4.3
700	23	8.2	24.2	23.8	1.3	0.7	0.6	2.4	5.0
700	53	9.7	29.2	28.8	1.5	0.7	0.6	2.2	5.0
700	77	8.2	24.9	24.4	1.3	0.5	0.6	1.4	3.8
700	99	8.4	25.4	25.0	1.3	0.4	0.5	1.4	3.6
700	122	8.8	26.8	26.3	1.4	0.5	0.4	1.3	3.6

**Table 5.4.3** Product Yields for the Straight Dehydrogenation of Butane using 0.5% Pt/Al<sub>2</sub>O<sub>3</sub> Support Material.

Temp. (°C)	Time (mins)	Met. Yield (%)	Eth. Yield (%)	Iso Yield (%)	B-1 Yield (%)	Trans B-2 Yield (%)	Cis B-2 Yield (%)	Diene Yield (%)	Dehydro. Yield (%)
500	0	0	0	0.09	0	0	0	0	0
500	23	0	0	0	0	0	0	0	0
500	49	0	0	0.10	0	0	0	0	0
500	71	0	0	0	0	0	0	0	0
500	101	0	0	0	0	0	0	0	0
600	0	0.36	0.92	1.40	0	0.11	0	0	0.11
600	21	0.38	0.97	1.47	0	0.08	0	0	0.08
600	46	0.38	0.94	1.45	0	0	0	0	0
600	73	0.40	1.00	1.59	0	0.10	0	0	0.10
600	112	0.37	0.93	1.45	0	0.10	0	0	0.10
600	162	0.36	0.88	1.52	0	0.16	0	0	0.16
700	0	4.41	12.49	12.42	0.90	0.45	0.37	1.50	3.22
700	23	5.53	16.44	16.04	0.88	0.47	0.40	1.62	3.37
700	53	6.12	18.42	18.17	0.95	0.44	0.38	1.39	3.16
700	77	5.49	16.38	16.35	0.87	0.34	0.40	0.94	2.55
700	99	5.57	16.34	16.58	0.86	0.26	0.33	0.93	2.39
700	122	5.79	17.63	17.30	0.92	0.33	0.26	0.86	2.37

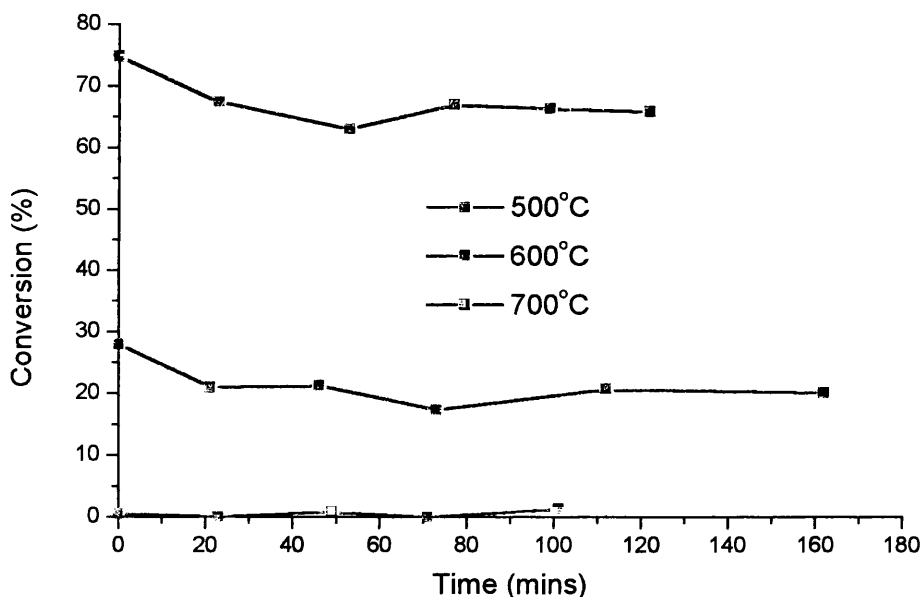


**Fig. 5.4.1** Conversion as a function of Time during the Straight Dehydrogenation of Butane at various Temperatures using the Support Material.

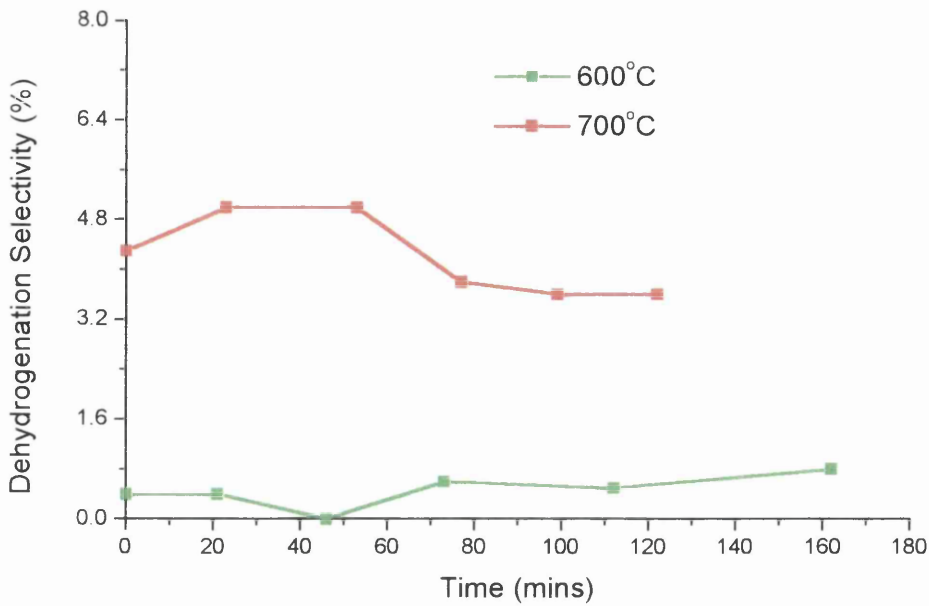


**Fig. 5.4.2** Dehydrogenation Selectivity as a function of Time during the Straight Dehydrogenation of Butane at various Temperatures using the Support Material.

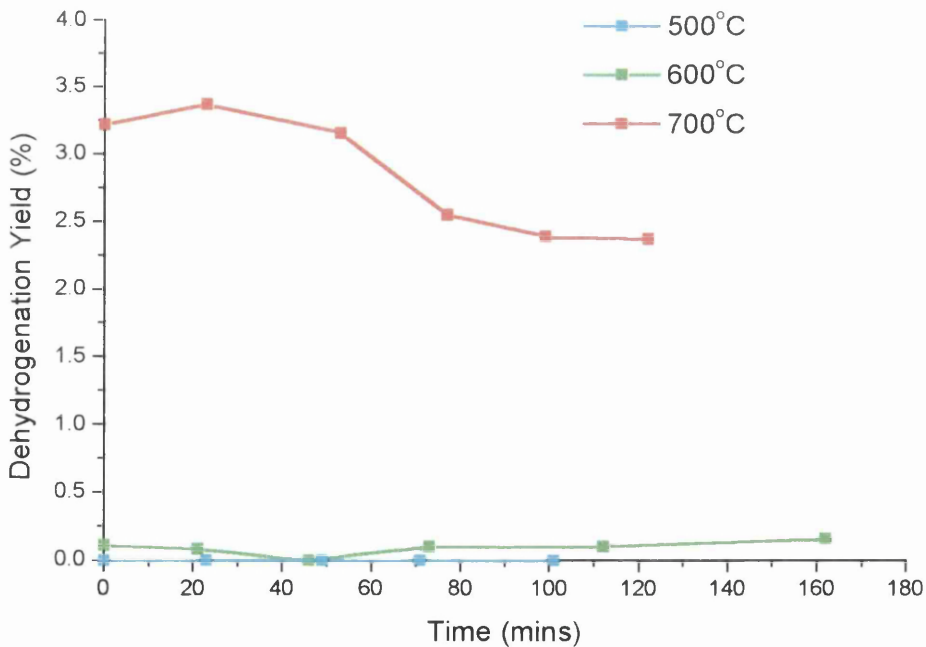


**Fig. 5.4.3** Dehydrogenation Yield as a function of Time during the Straight Dehydrogenation of Butane at various Temperatures using the Support Material.

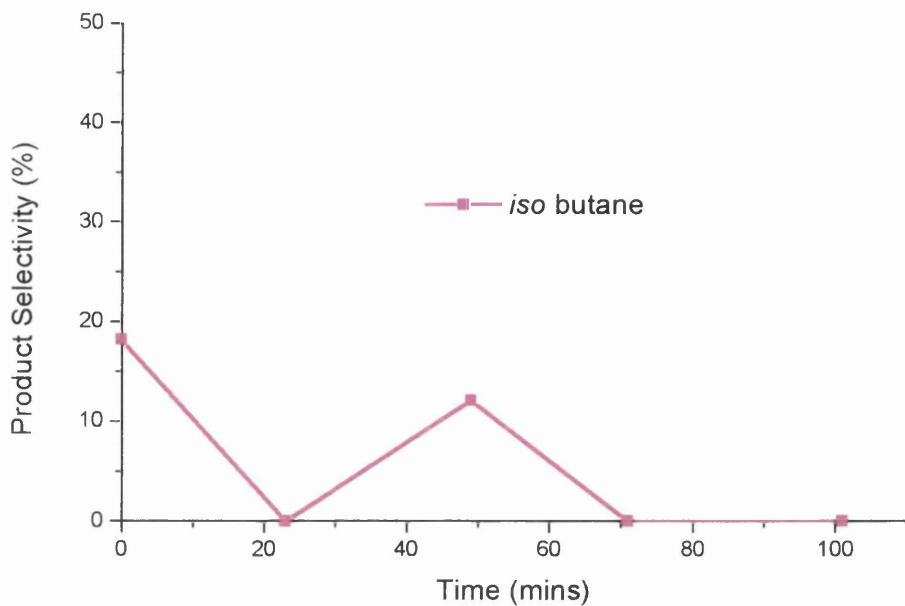


**Fig. 5.4.4** Product Selectivity as a function of Time during the Straight Dehydrogenation of Butane using the Support Material at 500°C.

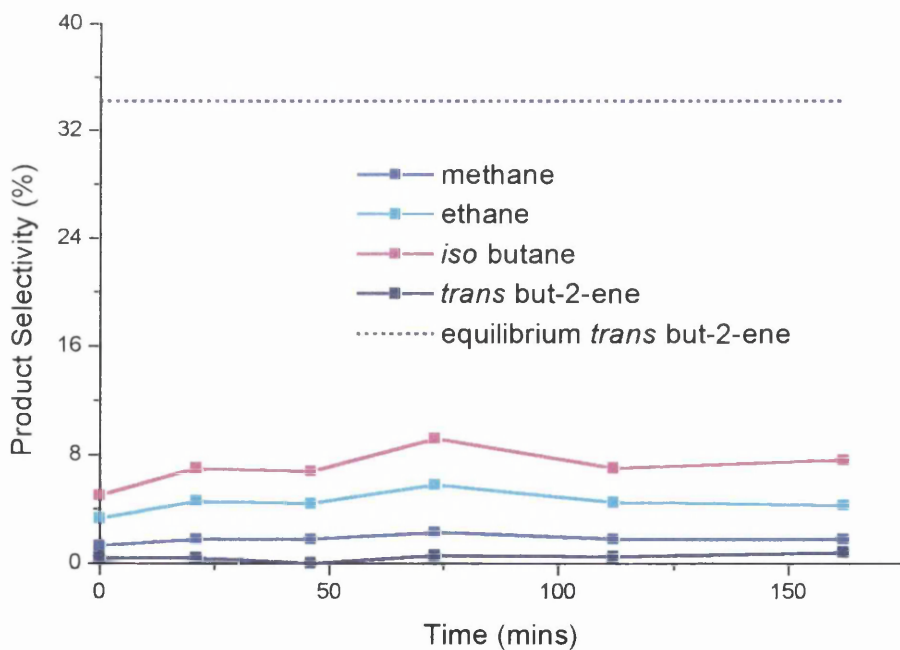


**Fig. 5.4.5** Product Selectivity as a function of Time during the Straight Dehydrogenation of Butane using the Support Material at 600°C.

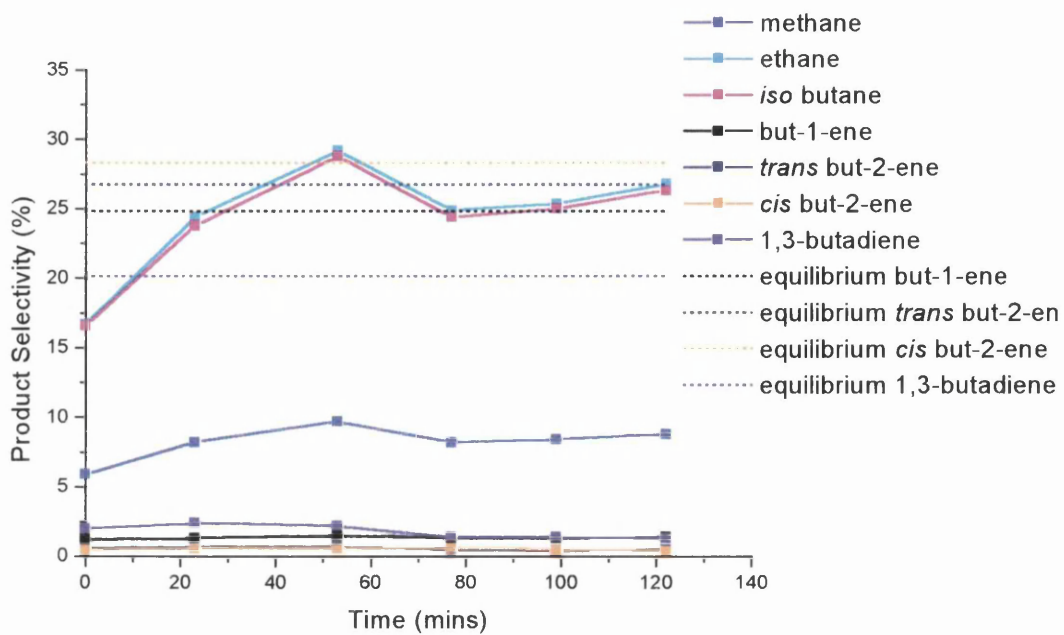


**Fig. 5.4.6** Product Selectivity as a function of Time during the Straight Dehydrogenation of Butane using the Support Material at 700°C.

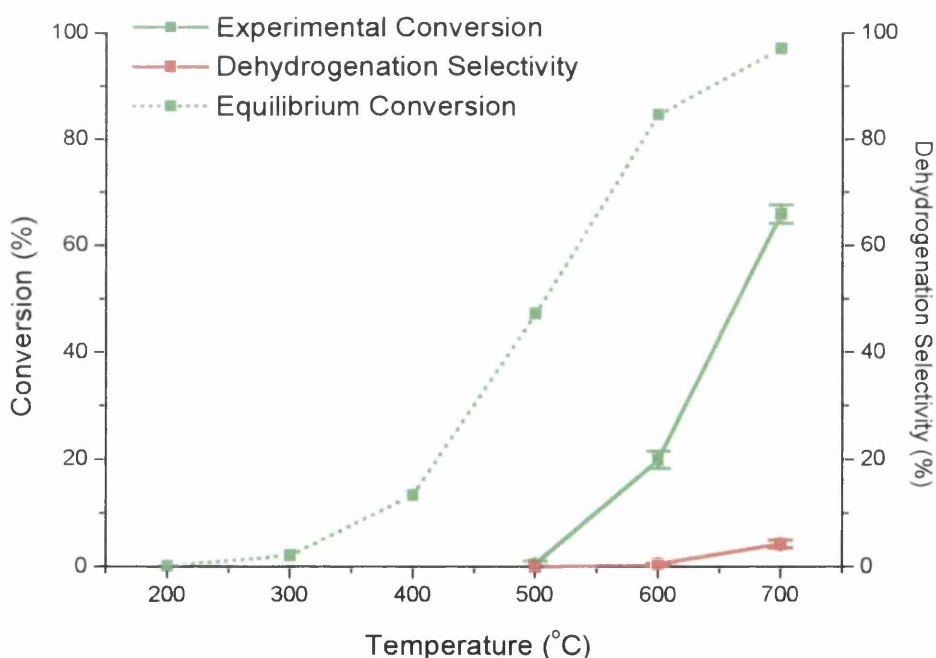


**Fig. 5.4.7** Experimental and Equilibrium Conversion and Dehydrogenation Selectivity during the Straight Dehydrogenation of Butane using the Support Material.

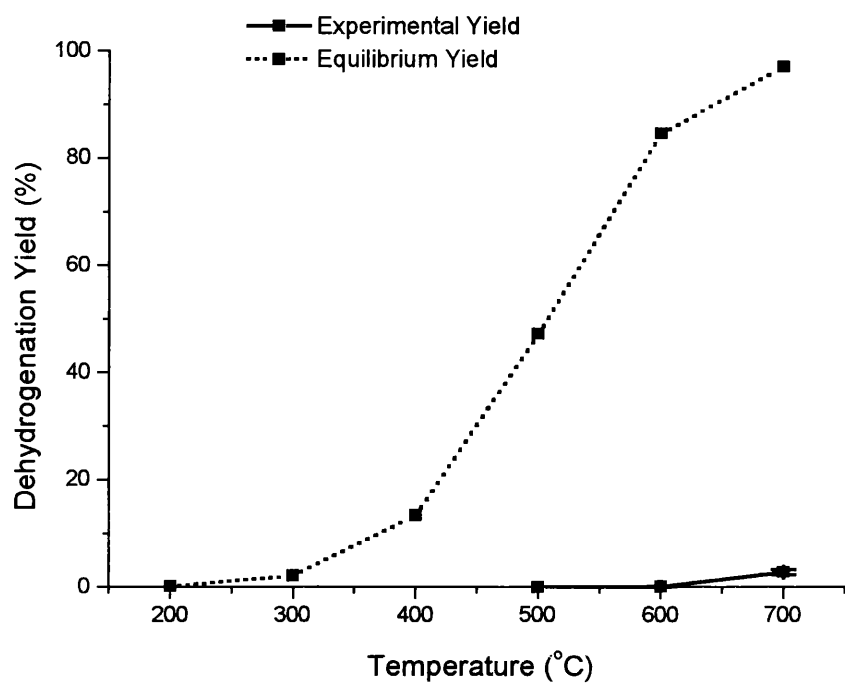


**Fig. 5.4.8** Experimental and Equilibrium Dehydrogenation Yield during the Straight Dehydrogenation of Butane using the Support Material.

**Table 5.4.4** Conversion and Product Molar Quantities for the Oxidative Dehydrogenation of Butane using 0.5% Pt/Al<sub>2</sub>O<sub>3</sub> Support Material.

Temp. (°C)	Time (mins)	Moles Bypass (x10 <sup>-7</sup> )	Moles Reacted (x10 <sup>-7</sup> )	Conv. (%)	CO <sub>2</sub> /Pr (x10 <sup>-7</sup> )	CO (x10 <sup>-7</sup> )	Met. (x10 <sup>-7</sup> )	Eth. (x10 <sup>-7</sup> )	Iso (x10 <sup>-7</sup> )	B-1 (x10 <sup>-7</sup> )	Trans B-2 (x10 <sup>-7</sup> )	Cis B-2 (x10 <sup>-7</sup> )	Diene (x10 <sup>-7</sup> )
400	0	46.93	10.41	22.2	0.77	1.44	0	0.30	0.24	1.19	0.58	0.49	0
400	52	46.93	8.31	17.7	0.78	2.15	0.24	0.46	0.32	1.39	0.67	0.56	0
400	107	46.93	7.55	16.1	0.77	1.49	0	0.29	0.19	1.06	0.50	0.35	0
400	161	46.93	3.28	7	0.66	1.02	0	0.18	0.12	0.83	0.45	0.33	0
400	209	46.93	4.89	10.4	0.67	0.92	0.06	0.17	0.11	0.81	0.44	0.27	0
500	0	46.93	6.82	14.5	1.55	2.40	0.60	0.72	0.77	0.62	0.31	0.27	0.10
500	53	46.93	5.36	11.4	2.21	2.55	1.45	1.23	1.45	0.72	0.45	0.42	0.14
500	108	46.93	10.72	22.8	2.38	2.59	1.92	1.76	1.88	0.73	0.42	0.44	0.10
500	158	46.93	6.6	14.1	2.16	2.56	1.57	1.25	1.58	0.72	0.46	0.45	0.07
500	223	46.93	7.59	16.2	2.30	2.40	1.86	1.25	1.58	0.68	0.42	0.40	0.11
600	0	46.93	20.17	43	1.40	3.71	6.39	7.34	5.53	0.59	0.47	0.43	0.14
600	50	46.93	30.03	64	1.33	5.12	6.55	7.63	5.57	0.90	0.46	0.35	0.17
600	110	46.93	30.95	65.9	1.08	5.32	6.83	7.63	5.48	0.81	0.41	0.39	0.24
600	157	46.93	24.34	51.9	0.93	4.12	7.16	7.49	5.99	0.97	0.41	0.28	0.18

**Table 5.4.5** Product Selectivity for the Oxidative Dehydrogenation of Butane using 0.5% Pt/Al<sub>2</sub>O<sub>3</sub> Support Material.

Temp. (°C)	Time (mins)	CO <sub>2</sub> /Pr Sel. (%)	CO Sel. (%)	Met. Sel. (%)	Eth. Sel. (%)	Iso Sel. (%)	B-1 Sel. (%)	Trans B-2 Sel. (%)	Cis B-2 Sel. (%)	Diene Sel. (%)	Dehydro. Sel. (%)
400	0	1.8	3.4	0	1.4	2.3	11.4	5.6	4.7	0	21.7
400	52	2.3	6.5	0.7	2.8	3.8	16.7	8.1	6.7	0	31.5
400	107	2.5	4.9	0	1.9	2.5	14.0	6.6	4.6	0	25.3
400	161	5.0	7.8	0	2.7	3.6	25.3	13.7	10.1	0	49.1
400	209	3.4	4.7	0.3	1.7	2.2	16.6	9.0	5.5	0	31.1
500	0	5.7	8.8	2.2	5.3	11.3	9.1	4.5	4.0	1.5	19.1
500	53	10.3	11.9	6.8	11.5	27.0	13.4	8.4	7.8	2.6	32.3
500	108	5.6	6.0	4.5	8.2	17.5	6.8	3.9	4.1	0.9	15.8
500	158	8.2	9.7	5.9	9.5	23.9	10.9	7.0	6.8	1.1	25.8
500	223	7.6	7.9	6.1	8.2	20.8	9.0	5.5	5.3	1.4	21.2
600	0	1.7	4.6	7.9	18.2	27.4	2.9	2.3	2.1	0.7	8.1
600	50	1.1	4.3	5.4	12.7	18.4	3.0	1.5	1.2	0.6	6.3
600	110	0.9	4.3	5.5	12.3	17.7	2.6	1.3	1.3	0.8	6.0
600	157	1.0	4.2	7.4	15.4	24.6	4.0	1.7	1.2	0.7	7.6

**Table 5.4.6** Product Yields for the Oxidative Dehydrogenation of Butane using 0.5% Pt/Al<sub>2</sub>O<sub>3</sub> Support Material.

Temp. (°C)	Time (mins)	CO <sub>2</sub> /Pr Yield (%)	CO Yield (%)	Met. Yield (%)	Eth. Yield (%)	Iso Yield (%)	B-1 Yield (%)	Trans B-2 Yield (%)	Cis B-2 Yield (%)	Diene Yield (%)	Dehydro. Yield (%)
400	0	0.41	0.77	0	0.32	0.51	2.54	1.24	1.04	0	4.82
400	52	0.42	1.14	0.13	0.49	0.68	2.96	1.43	1.19	0	5.58
400	107	0.41	0.79	0	0.31	0.40	2.26	1.06	0.74	0	4.07
400	161	0.35	0.54	0	0.19	0.26	1.77	0.96	0.7	0	3.43
400	209	0.36	0.49	0.03	0.18	0.23	1.72	0.94	0.58	0	3.24
500	0	0.82	1.28	0.32	0.77	1.64	1.32	0.66	0.57	0.21	2.77
500	53	1.18	1.36	0.77	1.31	3.09	1.53	0.96	0.89	0.3	3.69
500	108	1.27	1.37	1.02	1.88	4.00	1.56	0.89	0.94	0.21	3.6
500	158	1.15	1.36	0.84	1.33	3.37	1.53	0.98	0.96	0.15	3.62
500	223	1.22	1.28	0.99	1.33	3.37	1.45	0.89	0.85	0.23	3.43
600	0	0.74	1.98	3.40	7.82	11.78	1.26	1	0.92	0.3	3.47
600	50	0.71	2.73	3.49	8.13	11.87	1.92	0.98	0.74	0.36	4
600	110	0.58	2.83	3.64	8.13	11.68	1.72	0.87	0.83	0.51	3.94
600	157	0.50	2.19	3.81	7.98	12.76	2.07	0.87	0.6	0.38	3.92

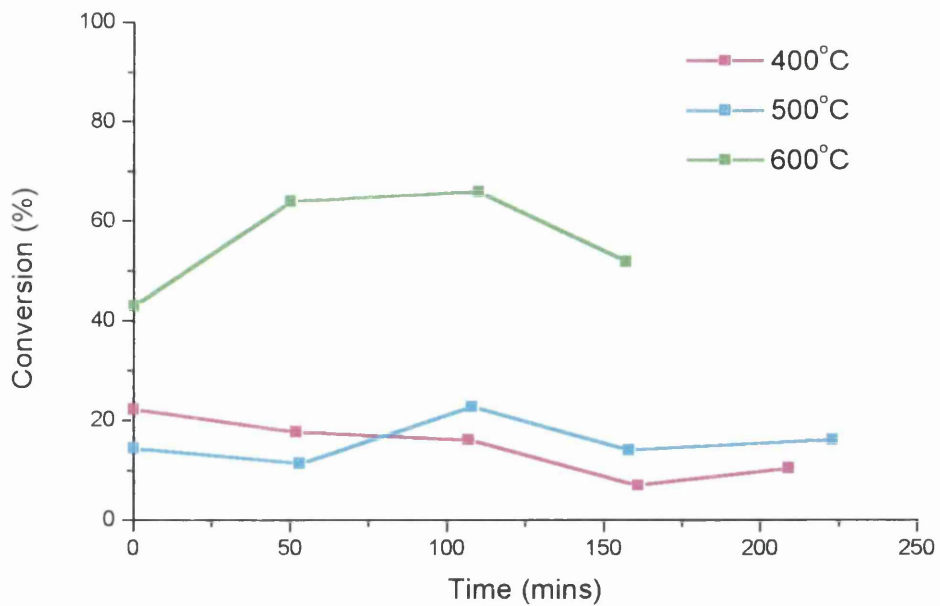


**Fig. 5.4.9** Conversion as a function of Time during the Oxidative Dehydrogenation of Butane using the Support Material.

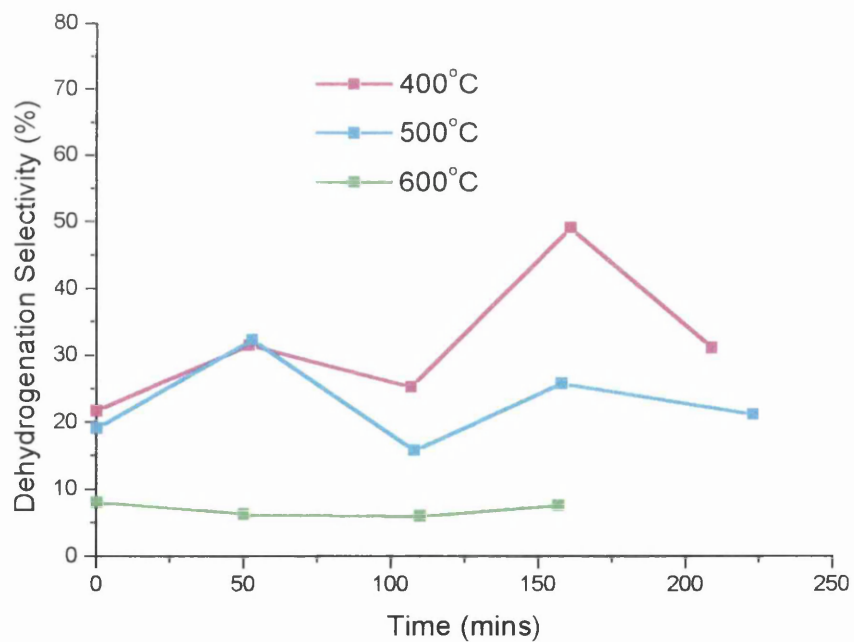


**Fig. 5.4.10** Dehydrogenation Selectivity as a function of Time during the Oxidative Dehydrogenation of Butane using the Support Material.

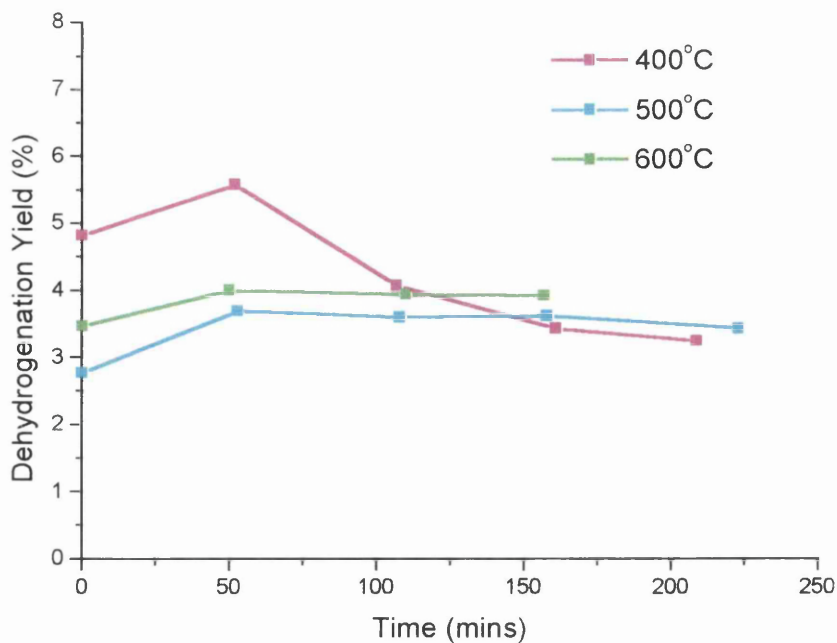


**Fig. 5.4.11** Dehydrogenation Yield as a function of Time during the Oxidative Dehydrogenation of Butane using the Support Material.

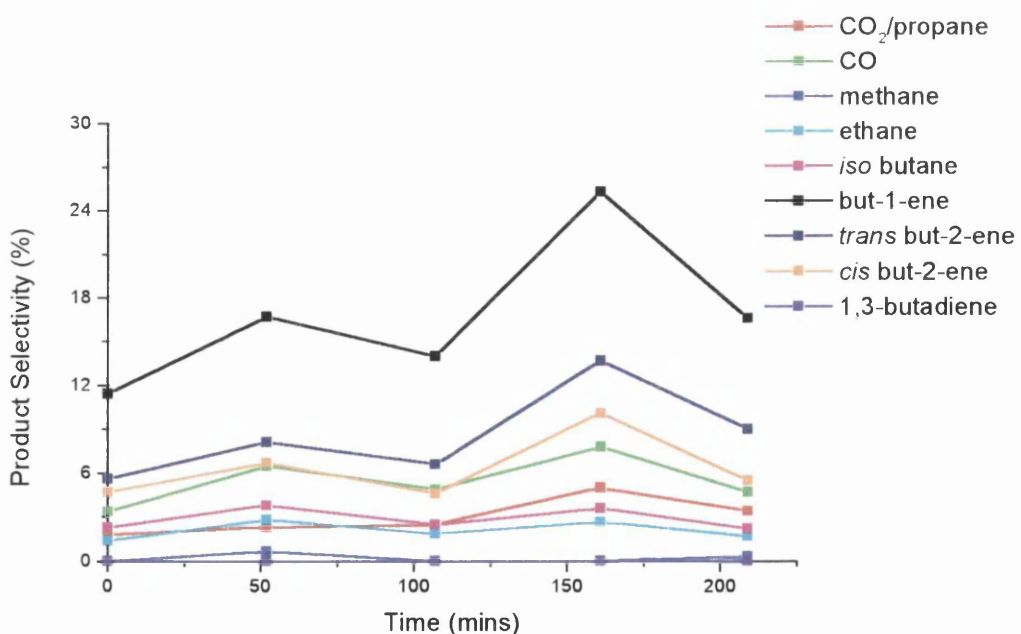


**Fig. 5.4.12** Product Selectivity as a function of Time during the Oxidative Dehydrogenation of Butane using the Support Material at 400°C.

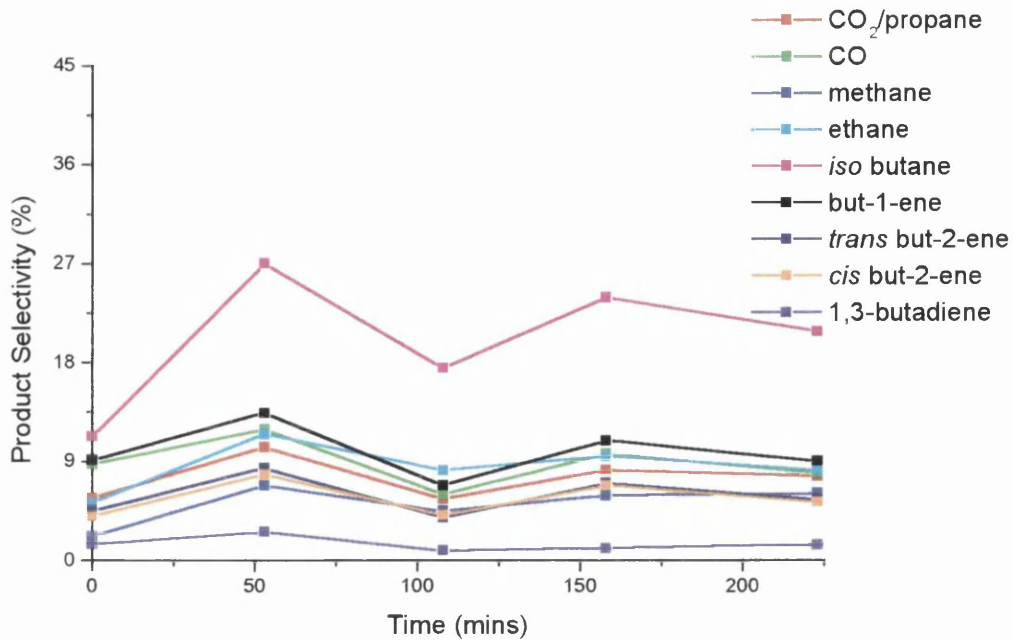


**Fig. 5.4.13** Product Selectivity as a function of Time during the Oxidative Dehydrogenation of Butane using the Support Material at 500°C.

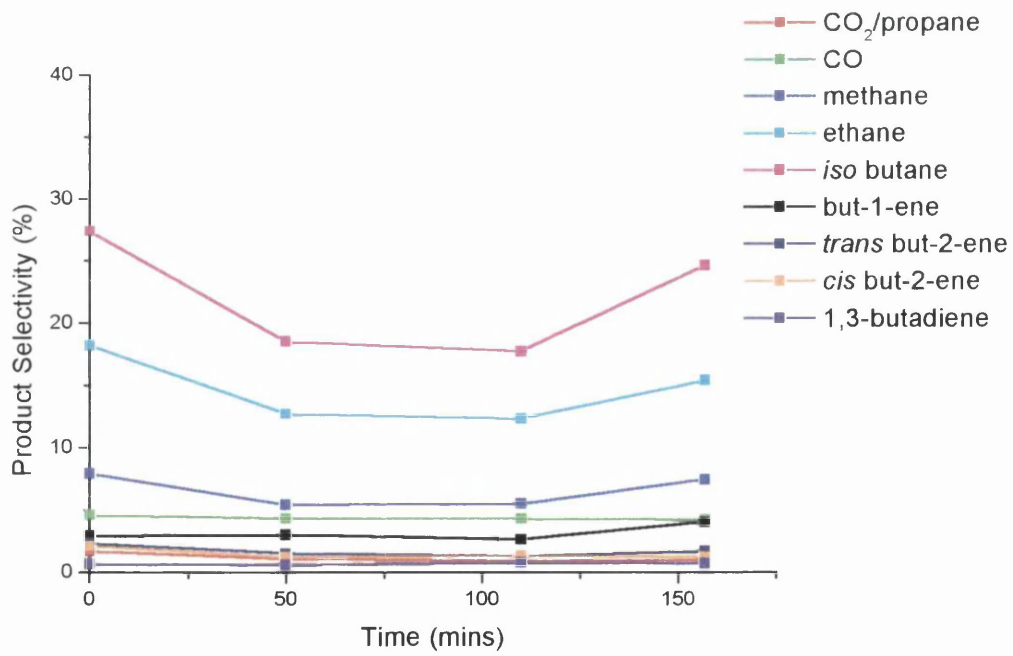


**Fig. 5.4.14** Product Selectivity as a function of Time during the Oxidative Dehydrogenation of Butane using the Support Material at 600°C.

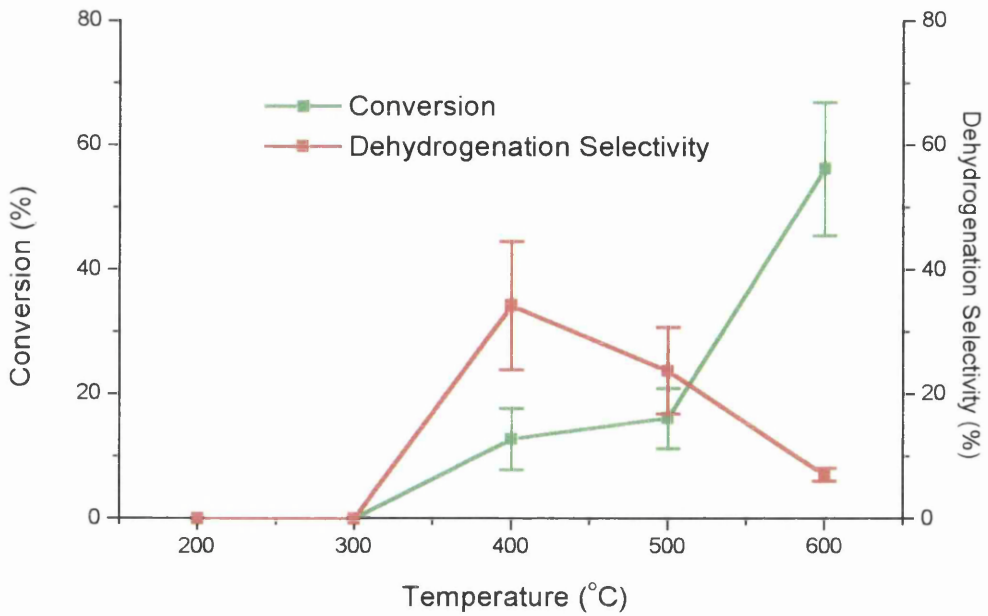


**Fig. 5.4.15** Conversion and Dehydrogenation Selectivity during the Oxidative Dehydrogenation of Butane using the Support Material.

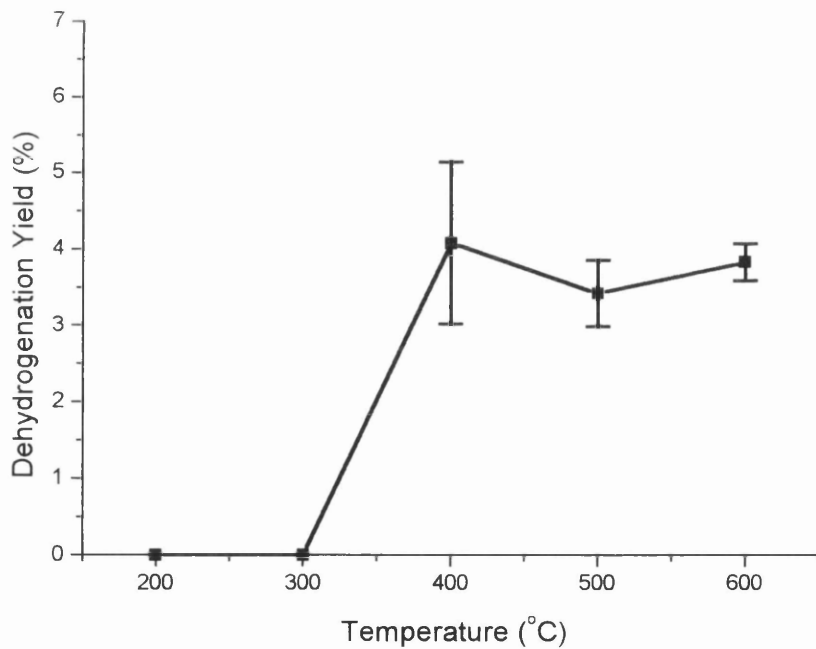


**Fig. 5.4.16** Dehydrogenation Yield during the Oxidative Dehydrogenation of Butane using the Support Material.

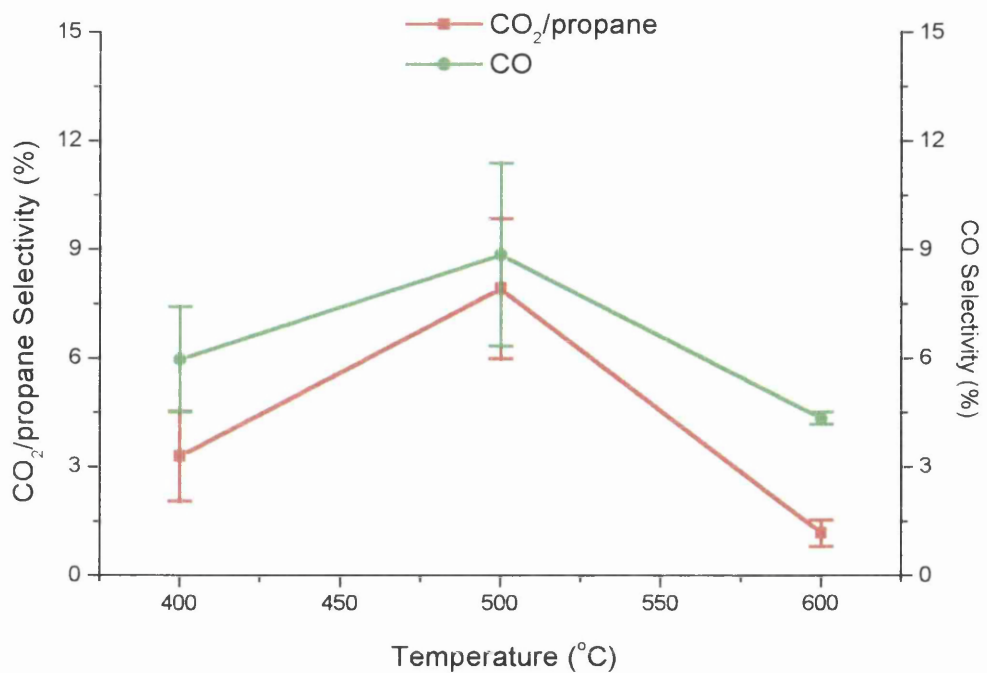


**Fig. 5.4.17** Oxygenate Selectivity observed during the Oxidative Dehydrogenation of Butane using the Support Material.

## **5.5      *The Straight and Oxidative Dehydrogenation of Butane using 0.5% Pt/Al<sub>2</sub>O<sub>3</sub>***

Throughout the following sections of the thesis the results from the catalyst testing are illustrated. Many reactions have been carried out with the formation of a variety of products, therefore the discussion of these results is non-trivial. In order to simplify the remaining sections the following format has been adopted. The beginning of each section will consist of tables containing the data collected from all the experiments carried out on each particular catalyst *e.g.* straight dehydrogenation as a function of temperature or oxidative dehydrogenation as a function of flow-rate. This is then followed by the corresponding plots and at the end all the results from the straight and oxidative dehydrogenation on each particular catalyst are summarised.

### **5.5.1    The Straight Dehydrogenation of Butane as a function of Temperature under Continuous-flow conditions using 0.5% Pt/Al<sub>2</sub>O<sub>3</sub>**

Tables 5.5.1, 5.5.2 and 5.5.3 contain the conversion and product molar quantities, the product selectivity and the product yield values respectively for the straight dehydrogenation of butane using 0.5% Pt/Al<sub>2</sub>O<sub>3</sub> as a function of temperature. Figures 5.5.1 - 5.5.10 graphically represent these results with respect to the conversion, individual product selectivity, dehydrogenation selectivity and dehydrogenation yield as a function of time and temperature, showing the equilibrium results, where appropriate, for comparison. Section 4.1.3 describes the procedure used to carry out the experiments.

**Table 5.5.1** Conversion and Product Molar Quantities for the Straight Dehydrogenation of Butane using 0.5% Pt/Al<sub>2</sub>O<sub>3</sub>.

Temp. (°C)	Time (mins)	Moles Bypass (x10 <sup>-7</sup> )	Moles React. (x10 <sup>-7</sup> )	Conv. (%)	Met. (x10 <sup>-7</sup> )	Eth. (x10 <sup>-7</sup> )	Iso. (x10 <sup>-7</sup> )	B-1 (x10 <sup>-7</sup> )	Trans B-2 (x10 <sup>-7</sup> )	Cis B-2 (x10 <sup>-7</sup> )	Diene (x10 <sup>-7</sup> )
200	0	42.83	2.31	5.4	0	0	0	0	0	0	0
200	21	42.83	0.73	1.7	0	0	0	0	0	0	0
200	40	42.83	0.07	0.2	0	0	0	0	0	0	0
200	59	42.83	0.37	0.9	0	0	0	0	0	0	0
300	0	43.58	3.90	8.9	0	0	0	0	0.23	0.17	0
300	20	43.58	3.07	7.0	0	0	0	0	0.17	0.12	0
300	42	43.58	1.58	3.6	0	0	0	0	0.14	0.11	0
300	64	43.58	1.82	4.2	0	0	0	0	0.12	0.07	0
300	87	43.58	2.76	6.3	0	0	0	0	0.10	0.06	0
300	109	43.58	1.89	4.3	0	0	0	0	0.08	0.06	0
300	131	43.58	1.80	4.1	0	0	0	0	0.08	0.06	0
300	155	43.58	2.51	5.8	0	0	0	0	0.05	0.05	0
300	175	43.58	1.80	4.1	0	0	0	0	0.04	0.05	0
400	0	40.97	3.49	8.5	0	0	0	0.15	0.37	0.30	0
400	26	40.97	0.84	2.0	0	0	0	0.01	0	0	0
400	48	40.97	0	0	0	0	0	0	0	0	0
400	64	40.97	0.98	2.4	0	0	0	0	0	0	0
400	85	40.97	0.67	1.6	0	0	0	0	0	0	0
400	100	40.97	0.88	2.1	0	0	0	0	0	0	0
500	0	41.29	5.23	12.7	0.22	0	0.03	0.26	0.33	0.31	0.13
500	22	41.29	1.13	2.7	0.07	0	0	0.09	0.11	0.08	0
500	44	41.29	1.44	3.5	0	0	0	0.05	0.08	0	0
500	62	41.29	1.58	3.8	0	0	0	0.04	0.06	0	0
500	84	41.29	0.35	0.7	0	0	0	0.04	0.04	0	0
500	112	41.29	1.11	2.7	0	0	0	0.02	0.04	0	0
500	129	41.29	0.31	0.8	0	0	0	0	0	0	0
600	0	41.63	4.65	11.2	0.86	0.66	0.51	0.46	0.62	0.60	0.42
600	25	41.63	3.17	7.6	0.76	0.85	0.61	0.18	0.33	0.27	0.12
600	48	41.63	5.26	12.6	0.67	0.76	0.61	0.12	0.24	0.22	0.08
600	71	41.63	4.75	11.4	0.70	0.72	0.64	0.10	0.20	0.15	0
600	96	41.63	2.83	6.8	0.76	0.86	0.71	0.09	0.18	0.15	0.08
600	117	41.63	2.65	6.4	0.76	0.90	0.70	0.08	0.20	0.16	0
600	147	41.63	2.53	6.1	0.76	0.92	0.72	0.08	0.20	0.14	0
600	166	41.63	3.03	7.3	0.72	0.83	0.70	0.06	0.16	0.11	0.07
600	211	41.63	2.22	5.3	0.76	0.98	0.75	0.06	0.15	0.13	0
700	0	41.00	24.76	60.4	7.96	11.28	5.97	0.36	0.24	0.22	0.50
700	24	41.00	23.48	57.3	8.16	12.06	6.39	0.31	0.18	0.14	0.35
700	46	41.00	23.70	57.8	8.11	11.99	6.46	0.32	0.18	0.15	0.30
700	70	41.00	22.98	56.0	8.48	12.59	6.80	0.34	0.18	0.15	0.27
700	93	41.00	22.98	56.0	8.46	12.53	6.80	0.36	0.19	0.15	0.27
700	116	41.00	22.84	55.7	8.35	12.42	6.74	0.36	0.18	0.19	0.26
700	136	41.00	22.85	55.7	8.63	12.73	6.90	0.38	0.19	0.13	0.26
700	166	41.00	21.90	53.4	8.98	13.39	7.28	0.38	0.17	0.14	0.26
700	193	41.00	22.50	54.9	8.68	12.97	7.02	0.37	0.16	0.14	0.52

**Table 5.5.2** Product Selectivity for the Straight Dehydrogenation of Butane as a function of Temperature using 0.5% Pt/Al<sub>2</sub>O<sub>3</sub>.

Temp. (°C)	Time (mins)	Met. Sel. (%)	Eth. Sel. (%)	Iso Sel. (%)	B-1 Sel. (%)	Trans B-2 Sel. (%)	Cis B-2 Sel. (%)	Diene Sel. (%)	Dehydro. Sel. (%)
200	0	0	0	0	0	0	0	0	0
200	21	0	0	0	0	0	0	0	0
200	40	0	0	0	0	0	0	0	0
200	59	0	0	0	0	0	0	0	0
300	0	0	0	0	0	5.9	4.4	0	10.3
300	20	0	0	0	0	5.5	3.9	0	9.4
300	42	0	0	0	0	8.8	7.0	0	15.8
300	64	0	0	0	0	6.6	3.8	0	10.4
300	87	0	0	0	0	3.6	2.2	0	5.8
300	109	0	0	0	0	4.2	3.2	0	7.4
300	131	0	0	0	0	4.4	3.3	0	7.7
300	155	0	0	0	0	2.0	2.0	0	4.0
300	175	0	0	0	0	2.2	2.8	0	5.0
400	0	0	0	0	4.3	10.6	8.6	0	23.5
400	26	0	0	0	1.2	0	0	0	1.2
400	48	0	0	0	0	0	0	0	0
400	64	0	0	0	0	0	0	0	0
400	85	0	0	0	0	0	0	0	0
400	100	0	0	0	0	0	0	0	0
500	0	1.0	0	0.6	5.0	6.3	5.9	2.5	19.7
500	22	1.5	0	0	8.0	9.7	7.1	0	24.8
500	44	0	0	0	3.5	5.6	0	0	9.1
500	62	0	0	0	2.5	3.8	0	0	6.3
500	84	0	0	0	11.4	11.4	0	0	22.8
500	112	0	0	0	1.8	3.6	0	0	5.4
500	129	0	0	0	0	0	0	0	0
600	0	4.6	7.1	11.0	10.0	13.3	12.9	9.0	45.2
600	25	6.0	13.4	19.2	5.7	10.4	8.5	3.8	28.5
600	48	3.2	7.2	11.6	2.3	4.6	4.2	1.5	12.6
600	71	3.7	7.6	13.5	2.1	4.2	3.2	0	7.5
600	96	6.7	15.2	25.1	3.2	6.4	5.3	2.8	17.7
600	117	7.2	17.0	26.4	3.0	7.5	6.0	0	16.5
600	147	7.5	18.2	28.4	3.2	7.9	5.5	0	16.6
600	166	5.9	13.7	23.1	2.0	5.3	3.6	2.3	11.2
600	211	8.6	22.1	33.8	2.7	6.8	5.8	0	16.3
700	0	8.0	22.8	24.1	1.4	1.0	0.9	2.0	5.3
700	24	8.7	25.7	27.2	1.3	0.8	0.6	1.5	4.2
700	46	8.6	25.3	27.2	1.4	0.8	0.6	1.3	4.1
700	70	9.2	27.4	29.6	1.5	0.8	0.6	1.2	4.1
700	93	9.2	27.3	29.6	1.6	0.8	0.6	1.2	4.2
700	116	9.1	27.2	29.5	1.6	0.8	0.8	1.1	4.3
700	136	9.4	27.8	30.2	1.7	0.8	0.6	1.1	4.2
700	166	10.2	30.6	33.2	1.7	0.8	0.6	1.2	4.3
700	193	9.6	28.8	31.2	1.6	0.7	0.6	2.3	5.2

**Table 5.5.3** Product Yields for the Straight Dehydrogenation of Butane as a function of Temperature using 0.5% Pt/Al<sub>2</sub>O<sub>3</sub>.

Temp. (°C)	Time (mins)	Met. Yield (%)	Eth. Yield (%)	Iso Yield (%)	B-1 Yield (%)	Trans B-2 Yield (%)	Cis B-2 Yield (%)	Diene Yield (%)	Dehydro. Yield (%)
200	0	0	0	0	0	0	0	0	0
200	21	0	0	0	0	0	0	0	0
200	40	0	0	0	0	0	0	0	0
200	59	0	0	0	0	0	0	0	0
300	0	0	0	0	0	0.52	0.39	0	0.91
300	20	0	0	0	0	0.38	0.27	0	0.65
300	42	0	0	0	0	0.32	0.25	0	0.57
300	64	0	0	0	0	0.28	0.16	0	0.44
300	87	0	0	0	0	0.23	0.14	0	0.37
300	109	0	0	0	0	0.18	0.14	0	0.32
300	131	0	0	0	0	0.18	0.14	0	0.32
300	155	0	0	0	0	0.11	0.12	0	0.23
300	175	0	0	0	0	0.09	0.11	0	0.20
400	0	0	0	0	0.36	0.90	0.73	0	1.99
400	26	0	0	0	0.02	0	0	0	0.02
400	48	0	0	0	0	0	0	0	0
400	64	0	0	0	0	0	0	0	0
400	85	0	0	0	0	0	0	0	0
400	100	0	0	0	0	0	0	0	0
500	0	0.13	0	0.08	0.63	0.80	0.75	0.32	2.50
500	22	0.04	0	0	0.22	0.26	0.19	0	0.67
500	44	0	0	0	0.12	0.20	0	0	0.32
500	62	0	0	0	0.10	0.14	0	0	0.24
500	84	0	0	0	0.09	0.09	0	0	0.18
500	112	0	0	0	0.05	0.10	0	0	0.15
500	129	0	0	0	0	0	0	0	0
600	0	0.5	0.8	1.2	1.1	1.5	1.4	1.0	5.0
600	25	0.4	1.0	1.4	0.4	0.8	0.6	0.3	2.1
600	48	0.4	0.9	1.5	0.3	0.6	0.5	0.2	1.6
600	71	0.4	0.9	1.5	0.2	0.5	0.4	0	1.1
600	96	0.4	1.0	1.7	0.2	0.4	0.4	0.2	1.2
600	117	0.5	1.1	1.7	0.2	0.5	0.4	0	1.1
600	147	0.4	1.1	1.7	0.2	0.5	0.3	0	1.0
600	166	0.4	1.0	1.7	0.1	0.4	0.3	0.2	1.0
600	211	0.4	1.2	1.8	0.1	0.4	0.3	0	0.8
700	0	4.8	13.8	14.6	0.8	0.6	0.5	1.2	3.1
700	24	5.0	14.7	15.6	0.7	0.4	0.3	0.8	2.2
700	46	5.0	14.6	15.7	0.8	0.5	0.3	0.8	2.4
700	70	5.2	15.3	16.6	0.8	0.4	0.3	0.7	2.2
700	93	5.2	15.3	16.6	0.9	0.4	0.3	0.7	2.3
700	116	5.1	15.2	16.4	0.9	0.4	0.4	0.6	2.3
700	136	5.2	15.5	16.8	0.9	0.4	0.3	0.6	2.2
700	166	5.4	16.3	17.7	0.9	0.4	0.3	0.6	2.2
700	193	5.3	15.8	17.1	0.9	0.4	0.3	1.3	2.9

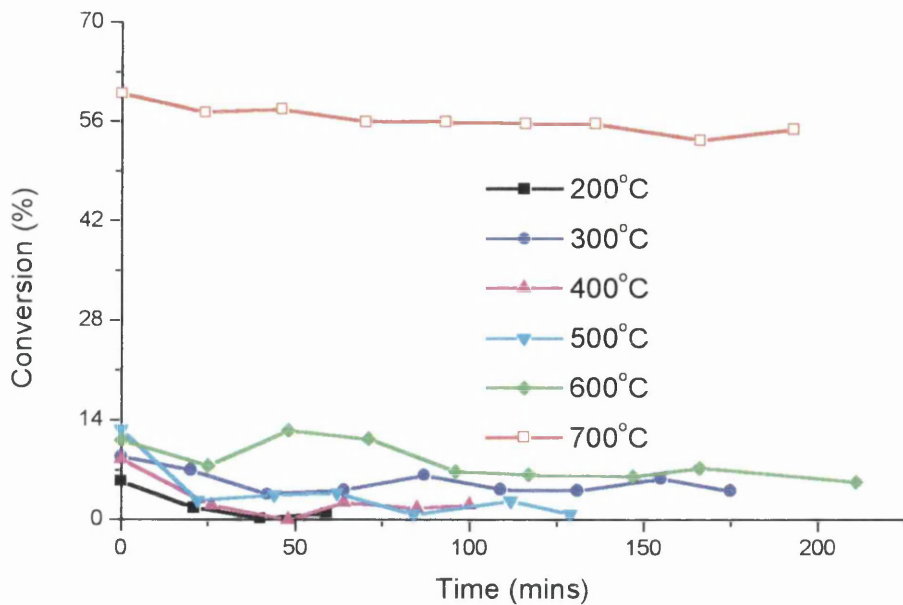


**Fig. 5.5.1** Conversion as a function of Time during the Straight Dehydrogenation of Butane at various Temperatures using 0.5% Pt/Al<sub>2</sub>O<sub>3</sub>.

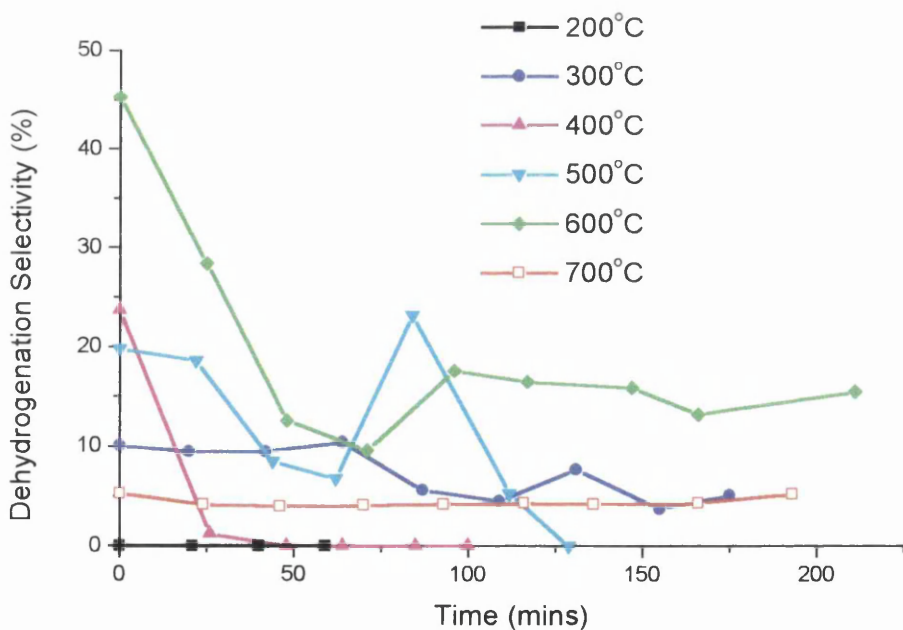


**Fig. 5.5.2** Dehydrogenation Selectivity as a function of Time during the Straight Dehydrogenation of Butane at various Temperatures using 0.5% Pt/Al<sub>2</sub>O<sub>3</sub>.

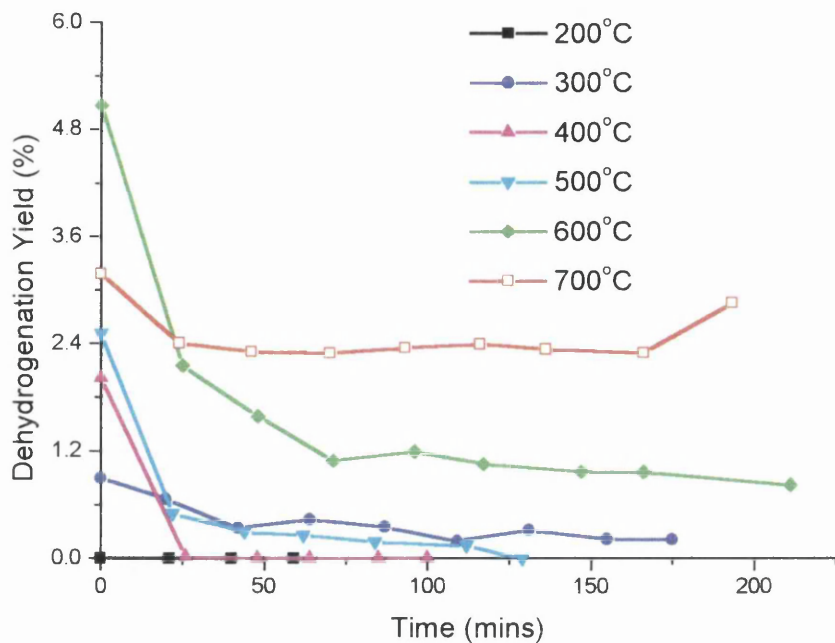


**Fig. 5.5.3** Dehydrogenation Yield as a function of Time during the Straight Dehydrogenation of Butane at various Temperatures using 0.5% Pt/Al<sub>2</sub>O<sub>3</sub>.

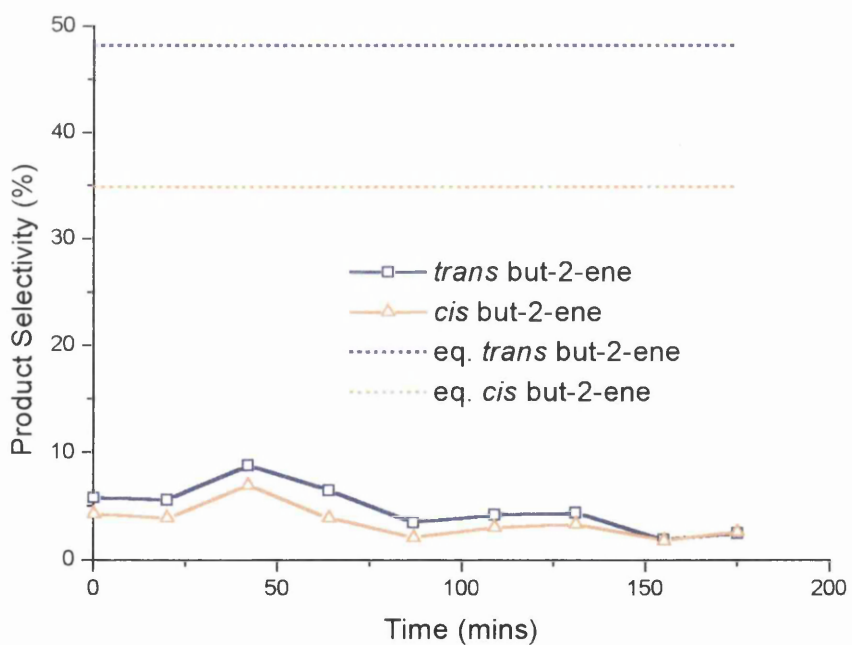


**Fig. 5.5.4** Product Selectivity as a function of Time during the Straight Dehydrogenation of Butane using the 0.5% Pt/Al<sub>2</sub>O<sub>3</sub> at 300°C.

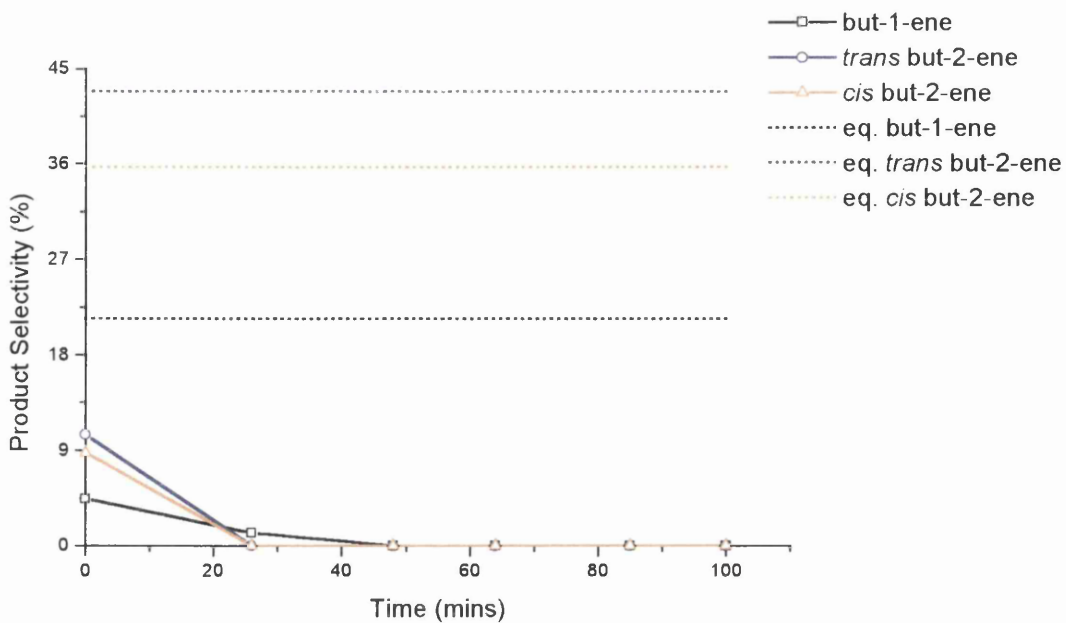


**Fig. 5.5.5** Product Selectivity as a function of Time during the Straight Dehydrogenation of Butane using the 0.5% Pt/Al<sub>2</sub>O<sub>3</sub> at 400°C.

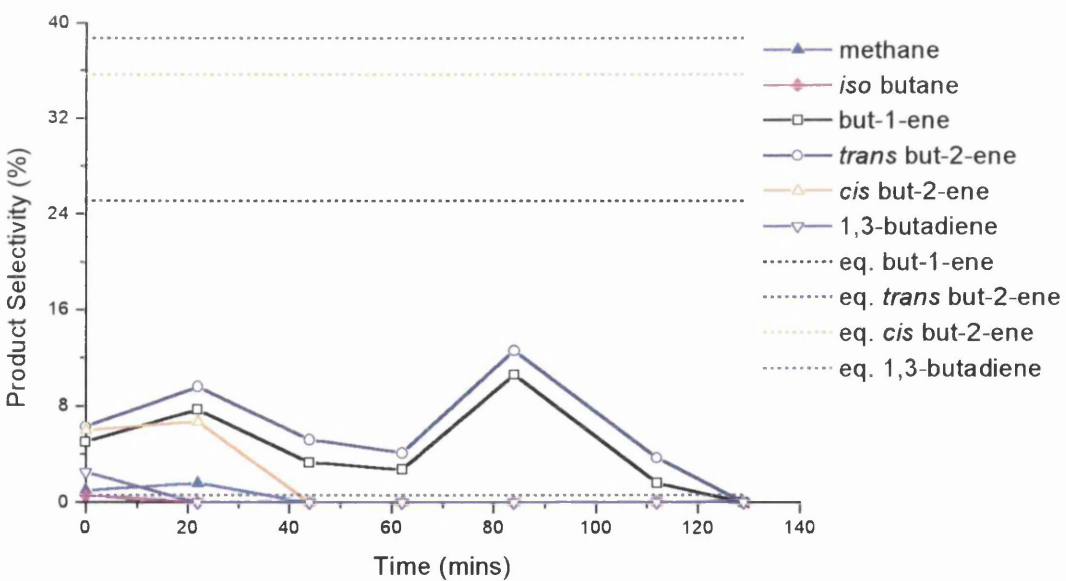


**Fig. 5.5.6** Product Selectivity as a function of Time during the Straight Dehydrogenation of Butane using the 0.5% Pt/Al<sub>2</sub>O<sub>3</sub> at 500°C.

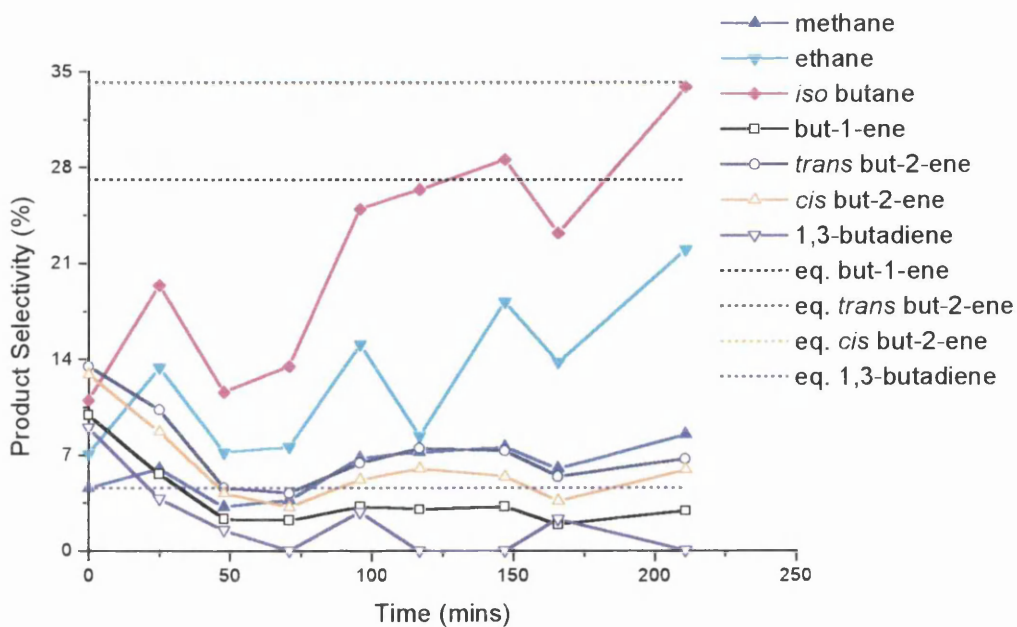


**Fig. 5.5.7** Product Selectivity as a function of Time during the Straight Dehydrogenation of Butane using the 0.5% Pt/Al<sub>2</sub>O<sub>3</sub> at 600°C.

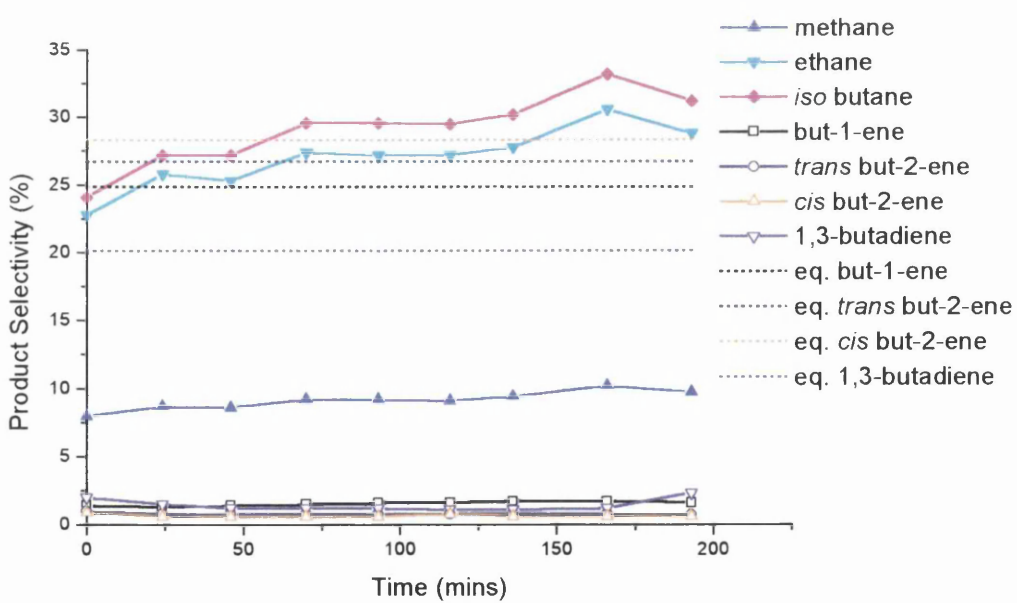


**Fig. 5.5.8** Product Selectivity as a function of Time during the Straight Dehydrogenation of Butane using the 0.5% Pt/Al<sub>2</sub>O<sub>3</sub> at 700°C.

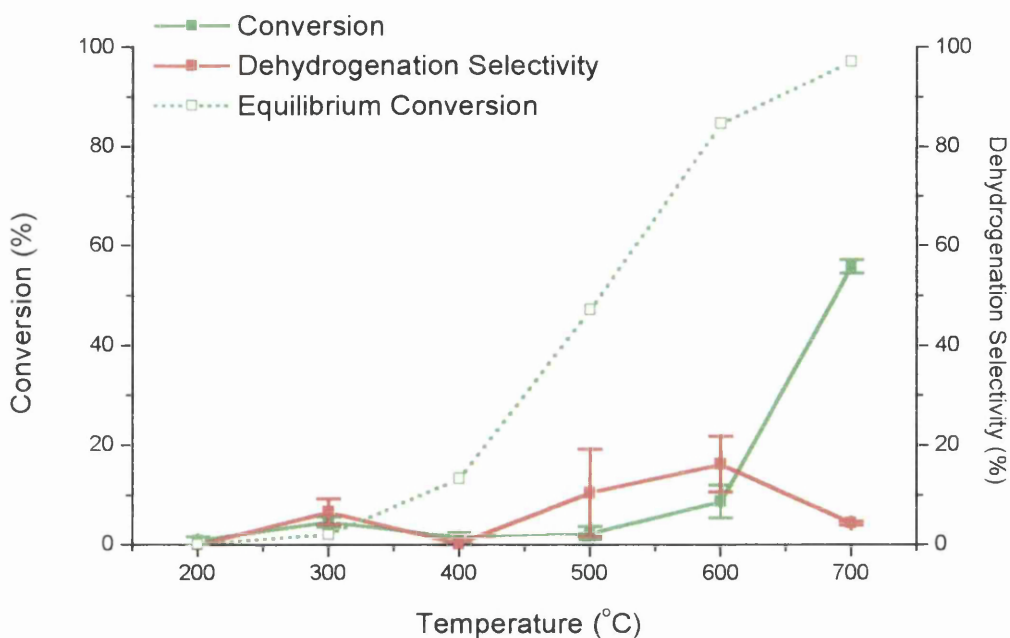


**Fig. 5.5.9** Conversion and Dehydrogenation Selectivity as a function of Temperature during the Straight Dehydrogenation of Butane using 0.5% Pt/Al<sub>2</sub>O<sub>3</sub>.

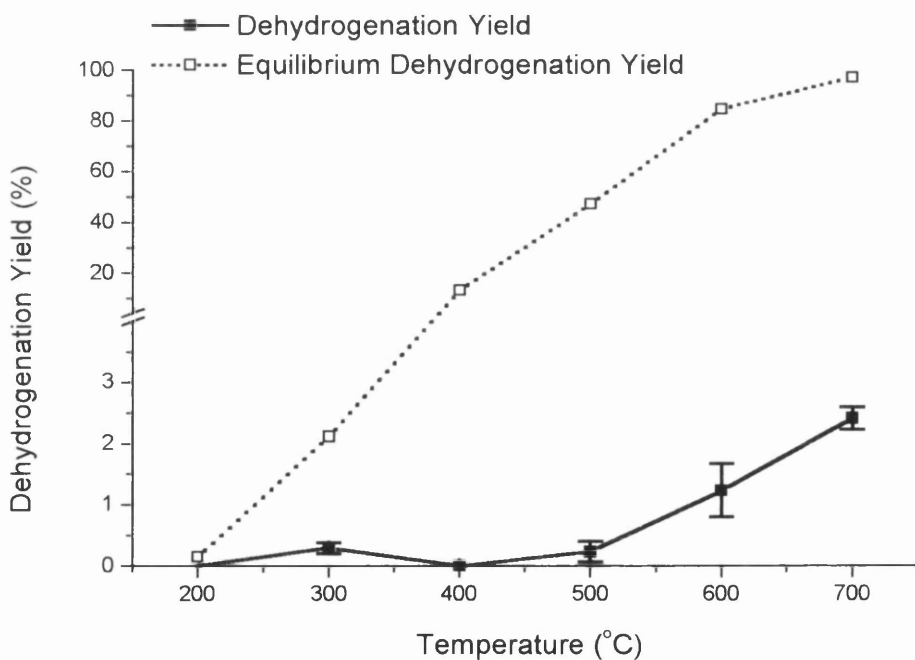


**Fig. 5.5.10** Dehydrogenation Yield as a function of Temperature during the Straight Dehydrogenation of Butane using 0.5% Pt/Al<sub>2</sub>O<sub>3</sub>.

## 5.5.2 The Oxidative Dehydrogenation of Butane as a function of Temperature under Continuous-flow conditions using 0.5% Pt/Al<sub>2</sub>O<sub>3</sub>

Tables 5.5.4, 5.5.5 and 5.5.6 contain the conversion and product molar quantities, the product selectivity and the product yield values respectively for the oxidative dehydrogenation of butane using 0.5% Pt/Al<sub>2</sub>O<sub>3</sub> as a function of temperature. Figures 5.5.11 - 5.5.21 graphically represent these results with respect to the conversion, individual product selectivity, dehydrogenation selectivity and dehydrogenation yield as a function of time and temperature. The procedure used to carry out these experiments is described in section 4.1.3.

**Table 5.5.4 Conversion and Product Molar Quantities for the Oxidative Dehydrogenation of Butane using 0.5% Pt/Al<sub>2</sub>O<sub>3</sub>.**

Temp. (°C)	Time (mins)	Moles Bypass (x10 <sup>-7</sup> )	Moles Reacted (x10 <sup>-7</sup> )	Conv. (%)	CO <sub>2</sub> /Pr (x10 <sup>-7</sup> )	CO (x10 <sup>-7</sup> )	Met. (x10 <sup>-7</sup> )	Eth. (x10 <sup>-7</sup> )	Iso (x10 <sup>-7</sup> )	B-1 (x10 <sup>-7</sup> )	Trans B-2 (x10 <sup>-7</sup> )	Cis B-2 (x10 <sup>-7</sup> )	Diene (x10 <sup>-7</sup> )
200	0	46.93	4.88	10.4	4.69	0	0	0	0	0	0	0	0
200	46	46.93	8.56	18.2	4.61	0	0	0	0	0	0	0	0
200	90	46.93	10.88	23.2	5.05	0	0	0	0	0	0	0	0
200	123	46.93	6.38	13.6	4.70	0	0	0	0	0	0	0	0
200	165	46.93	3.28	7.0	4.44	0	0	0	0	0	0	0	0
300	0	46.93	6.59	14.0	3.89	0	0	0	0	0.07	0.35	0.31	0
300	53	46.93	6.11	13.0	4.25	0	0	0	0	0	0	0	0
300	100	46.93	7.77	16.6	4.35	0	0	0	0	0	0	0	0
300	137	46.93	7.29	15.5	4.29	0	0	0	0	0	0	0	0
300	184	46.93	13.68	29.1	4.94	0	0	0	0	0	0	0	0
400	0	46.93	11.95	25.5	4.80	3.38	0	0	0	0.16	0.20	0.18	0
400	49	46.93	4.41	9.4	4.37	0	0	0	0	0.06	0	0	0
400	95	46.93	5.04	10.7	4.57	0	0	0	0	0.04	0	0	0
400	128	46.93	6.12	13.0	4.63	0	0	0	0	0.04	0	0	0
400	176	46.93	5.38	11.5	4.70	0	0	0	0	0.03	0	0	0
400	205	46.93	5.65	12.0	4.59	0	0	0	0	0.03	0	0	0
500	0	46.93	11.17	23.8	3.96	2.07	0.38	0	0	0.23	0.24	0.24	0.08
500	52	46.93	7.36	15.7	4.19	1.96	0.08	0	0	0.17	0.10	0.07	0
500	98	46.93	7.51	16.0	4.22	0.87	0.09	0	0	0.16	0.08	0.09	0
500	160	46.93	6.57	14.0	4.17	0.41	0	0	0	1.47	0.09	0.09	0
500	218	46.93	6.36	13.6	4.34	0.47	0	0	0	1.42	0.09	0.08	0
500	264	46.93	6.17	13.1	4.36	0.35	0	0	0	1.38	0.10	0.08	0
600	0	46.93	15.98	34.0	2.82	6.09	0.21	0.60	0.68	0.66	0.31	0.27	0.17
600	53	46.93	10.65	22.7	3.34	3.66	0.11	0.61	1.11	0.24	0.18	0.17	0.04
600	109	46.93	10.50	22.4	3.32	2.97	0.09	0.57	1.15	0.21	0.17	0.16	0.06
600	182	46.93	10.82	23.0	3.61	2.53	0	0.63	1.28	0.22	0.19	0.17	0
600	238	46.93	9.99	21.3	3.54	2.42	0	0.65	1.37	0.24	0.19	0.17	0
600	279	46.93	10.29	21.9	3.53	2.09	0	0.67	1.41	0.23	0.20	0.19	0

**Table 5.5.5** Product Selectivity for the Oxidative Dehydrogenation of Butane using 0.5% Pt/Al<sub>2</sub>O<sub>3</sub>.

Temp. (°C)	Time (mins)	CO <sub>2</sub> /Pr Sel. (%)	CO Sel. (%)	Met. Sel. (%)	Eth. Sel. (%)	Iso Sel. (%)	B-1 Sel. (%)	Trans B-2 Sel. (%)	Cis B-2 Sel. (%)	Diene Sel. (%)	Dehydro. Sel. (%)
200	0	24.0	0	0	0	0	0	0	0	0	0
200	46	13.5	0	0	0	0	0	0	0	0	0
200	90	11.6	0	0	0	0	0	0	0	0	0
200	123	18.4	0	0	0	0	0	0	0	0	0
200	165	33.8	0	0	0	0	0	0	0	0	0
300	0	14.8	0	0	0	0	1.1	5.3	4.7	0	11.1
300	53	17.4	0	0	0	0	0	0	0	0	0
300	100	14.0	0	0	0	0	0	0	0	0	0
300	137	14.7	0	0	0	0	0	0	0	0	0
300	184	9.0	0	0	0	0	0	0	0	0	0
400	0	10.0	0.7	0	0	0	1.3	1.7	1.5	0	4.5
400	49	24.8	0	0	0	0	1.4	0	0	0	1.4
400	95	22.7	0	0	0	0	0.8	0	0	0	0.8
400	128	18.9	0	0	0	0	0.6	0	0	0	0.6
400	176	22.1	0	0	0	0	0.6	0	0	0	0.6
400	205	20.3	0	0	0	0	0.7	0	0	0	0.7
500	0	8.9	4.3	0.8	0	0	2.0	2.1	2.1	0.7	6.9
500	52	14.2	6.6	0.3	0	0	2.3	1.4	1	0	4.7
500	98	14.0	2.9	0.3	0	0	2.1	1.1	1.2	0	4.4
500	160	15.9	1.6	0	0	0	2.3	1.4	1.4	0	5.1
500	218	17.0	1.8	0	0	0	2.2	1.4	1.2	0	4.8
500	264	17.7	1.4	0	0	0	2.3	1.6	1.3	0	5.2
600	0	4.4	9.5	0.3	1.9	4.2	4.1	1.9	1.7	1.1	8.8
600	53	7.8	8.6	0.3	2.9	10.4	2.2	1.7	1.6	0.4	5.9
600	109	7.9	7.1	0.2	2.7	10.0	2.0	1.6	1.6	0.6	5.8
600	182	8.3	5.8	0	2.9	11.8	2.0	1.8	1.6	0	5.4
600	238	8.8	6.0	0	3.2	13.7	2.4	1.9	1.7	0	6.0
600	279	8.6	5.1	0	3.2	13.7	2.2	1.9	1.8	0	5.9

**Table 5.5.6** Product Yields for the Oxidative Dehydrogenation of Butane using 0.5% Pt/Al<sub>2</sub>O<sub>3</sub>.

Temp. (°C)	Time (mins)	CO <sub>2</sub> /Pr Yield (%)	CO Yield (%)	Met. Yield (%)	Eth. Yield (%)	Iso Yield (%)	B-1 Yield (%)	Trans B-2 Yield (%)	Cis B-2 Yield (%)	Diene Yield (%)	Dehydro. Yield (%)
200	0	2.50	0	0	0	0	0	0	0	0	0
200	46	2.46	0	0	0	0	0	0	0	0	0
200	90	2.69	0	0	0	0	0	0	0	0	0
200	123	2.50	0	0	0	0	0	0	0	0	0
200	165	2.37	0	0	0	0	0	0	0	0	0
300	0	2.07	0	0	0	0.15	0.74	0.66	0	0	1.55
300	53	2.26	0	0	0	0	0	0	0	0	0
300	100	2.32	0	0	0	0	0	0	0	0	0
300	137	2.78	0	0	0	0	0	0	0	0	0
300	184	2.62	0	0	0	0	0	0	0	0	0
400	0	2.55	0.18	0	0	0	0.33	0.43	0.38	0	1.15
400	49	2.33	0	0	0	0	0.13	0	0	0	0.13
400	95	2.43	0	0	0	0	0.08	0	0	0	0.08
400	128	2.56	0	0	0	0	0.08	0	0	0	0.08
400	176	2.54	0	0	0	0	0.07	0	0	0	0.07
400	205	2.44	0	0	0	0	0.08	0	0	0	0.08
500	0	2.12	1.02	0.19	0	0	0.48	0.50	0.50	0.17	1.64
500	52	2.23	1.04	0.05	0	0	0.36	0.22	0.16	0	0.74
500	98	2.24	0.46	0.05	0	0	0.34	0.18	0.19	0	0.70
500	160	2.23	0.22	0	0	0	0.32	0.20	0.20	0	0.71
500	218	2.31	0.24	0	0	0	0.30	0.19	0.16	0	0.65
500	264	2.32	0.18	0	0	0	0.30	0.21	0.17	0	0.68
600	0	1.50	3.23	0.65	1.43	1.39	0.65	0.58	0.37	0	2.99
600	53	1.77	1.95	1.95	0.66	2.36	0.50	0.38	0.36	0.09	1.34
600	109	1.77	1.59	1.59	0.60	2.24	0.45	0.36	0.36	0.13	1.30
600	182	1.91	1.33	1.33	0.67	2.71	0.46	0.41	0.37	0	1.24
600	238	1.87	1.28	1.28	0.68	2.92	0.51	0.40	0.36	0	1.28
600	279	1.88	1.12	1.12	0.70	3.00	0.48	0.42	0.39	0	1.29

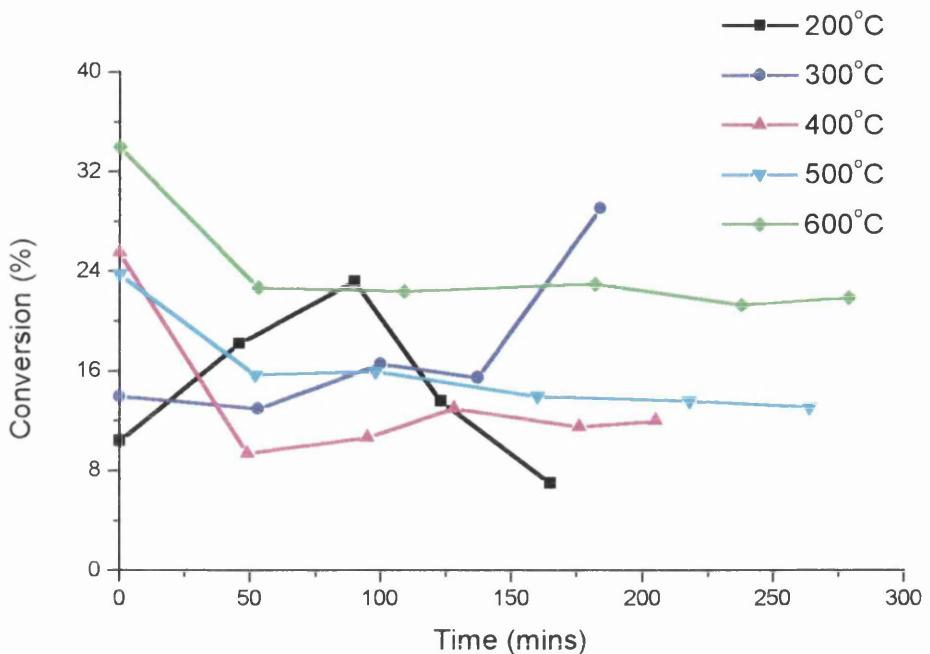


**Fig. 5.5.11** Conversion as a function of Time during the Oxidative Dehydrogenation of Butane at various Temperatures using 0.5% Pt/Al<sub>2</sub>O<sub>3</sub>.

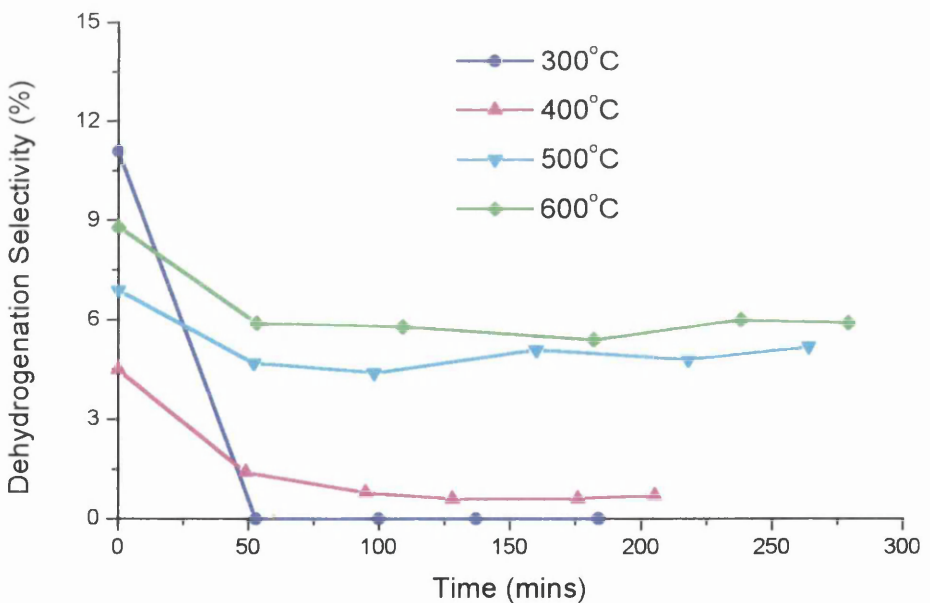


**Fig. 5.5.12** Dehydrogenation Selectivity as a function of Time during the Oxidative Dehydrogenation of Butane at various Temperatures using 0.5% Pt/Al<sub>2</sub>O<sub>3</sub>.

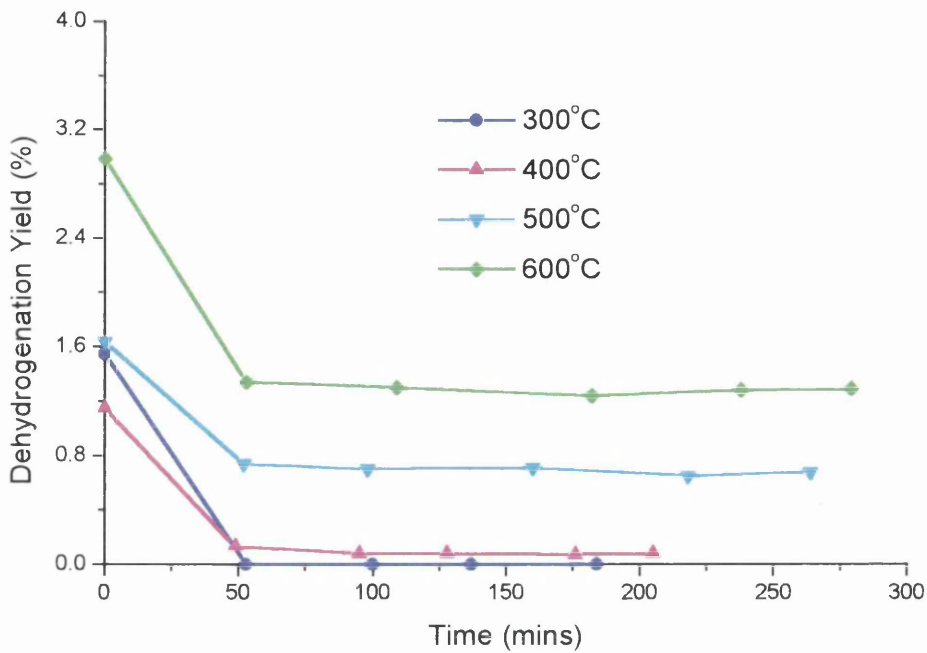


**Fig. 5.5.13** Dehydrogenation Yield as a function of Time during the Oxidative Dehydrogenation of Butane at various Temperatures using 0.5% Pt/Al<sub>2</sub>O<sub>3</sub>.

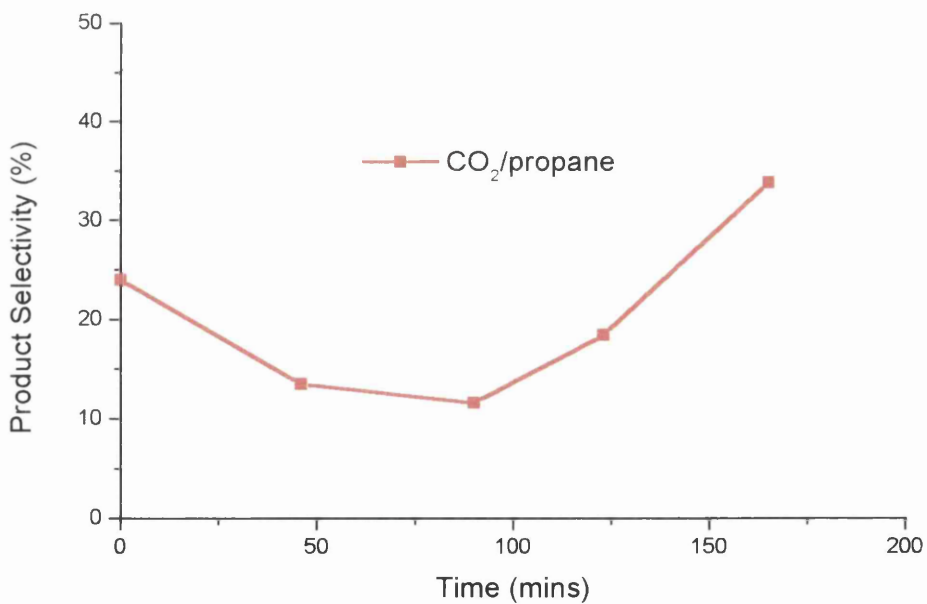


**Fig. 5.5.14** Product Selectivity as a function of Time during the Oxidative Dehydrogenation of Butane using the 0.5% Pt/Al<sub>2</sub>O<sub>3</sub> at 200°C.

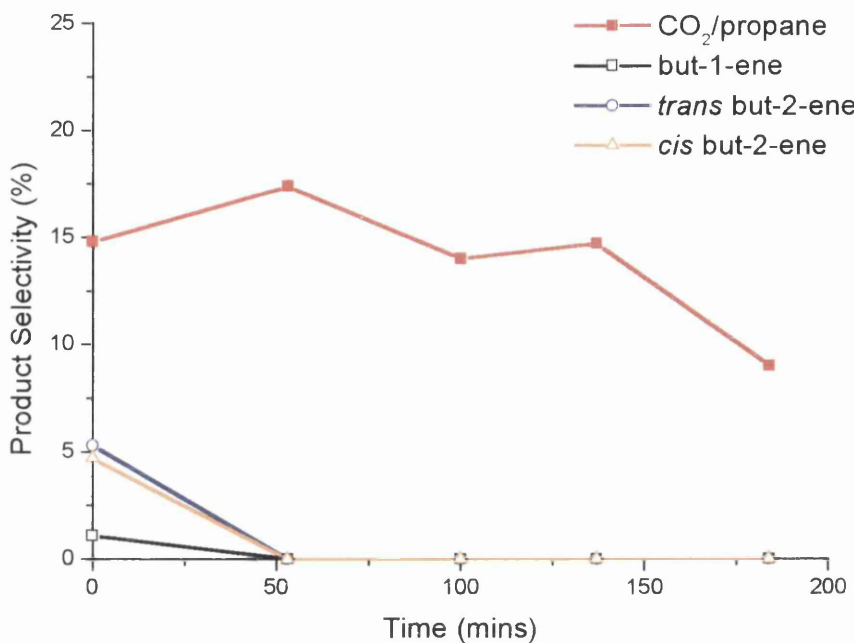


**Fig. 5.5.15** Product Selectivity as a function of Time during the Oxidative Dehydrogenation of Butane using the 0.5% Pt/Al<sub>2</sub>O<sub>3</sub> at 300°C.

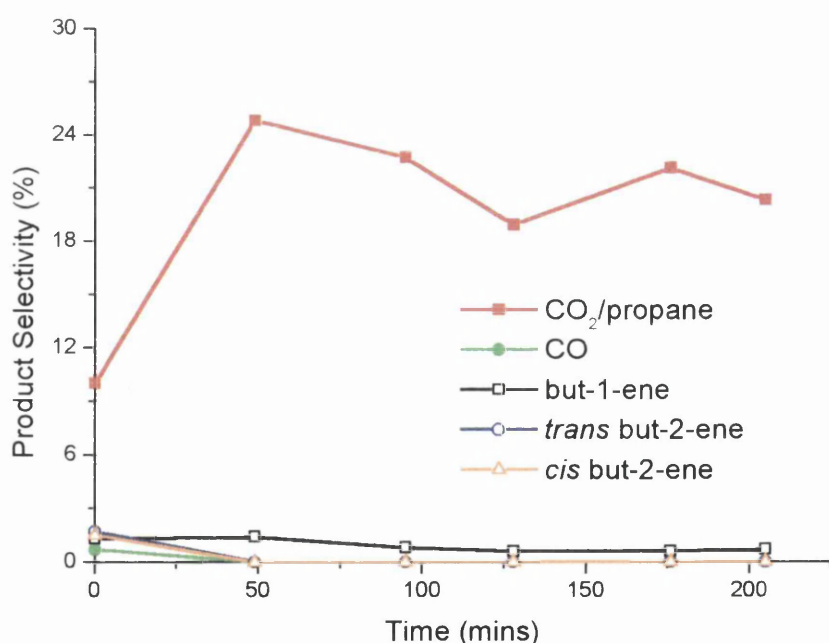


**Fig. 5.5.16** Product Selectivity as a function of Time during the Oxidative Dehydrogenation of Butane using the 0.5% Pt/Al<sub>2</sub>O<sub>3</sub> at 400°C.

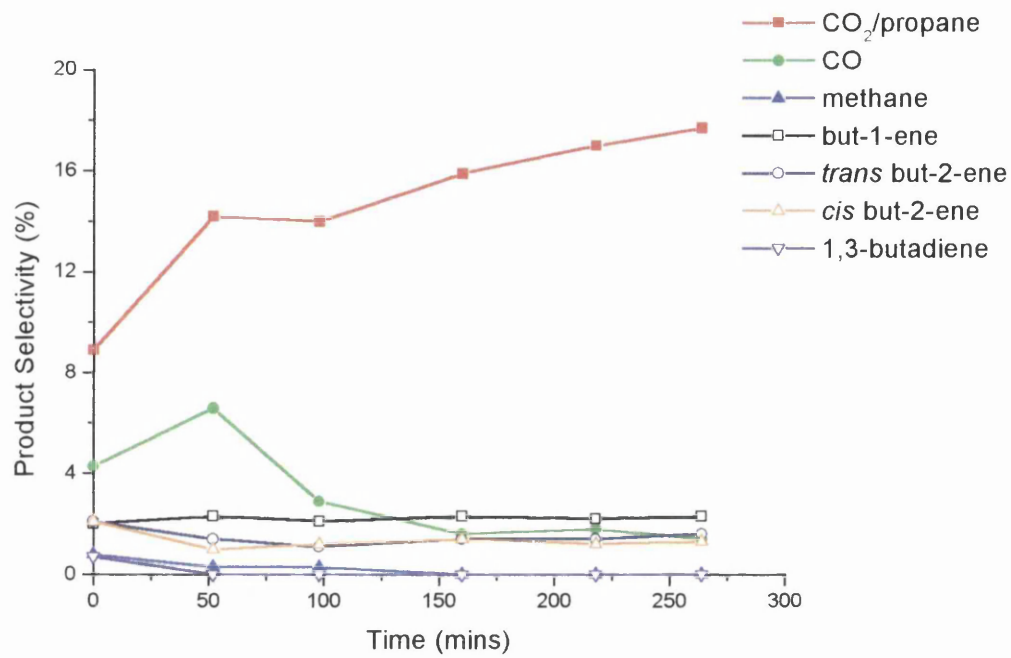


**Fig. 5.5.17** Product Selectivity as a function of Time during the Oxidative Dehydrogenation of Butane using the 0.5% Pt/Al<sub>2</sub>O<sub>3</sub> at 500°C.

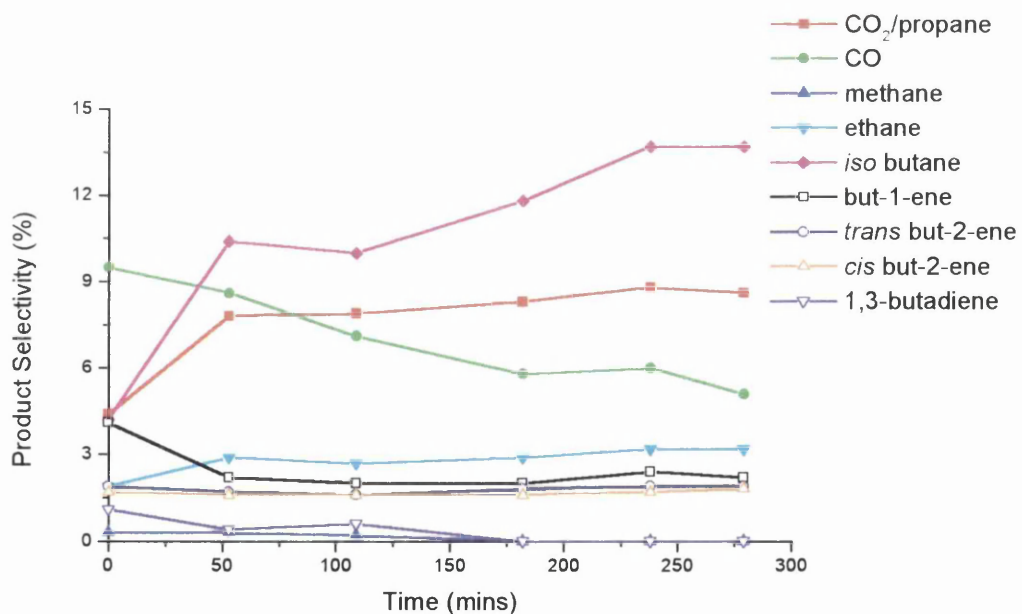


**Fig. 5.5.18** Product Selectivity as a function of Time during the Oxidative Dehydrogenation of Butane using the 0.5% Pt/Al<sub>2</sub>O<sub>3</sub> at 600°C.

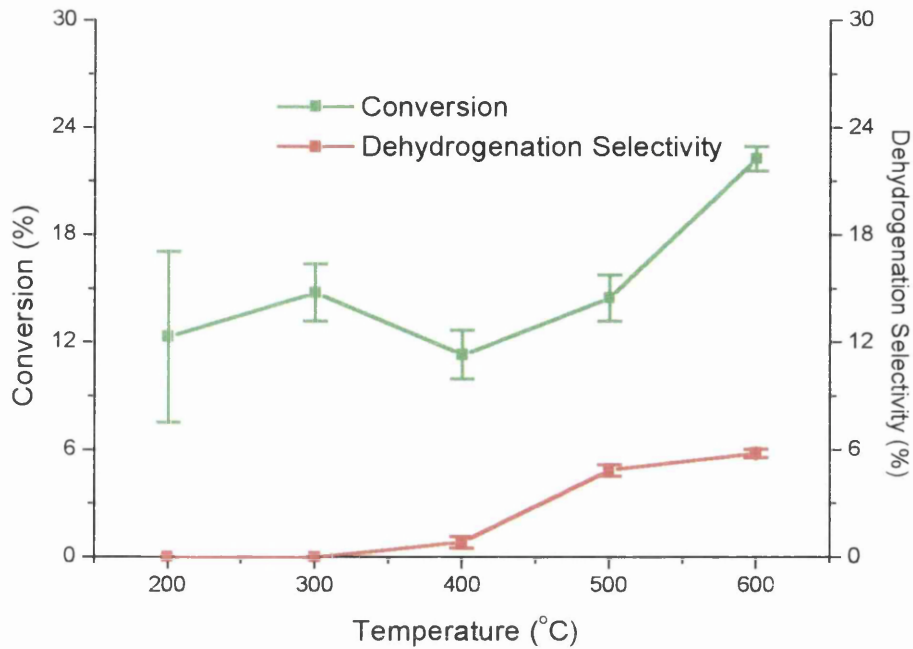


**Fig. 5.5.19** Conversion and Dehydrogenation Selectivity as a function of Temperature during the Oxidative Dehydrogenation of Butane using 0.5% Pt/Al<sub>2</sub>O<sub>3</sub>.

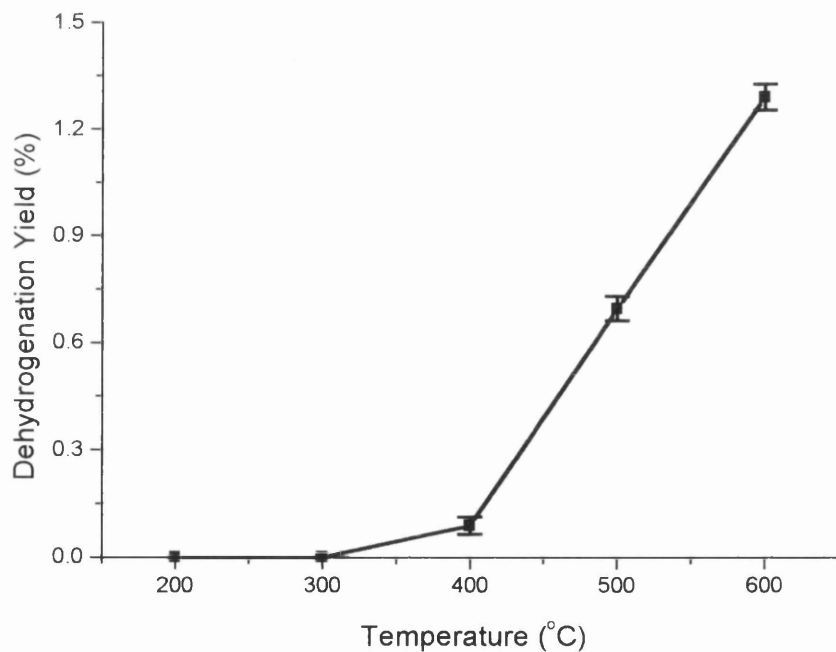


**Fig. 5.5.20** Dehydrogenation Yield as a function of Temperature during the Oxidative Dehydrogenation of Butane using 0.5% Pt/Al<sub>2</sub>O<sub>3</sub>.

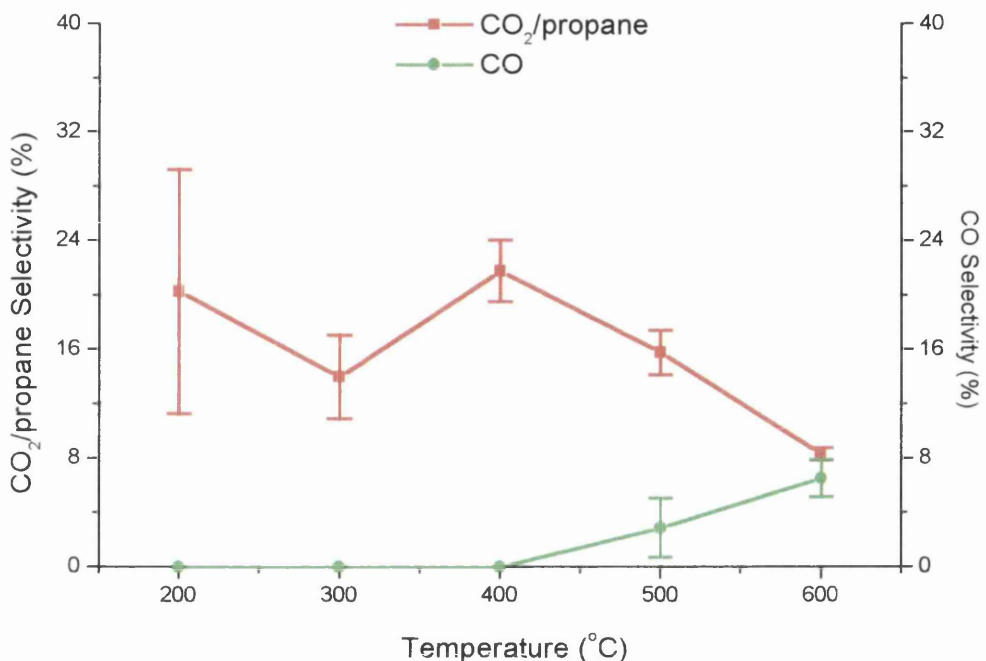


**Fig. 5.5.21**  $\text{CO}_2$  and CO Product Selectivity during the Oxidative Dehydrogenation of Butane using 0.5%  $\text{Pt}/\text{Al}_2\text{O}_3$ .

### 5.5.3 The Straight Dehydrogenation of Butane as a function of Flow-rate under Continuous-flow conditions using 0.5% $\text{Pt}/\text{Al}_2\text{O}_3$

Tables 5.5.7, 5.5.8 and 5.5.9 contain the conversion and product molar quantities, the product selectivity and the product yield values respectively for the straight dehydrogenation of butane using 0.5%  $\text{Pt}/\text{Al}_2\text{O}_3$  as a function of flow-rate. Figures 5.5.22 - 5.5.30 graphically represent these results with respect to the conversion, individual product selectivity, dehydrogenation selectivity and dehydrogenation yield as a function of time and temperature, showing the equilibrium results, where appropriate, for comparison. Section 4.1.3 describes the procedure used to carry out the experiments.

**Table 5.5.7** Conversion and Product Molar Quantities for the Straight Dehydrogenation of Butane as a function of Flow-rate using 0.5% Pt/Al<sub>2</sub>O<sub>3</sub>.

Flow-rate (ml min <sup>-1</sup> )	Time (mins)	Moles Bypass (x10 <sup>-7</sup> )	Moles Reacted (x10 <sup>-7</sup> )	Conv. (%)	Met. (x10 <sup>-7</sup> )	Eth. (x10 <sup>-7</sup> )	Iso (x10 <sup>-7</sup> )	B-1 (x10 <sup>-7</sup> )	Trans B-2 (x10 <sup>-7</sup> )	Cis B-2 (x10 <sup>-7</sup> )	Diene (x10 <sup>-7</sup> )
30	0	59.62	20.16	33.8	0.18	0	0.03	0.38	0.62	0.56	0.29
30	93	59.62	6.42	10.8	0	0	0.04	0.03	0.14	0.10	0
30	113	59.62	7.87	13.2	0	0	0.03	0.03	0.10	0.06	0
30	133	59.62	7.17	12	0	0	0.04	0	0.11	0.10	0
30	153	59.62	11.13	18.7	0	0	0	0	0	0	0
100	0	26.90	4.36	16.2	0	0	0	0.07	0.10	0.09	0
100	25	26.90	1.28	4.8	0	0	0	0.06	0.08	0.04	0.09
100	46	26.90	1.44	5.4	0	0	0	0.06	0.07	0	0
100	69	26.90	0.62	2.3	0	0	0	0.01	0.03	0	0.02
100	114	26.90	2.79	10.4	0	0	0	0.01	0	0	0
100	133	26.90	2.86	10.6	0	0	0	0	0	0	0
130	0	17.72	1.22	6.9	0	0	0	0.17	0.07	0	0
130	22	17.72	0.43	2.4	0	0	0	0.06	0	0	0
130	39	17.72	0.37	2.1	0	0	0	0.06	0	0	0
130	63	17.72	0.57	3.2	0	0	0	0.04	0	0	0
130	82	17.72	0.33	1.9	0	0	0	0.04	0	0	0

**Table 5.5.8** Product Selectivity for the Straight Dehydrogenation of Butane as a function of Flow-rate using 0.5% Pt/Al<sub>2</sub>O<sub>3</sub>.

Flow-rate (ml min <sup>-1</sup> )	Time (mins)	Met. Sel. (%)	Eth. Sel. (%)	Iso Sel. (%)	B-1 Sel. (%)	Trans B-2 Sel. (%)	Cis B-2 Sel. (%)	Diene Sel. (%)	Dehydro. Sel. (%)
30	0	0.2	0	0.1	1.9	3.1	2.8	1.4	9.2
30	93	0	0	0.6	0.4	2.2	1.6	0	4.2
30	113	0	0	0.4	0.4	1.3	0.8	0	2.5
30	133	0	0	0.6	0	1.5	1.4	0	2.9
30	153	0	0	0	0	0	0	0	0
100	0	0	0	0	1.6	2.3	2.1	0	6
100	25	0	0	0	4.7	6.2	3.1	7	21
100	46	0	0	0	1.6	4.9	0	0	6.5
100	69	0	0	0	1.6	4.8	0	3.2	9.6
100	114	0	0	0	0.4	0	0	0	0.4
100	133	0	0	0	0	0	0	0	0
130	0	0	0	0	13.9	5.7	0	0	19.6
130	22	0	0	0	14	0	0	0	14
130	39	0	0	0	16.2	0	0	0	16.2
130	63	0	0	0	7	0	0	0	7
130	82	0	0	0	12.1	0	0	0	12.1

**Table 5.5.9** Product Yields for the Straight Dehydrogenation of Butane as a function of Flow-rate using 0.5% Pt/Al<sub>2</sub>O<sub>3</sub>.

Flow-rate (ml min <sup>-1</sup> )	Time (mins)	Met. Yield (%)	Eth. Yield (%)	Iso Yield (%)	B-1 Yield (%)	Trans B-2 Yield (%)	Cis B-2 Yield (%)	Diene Yield (%)	Dehydro. Yield (%)
30	0	0.07	0	0.03	0.64	1.05	0.95	0.47	3.11
30	93	0	0	0.06	0.04	0.24	0.17	0	0.45
30	113	0	0	0.05	0.05	0.17	0.10	0	0.33
30	133	0	0	0.07	0	0.18	0.17	0	0.35
30	153	0	0	0	0	0	0	0	0
100	0	0	0	0	0.26	0.37	0.34	0	0.97
100	25	0	0	0	0.22	0.30	0.15	0.34	1.01
100	46	0	0	0	0.09	0.26	0	0	0.35
100	69	0	0	0	0.04	0.11	0	0.07	0.22
100	114	0	0	0	0.04	0	0	0	0.04
100	133	0	0	0	0	0	0	0	0
130	0	0	0	0	0.96	0.39	0	0	1.35
130	22	0	0	0	0.34	0	0	0	0.34
130	39	0	0	0	0.34	0	0	0	0.34
130	63	0	0	0	0.22	0	0	0	0.22
130	82	0	0	0	0.23	0	0	0	0.23

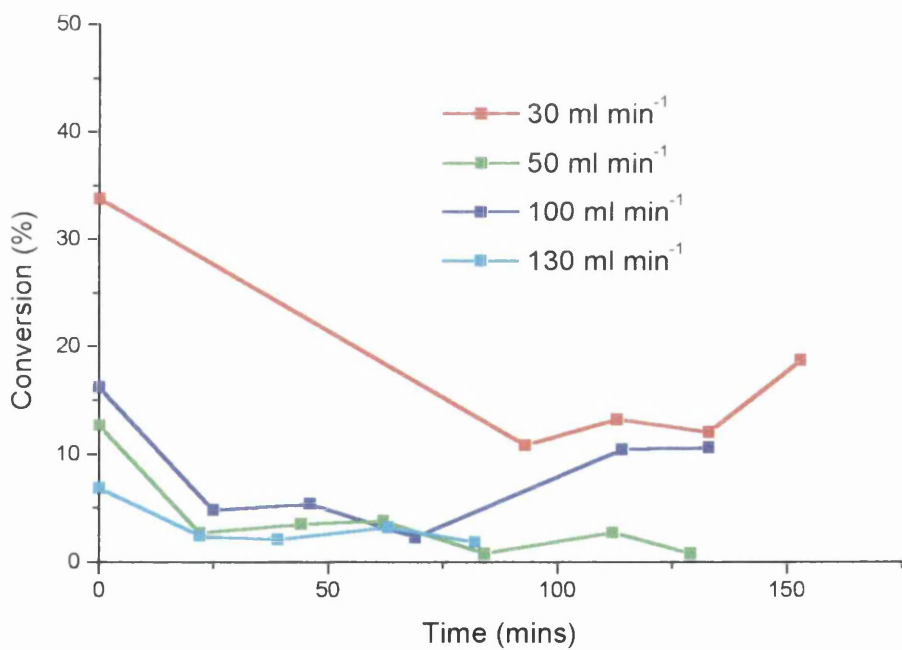


**Fig. 5.5.22** Conversion as a function of Time during the Straight Dehydrogenation of Butane at various Flow-rates using 0.5% Pt/Al<sub>2</sub>O<sub>3</sub>.

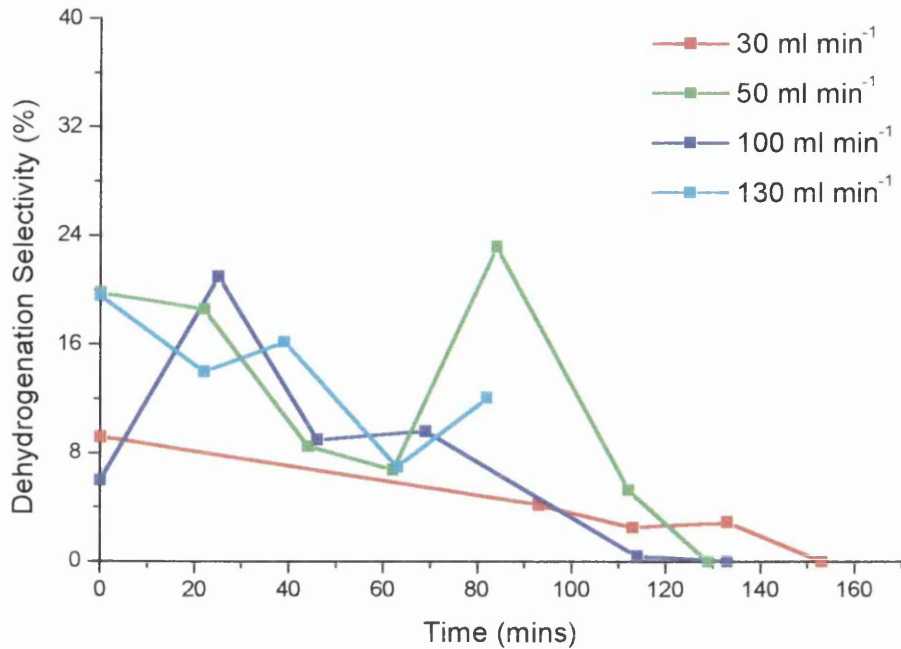


**Fig. 5.5.23** Dehydrogenation Selectivity as a function of Time during the Straight Dehydrogenation of Butane at various Flow-rates using 0.5% Pt/ $\text{Al}_2\text{O}_3$ .

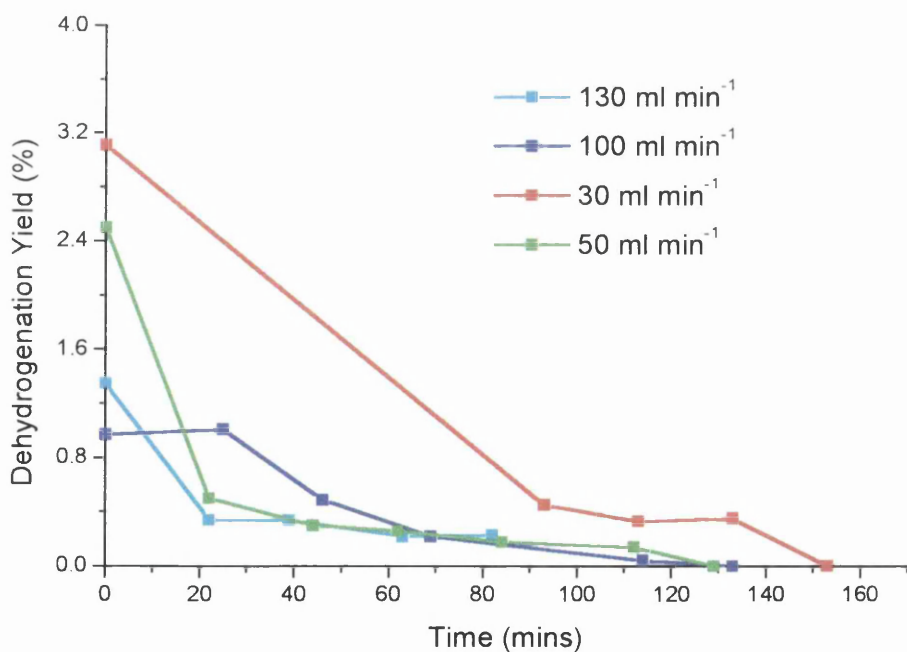


**Fig. 5.5.24** Dehydrogenation Yield as a function of Time during the Straight Dehydrogenation of Butane at various Flow-rates using 0.5% Pt/ $\text{Al}_2\text{O}_3$ .

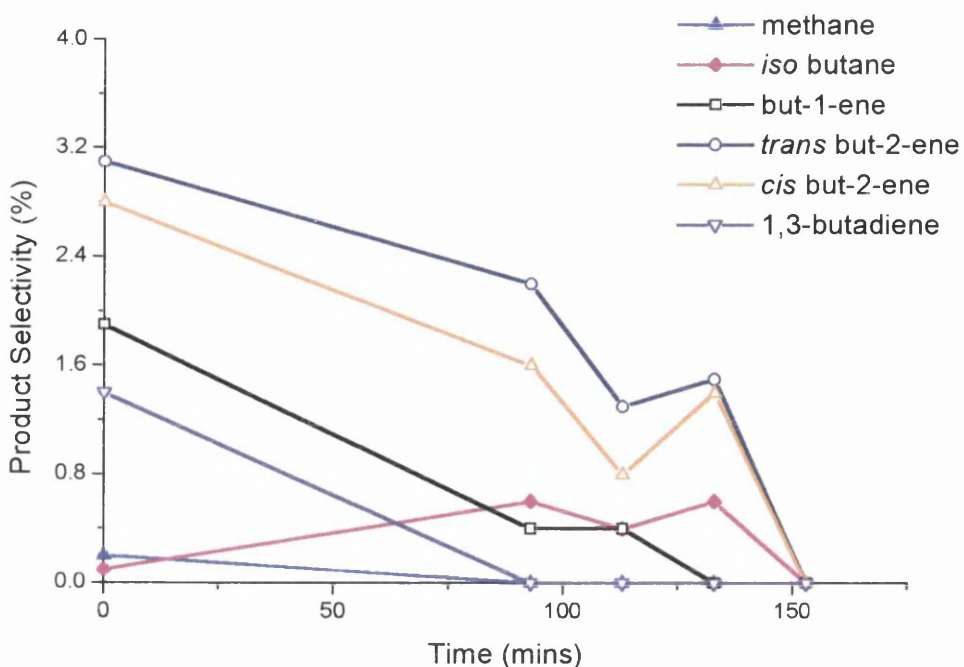


**Fig. 5.5.25** Product Selectivity as a function of Time during the Straight Dehydrogenation of Butane using the 0.5% Pt/Al<sub>2</sub>O<sub>3</sub> at 30 ml min<sup>-1</sup>.

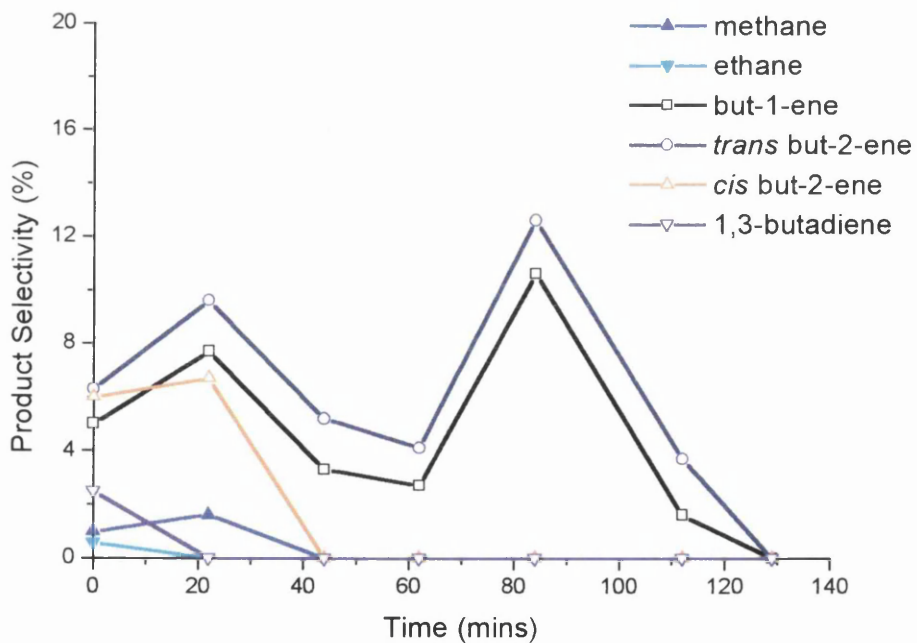


**Fig. 5.5.26** Product Selectivity as a function of Time during the Straight Dehydrogenation of Butane using the 0.5% Pt/Al<sub>2</sub>O<sub>3</sub> at 50 ml min<sup>-1</sup>.

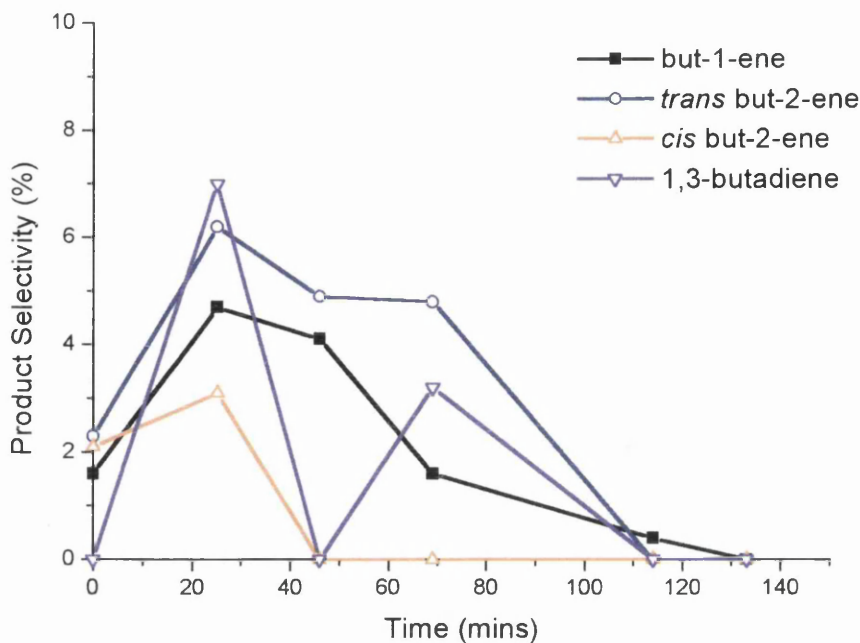


**Fig. 5.5.27** Product Selectivity as a function of Time during the Straight Dehydrogenation of Butane using the 0.5% Pt/Al<sub>2</sub>O<sub>3</sub> at 100 ml min<sup>-1</sup>.

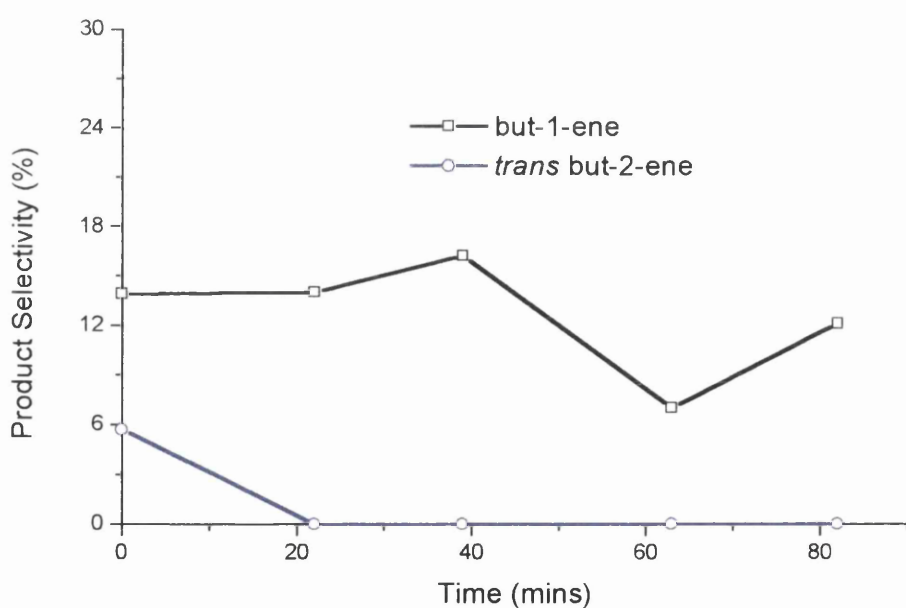


**Fig. 5.5.28** Product Selectivity as a function of Time during the Straight Dehydrogenation of Butane using the 0.5% Pt/Al<sub>2</sub>O<sub>3</sub> at 130 ml min<sup>-1</sup>.

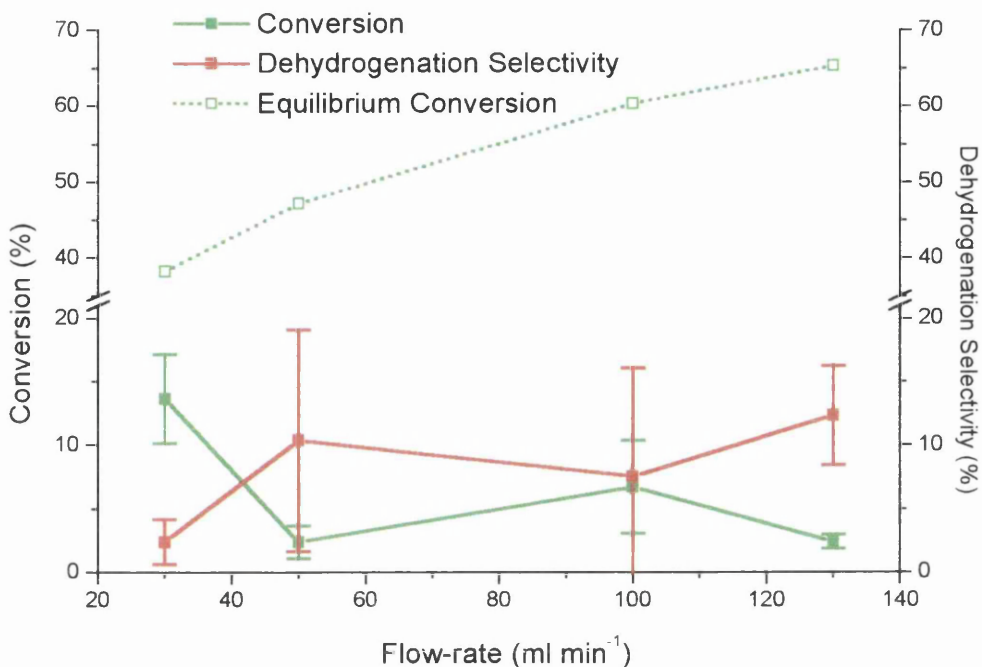


**Fig. 5.5.29** Conversion and Dehydrogenation Selectivity as a function of Flow-rate during the Straight Dehydrogenation of Butane using 0.5% Pt/Al<sub>2</sub>O<sub>3</sub> at 500°C.

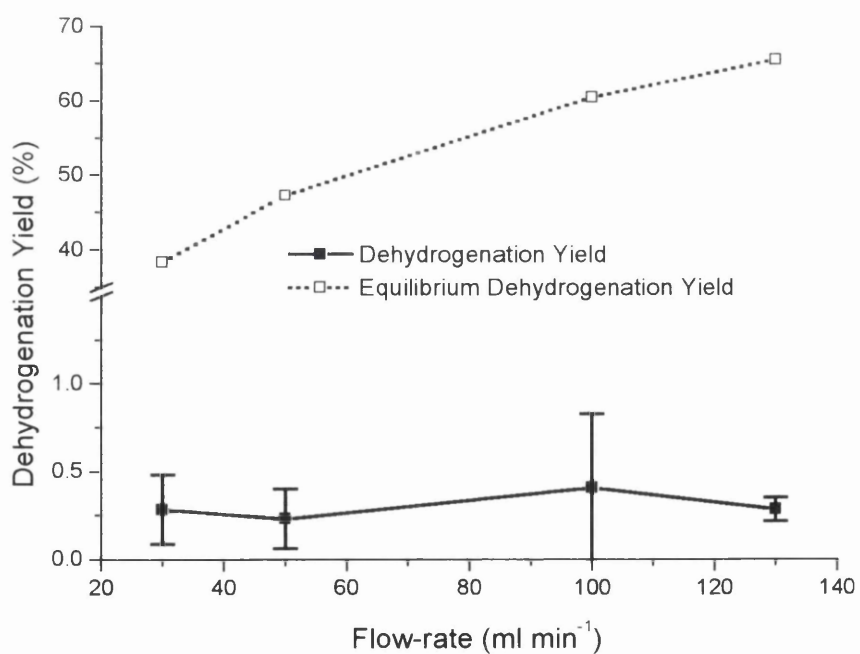


**Fig. 5.5.30** Dehydrogenation Yield as a function of Flow-rate during the Straight Dehydrogenation of Butane using 0.5% Pt/Al<sub>2</sub>O<sub>3</sub> at 500°C.

### 5.5.4 The Oxidative Dehydrogenation of Butane as a function of Flow-rate under Continuous-flow conditions using 0.5% Pt/Al<sub>2</sub>O<sub>3</sub>

Tables 5.5.10, 5.5.11 and 5.5.12 contain the conversion and product molar quantities, the product selectivity and the product yield values respectively for the oxidative dehydrogenation of butane using 0.5% Pt/Al<sub>2</sub>O<sub>3</sub> as a function of flow-rate. Figures 5.5.31 - 5.5.39 graphically represent these results with respect to the conversion, individual product selectivity, dehydrogenation selectivity and dehydrogenation yield as a function of time and temperature. A description of the experimental procedure is detailed in section 4.1.3.

**Table 5.5.10** Conversion and Product Molar Quantities for the Oxidative Dehydrogenation of Butane using 0.5% Pt/Al<sub>2</sub>O<sub>3</sub> as a function of Flow-rate.

Flow-rate (ml min <sup>-1</sup> )	Time (mins)	Moles Bypass (x10 <sup>-7</sup> )	Moles Reacted (x10 <sup>-7</sup> )	Conv. (%)	CO <sub>2</sub> /Pr (x10 <sup>-7</sup> )	CO (x10 <sup>-7</sup> )	Met. (x10 <sup>-7</sup> )	Eth. (x10 <sup>-7</sup> )	Iso (x10 <sup>-7</sup> )	B-1 (x10 <sup>-7</sup> )	Trans B-2 (x10 <sup>-7</sup> )	Cis B-2 (x10 <sup>-7</sup> )	Diene (x10 <sup>-7</sup> )
100	0	28.02	7.87	28.1	2.06	1.38	0	0	0	0.30	0.08	0.05	0
100	56	28.02	7.44	26.6	2.30	0.65	0	0	0	0.17	0	0	0
100	110	28.02	7.78	27.8	2.41	0.42	0	0	0	0.18	0	0	0
100	158	28.02	7.26	25.9	2.18	0.31	0	0	0	0.10	0.06	0	0
100	225	28.02	7.18	25.6	2.30	0.58	0	0	0	0.06	0	0	0
100	286	28.02	7.62	27.2	2.22	0.44	0	0	0	0.07	0	0	0
130	0	23.52	8.10	34.4	1.84	1.50	0	0	0	0.12	0.06	0	0
130	59	23.52	6.35	27	1.86	0.54	0	0	0	0.07	0	0	0
130	107	23.52	6.53	27.8	1.69	0.43	0	0	0	0.05	0	0	0
130	156	23.52	6.14	26.1	1.90	0.44	0	0	0	0.04	0	0	0
130	211	23.52	6.95	29.5	1.76	0.33	0	0	0	0.05	0	0	0
130	256	23.52	7.07	30	1.63	0.43	0	0	0	0.03	0	0	0

**Table 5.5.11** Product Selectivity for the Oxidative Dehydrogenation of Butane using 0.5% Pt/Al<sub>2</sub>O<sub>3</sub> as a function of Flow-rate.

Flow-rate (ml min <sup>-1</sup> )	Time (mins)	CO <sub>2</sub> /Pr Sel. (%)	CO Sel. (%)	Met. Sel. (%)	Eth. Sel. (%)	Iso Sel. (%)	B-1 Sel. (%)	Trans B-2 Sel. (%)	Cis B-2 Sel. (%)	Diene Sel. (%)	Dehydro. Sel. (%)
100	0	6.5	4.4	0	0	0	3.8	1.0	0.6	0	5.4
100	56	7.7	2.2	0	0	0	2.3	0	0	0	2.3
100	110	7.7	1.3	0	0	0	2.3	0	0	0	2.3
100	158	7.5	1.1	0	0	0	1.4	0.8	0	0	2.2
100	225	8.0	2.0	0	0	0	0.8	0	0	0	0.8
100	286	7.3	1.4	0	0	0	0.9	0	0	0	0.9
130	0	5.7	4.6	0	0	0	1.5	0.7	0	0	2.2
130	59	7.3	2.1	0	0	0	1.1	0	0	0	1.1
130	107	6.5	1.6	0	0	0	0.8	0	0	0	0.8
130	156	7.7	1.8	0	0	0	0.6	0	0	0	0.6
130	211	6.3	1.2	0	0	0	0.7	0	0	0	0.7
130	256	5.8	1.5	0	0	0	0.4	0	0	0	0.4

**Table 5.5.12** Product Yields for the Oxidative Dehydrogenation of Butane using 0.5% Pt/Al<sub>2</sub>O<sub>3</sub> as a function of Flow-rate.

Flow-rate (ml min <sup>-1</sup> )	Time (mins)	CO <sub>2</sub> /Pr Yield (%)	CO Yield (%)	Met. Yield (%)	Eth. Yield (%)	Iso Yield (%)	B-1 Yield (%)	Trans-B-2 Yield (%)	Cis-B-2 Yield (%)	Diene Yield (%)	Dehydro. Yield (%)
100	0	1.83	1.24	0	0	0	1.07	0.28	0.17	0	1.52
100	56	2.05	0.58	0	0	0	0.61	0	0	0	0.61
100	110	2.14	0.36	0	0	0	0.64	0	0	0	0.64
100	158	1.94	0.24	0	0	0	0.36	0.21	0	0	0.57
100	225	2.05	0.51	0	0	0	0.20	0	0	0	0.20
100	286	1.98	0.38	0	0	0	0.24	0	0	0	0.24
130	0	1.96	1.58	0	0	0	0.52	0.24	0	0	0.76
130	59	1.97	0.57	0	0	0	0.30	0	0	0	0.30
130	107	1.81	0.44	0	0	0	0.22	0	0	0	0.22
130	156	2.01	0.47	0	0	0	0.16	0	0	0	0.16
130	211	1.86	0.35	0	0	0	0.21	0	0	0	0.21
130	256	1.74	0.45	0	0	0	0.12	0	0	0	0.12

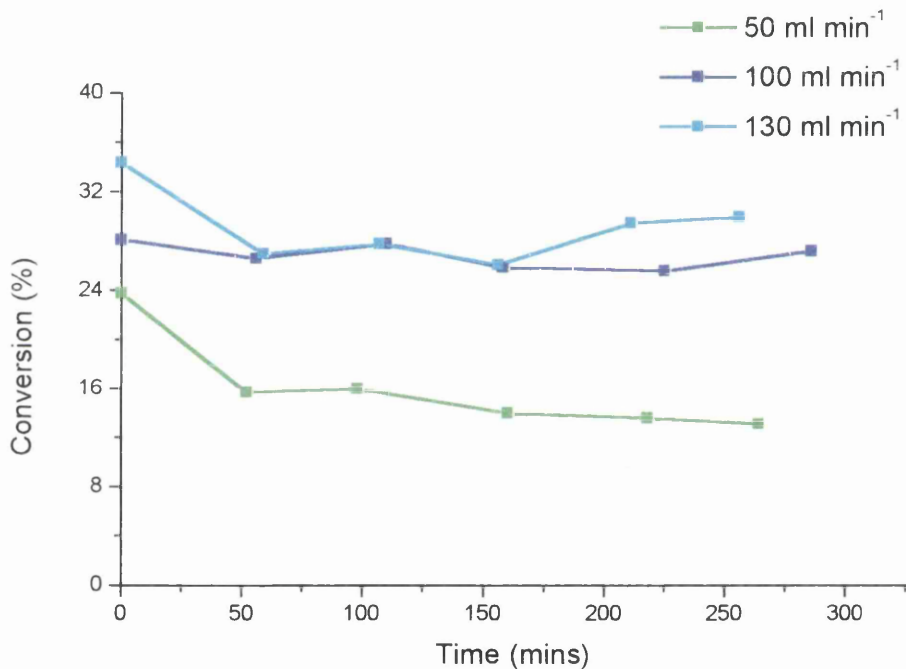


**Fig. 5.5.31** Conversion as a function of Time during the Oxidative Dehydrogenation of Butane at various Flow-rates using 0.5% Pt/Al<sub>2</sub>O<sub>3</sub>.

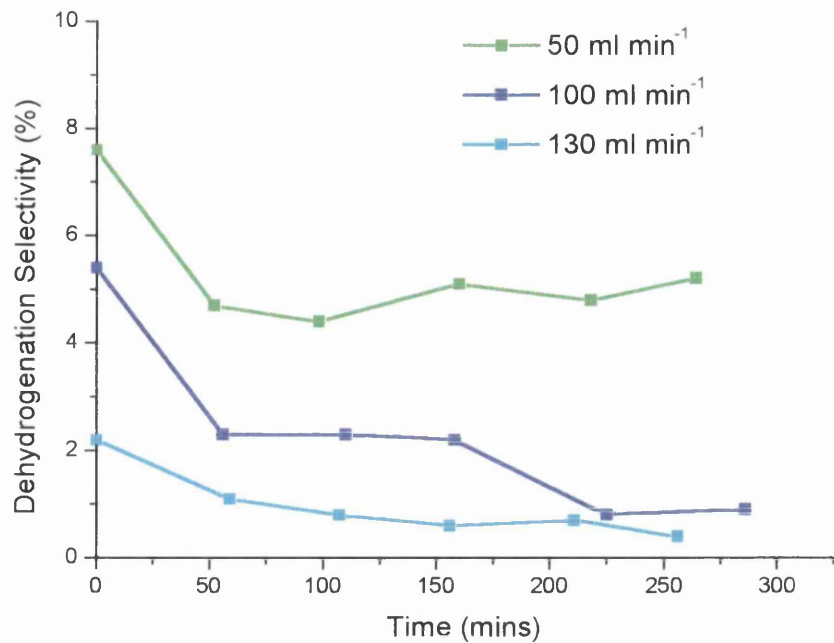


**Fig. 5.5.32** Dehydrogenation Selectivity as a function of Time during the Oxidative Dehydrogenation of Butane at various Flow-rates using 0.5% Pt/Al<sub>2</sub>O<sub>3</sub>.

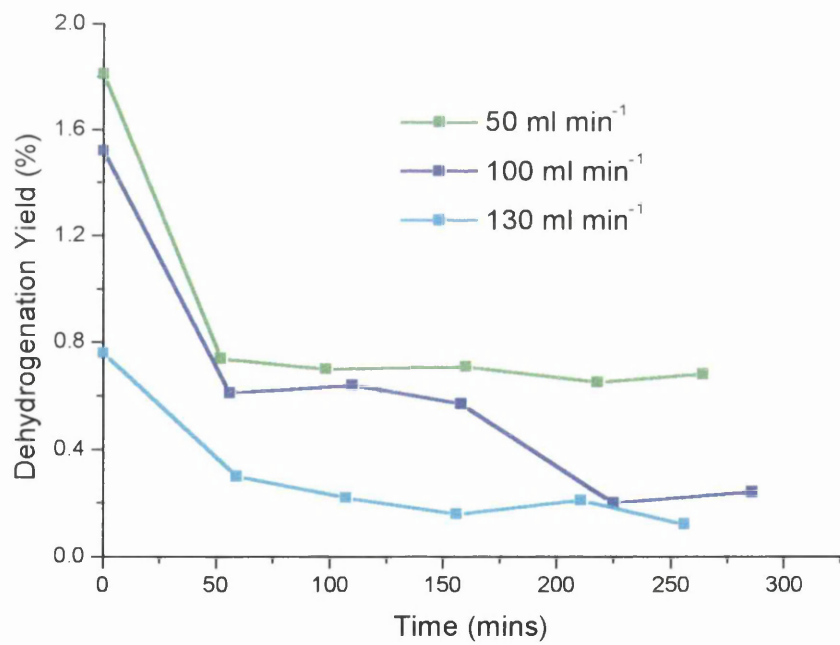


**Fig. 5.5.33** Dehydrogenation Yield as a function of Time during the Oxidative Dehydrogenation of Butane at various Flow-rates using 0.5% Pt/Al<sub>2</sub>O<sub>3</sub>.

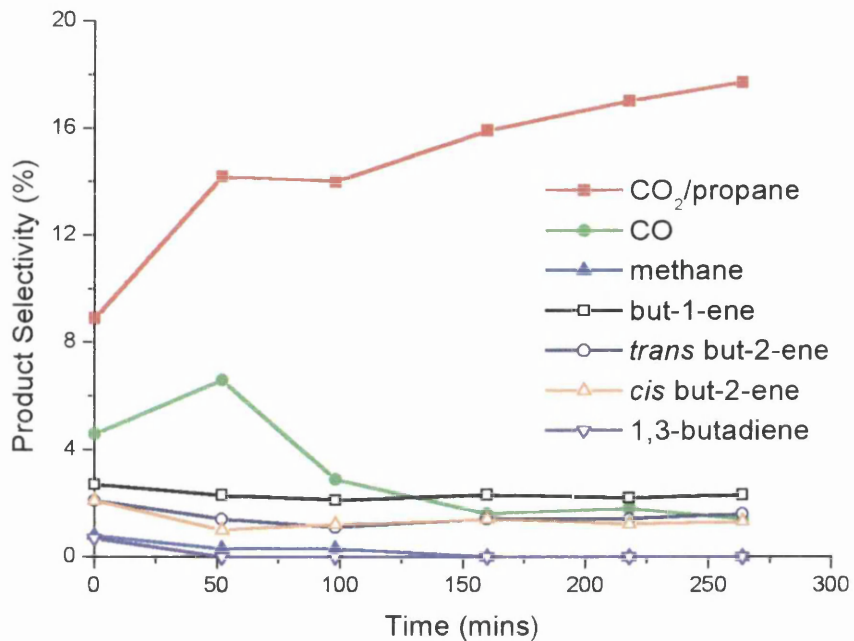


**Fig. 5.5.34** Product Selectivity as a function of Time during the Oxidative Dehydrogenation of Butane using the 0.5% Pt/Al<sub>2</sub>O<sub>3</sub> at 50 ml min<sup>-1</sup>.

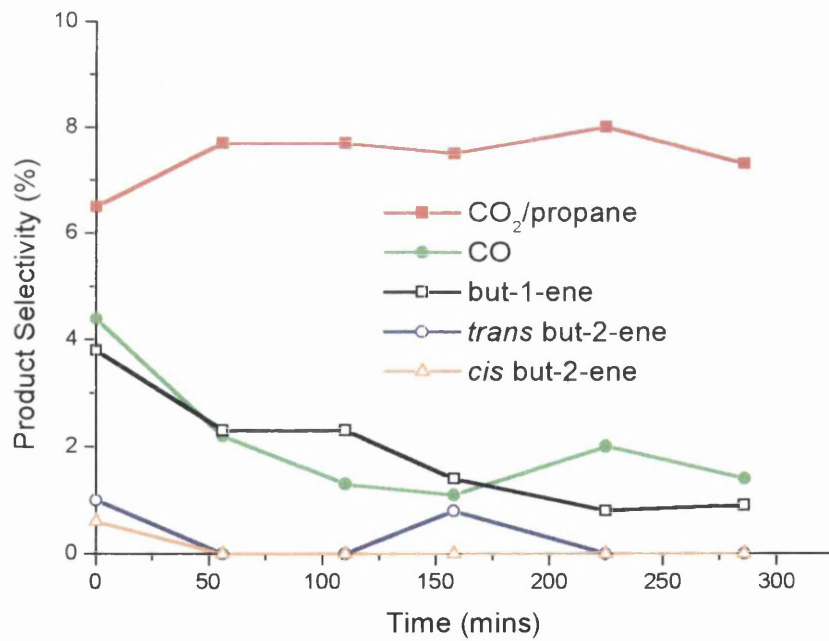


**Fig. 5.5.35** Product Selectivity as a function of Time during the Oxidative Dehydrogenation of Butane using the 0.5% Pt/Al<sub>2</sub>O<sub>3</sub> at 100 ml min<sup>-1</sup>.

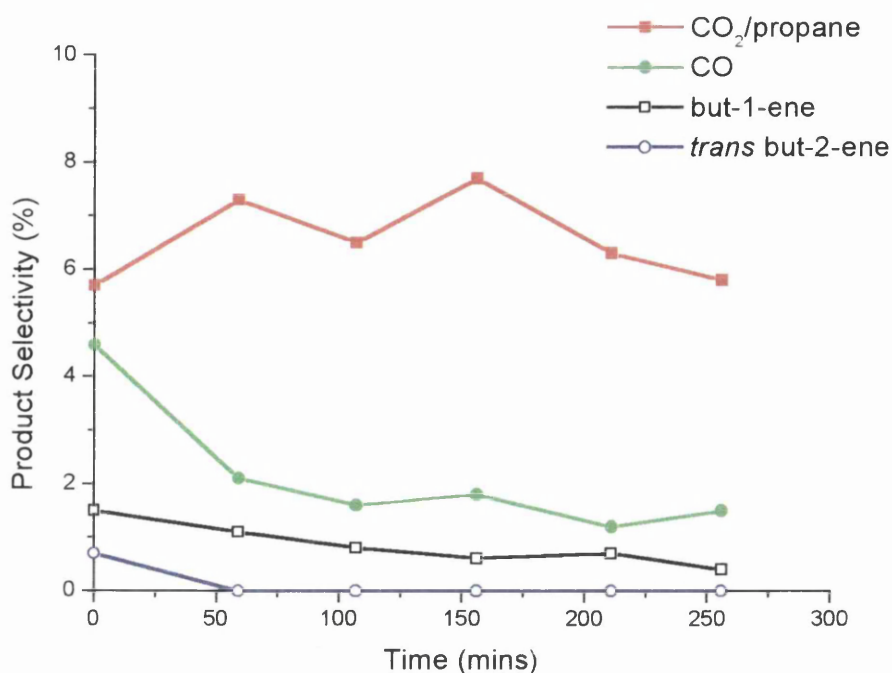


**Fig. 5.5.36** Product Selectivity as a function of Time during the Oxidative Dehydrogenation of Butane using the 0.5% Pt/Al<sub>2</sub>O<sub>3</sub> at 130 ml min<sup>-1</sup>.

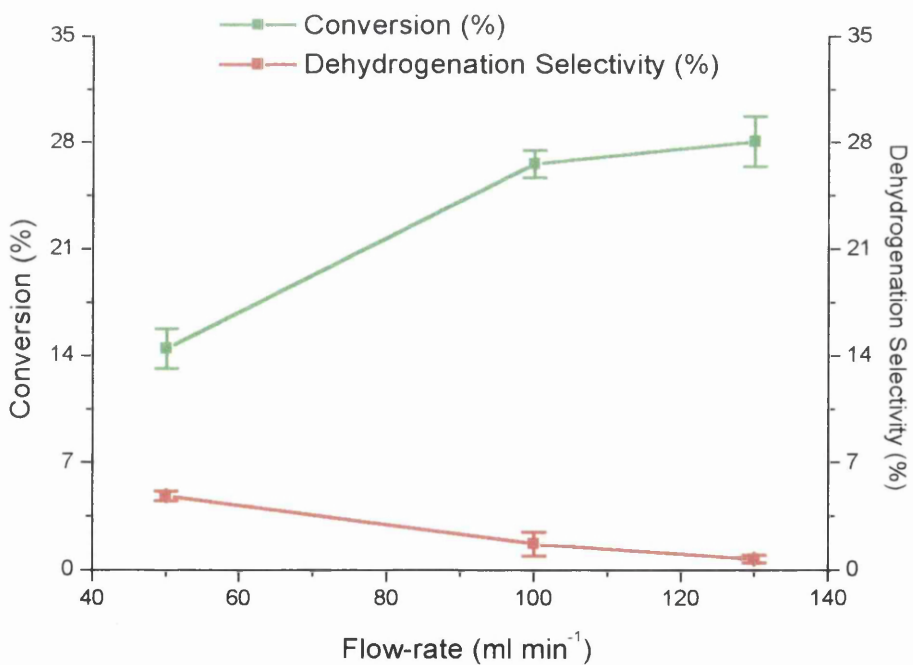


**Fig. 5.5.37** Conversion and Dehydrogenation Selectivity as a function of Flow-rate during the Oxidative Dehydrogenation of Butane using 0.5% Pt/Al<sub>2</sub>O<sub>3</sub> at 500°C.

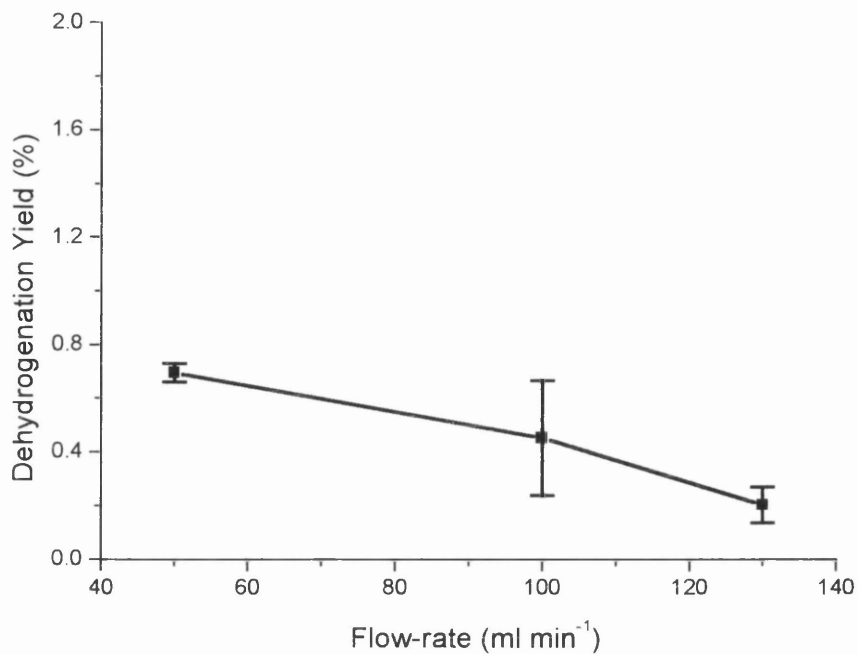


**Fig. 5.5.38** Dehydrogenation Yield as a function of Flow-rate during the Oxidative Dehydrogenation of Butane using 0.5% Pt/ $\text{Al}_2\text{O}_3$  at 500°C.

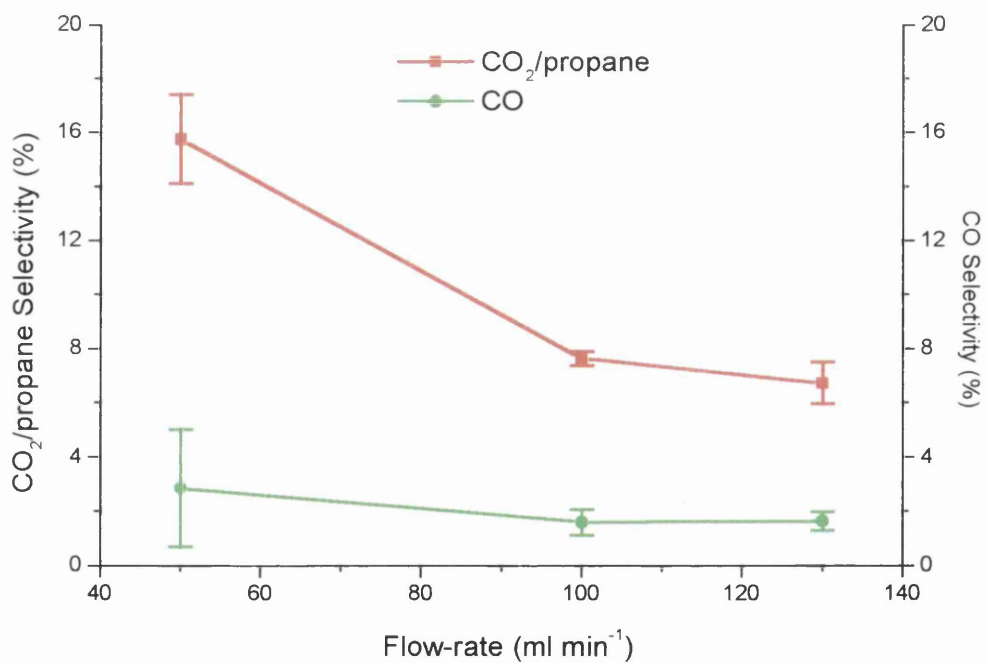


**Fig. 5.5.39**  $\text{CO}_2$  and CO Product Selectivity during the Oxidative Dehydrogenation of Butane using 0.5% Pt/ $\text{Al}_2\text{O}_3$  at 500°C.

### **5.5.5 Summary of the Testing Reactions of the 0.5% Pt/Al<sub>2</sub>O<sub>3</sub> Catalyst under Continuous-flow conditions**

The straight and oxidative dehydrogenation reactions of butane have been carried out using the 0.5% Pt/Al<sub>2</sub>O<sub>3</sub> catalyst. Comparison of figure 5.5.9 and 5.5.19 illustrates the differences between the two processes in terms of conversion. It can be observed that overall the activity of the catalyst in the case of the oxidative dehydrogenation is higher than that for the straight dehydrogenation. This is especially important at the lower temperatures (200-400°C) before the onset of homogeneous gas phase reactions, the temperature of which were determined in section 5.3. It is also apparent that the homogeneous reactions begin at lower temperatures in the case of the oxidative dehydrogenation compared to those in the straight dehydrogenation [58]. As described earlier this is a result of the activating power of the oxygen towards the hydrocarbon molecule leading to radical reactions as well as the thermodynamic drive to produce water, as explained in section 5.1.2.

Figures 5.5.9 and 5.5.19 contain the dehydrogenation selectivity for the straight and oxidative dehydrogenation respectively. It is clear that very low amounts of olefin products are formed during both methods. In fact when compared to the empty reactor and the support material (figures 5.3.3 and 5.4.15 respectively) it is apparent that the best results occur when no catalyst is used, in the case of oxidative dehydrogenation at 400 and 500°C, as shown by Burch and Crabb [58]. In fact the poorest result is observed for the oxidative dehydrogenation using the catalyst. This suggests that the catalyst is in fact breaking up the butane molecules on its surface resulting in combustion and therefore a higher selectivity towards C<sub>1</sub> products, in particular CO<sub>2</sub> [10].

The results obtained from the straight dehydrogenation carried out over the catalyst present some interesting results. Figure 5.5.9 shows that the selectivity towards olefin formation is at its highest at approximately 600°C decreasing as the homogeneous reaction, forming cracking products and *iso*-butane, become more apparent. However, there is a smaller maximum found at 300°C which, if real, suggests that there is a window, under milder conditions, where dehydrogenation can occur but is too weak to enforce total carbon backbone break-up. This effect is completely catalytic as it is not observed with the empty reactor vessel or the support material. It

should also be noted that the observed values at 300°C, with respect to their associated error bars obtained from reproducibility measurements, indicate this to be a valid result.

The results also show that deactivation is a major issue that has to be considered. Figure 5.5.1 and 5.5.2 illustrates deactivation under straight dehydrogenation conditions. Initial selectivity of 45% towards dehydrogenation products is obtained at 600°C decreasing to 20% after the first injections. Similarly at 400°C, 25% dehydrogenation selectivity is obtained which subsequently falls to approximately zero after the initial samples have been taken.

Likewise under oxidative dehydrogenation conditions figure 5.5.12 shows that deactivation of the catalyst takes place. At 300°C the dehydrogenation selectivity is approximately 11%, which then falls to zero as the catalyst begins to deactivate with respect to olefin production. This can also be seen for the other temperatures to a lesser extent.

Deactivation of the catalyst happens as a consequence of blockage of the active metal sites where reactions to form butene species take place. Carbonaceous material is deposited on the metal atoms as well as blocking up the pores of the support material, resulting in restricted access of the reactant gases to the active catalyst surface [46, 47]. In the oxidative dehydrogenation process it is possible that deactivation could also be occurring due to sintering of the metal crystallites, accelerated by the presence of water, which is a by-product of both dehydrogenation and combustion [15].

The other two important types of reaction which occur in these systems are the break-up of the butane backbone, forming lower alkanes and oxygenates in the case of oxidative dehydrogenation, and isomerisation to form *iso*-butane. Figures 5.5.4 - 5.5.8 and 5.5.14 - 5.5.18 illustrate the product selectivity for each of the various reactions studied. In the case of straight dehydrogenation C<sub>1</sub> production is insignificant and it is the formation of ethane by cleavage of the C<sub>2</sub> and C<sub>3</sub> carbon atoms, as well as the production of *iso*-butane from isomerisation of the butane starting material that occurs most readily as the conversion is increased. Comparison with the empty reactor and support material tests show that these processes are almost exclusively homogeneous transformations.

In the case of the oxidative dehydrogenation C<sub>1</sub> production becomes more relevant. When the catalyst is used CO<sub>2</sub> is the major product detected. CO is also formed at the high temperatures where the carbon - carbon break-up occurs more readily with the result that the amount of oxygen in the mixture becomes less in relation to the amount of carbon available. Methane production again is minimal but is sustained at all temperatures.

It is thought that the CO<sub>2</sub> produced in this reaction is formed by the oxygen reacting with the carbon (combustion), which causes the deactivation in the straight dehydrogenation system, deposited on the metal surface [76]. This is studied and explained in more detail in the pulse-flow section below. This is also supported by the fact that when similar reactions are carried out using the support material only, and the empty reactor, the amount of CO<sub>2</sub> formed is minimal. CO as mentioned above is also minimal throughout these reactions and again isomerisation between 500-600°C with ethane also being dominant at the high temperatures.

The final parameter to be varied was the linear velocity. Figures 5.5.22 - 5.5.30 describe the results obtained for the straight dehydrogenation as a function of flow-rate while figures 5.5.31 - 5.5.38 represent the outcome of equivalent experiments carried out under oxidative conditions. The results from the straight dehydrogenation behave as expected. Figure 5.5.29 shows that as the linear velocity is increased the conversion tends to decrease as a consequence of the reduction in contact time. It is also interesting to see that as the contact time is reduced the selectivity towards the dehydrogenation products increases. When it is studied in greater detail (table 5.5.8), it can be seen that in fact there is an increase in the selectivity towards the but-1-ene species and a decrease in the remaining olefin products. This could suggest that there is an isomerisation process taking place converting but-1-ene species to but-2-ene species, which can be controlled to a certain extent by manipulation of the linear velocity.

In the case of oxidative dehydrogenation it is interesting to see from figure 5.5.37 that the conversion increases as the linear velocity is increased. In terms of the product selectivity, there is a decrease in the amount of all products formed. This is most apparent in the case of CO<sub>2</sub> (figure 5.5.39). The dehydrogenation products remain steady but are found at very low levels. Decomposition processes, leading to oligomer formation, are responsible for the observed increase in conversion. The

oligomer species were detected purely by visual observation, as a brown/yellow substance on the exhaust side of the reactor vessel at the exit of the furnace. Figure 5.5.40 is a diagrammatic representation of where the oligomer material collected on the reactor walls of the reactor after one of these reactions. The identity of this/these species is unknown, however GC-MS has confirmed the existence of high molecular weight compounds ( $>70$  amu) with  $^1\text{H}$  NMR providing evidence to suggest that these are aromatic in nature, possibly consisting of extended ring structures and heterocycles [100]. The formation of oligomer species is well known under these conditions [1].

### **5.5.6 Post-reaction Analysis of the 0.5% Pt/Al<sub>2</sub>O<sub>3</sub> Catalyst after Continuous-flow Experiments**

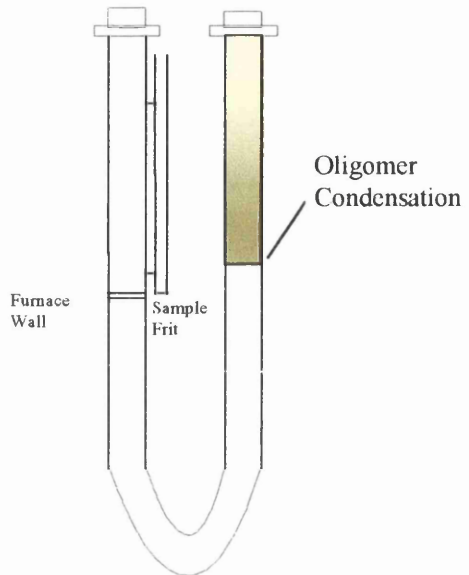
The post-reaction analysis of the 0.5% Pt/Al<sub>2</sub>O<sub>3</sub> catalyst was carried out in an attempt to see if any changes were made to the size and composition of the catalyst after being subject to straight and oxidative dehydrogenation reactions under continuous-flow. Two measurements were carried out. Temperature programmed oxidation (TPO) was carried out in order to observe any changes to the catalyst surface in terms of carbon deposition while TEM was conducted to see if there was any change to the particle size through sintering of the metal crystallites.

Figure 5.5.41 illustrates the outcome of the TPO experiments with section 4.3.6 describing the method used to carry out the experiments. Both spectra show the presence of a peak centered at approximately 395°C. Data obtained from the literature suggest that this results from carbonaceous material deposited on the alumina support material [41]. It was also suggested that carbonaceous material associated with the metal would be found at a lower temperature. However, this is not observed in this set of spectra possibly because the surface area of the metal is very much smaller than that of the support material, thus it is conceivable that the resultant peak would be small in comparison to that associated with the support material.

The peak observed at approximately 475°C is not observed in the literature, but could be attributed to the oxidation of the oligomer products observed in the oxidative dehydrogenation reactions.

Unfortunately, resolution problems with the electron microscope has resulted in uninformative micrographs. Figure 5.5.42 and 5.5.43 shows no sign of any metal

particles. It was hoped that changes in the particle size could be observed, especially with the oxidative dehydrogenation, where the large amounts of water that form almost certainly result in sintering [15].



**Fig. 5.5.40** Diagrammatic Representation of the Oligomer Formation on the Quartz Reactor.

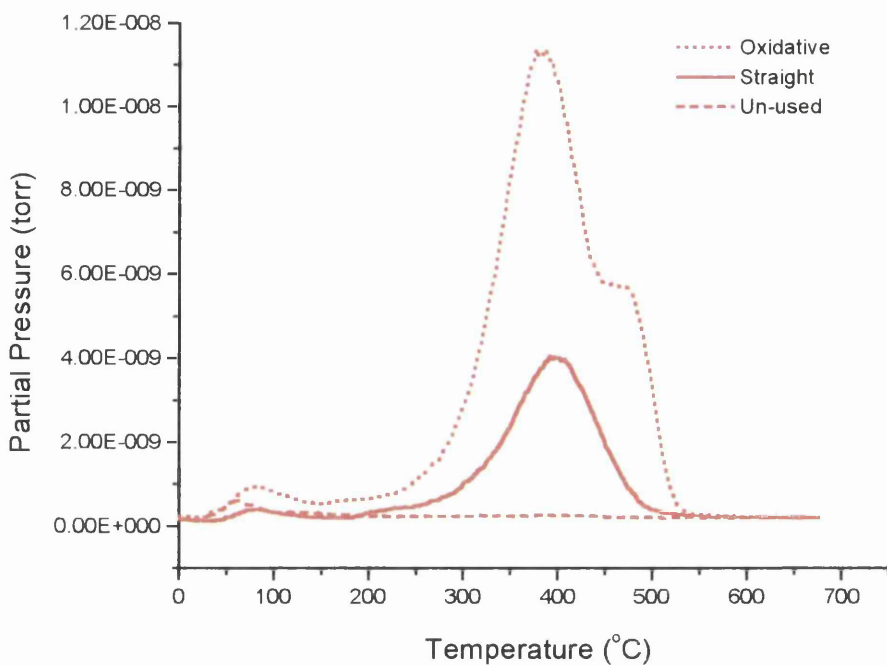


**Fig. 5.5.41** TPO of the 0.5% Pt/Al<sub>2</sub>O<sub>3</sub> Catalysts (following mass 44).

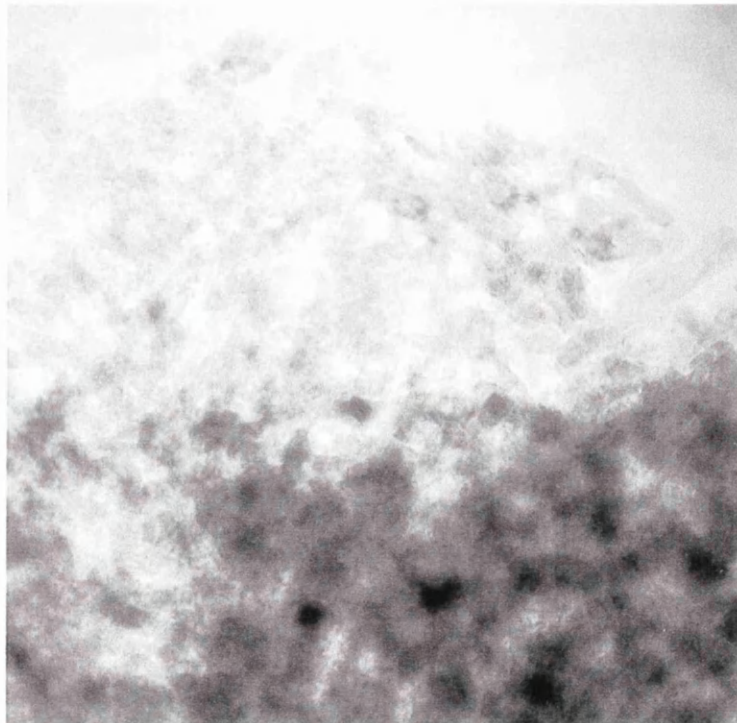


**Fig. 5.5.42** TEM Micrograph of the 0.5% Pt/Al<sub>2</sub>O<sub>3</sub> Catalyst after Straight Dehydrogenation.

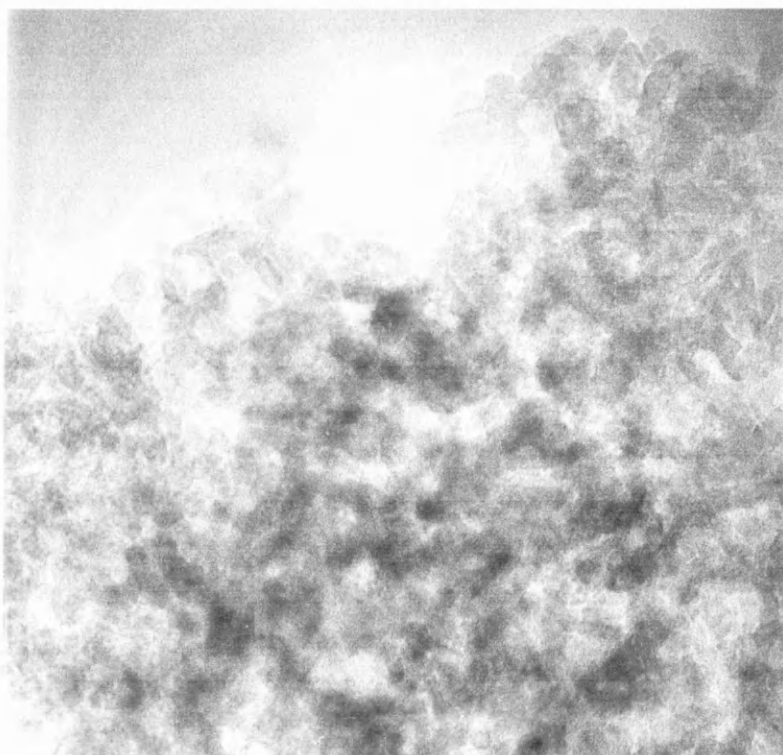


**Fig. 5.5.43** TEM Micrograph of the 0.5% Pt/Al<sub>2</sub>O<sub>3</sub> Catalyst after Oxidative Dehydrogenation.

## *5.6 The Straight and Oxidative Dehydrogenation of Butane using 0.65% Pt/Al<sub>2</sub>O<sub>3</sub>*

The reactions detailed above for the 0.5% Pt/Al<sub>2</sub>O<sub>3</sub> were repeated on an alternative 0.65% catalyst which has a very different dispersion (78% compared to 38% using CO as the adsorbate) in an attempt to change the behavior of the catalysts in favour of dehydrogenation. Section 5.2 describes the characteristics of both the catalysts and highlights the differences between them.

Further studies were carried out using this catalysts. As well as a temperature study and flow-rate variations, changing the catalyst mass and manipulation of hydrocarbon:oxygen ratio were also investigated to see if a set of conditions could be found where high dehydrogenation selectivity and conversion could be achieved. The results for all of these studies are compiled below and summarised in section 5.6.8.

### **5.6.1 The Straight Dehydrogenation of Butane as a function of Temperature under Continuous-flow conditions using 0.65% Pt/Al<sub>2</sub>O<sub>3</sub>**

Tables 5.6.1, 5.6.2 and 5.6.3 contain the conversion and product molar quantities, the product selectivity and the product yield values respectively for the straight dehydrogenation of butane using 0.65% Pt/Al<sub>2</sub>O<sub>3</sub> as a function of temperature. Figures 5.6.1 - 5.6.9 graphically represent these results with respect to the conversion, individual product selectivity, dehydrogenation selectivity and dehydrogenation yield as a function of time and temperature, showing the equilibrium results, where appropriate, for comparison. Section 4.1.3 describes the procedure used to carry out the experiments.

**Table 5.6.1** Conversion and Product Molar Quantities for the Straight Dehydrogenation of Butane using 0.65% Pt/Al<sub>2</sub>O<sub>3</sub>.

Temp. (°C)	Time (mins)	Moles Bypass (x10 <sup>-7</sup> )	Moles React. (x10 <sup>-7</sup> )	Conv. (%)	Met. (x10 <sup>-7</sup> )	Eth. (x10 <sup>-7</sup> )	Iso. (x10 <sup>-7</sup> )	B-1 (x10 <sup>-7</sup> )	Trans B-2 (x10 <sup>-7</sup> )	Cis B-2 (x10 <sup>-7</sup> )	Diene (x10 <sup>-7</sup> )
200	0	38.91	0	0	0	0	0	0	0	0	0
200	24	38.91	0	0	0	0	0	0	0	0	0
200	39	38.91	0	0	0	0	0	0	0	0	0
200	57	38.91	0	0	0	0	0	0	0	0	0
300	0	39.08	2.10	5.4	0	0	0	0.25	0.24	0.20	0
300	24	39.08	2.14	5.5	0	0	0	0.02	0.22	0.18	0
300	44	39.08	1.44	3.7	0	0	0	0	0.21	0.15	0
300	65	39.08	1.59	4.1	0	0	0	0	0.22	0.15	0
300	97	39.08	3.08	7.9	0	0	0	0	0.17	0.10	0
400	0	38.29	4.60	12.0	0.27	0.14	0.08	0.67	1.26	1.09	0
400	30	38.29	1.87	4.9	0.10	0	0	0.29	0.69	0.63	0
400	50	38.29	2.12	5.5	0.06	0	0	0.23	0.55	0.45	0
400	73	38.29	1.35	3.5	0	0	0	0.19	0.49	0.41	0
400	105	38.29	1.14	3.0	0	0	0	0.15	0.41	0.31	0
400	141	38.29	1.10	2.9	0	0	0	0.12	0.33	0.28	0
500	0	39.66	14.72	37.1	1.91	1.09	0.90	4.05	2.85	2.59	0.39
500	25	39.66	4.64	11.7	0.20	0	0.08	0.98	0.87	0.79	0.30
500	69	39.66	1.92	4.8	0.08	0	0	0.34	0.36	0.32	0.12
500	109	39.66	1.22	3.1	0.07	0	0	0.32	0.31	0.26	0.10
500	132	39.66	1.67	4.2	0.05	0	0	0.27	0.28	0.25	0.07
600	0	41.37	22.86	55.2	2.74	2.22	1.29	4.45	2.19	1.96	1.02
600	23	41.37	9.63	23.3	0.76	0.96	0.53	1.67	0.77	0.62	0.58
600	46	41.37	8.28	20.0	0.72	1.05	0.58	1.35	0.58	0.50	0.46
600	78	41.37	6.24	15.1	0.72	1.13	0.62	1.69	0.46	0.35	0.30
600	145	41.37	5.19	12.5	0.70	1.16	0.62	0.34	0.20	0.20	0.21
600	210	41.37	4.15	10.0	0.68	1.04	0.63	0	0.17	0.13	0.20
600	234	41.37	6.27	15.2	0.65	1.00	0.60	0.24	0.15	0.16	0.23

**Table 5.6.2** Product Selectivity for the Straight Dehydrogenation of Butane as a function of Temperature using 0.65% Pt/Al<sub>2</sub>O<sub>3</sub>.

Temp. (°C)	Time (mins)	Met. Sel. (%)	Eth. Sel. (%)	Iso. Sel. (%)	B-1 Sel. (%)	Trans B-2 Sel. (%)	Cis B-2 Sel. (%)	Diene Sel. (%)	Dehydro. Sel. (%)
200	0	0	0	0	0	0	0	0	0
200	24	0	0	0	0	0	0	0	0
200	39	0	0	0	0	0	0	0	0
200	57	0	0	0	0	0	0	0	0
300	0	0	0	0	1.0	11.4	9.5	0	21.9
300	24	0	0	0	0.9	10.3	8.4	0	19.6
300	44	0	0	0	0	14.6	10.4	0	25.0
300	65	0	0	0	0	13.8	9.4	0	23.2
300	97	0	0	0	0	5.5	3.2	0	8.7
400	0	1.5	1.5	1.7	14.6	27.4	23.7	0	65.7
400	30	1.3	0	0	15.5	36.9	33.7	0	86.1
400	50	0.7	0	0	10.8	25.9	21.2	0	57.9
400	73	0	0	0	14.1	36.3	30.4	0	80.8
400	105	0	0	0	13.2	36.0	27.2	0	76.4
400	141	0	0	0	10.9	30.0	25.4	0	66.3
500	0	3.2	3.7	6.1	27.5	19.4	17.6	2.6	67.1
500	25	1.1	0	1.7	21.1	18.8	17.0	6.5	63.4
500	69	1.0	0	0	17.7	18.8	16.7	6.2	59.4
500	109	1.4	0	0	26.2	25.4	21.3	8.2	81.1
500	132	0.7	0	0	16.2	16.8	15.0	4.2	52.2
600	0	3.0	4.8	5.6	19.5	9.6	8.6	4.5	42.2
600	23	2.0	5.0	5.5	17.3	8.0	6.4	6.0	37.7
600	46	2.2	6.3	7.0	16.3	7.0	6.0	5.6	34.9
600	78	2.9	9.0	9.9	27.1	7.4	5.6	4.8	44.9
600	145	3.4	11.2	11.9	6.6	3.8	3.8	4.0	18.2
600	210	4.1	12.5	15.2	0	4.1	3.1	4.8	12.0
600	234	2.6	8.0	9.6	3.8	2.4	2.6	3.7	12.5

**Table 5.6.3** Product Yields for the Straight Dehydrogenation of Butane as a function of Temperature using 0.65% Pt/Al<sub>2</sub>O<sub>3</sub>.

Temp. (°C)	Time (mins)	Met. Yield (%)	Eth. Yield (%)	Iso Yield (%)	B-1 Yield (%)	Trans B-2 Yield (%)	Cis B-2 Yield (%)	Diene Yield (%)	Dehydro. Yield (%)
200	0	0	0	0	0	0	0	0	0
200	24	0	0	0	0	0	0	0	0
200	39	0	0	0	0	0	0	0	0
200	57	0	0	0	0	0	0	0	0
300	0	0	0	0	0.05	0.62	0.51	0	1.18
300	24	0	0	0	0.05	0.57	0.46	0	1.08
300	44	0	0	0	0	0.54	0.38	0	0.92
300	65	0	0	0	0	0.56	0.38	0	0.95
300	97	0	0	0	0	0.43	0.25	0	0.69
400	0	0.18	0.18	0.20	1.75	3.29	2.84	0	7.88
400	30	0.06	0	0	0.76	1.81	1.65	0	4.22
400	50	0.04	0	0	0.59	1.42	1.17	0	3.18
400	73	0	0	0	0.49	1.27	1.06	0	2.83
400	105	0	0	0	0.40	1.08	0.82	0	2.29
400	141	0	0	0	0.32	0.87	0.74	0	1.92
500	0	1.19	1.37	2.26	10.20	7.20	6.53	0.96	24.89
500	25	0.13	0	0.20	2.47	2.20	1.99	0.76	7.42
500	69	0.05	0	0	0.85	0.90	0.80	0.30	2.85
500	109	0.04	0	0	0.81	0.79	0.66	0.25	2.51
500	132	0.03	0	0	0.68	0.70	0.63	0.18	2.19
600	0	1.66	2.65	3.09	10.76	5.30	4.75	2.48	23.29
600	23	0.47	1.16	1.28	4.03	1.86	1.49	1.40	8.78
600	46	0.44	1.26	1.40	3.26	1.40	1.20	1.12	6.98
600	78	0.44	1.36	1.49	4.09	1.12	0.84	0.72	6.78
600	145	0.42	1.40	1.49	0.82	0.48	0.48	0.50	2.28
600	210	0.41	1.25	1.52	0	0.41	0.31	0.48	1.20
600	234	0.40	1.22	1.46	0.58	0.36	0.40	0.56	1.90

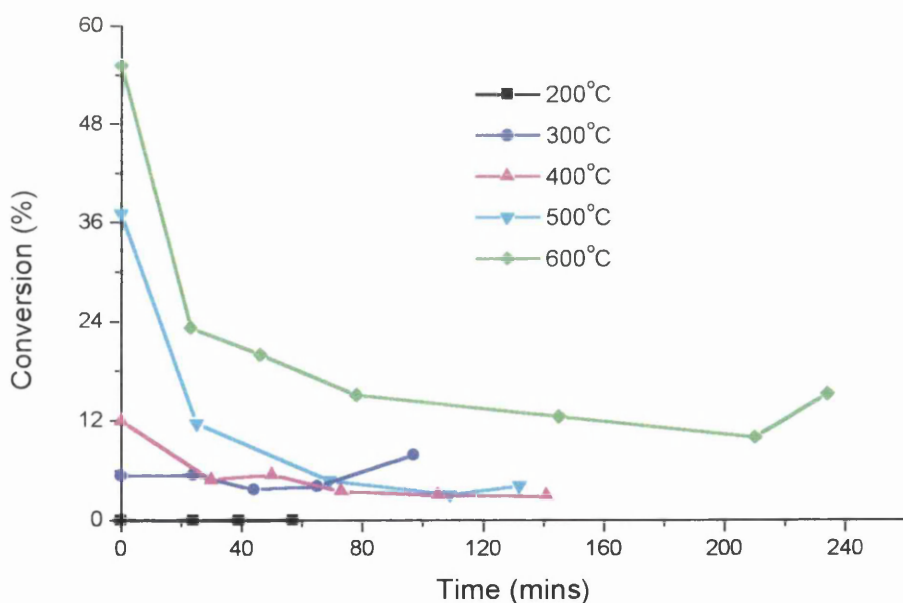


**Fig. 5.6.1** Conversion as a function of Time during the Straight Dehydrogenation of Butane at various Temperatures using 0.65% Pt/Al<sub>2</sub>O<sub>3</sub>.

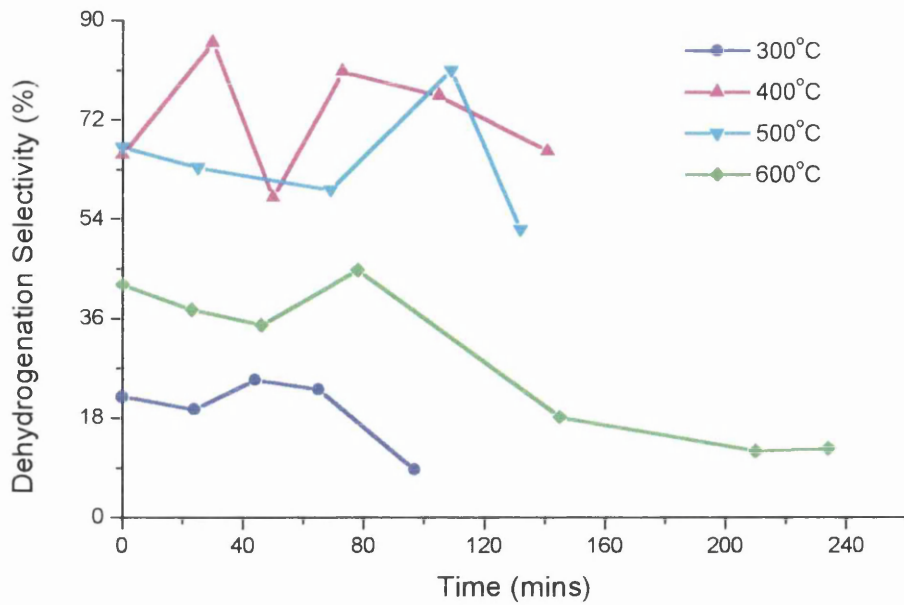


**Fig. 5.6.2** Dehydrogenation Selectivity as a function of Time during the Straight Dehydrogenation of Butane at various Temperatures using 0.65% Pt/Al<sub>2</sub>O<sub>3</sub>.

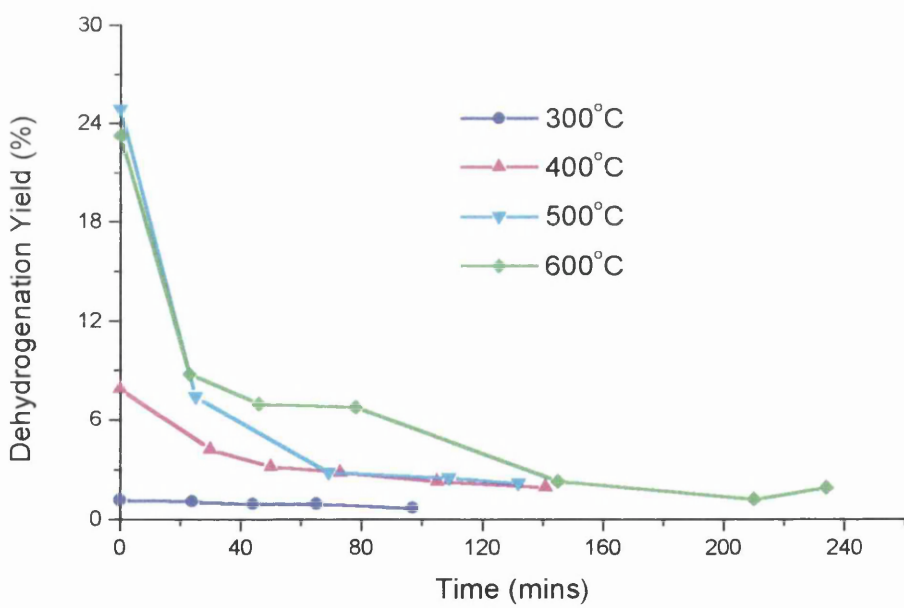


**Fig. 5.6.3** Dehydrogenation Yield as a function of Time during the Straight Dehydrogenation of Butane at various Temperatures using 0.65% Pt/Al<sub>2</sub>O<sub>3</sub>.

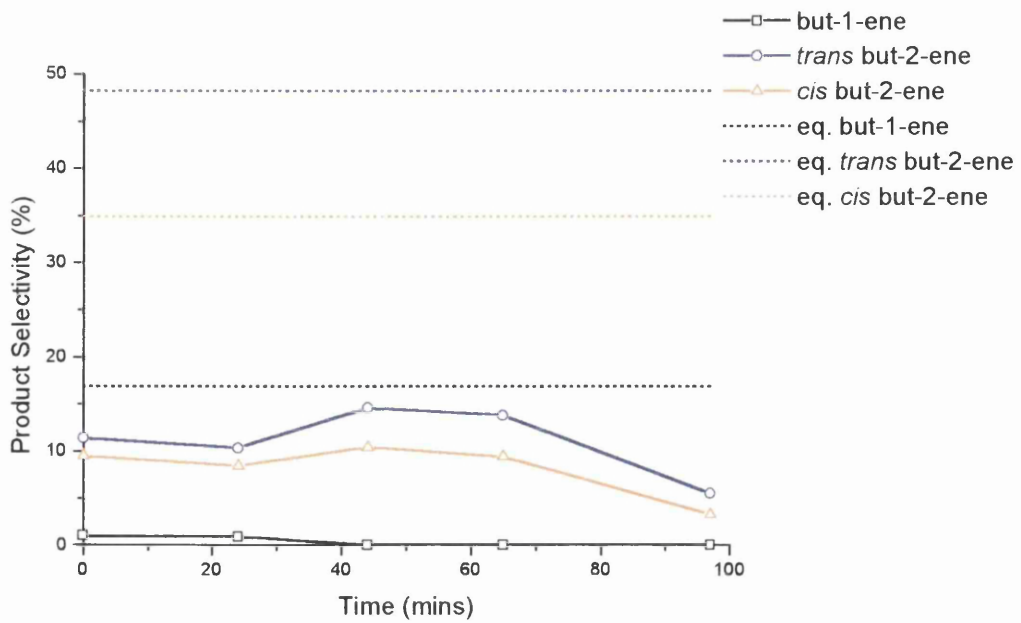


**Fig. 5.6.4** Product Selectivity as a function of Time during the Straight Dehydrogenation of Butane using the 0.65% Pt/Al<sub>2</sub>O<sub>3</sub> at 300°C.

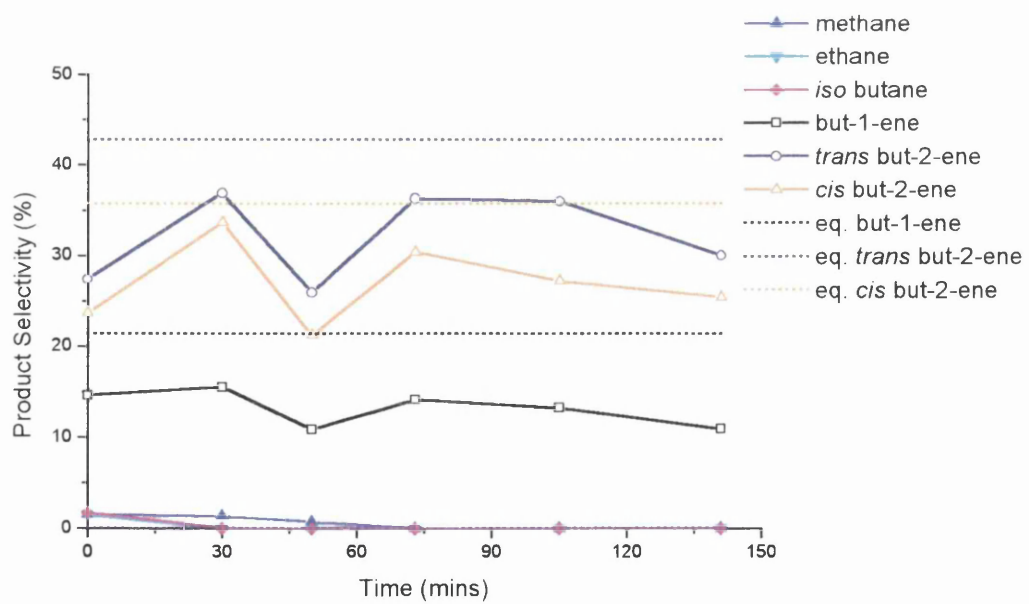


**Fig. 5.6.5** Product Selectivity as a function of Time during the Straight Dehydrogenation of Butane using the 0.65% Pt/Al<sub>2</sub>O<sub>3</sub> at 400°C.

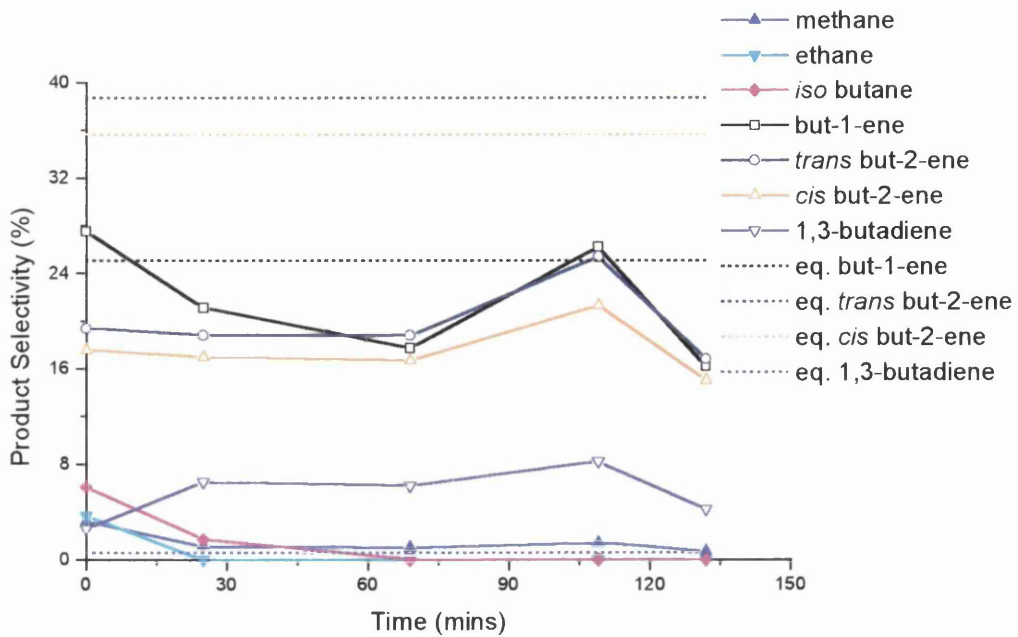


**Fig. 5.6.6** Product Selectivity as a function of Time during the Straight Dehydrogenation of Butane using the 0.65% Pt/Al<sub>2</sub>O<sub>3</sub> at 500°C.

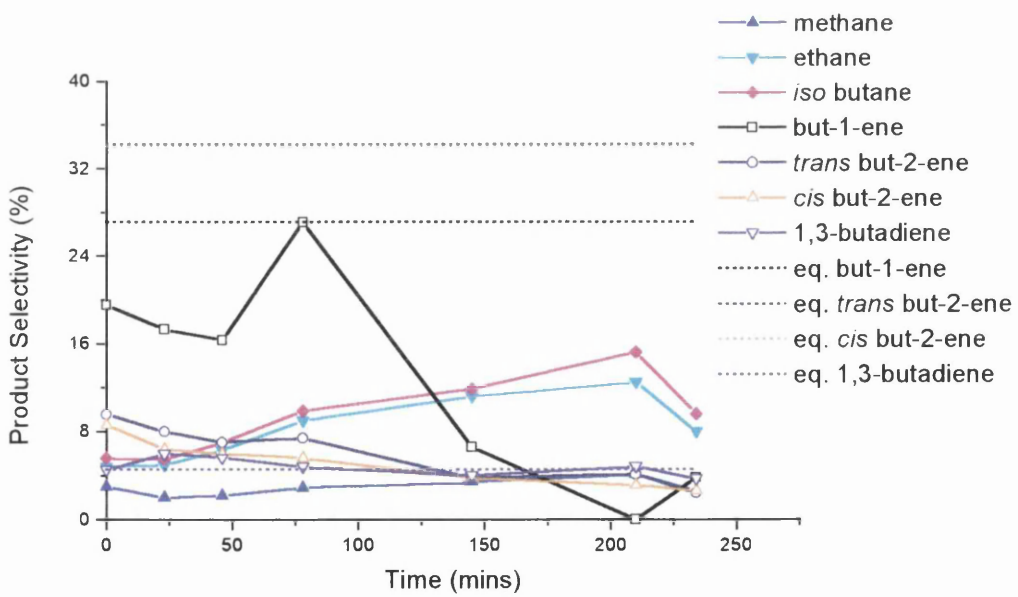


**Fig. 5.6.7** Product Selectivity as a function of Time during the Straight Dehydrogenation of Butane using the 0.65% Pt/Al<sub>2</sub>O<sub>3</sub> at 600°C.

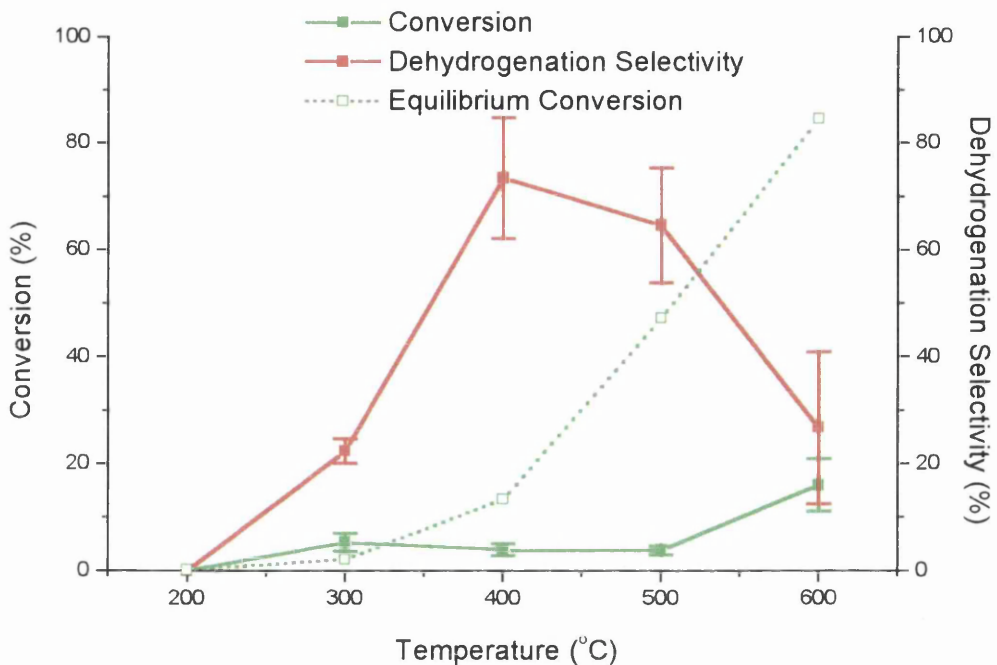


**Fig. 5.6.8** Conversion and Dehydrogenation Selectivity as a function of Temperature during the Straight Dehydrogenation of Butane using 0.65% Pt/Al<sub>2</sub>O<sub>3</sub>.

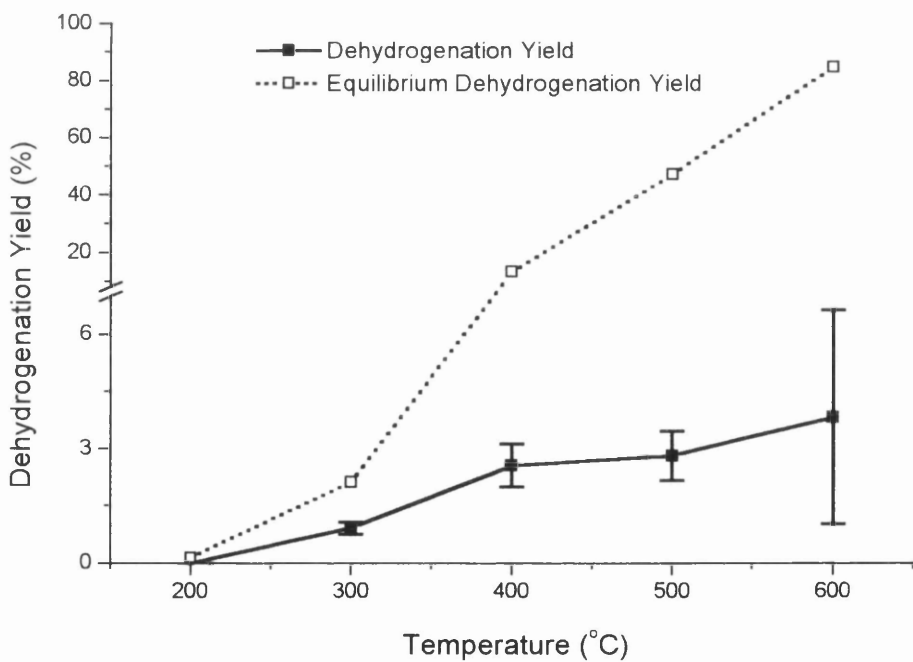


**Fig. 5.6.9** Dehydrogenation Yield as a function of Temperature during the Straight Dehydrogenation of Butane using 0.65% Pt/Al<sub>2</sub>O<sub>3</sub>.

## 5.6.2 The Oxidative Dehydrogenation of Butane as a function of Temperature under Continuous-flow conditions using 0.65% Pt/Al<sub>2</sub>O<sub>3</sub>

Tables 5.6.4, 5.6.5 and 5.6.6 contain the conversion and product molar quantities, the product selectivity and the product yield values respectively for the oxidative dehydrogenation of butane using 0.65% Pt/Al<sub>2</sub>O<sub>3</sub> as a function of temperature. Figures 5.6.10 - 5.6.20 graphically represent these results with respect to the conversion, individual product selectivity, dehydrogenation selectivity and dehydrogenation yield as a function of time and temperature. Section 4.1.3 describes the procedure used to carry out the experiments.

**Table 5.6.4 Conversion and Product Molar Quantities for the Oxidative Dehydrogenation of Butane using 0.65% Pt/Al<sub>2</sub>O<sub>3</sub>.**

Temp. (°C)	Time (mins)	Moles Bypass (x10 <sup>-7</sup> )	Moles Reacted (x10 <sup>-7</sup> )	Conv. (%)	CO <sub>2</sub> /Pr (x10 <sup>-7</sup> )	CO (x10 <sup>-7</sup> )	Met. (x10 <sup>-7</sup> )	Eth. (x10 <sup>-7</sup> )	Iso (x10 <sup>-7</sup> )	B-1 (x10 <sup>-7</sup> )	Trans B-2 (x10 <sup>-7</sup> )	Cis B-2 (x10 <sup>-7</sup> )	Diene (x10 <sup>-7</sup> )
200	0	44.90	7.92	17.6	1.19	0	0.54	0	0	0	0	0	0
200	55	44.90	8.19	18.2	4.02	0	0	0	0	0	0	0	0
200	102	44.90	6.79	15.1	3.87	0	0	0	0	0	0	0	0
200	198	44.90	8.65	19.3	4.40	0	0	0	0	0	0	0	0
300	0	44.90	7.79	17.3	3.68	0	0	0	0	0.19	0.74	0.58	0
300	64	44.90	4.97	11.1	5.07	0	0	0	0	0.09	0.12	0.12	0
300	113	44.90	6.07	13.5	4.45	0	0	0	0	0	0.14	0.11	0
300	195	44.90	6.01	13.4	4.27	0	0	0	0	0	0.10	0.09	0
300	256	44.90	5.51	12.3	4.26	0	0	0	0	0	0.09	0.09	0
400	0	44.90	12.55	28.0	3.19	1.06	0.23	0.13	0.31	0.64	1.20	1.05	0
400	55	44.90	7.59	16.9	3.83	0.17	0	0	0	0.04	0.18	0.15	0
400	105	44.90	5.96	13.3	4.33	0	0	0	0	0.02	0.14	0.11	0
400	180	44.90	6.20	13.8	4.64	0.12	0	0	0	0.02	0.14	0.16	0
400	229	44.90	5.54	12.3	4.89	0	0	0	0	0.02	0.17	0.14	0
500	0	44.90	20.21	45.0	2.26	5.56	1.45	0.41	0.70	1.08	0.94	0.84	0.16
500	67	44.90	12.33	27.5	3.63	1.51	0.17	0	0.01	0.13	0.24	0.20	0
500	151	44.90	11.44	25.5	3.76	1.17	0.16	0	0	0.10	0.22	0.18	0
500	201	44.90	10.96	24.4	4.00	1.18	0.19	0	0	0.07	0.20	0.19	0
500	254	44.90	11.21	25.0	4.59	1.10	0.15	0	0	0.08	0.21	0.18	0
600	0	44.90	31.51	70.2	1.02	10.36	9.28	2.96	2.55	1.20	0.52	0.45	0.39
600	63	44.90	26.40	58.8	2.16	5.37	6.49	5.96	5.06	0.53	0.30	0.27	0.28
600	125	44.90	26.02	58.0	2.34	4.46	6.28	6.20	5.42	0.62	0.30	0.23	0.15
600	176	44.90	26.17	58.3	2.33	4.17	6.39	6.49	5.44	0.60	0.27	0.21	0.13
600	225	44.90	25.80	57.5	2.55	4.13	6.41	6.90	5.58	0.62	0.27	0.21	0.20

**Table 5.6.5** Product Selectivity for the Oxidative Dehydrogenation of Butane using 0.65% Pt/Al<sub>2</sub>O<sub>3</sub>.

Temp. (°C)	Time (mins)	CO <sub>2</sub> /Pr Sel. (%)	CO Sel. (%)	Met. Sel. (%)	Eth. Sel. (%)	Iso Sel. (%)	B-1 Sel. (%)	Trans B-2 Sel. (%)	Cis B-2 Sel. (%)	Diene Sel. (%)	Dehydro. Sel. (%)
200	0	3.8	0	1.7	0	0	0	0	0	0	0
200	55	12.3	0	0	0	0	0	0	0	0	0
200	102	14.2	0	0	0	0	0	0	0	0	0
200	198	12.7	0	0	0	0	0	0	0	0	0
300	0	11.8	0	0	0	0	2.4	9.5	7.4	0	19.3
300	64	25.5	0	0	0	0	0.2	2.4	2.4	0	5.0
300	113	18.3	0	0	0	0	0	2.3	1.8	0	4.1
300	195	17.8	0	0	0	0	0	1.7	1.5	0	3.2
300	256	19.3	0	0	0	0	0	1.6	1.6	0	3.2
400	0	6.4	2.1	0.4	0.5	2.5	5.1	9.6	8.4	0	23.1
400	55	12.6	5.6	0	0	0	0.5	2.4	2.0	0	4.9
400	105	18.2	0	0	0	0	0.3	2.3	1.8	0	4.4
400	180	18.7	5.1	0	0	0	0.3	2.2	2.6	0	5.1
400	229	22.1	0	0	0	0	0.4	3.1	2.5	0	6.0
500	0	2.8	6.9	1.8	1.0	3.5	5.3	4.6	4.2	0.8	14.9
500	67	7.4	3.1	0.3	0	0.1	1.0	1.9	1.6	0	4.5
500	151	8.3	2.6	0.3	0	0	0.9	1.9	1.6	0	4.4
500	201	9.1	2.7	0.4	0	0	0.6	1.8	1.7	0	4.1
500	254	10.2	2.4	0.3	0	0	0.7	1.9	1.6	0	4.2
600	0	0.8	8.2	7.4	4.7	8.1	3.8	1.6	1.4	1.2	8.0
600	63	2.0	5.1	6.1	11.3	19.2	2.0	1.1	1.0	1.1	5.2
600	125	2.2	4.3	6.0	11.9	20.8	2.4	1.2	0.9	0.6	5.1
600	176	2.2	4.0	6.1	12.4	20.8	2.3	1.0	0.8	0.5	4.6
600	225	2.5	4.0	6.2	13.4	21.6	2.4	1.0	0.8	0.8	5.0

**Table 5.6.6** Product Yields for the Oxidative Dehydrogenation of Butane using 0.65% Pt/Al<sub>2</sub>O<sub>3</sub>.

Temp. (°C)	Time (mins)	CO <sub>2</sub> /Pr Yield (%)	CO Yield (%)	Met. Yield (%)	Eth. Yield (%)	Iso Yield (%)	B-1 Yield (%)	Trans B-2 Yield (%)	Cis B-2 Yield (%)	Diene Yield (%)	Dehydro. Yield (%)
200	0	0.67	0	0.30	0	0	0	0	0	0	0
200	55	2.24	0	0	0	0	0	0	0	0	0
200	102	2.14	0	0	0	0	0	0	0	0	0
200	198	2.45	0	0	0	0	0	0	0	0	0
300	0	2.04	0	0	0	0	0.42	1.64	1.28	0	3.34
300	64	2.83	0	0	0	0	0.02	0.27	0.27	0	0.56
300	113	2.47	0	0	0	0	0	0.31	0.24	0	0.55
300	195	2.38	0	0	0	0	0	0.23	0.20	0	0.43
300	256	2.37	0	0	0	0	0	0.20	0.20	0	0.39
400	0	1.79	0.59	0.11	0.14	0.70	1.43	2.69	2.35	0	6.47
400	55	2.13	0.95	0	0	0	0.08	0.40	0.34	0	0.83
400	105	2.42	0	0	0	0	0.04	0.30	0.24	0	0.58
400	180	2.58	0.70	0	0	0	0.04	0.30	0.36	0	0.70
400	229	2.72	0	0	0	0	0.05	0.40	0.31	0	0.74
500	0	1.26	3.10	0.81	0.45	1.58	2.38	2.07	1.89	0.36	6.70
500	67	2.04	0.85	0.08	0	0.03	0.28	0.52	0.44	0	1.24
500	151	2.12	0.66	0.08	0	0	0.23	0.48	0.41	0	1.12
500	201	2.22	0.66	0.10	0	0	0.15	0.44	0.41	0	1.00
500	254	2.55	0.60	0.08	0	0	0.18	0.48	0.40	0	1.05
600	0	0.56	5.76	5.19	3.30	5.69	2.67	1.12	0.98	0.84	5.62
600	63	1.18	3.00	3.59	6.64	11.29	1.18	0.65	0.59	0.65	3.06
600	125	1.28	2.49	3.48	6.90	12.06	1.39	0.70	0.52	0.35	2.96
600	176	1.28	2.33	3.56	7.23	12.13	1.34	0.58	0.47	0.29	2.68
600	225	1.44	2.30	3.56	7.70	12.42	1.38	0.58	0.46	0.46	2.88

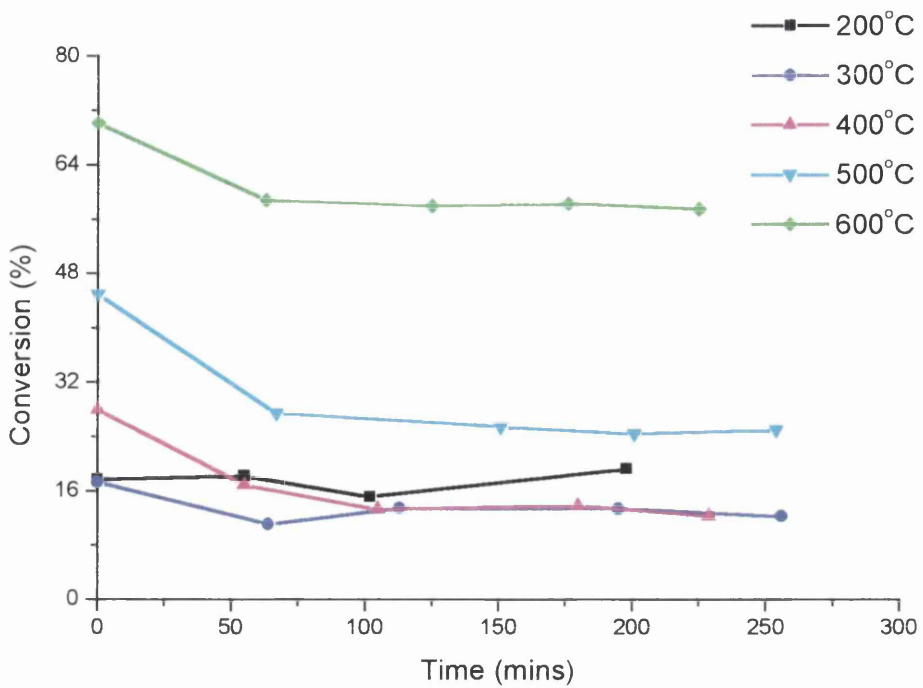


**Fig. 5.6.10** Conversion as a function of Time during the Oxidative Dehydrogenation of Butane at various Temperatures using 0.65% Pt/Al<sub>2</sub>O<sub>3</sub>.

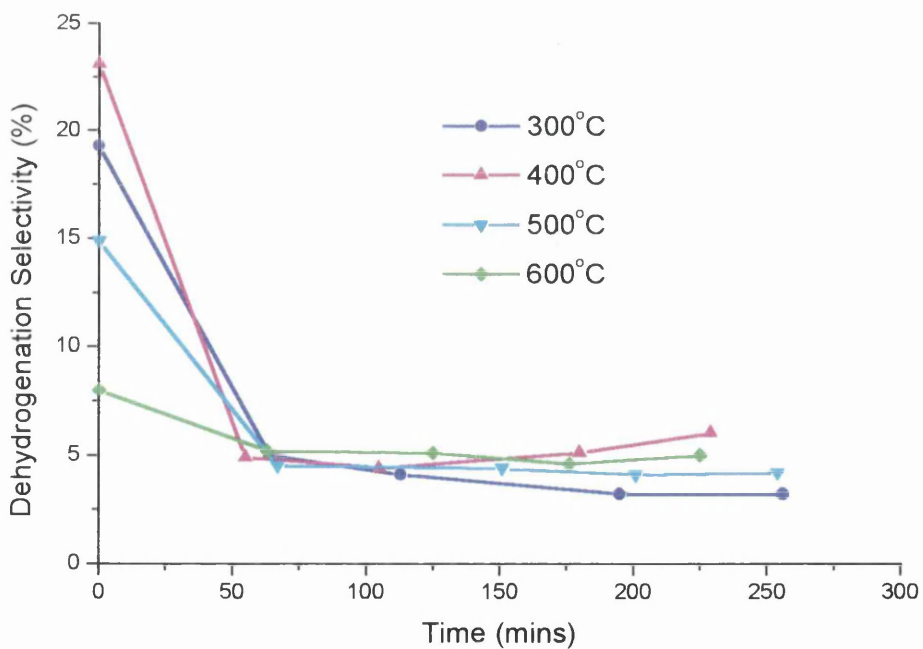


**Fig. 5.6.11** Dehydrogenation Selectivity as a function of Time during the Oxidative Dehydrogenation of Butane at various Temperatures using 0.65% Pt/Al<sub>2</sub>O<sub>3</sub>.

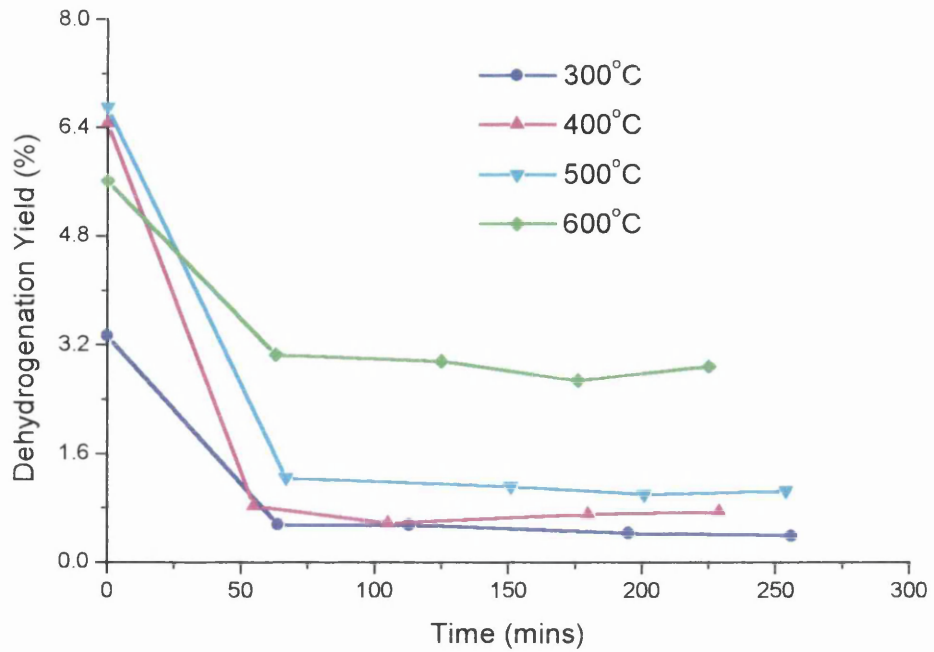


**Fig. 5.6.12** Dehydrogenation Yield as a function of Time during the Oxidative Dehydrogenation of Butane at various Temperatures using 0.65% Pt/Al<sub>2</sub>O<sub>3</sub>.

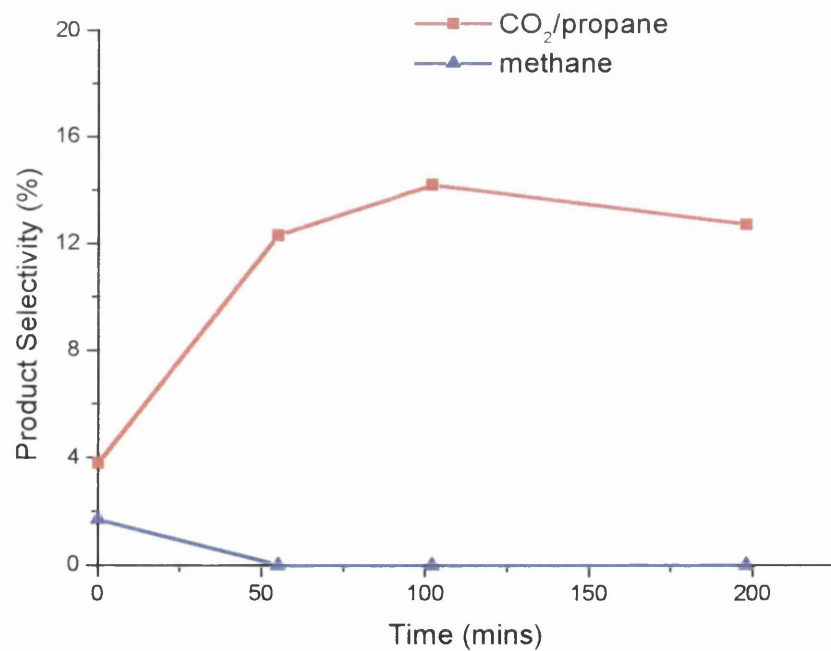


**Fig. 5.6.13** Product Selectivity as a function of Time during the Oxidative Dehydrogenation of Butane using the 0.65% Pt/Al<sub>2</sub>O<sub>3</sub> at 200°C.

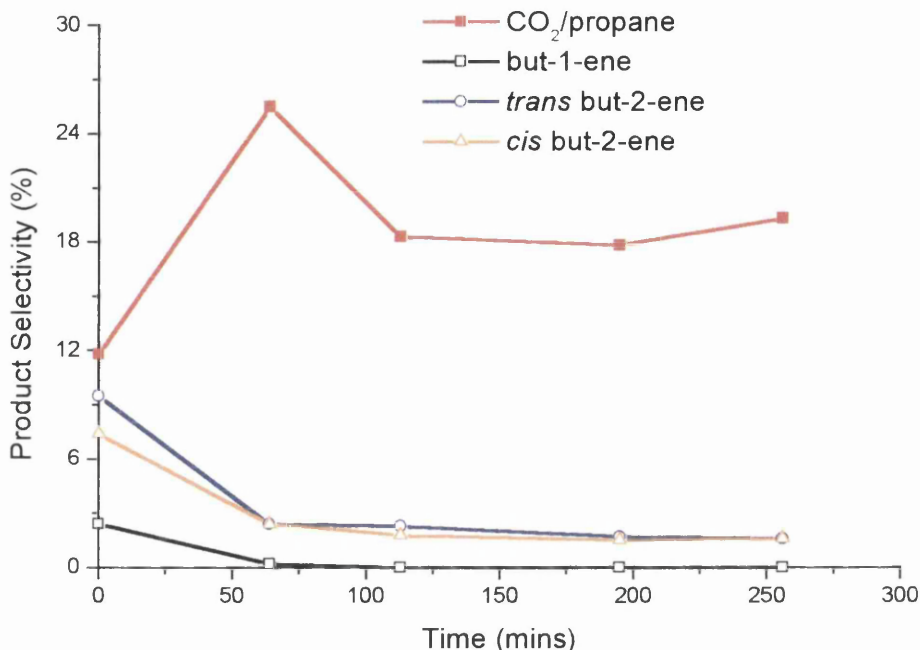


**Fig. 5.6.14** Product Selectivity as a function of Time during the Oxidative Dehydrogenation of Butane using the 0.65% Pt/Al<sub>2</sub>O<sub>3</sub> at 300°C.

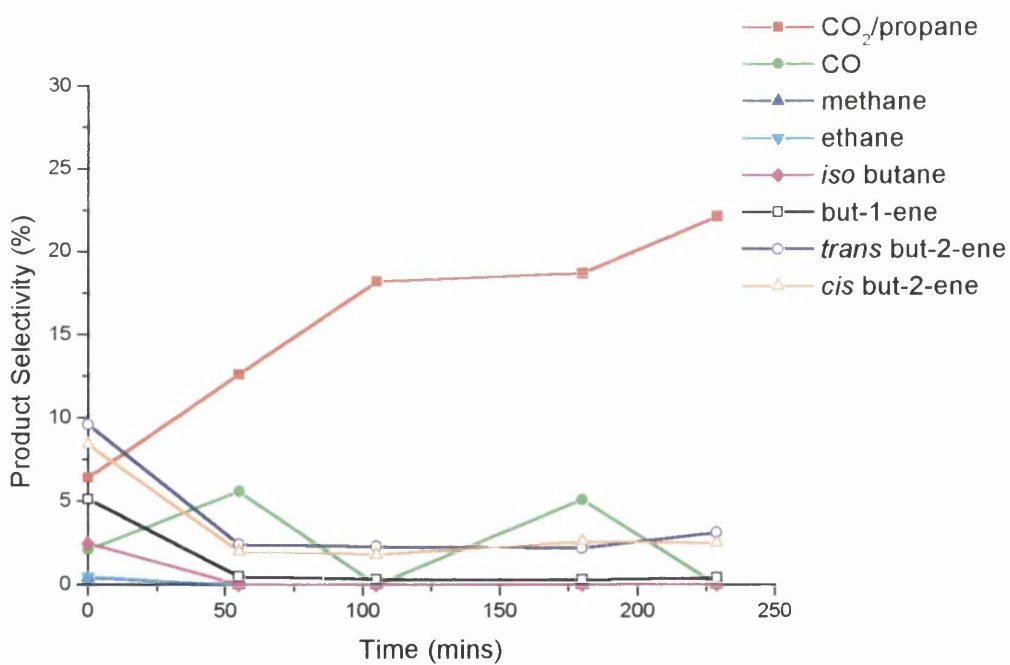


**Fig. 5.6.15** Product Selectivity as a function of Time during the Oxidative Dehydrogenation of Butane using the 0.65% Pt/Al<sub>2</sub>O<sub>3</sub> at 400°C.

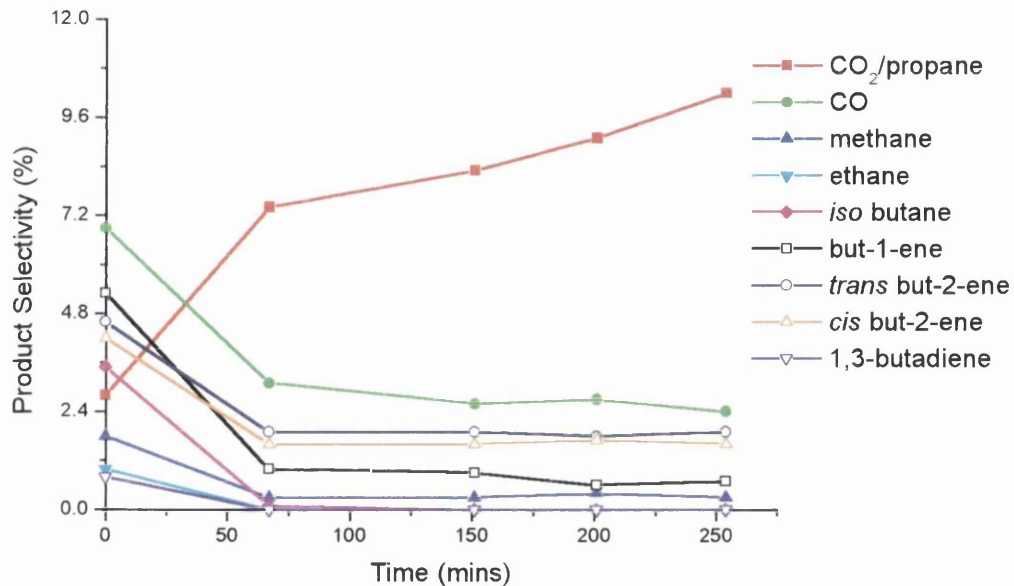


**Fig. 5.6.16** Product Selectivity as a function of Time during the Oxidative Dehydrogenation of Butane using the 0.65% Pt/Al<sub>2</sub>O<sub>3</sub> at 500°C.

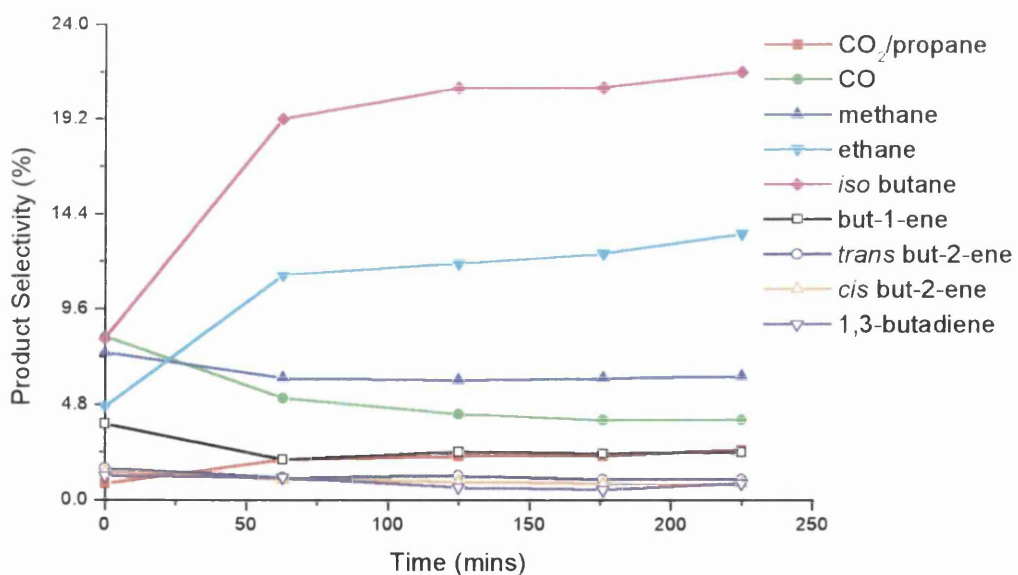


**Fig. 5.6.17** Product Selectivity as a function of Time during the Oxidative Dehydrogenation of Butane using the 0.65% Pt/Al<sub>2</sub>O<sub>3</sub> at 600°C.

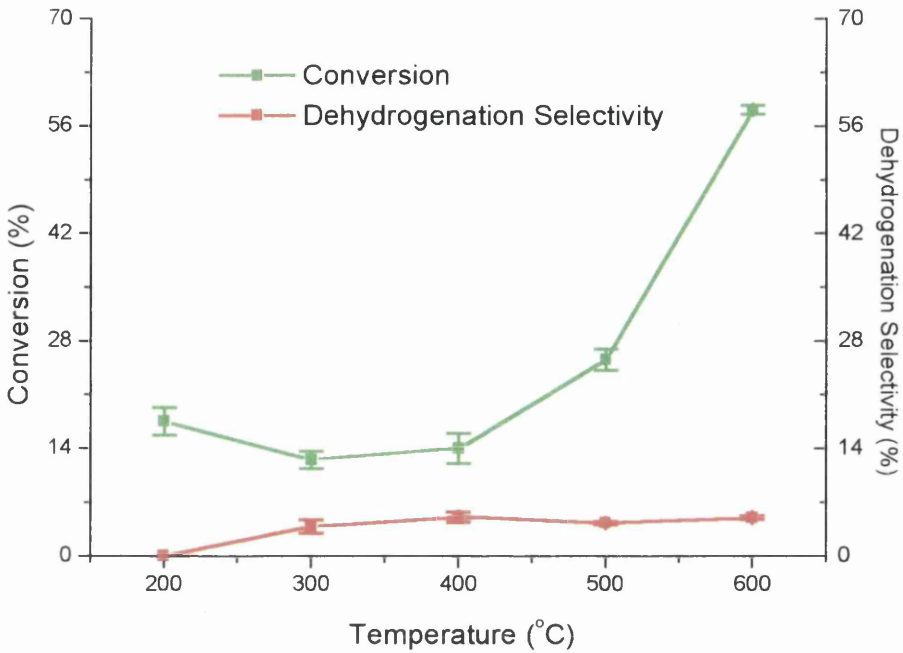


**Fig. 5.6.18** Conversion and Dehydrogenation Selectivity as a function of Temperature during the Oxidative Dehydrogenation of Butane using 0.65% Pt/Al<sub>2</sub>O<sub>3</sub>.

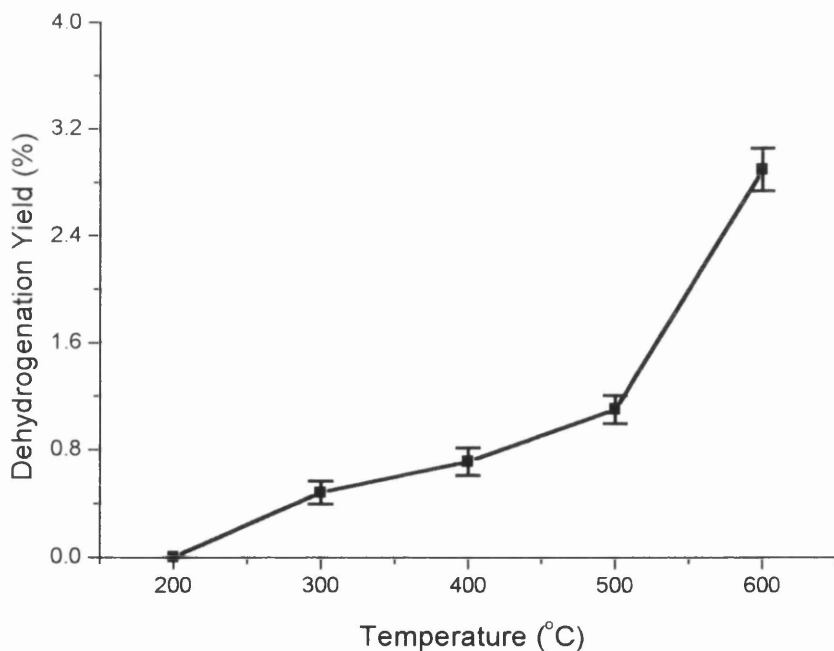


**Fig. 5.6.19** Dehydrogenation Yield as a function of Temperature during the Oxidative Dehydrogenation of Butane using 0.65% Pt/Al<sub>2</sub>O<sub>3</sub>.

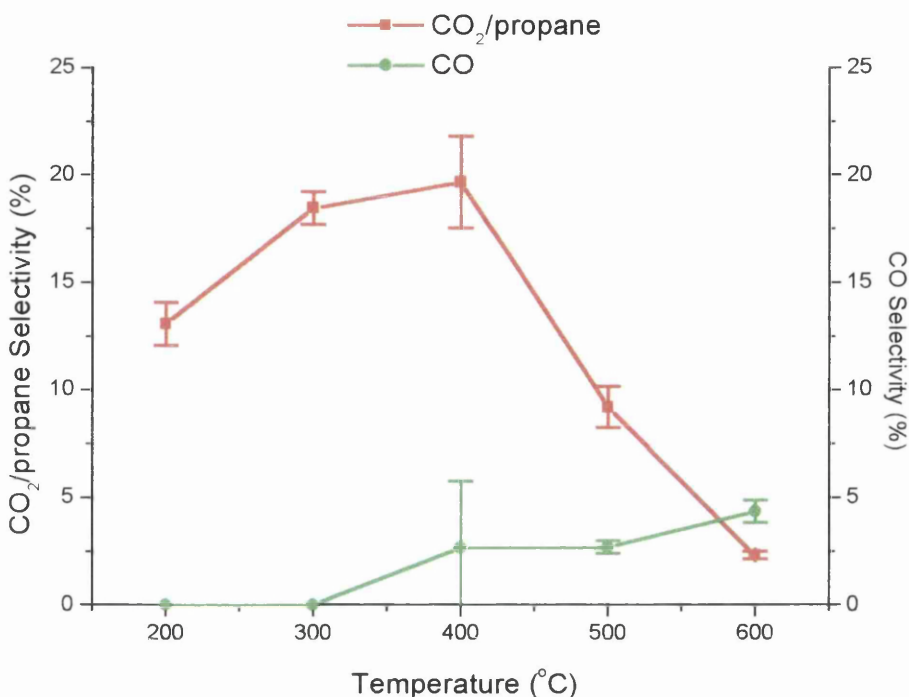


**Fig. 5.6.20**  $\text{CO}_2$  and CO Product Selectivity during the Oxidative Dehydrogenation of Butane using 0.65% Pt/ $\text{Al}_2\text{O}_3$ .

### 5.6.3 The Straight Dehydrogenation of Butane as a function of Flow-rate under Continuous-flow conditions using 0.65% Pt/ $\text{Al}_2\text{O}_3$

Tables 5.6.7, 5.6.8 and 5.6.9 contain the conversion and product molar quantities, the product selectivity and the product yield values respectively for the straight dehydrogenation of butane using 0.65% Pt/ $\text{Al}_2\text{O}_3$  as a function of flow-rate. Figures 5.6.21 - 5.6.29 graphically represent these results with respect to the conversion, individual product selectivity, dehydrogenation selectivity and dehydrogenation yield as a function of time and temperature, showing the equilibrium results, where appropriate, for comparison. Section 4.1.3 describes the procedure used to carry out the experiments.

**Table 5.6.7** Conversion and Product Molar Quantities for the Straight Dehydrogenation of Butane as a function of Flow-rate using 0.65% Pt/Al<sub>2</sub>O<sub>3</sub>.

Flow-rate (ml min <sup>-1</sup> )	Time (mins)	Moles Bypass (x10 <sup>-7</sup> )	Moles Reacted (x10 <sup>-7</sup> )	Conv. (%)	Met. (x10 <sup>-7</sup> )	Eth. (x10 <sup>-7</sup> )	Iso (x10 <sup>-7</sup> )	B-1 (x10 <sup>-7</sup> )	Trans B-2 (x10 <sup>-7</sup> )	Cis B-2 (x10 <sup>-7</sup> )	Diene (x10 <sup>-7</sup> )
30	0	62.72	13.25	21.1	0.87	0.43	0.27	0.77	1.70	1.34	0
30	25	62.72	4.05	6.4	0.19	0	0.06	0.62	1.55	1.37	0
30	47	62.72	3.08	4.9	0.13	0	0	0.46	1.24	1.08	0
30	77	62.72	3.43	5.5	0.10	0	0	0.43	1.16	0.99	0
30	102	62.72	2.55	4.1	0.10	0	0	0.41	1.12	0.94	0
100	0	24.04	2.69	11.2	0.14	0	0.05	0.31	0.67	0.60	0
100	19	24.04	2.14	8.9	0.04	0	0	0.06	0.20	0.14	0
100	43	24.04	0.85	3.5	0	0	0	0.04	0.14	0.12	0
100	61	24.04	0.50	2.1	0	0	0	0.02	0.10	0.08	0
100	117	24.04	0.70	2.9	0	0	0	0	0.08	0.08	0
130	0	17.72	1.31	7.4	0.10	0	0	0.27	0.53	0.47	0
130	52	17.72	0.54	3.0	0	0	0	0.02	0.08	0.07	0
130	77	17.72	0.42	2.4	0	0	0	0.01	0.08	0.02	0
130	107	17.72	0.21	1.2	0	0	0	0.01	0.05	0.04	0
130	127	17.72	0.23	1.3	0	0	0	0	0.06	0	0

**Table 5.6.8** Product Selectivity for the Straight Dehydrogenation of Butane as a function of Flow-rate using 0.65% Pt/Al<sub>2</sub>O<sub>3</sub>.

Flow-rate (ml min <sup>-1</sup> )	Time (mins)	Met. Sel. (%)	Eth. Sel. (%)	Iso Sel. (%)	B-1 Sel. (%)	Trans B-2 Sel. (%)	Cis B-2 Sel. (%)	Diene Sel. (%)	Dehydro. Sel. (%)
30	0	1.6	1.6	2	5.8	12.8	10.1	0	28.7
30	25	1.2	0	15.3	15.3	38.3	33.8	0	87.4
30	47	1.0	0	0	14.9	40.2	35.1	0	90.2
30	77	0.7	0	0	12.5	33.8	28.9	0	75.2
30	102	1.0	0	0	16.1	43.9	36.9	0	96.9
100	0	1.3	0	1.8	11.5	24.9	22.3	0	58.7
100	19	0.5	0	0	2.8	9.3	6.5	0	18.6
100	43	0	0	0	4.7	16.5	14.1	0	35.3
100	61	0	0	0	4.0	20.0	16.0	0	40.0
100	117	0	0	0	0.6	11.4	11.4	0	23.4
130	0	1.9	0	0	20.6	40.4	35.9	0	96.9
130	52	0	0	0	3.7	14.8	13.0	0	31.5
130	77	0	0	0	2.4	19.0	4.8	0	26.2
130	107	0	0	0	3.3	23.8	19	0	46.1
130	127	0	0	0	0	26.1	0	0	26.1

**Table 5.6.9** Product Yields for the Straight Dehydrogenation of Butane as a function of Flow-rate using 0.65% Pt/Al<sub>2</sub>O<sub>3</sub>.

Flow-rate (ml min <sup>-1</sup> )	Time (mins)	Met. Yield (%)	Eth. Yield (%)	Iso Yield (%)	B-1 Yield (%)	Trans B-2 Yield (%)	Cis B-2 Yield (%)	Diene Yield (%)	Dehydro. Yield (%)
30	0	0.34	0.34	0.42	1.22	2.70	2.13	0	6.06
30	25	0.08	0	0.98	0.98	2.45	2.16	0	5.59
30	47	0.05	0	0	0.73	1.97	1.72	0	4.42
30	77	0.04	0	0	0.69	1.86	1.59	0	4.14
30	102	0.04	0	0	0.66	1.80	1.51	0	3.97
100	0	0.14	0	0.20	1.29	2.79	2.50	0	6.57
100	19	0.04	0	0	0.25	0.83	0.58	0	1.66
100	43	0	0	0	0.16	0.58	0.49	0	1.24
100	61	0	0	0	0.08	0.42	0.34	0	0.84
100	117	0	0	0	0.02	0.33	0.33	0	0.68
130	0	0.14	0	0	1.52	2.99	2.66	0	7.17
130	52	0	0	0	0.11	0.44	0.39	0	0.94
130	77	0	0	0	0.06	0.46	0.12	0	0.63
130	107	0	0	0	0.04	0.28	0.23	0	0.55
130	127	0	0	0	0	0.34	0	0	0.34

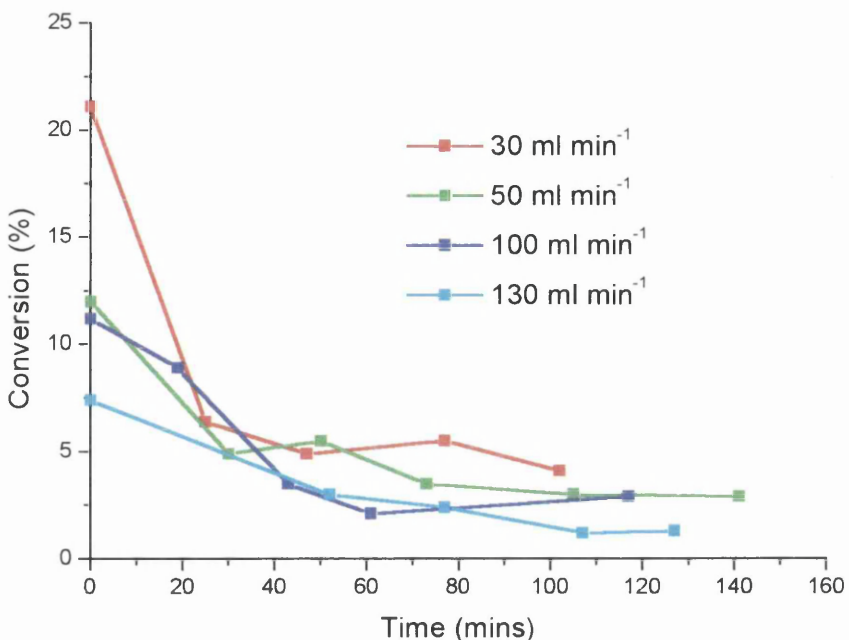


**Fig. 5.6.21** Conversion as a function of Time during the Straight Dehydrogenation of Butane at various Flow-rates using 0.65% Pt/Al<sub>2</sub>O<sub>3</sub>.

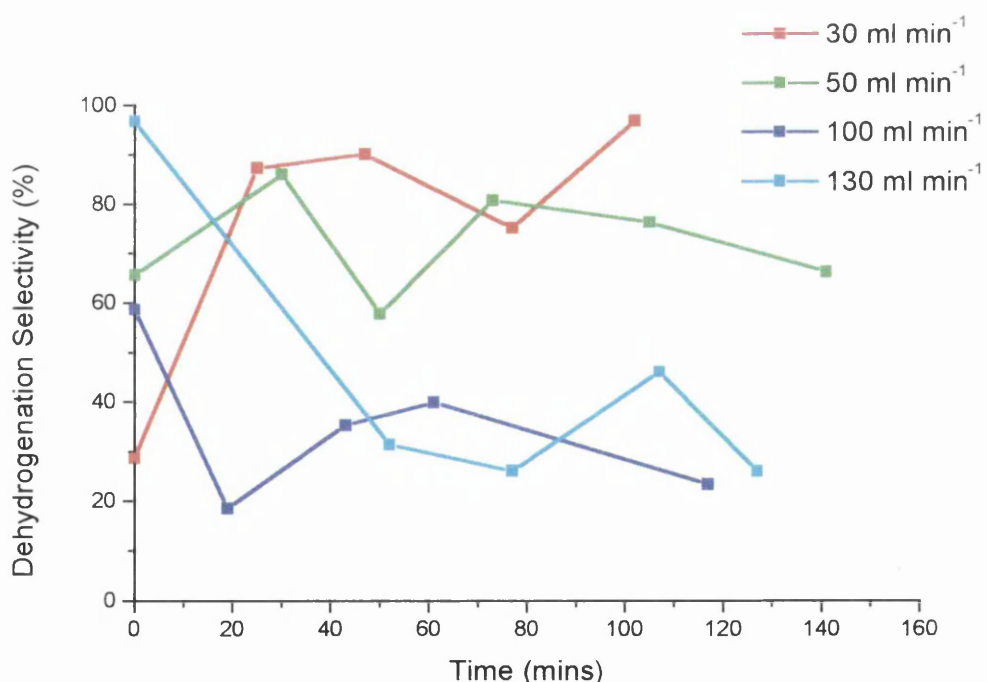


**Fig. 5.6.22** Dehydrogenation Selectivity as a function of Time during the Straight Dehydrogenation of Butane at various Flow-rates using 0.65% Pt/Al<sub>2</sub>O<sub>3</sub>.

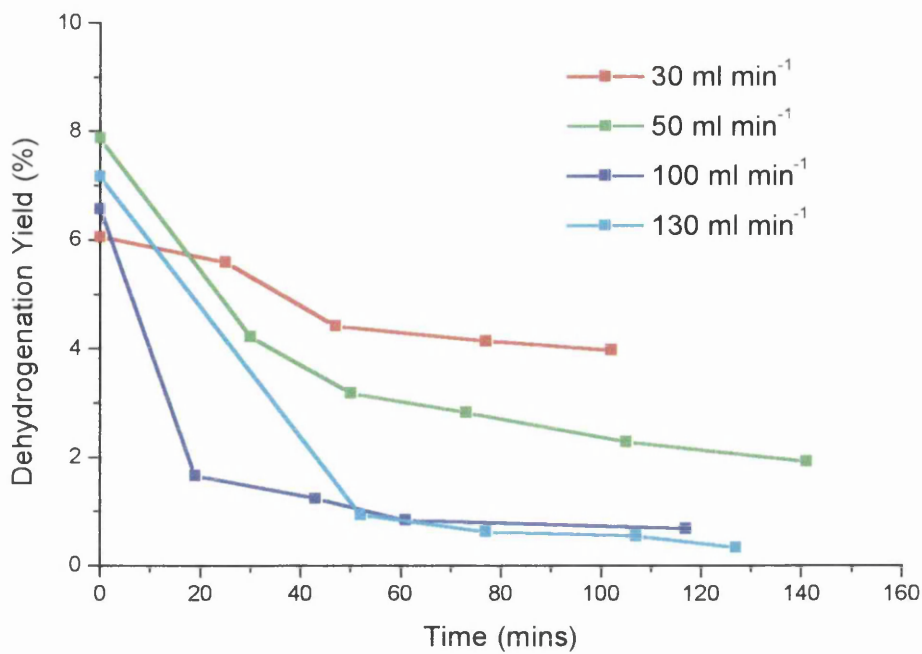


**Fig. 5.6.23** Dehydrogenation Yield as a function of Time during the Straight Dehydrogenation of Butane at various Flow-rates using 0.65% Pt/ $\text{Al}_2\text{O}_3$ .

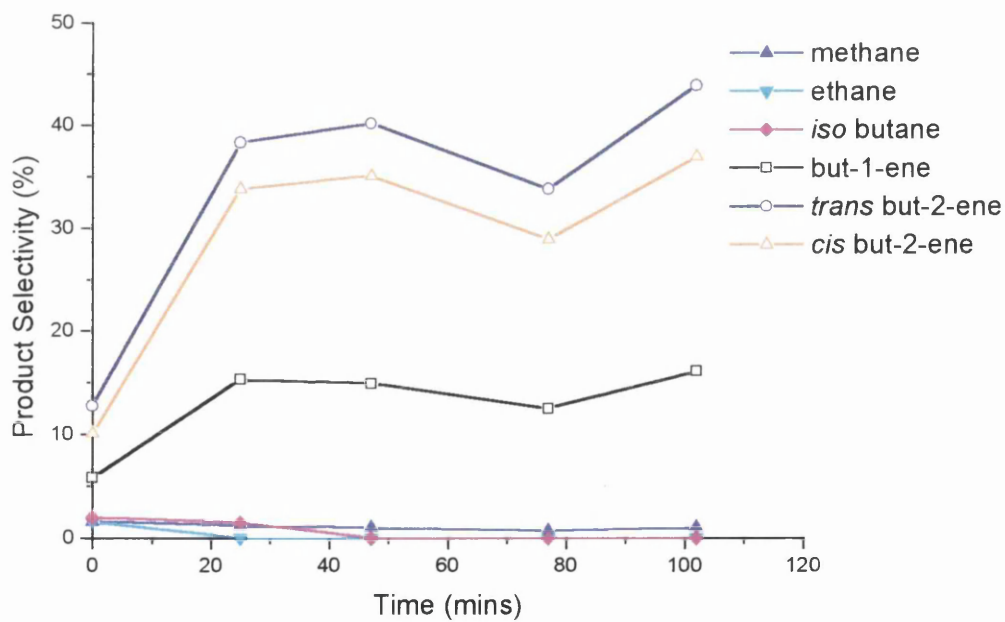


**Fig. 5.6.24** Product Selectivity as a function of Time during the Straight Dehydrogenation of Butane using the 0.65% Pt/ $\text{Al}_2\text{O}_3$  at 30  $\text{ml min}^{-1}$ .

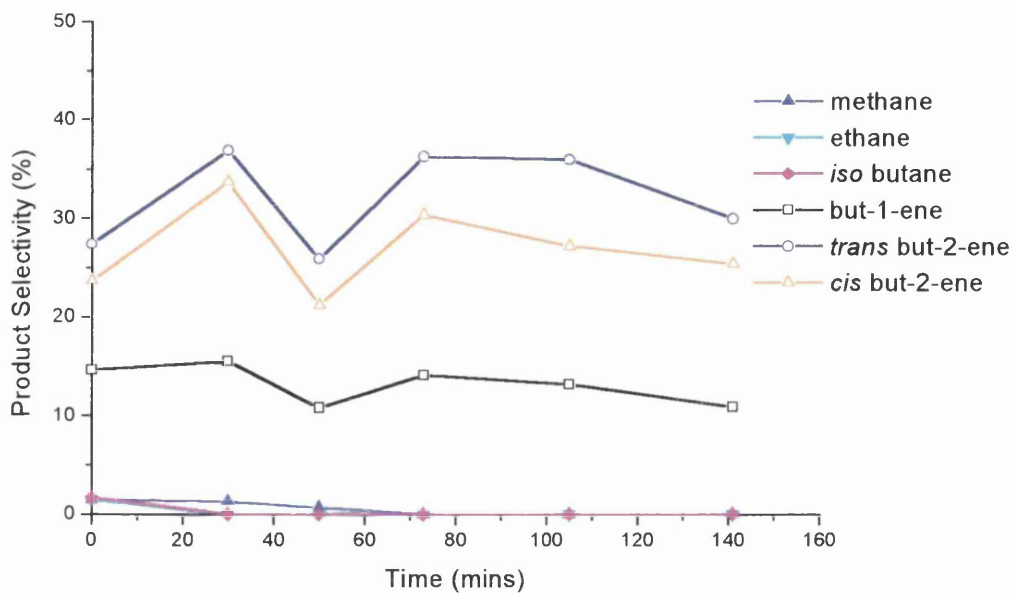


**Fig. 5.6.25** Product Selectivity as a function of Time during the Straight Dehydrogenation of Butane using the 0.5% Pt/Al<sub>2</sub>O<sub>3</sub> at 50 ml min<sup>-1</sup>.

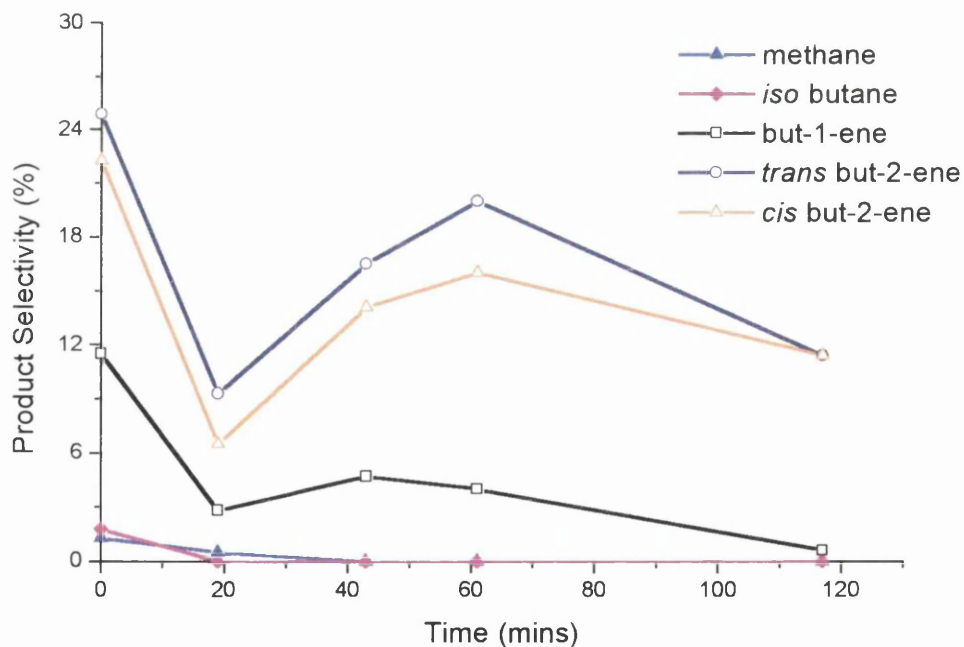


**Fig. 5.6.26** Product Selectivity as a function of Time during the Straight Dehydrogenation of Butane using the 0.65% Pt/Al<sub>2</sub>O<sub>3</sub> at 100 ml min<sup>-1</sup>.

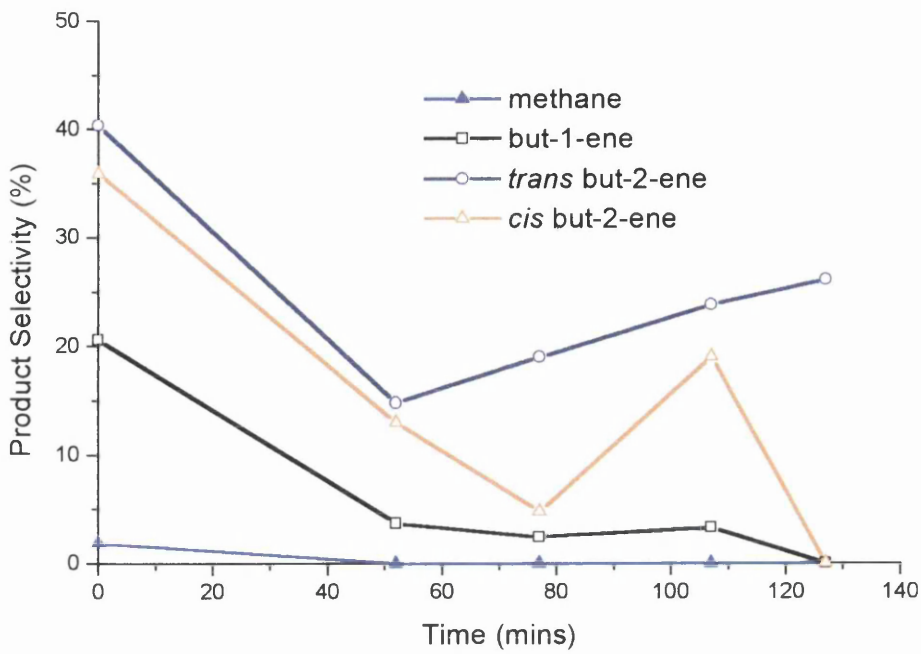


**Fig. 5.6.27** Product Selectivity as a function of Time during the Straight Dehydrogenation of Butane using the 0.65% Pt/Al<sub>2</sub>O<sub>3</sub> at 130 ml min<sup>-1</sup>.

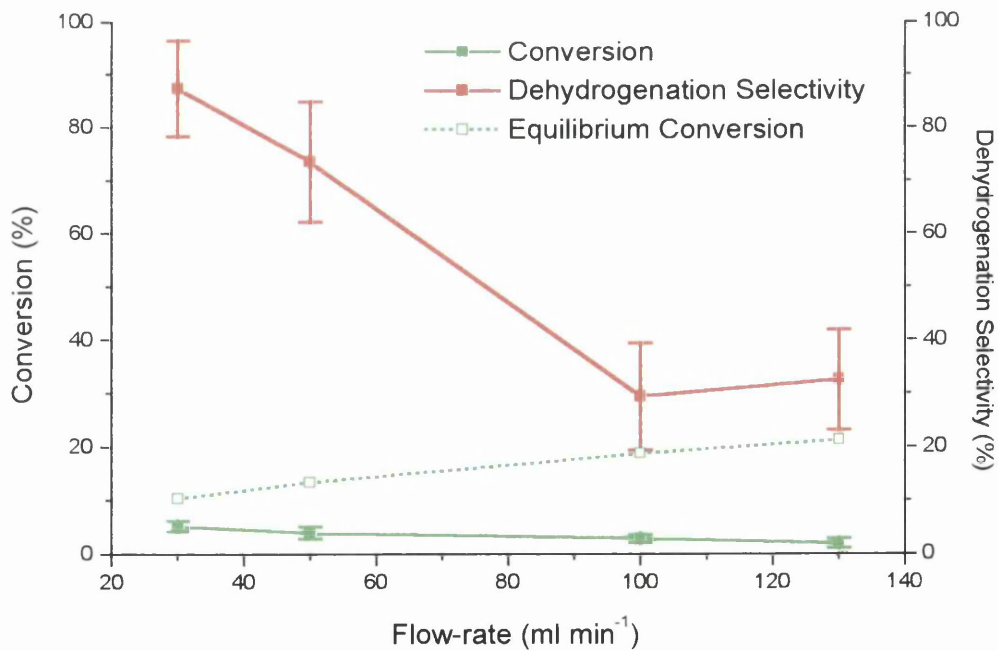


**Fig. 5.6.28** Conversion and Dehydrogenation Selectivity as a function of Flow-rate during the Straight Dehydrogenation of Butane using 0.65% Pt/Al<sub>2</sub>O<sub>3</sub> at 400°C.

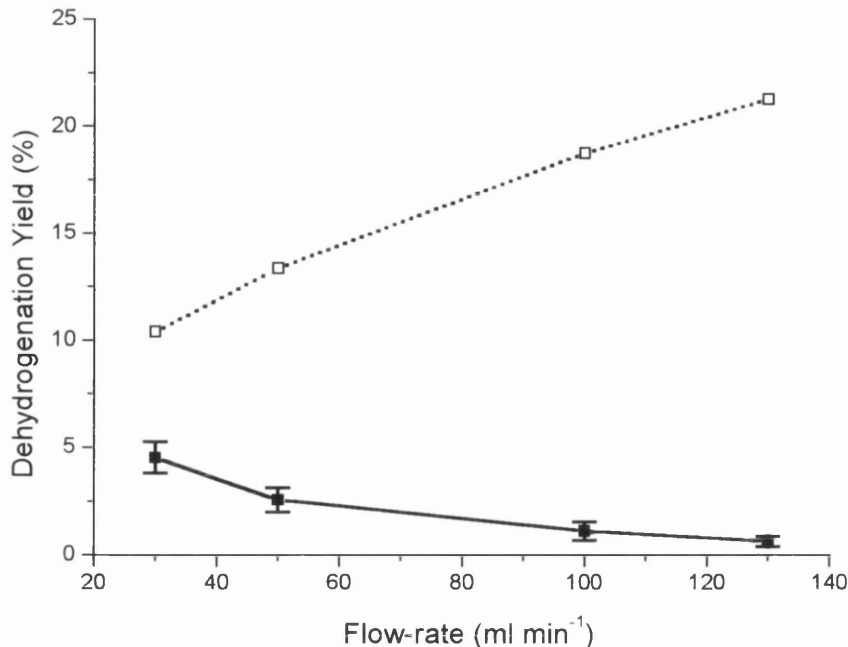


**Fig. 5.6.29** Dehydrogenation Yield as a function of Flow-rate during the Straight Dehydrogenation of Butane using 0.65% Pt/Al<sub>2</sub>O<sub>3</sub> at 400°C.

#### 5.6.4 The Oxidative Dehydrogenation of Butane as a function of Flow-rate under Continuous-flow conditions using 0.65% Pt/Al<sub>2</sub>O<sub>3</sub>

Tables 5.6.10, 5.6.11 and 5.6.12 contain the conversion and product molar quantities, the product selectivity and the product yield values respectively for the oxidative dehydrogenation of butane using 0.65% Pt/Al<sub>2</sub>O<sub>3</sub> as a function of flow-rate. Figures 5.6.30 - 5.6.38 graphically represent these results with respect to the conversion, individual product selectivity, dehydrogenation selectivity and dehydrogenation yield as a function of time and temperature. Section 4.1.3 describes the procedure used to carry out the experiments.

**Table 5.6.10** Conversion and Product Molar Quantities for the Oxidative Dehydrogenation of Butane using 0.65% Pt/Al<sub>2</sub>O<sub>3</sub> as a function of Flow-rate.

Flow-rate (ml min <sup>-1</sup> )	Time (mins)	Moles Bypass (x10 <sup>-7</sup> )	Moles Reacted (x10 <sup>-7</sup> )	Conv. (%)	CO <sub>2</sub> /Pr (x10 <sup>-7</sup> )	CO (x10 <sup>-7</sup> )	Met. (x10 <sup>-7</sup> )	Eth. (x10 <sup>-7</sup> )	Iso (x10 <sup>-7</sup> )	B-1 (x10 <sup>-7</sup> )	Trans B-2 (x10 <sup>-7</sup> )	Cis B-2 (x10 <sup>-7</sup> )	Diene (x10 <sup>-7</sup> )
100	0	28.02	11.26	40.2	1.73	0.88	0	0	0.11	0.23	0.44	0.35	0
100	51	28.02	9.17	32.7	1.96	0.15	0	0	0	0.03	0.10	0.07	0
100	101	28.02	8.97	32.0	2.08	0	0	0	0	0.02	0.10	0.09	0
100	138	28.02	9.10	32.5	2.32	0	0	0	0	0.02	0.07	0.05	0
100	198	28.02	9.01	32.2	2.51	0	0	0	0	0.02	0.08	0.10	0
130	0	23.52	8.35	35.5	1.47	0.60	0	0	0.09	0.14	0.29	0.26	0
130	63	23.52	6.82	29.0	1.55	0	0	0	0	0.02	0.09	0.07	0
130	103	23.52	7.48	31.8	1.77	0	0	0	0	0.02	0.08	0.08	0
130	183	23.52	7.46	31.7	1.41	0	0	0	0	0.02	0.05	0.04	0
130	213	23.52	7.23	30.7	1.82	0	0	0	0	0.01	0.07	0.03	0

**Table 5.6.11** Product Selectivity for the Oxidative Dehydrogenation of Butane using 0.65% Pt/Al<sub>2</sub>O<sub>3</sub> as a function of Flow-rate.

Flow-rate (ml min <sup>-1</sup> )	Time (mins)	CO <sub>2</sub> /Pr Sel. (%)	CO Sel. (%)	Met. Sel. (%)	Eth. Sel. (%)	Iso Sel. (%)	B-1 Sel. (%)	Trans B-2 Sel. (%)	Cis B-2 Sel. (%)	Diene Sel. (%)	Dehydro. Sel. (%)
100	0	3.8	2.0	0	0	1.0	2.0	3.9	3.1	0	9.0
100	51	5.3	0.4	0	0	0	0.3	1.1	0.8	0	2.2
100	101	5.8	0	0	0	0	0.2	1.1	1.0	0	2.3
100	138	6.4	0	0	0	0	0.1	0.8	0.5	0	1.4
100	198	7.0	0	0	0	0	0.2	0.9	1.1	0	2.2
130	0	4.4	1.8	0	0	1.1	1.7	3.5	3.1	0	8.3
130	63	5.7	0	0	0	0	0.3	1.3	1.0	0	2.6
130	103	5.9	0	0	0	0	0.3	1.1	1.1	0	2.5
130	183	4.7	0	0	0	0	0.3	0.7	0.5	0	1.5
130	213	6.3	0	0	0	0	0.1	1.0	0.4	0	1.5

**Table 5.6.12** Product Yields for the Oxidative Dehydrogenation of Butane using 0.65% Pt/Al<sub>2</sub>O<sub>3</sub> as a function of Flow-rate.

Flow-rate (ml min <sup>-1</sup> )	Time (mins)	CO <sub>2</sub> /Pr Yield (%)	CO Yield (%)	Met. Yield (%)	Eth. Yield (%)	Iso Yield (%)	B-1 Yield (%)	Trans B-2 Yield (%)	Cis B-2 Yield (%)	Diene Yield (%)	Dehydro. Yield (%)
100	0	1.53	0.80	0	0	0.40	0.80	1.57	1.25	0	3.62
100	51	1.73	0.13	0	0	0	0.10	0.36	0.26	0	0.72
100	101	1.86	0	0	0	0	0.06	0.35	0.32	0	0.74
100	138	2.08	0	0	0	0	0.03	0.26	0.16	0	0.46
100	198	2.25	0	0	0	0	0.06	0.29	0.35	0	0.71
130	0	1.56	0.64	0	0	0.39	0.60	1.24	1.10	0	2.95
130	63	1.65	0	0	0	0	0.09	0.38	0.29	0	0.75
130	103	1.88	0	0	0	0	0.10	0.35	0.35	0	0.80
130	183	1.49	0	0	0	0	0.10	0.22	0.16	0	0.48
130	213	1.93	0	0	0	0	0.03	0.31	0.12	0	0.46

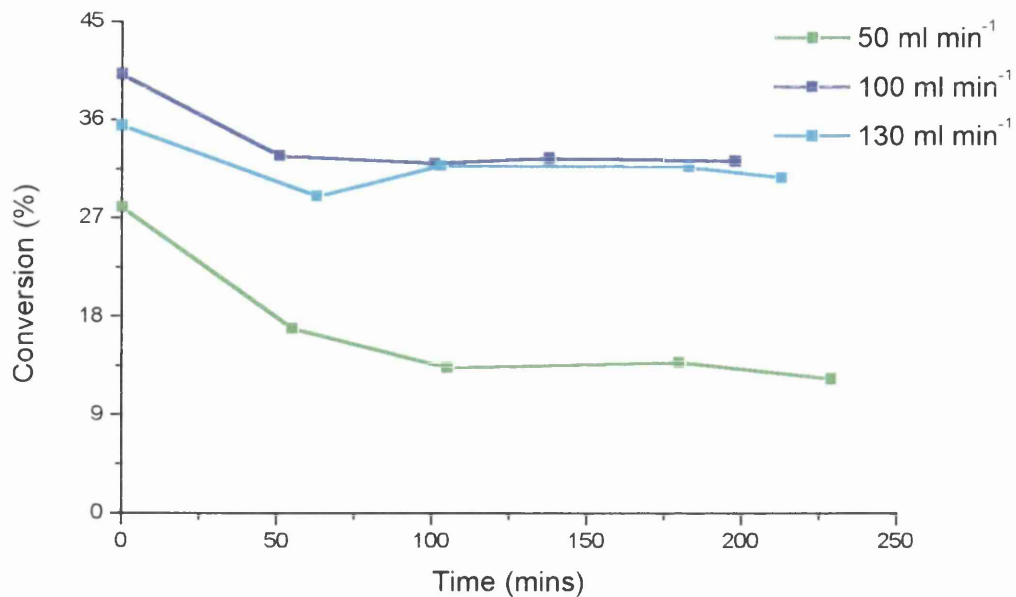


**Fig. 5.6.30** Conversion as a function of Time during the Oxidative Dehydrogenation of Butane at various Flow-rates using 0.65% Pt/Al<sub>2</sub>O<sub>3</sub>.

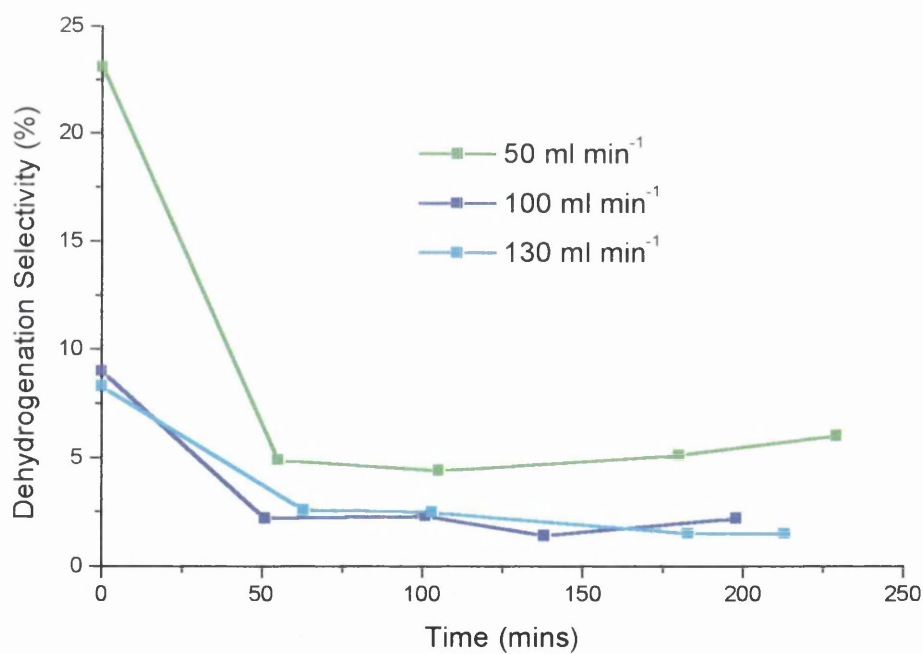


**Fig. 5.6.31** Dehydrogenation Selectivity as a function of Time during the Oxidative Dehydrogenation of Butane at various Flow-rates using 0.65% Pt/Al<sub>2</sub>O<sub>3</sub>.

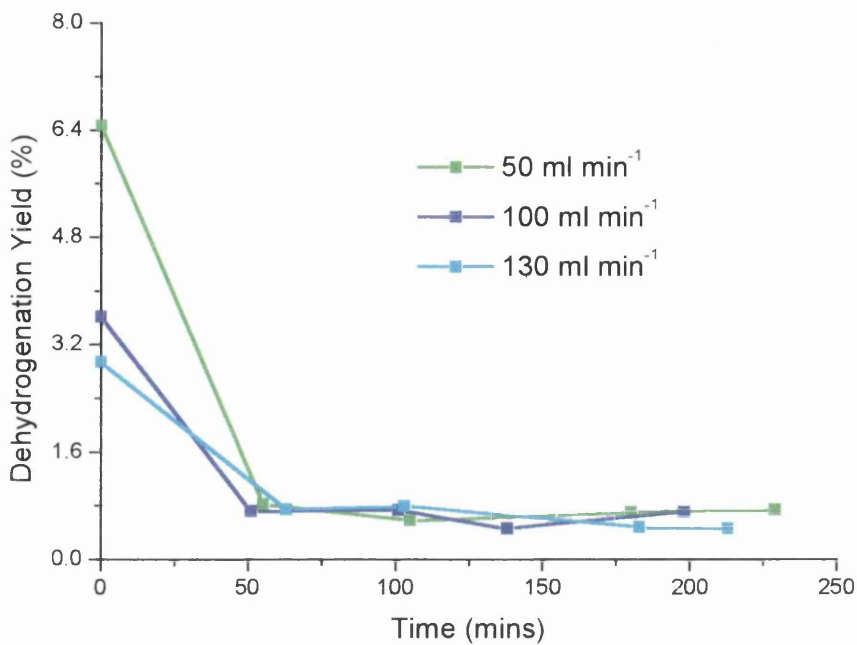


**Fig. 5.6.32** Dehydrogenation Yield as a function of Time during the Oxidative Dehydrogenation of Butane at various Flow-rates using 0.65% Pt/ $\text{Al}_2\text{O}_3$ .

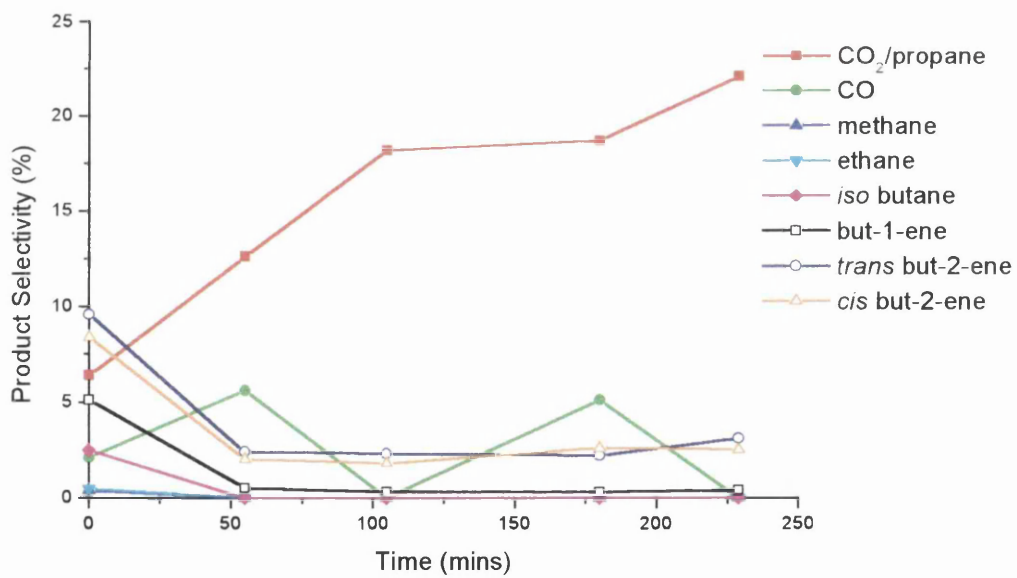


**Fig. 5.6.33** Product Selectivity as a function of Time during the Oxidative Dehydrogenation of Butane using the 0.65% Pt/ $\text{Al}_2\text{O}_3$  at 50  $\text{ml min}^{-1}$ .

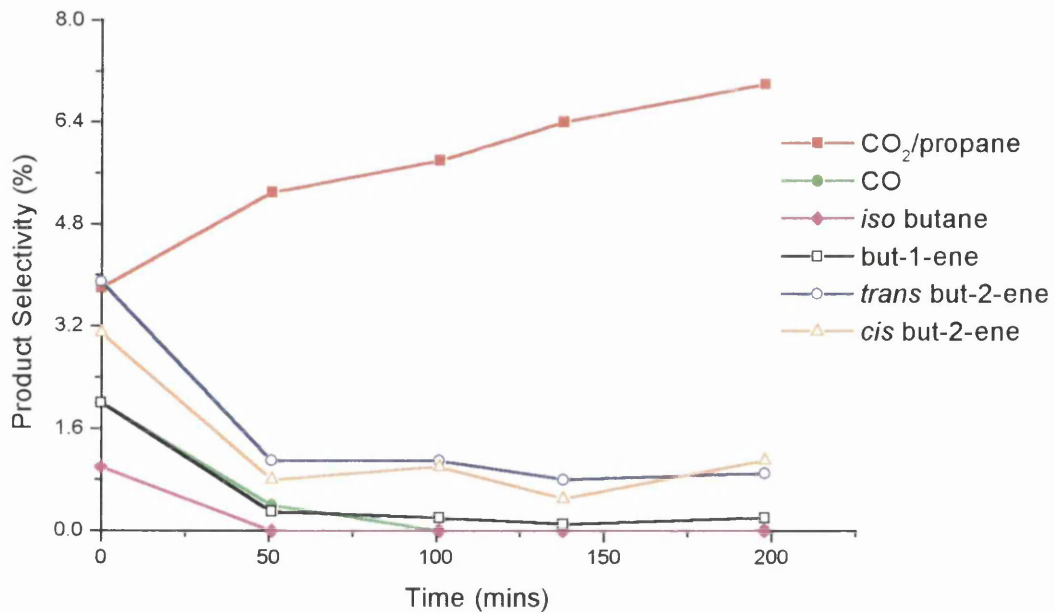


**Fig. 5.6.34** Product Selectivity as a function of Time during the Oxidative Dehydrogenation of Butane using the 0.65% Pt/Al<sub>2</sub>O<sub>3</sub> at 100 ml min<sup>-1</sup>.

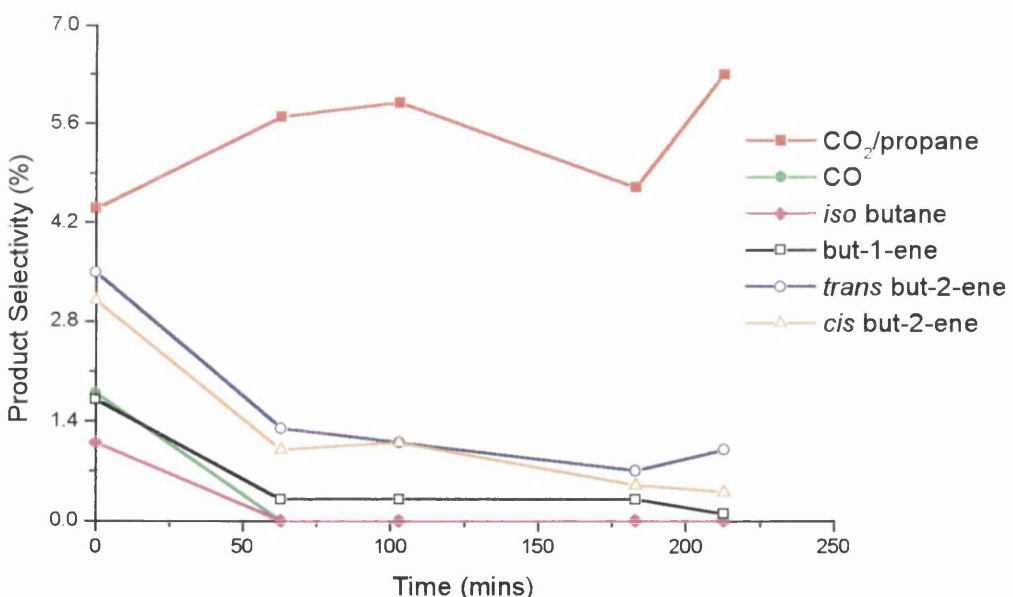


**Fig. 5.6.35** Product Selectivity as a function of Time during the Oxidative Dehydrogenation of Butane using the 0.65% Pt/Al<sub>2</sub>O<sub>3</sub> at 130 ml min<sup>-1</sup>.

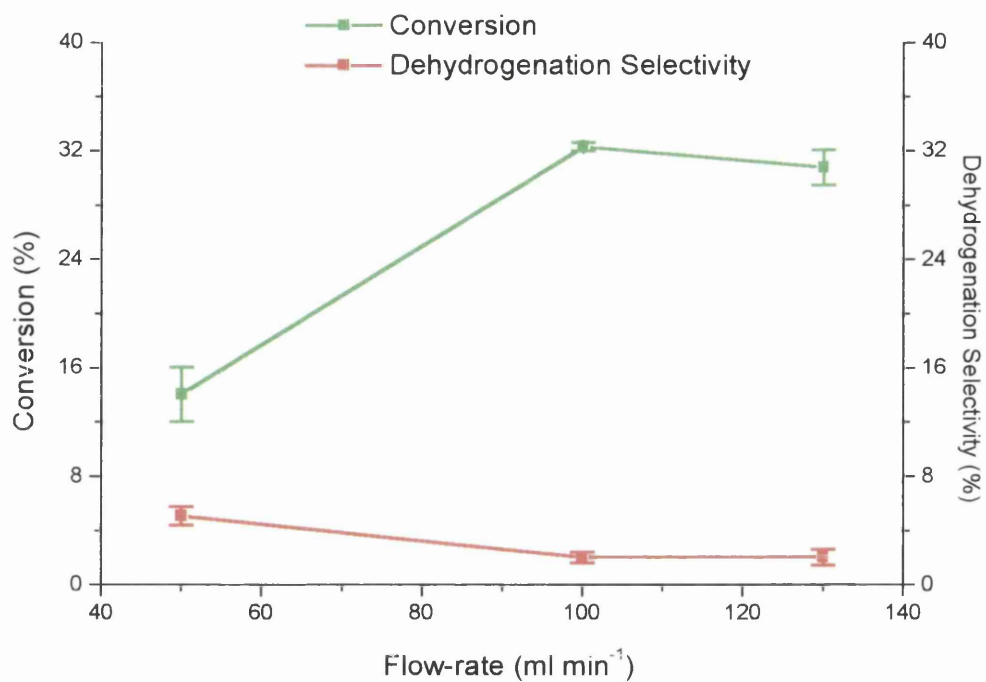


**Fig. 5.6.36** Conversion and Dehydrogenation Selectivity as a function of Flow-rate during the Oxidative Dehydrogenation of Butane using 0.65% Pt/Al<sub>2</sub>O<sub>3</sub> at 400°C.

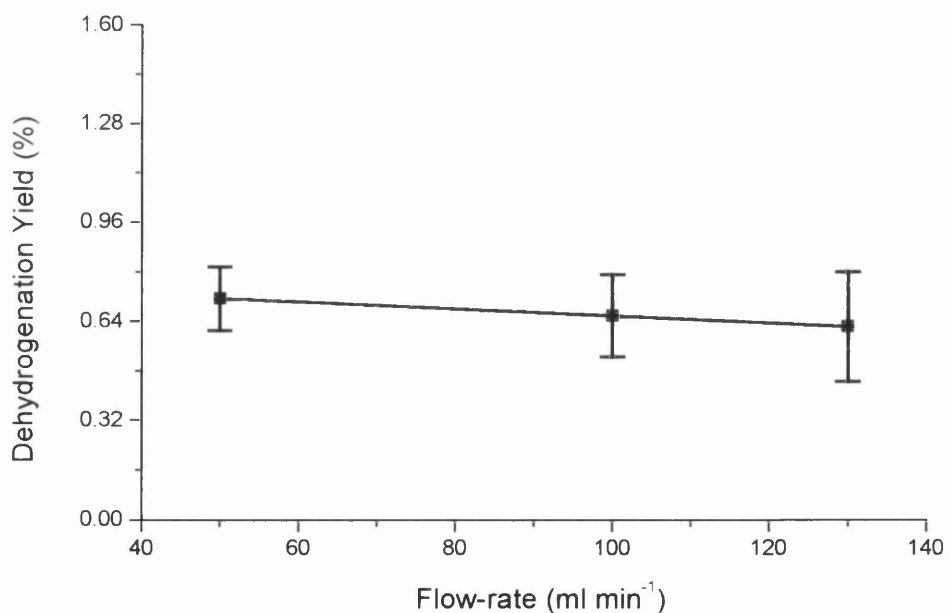


**Fig. 5.6.37** Dehydrogenation Yield as a function of Flow-rate during the Oxidative Dehydrogenation of Butane using 0.65% Pt/Al<sub>2</sub>O<sub>3</sub> at 400°C.

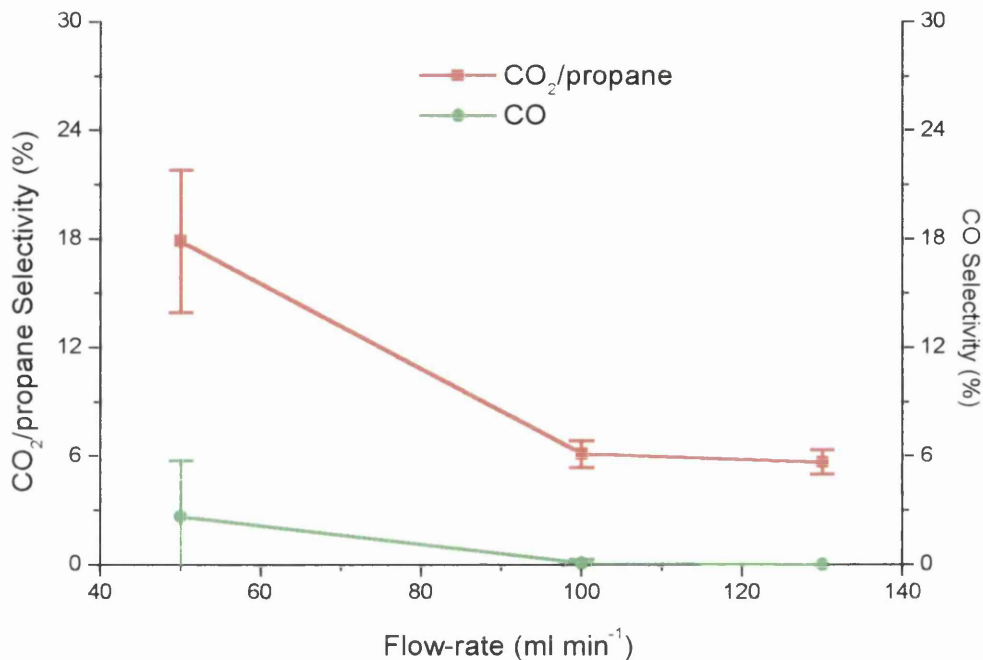


**Fig. 5.6.38**  $\text{CO}_2$  and CO Product Selectivity during the Oxidative Dehydrogenation of Butane using 0.65%  $\text{Pt}/\text{Al}_2\text{O}_3$  at  $400^\circ\text{C}$ .

### 5.6.5 The Straight Dehydrogenation of Butane as a function of Catalyst Mass under Continuous-flow conditions using 0.65% $\text{Pt}/\text{Al}_2\text{O}_3$

Tables 5.6.13, 5.6.14 and 5.6.15 contain the conversion and product molar quantities, the product selectivity and the product yield values respectively for the straight dehydrogenation of butane using 0.65%  $\text{Pt}/\text{Al}_2\text{O}_3$  as a function of catalyst mass. Figures 5.6.39 - 5.6.46 graphically represent these results with respect to the conversion, individual product selectivity, dehydrogenation selectivity and dehydrogenation yield as a function of time and catalyst mass, showing the equilibrium results, where appropriate, for comparison. Section 4.1.3 describes the procedure used to carry out the experiments.

**Table 5.6.13** Conversion and Product Molar Quantities for the Straight Dehydrogenation of Butane as a function of Catalyst Mass using 0.65% Pt/Al<sub>2</sub>O<sub>3</sub>.

Catalyst Mass (mg)	Time (mins)	Moles Bypass (x10 <sup>-7</sup> )	Moles Reacted (x10 <sup>-7</sup> )	Conv. (%)	Met. (x10 <sup>-7</sup> )	Eth. (x10 <sup>-7</sup> )	Iso (x10 <sup>-7</sup> )	B-1 (x10 <sup>-7</sup> )	Trans B-2 (x10 <sup>-7</sup> )	Cis B-2 (x10 <sup>-7</sup> )	Diene (x10 <sup>-7</sup> )
375	0	40.90	6.70	16.4	0.56	0.19	0.09	0.66	1.32	1.17	0
375	43	40.90	1.87	4.6	0.11	0	0	0.26	0.66	0.65	0
375	83	40.90	1.80	4.4	0.07	0	0	0.20	0.53	0.49	0
375	106	40.90	1.62	4.0	0.05	0	0	0.17	0.44	0.38	0
375	130	40.90	1.55	3.8	0.04	0	0	0.16	0.47	0.45	0
375	151	40.90	1.07	2.6	0	0	0	0.16	0.44	0.38	0
753	0	41.37	11.06	26.7	2.47	1.30	0.74	0.68	1.16	0.94	0
753	25	41.37	4.26	10.3	0.23	0	0.08	0.74	1.40	1.18	0
753	60	41.37	3.72	9.0	0.14	0	0.05	0.62	1.11	1.00	0
753	81	41.37	3.29	8.0	0.12	0	0.04	0.58	1.16	1.00	0
753	115	41.37	3.07	7.4	0.09	0	0	0.50	1.08	0.96	0

**Table 5.6.14** Product Selectivity for the Straight Dehydrogenation of Butane as a function of Catalyst Mass using 0.65% Pt/Al<sub>2</sub>O<sub>3</sub>.

Catalyst Mass (mg)	Time (mins)	Met. Sel. (%)	Eth. Sel. (%)	Iso Sel. (%)	B-1 Sel. (%)	Trans B-2 Sel. (%)	Cis B-2 Sel. (%)	Diene Sel. (%)	Dehydro. Sel. (%)
375	0	2.1	1.4	1.3	9.8	19.7	17.5	0	47.0
375	43	1.5	0	0	13.9	35.3	34.8	0	84.0
375	83	1.0	0	0	11.1	29.4	27.2	0	67.7
375	106	0.8	0	0	10.5	27.2	23.4	0	61.1
375	130	0.6	0	0	10.3	30.3	29.0	0	69.6
375	151	0	0	0	15.0	41.1	35.5	0	91.6
753	0	5.6	5.9	6.7	6.1	10.5	8.5	0	25.1
753	25	1.3	0	1.9	17.4	32.9	27.7	0	78.0
753	60	0.9	0	1.3	16.7	29.8	26.9	0	73.4
753	81	0.9	0	1.2	17.6	35.2	30.4	0	83.2
753	115	0.7	0	0	16.3	35.2	31.3	0	82.8

**Table 5.6.15** Product Yields for the Straight Dehydrogenation of Butane as a function of Catalyst Mass using 0.65% Pt/Al<sub>2</sub>O<sub>3</sub>.

Catalyst Mass (mg)	Time (mins)	Met. Yield (%)	Eth. Yield (%)	Iso Yield (%)	B-1 Yield (%)	Trans B-2 Yield (%)	Cis B-2 Yield (%)	Diene Yield (%)	Dehydro. Yield (%)
375	0	0.34	0.23	0.21	1.61	3.23	2.87	0	7.71
375	43	0.07	0	0	0.64	1.62	1.60	0	3.86
375	83	0.04	0	0	0.49	1.29	1.20	0	2.98
375	106	0.03	0	0	0.42	1.09	0.94	0	2.44
375	130	0.02	0	0	0.39	1.15	1.10	0	2.64
375	151	0	0	0	0.39	1.07	0.92	0	2.38
753	0	1.50	1.58	1.79	1.63	2.80	2.27	0	6.70
753	25	0.13	0	0.20	1.79	3.39	2.85	0	8.03
753	60	0.08	0	0.12	1.50	2.68	2.42	0	6.61
753	81	0.07	0	0.10	1.40	2.82	2.43	0	6.66
753	115	0.05	0	0	1.21	2.60	2.32	0	6.13

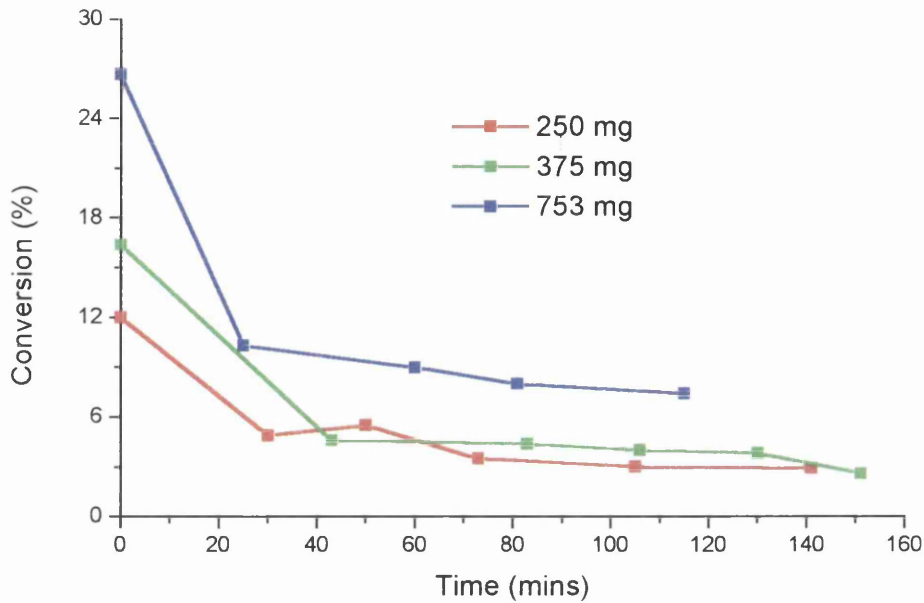


**Fig. 5.6.39** Conversion as a function of Time during the Straight Dehydrogenation of Butane at various Catalyst Masses using 0.65% Pt/Al<sub>2</sub>O<sub>3</sub>.

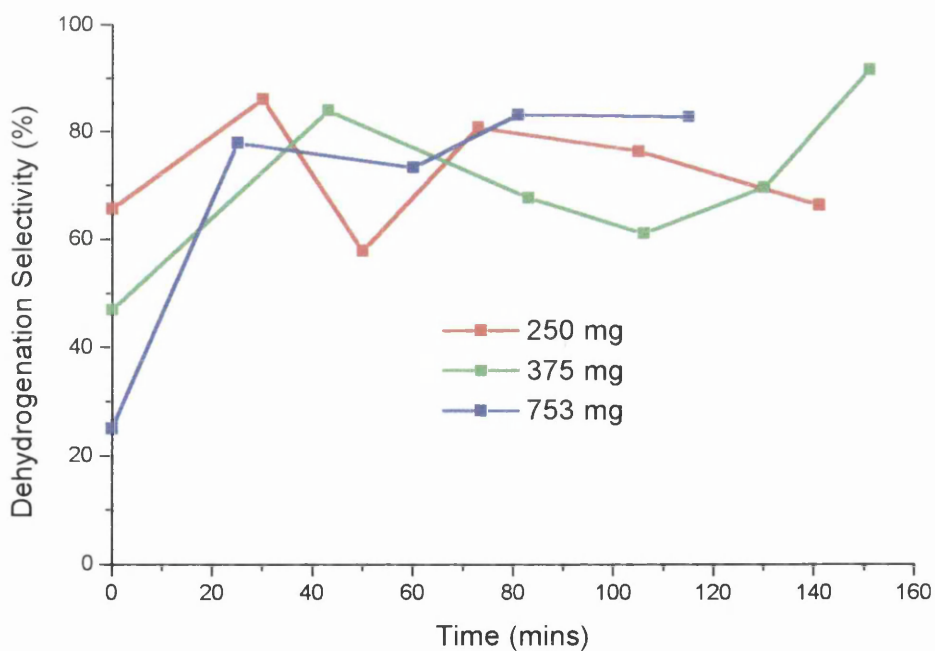


**Fig. 5.6.40** Dehydrogenation Selectivity as a function of Time during the Straight Dehydrogenation of Butane at various Catalyst Masses using 0.65% Pt/Al<sub>2</sub>O<sub>3</sub>.

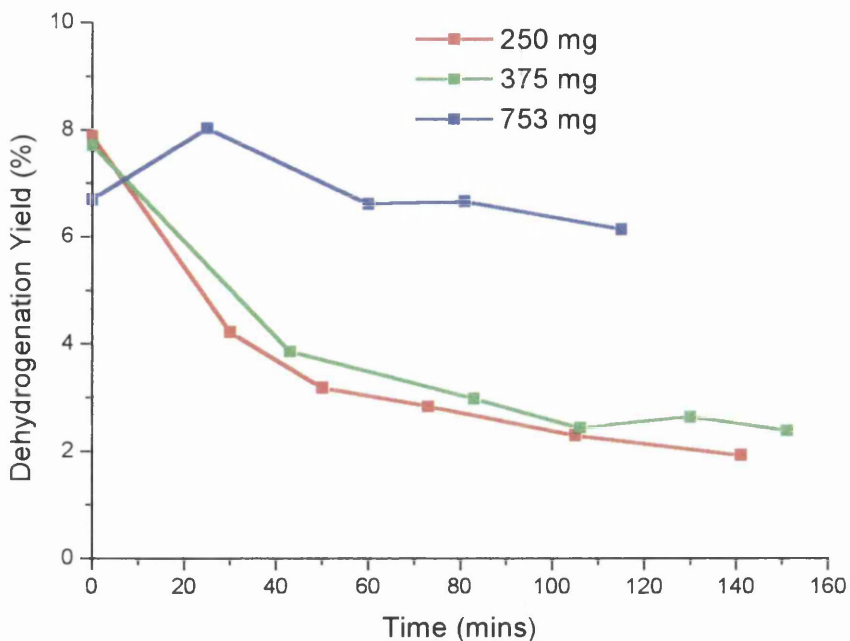


**Fig. 5.6.41** Dehydrogenation Yield as a function of Time during the Straight Dehydrogenation of Butane at various Catalyst Masses using 0.65% Pt/Al<sub>2</sub>O<sub>3</sub>.

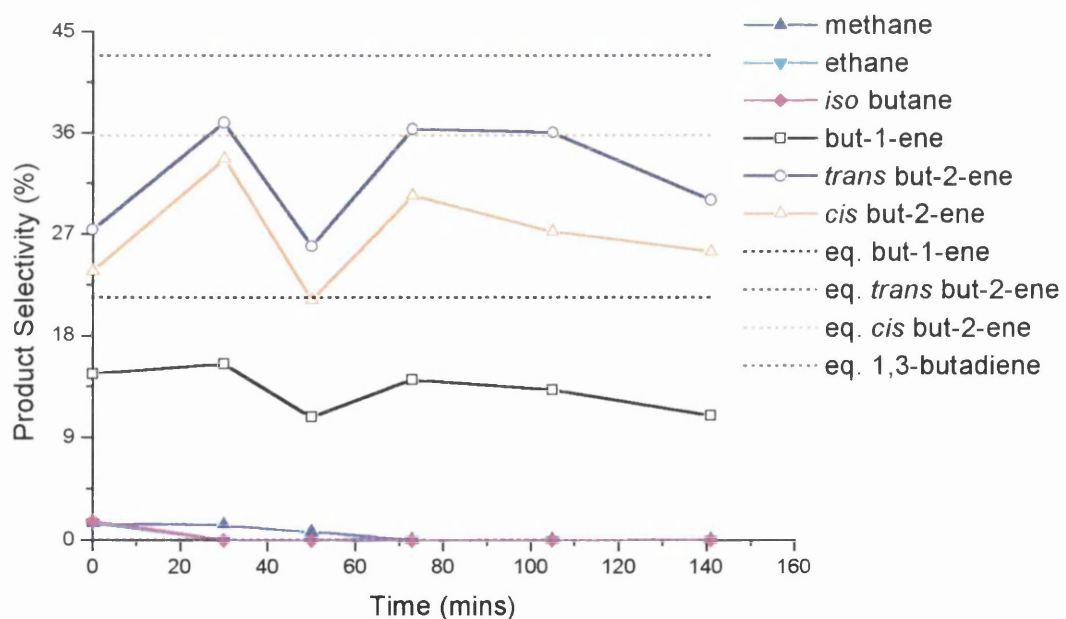


**Fig. 5.6.42** Product Selectivity as a function of Time during the Straight Dehydrogenation of Butane using 250mg of 0.65% Pt/Al<sub>2</sub>O<sub>3</sub>.

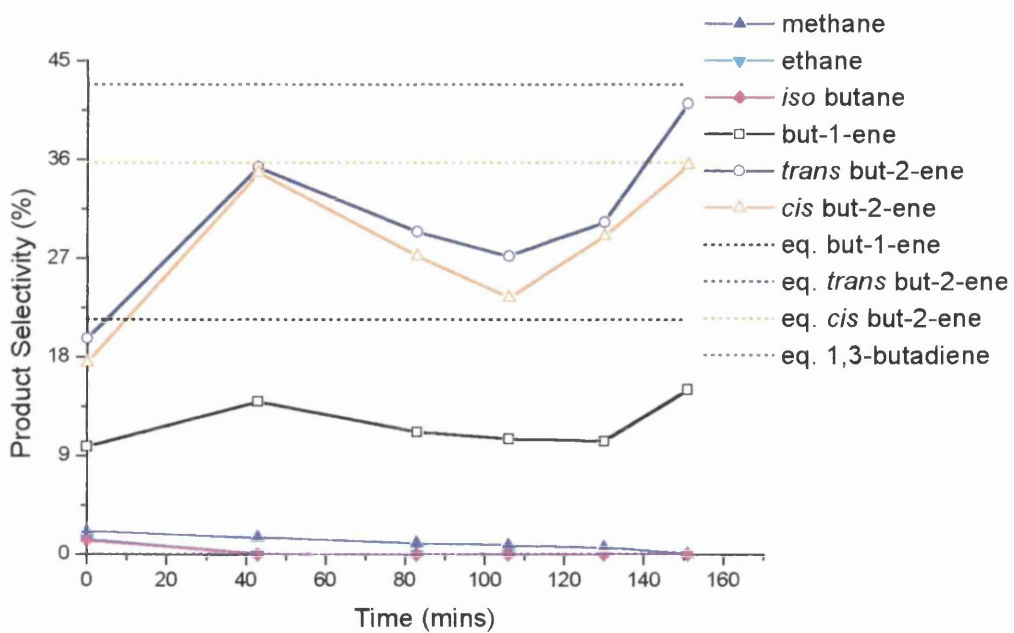


**Fig. 5.6.43** Product Selectivity as a function of Time during the Straight Dehydrogenation of Butane using 375mg of 0.65% Pt/Al<sub>2</sub>O<sub>3</sub>.

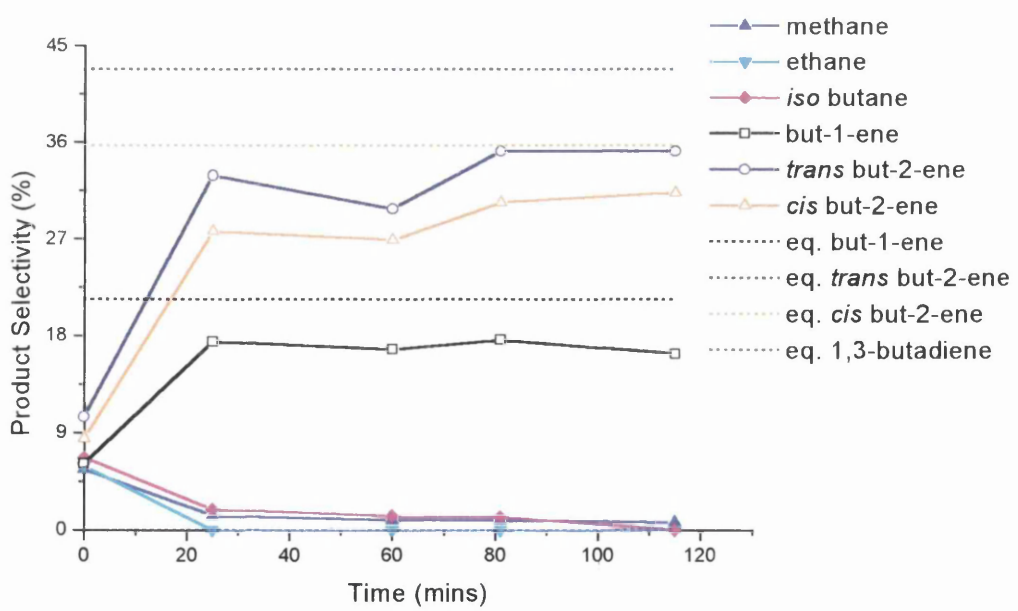


**Fig. 5.6.44** Product Selectivity as a function of Time during the Straight Dehydrogenation of Butane using 753mg of 0.65% Pt/Al<sub>2</sub>O<sub>3</sub>.

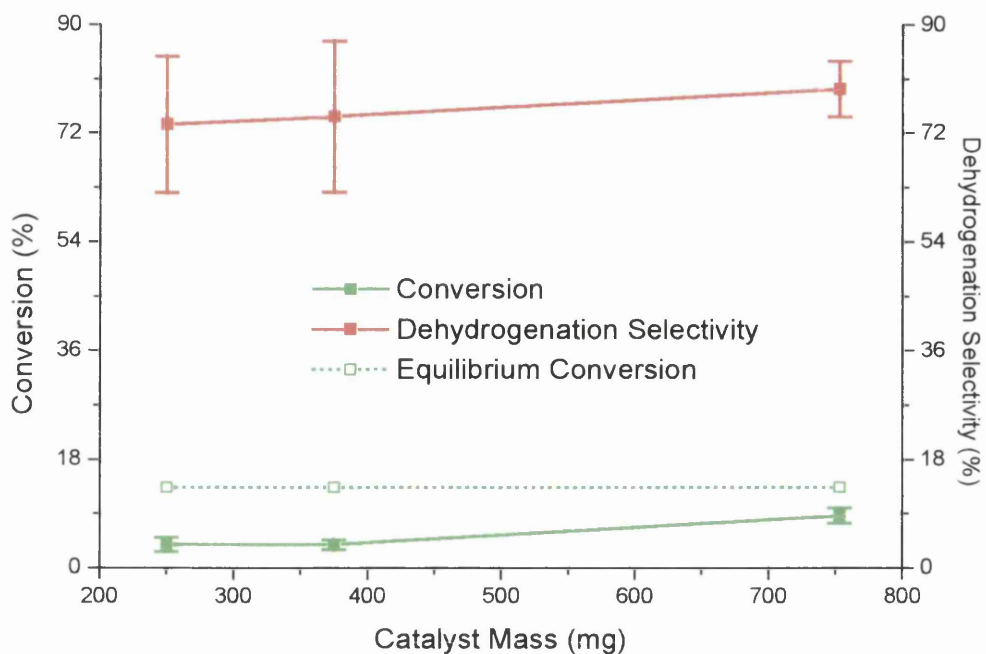


**Fig. 5.6.45** Conversion and Dehydrogenation Selectivity as a function of Catalyst Mass during the Straight Dehydrogenation of Butane using 0.65% Pt/Al<sub>2</sub>O<sub>3</sub> at 400°C.

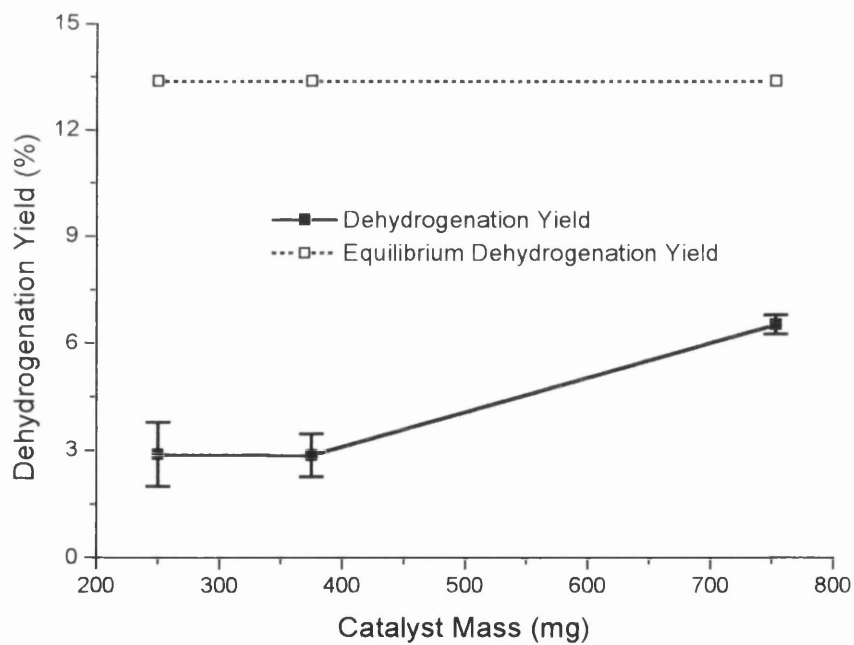


**Fig. 5.6.46** Dehydrogenation Yield as a function of Catalyst Mass during the Straight Dehydrogenation of Butane using 0.65% Pt/Al<sub>2</sub>O<sub>3</sub> at 400°C.

## 5.6.6 The Oxidative Dehydrogenation of Butane as a function of Catalyst Mass under Continuous-flow conditions using 0.65% Pt/Al<sub>2</sub>O<sub>3</sub>

Tables 5.6.16, 5.6.17 and 5.6.18 contain the conversion and product molar quantities, the product selectivity and the product yield values respectively for the oxidative dehydrogenation of butane using 0.65% Pt/Al<sub>2</sub>O<sub>3</sub> as a function of catalyst mass. Figures 5.6.47 - 5.6.55 graphically represent these results with respect to the conversion, individual product selectivity, dehydrogenation selectivity and dehydrogenation yield as a function of time and catalyst mass. Section 4.1.3 describes the procedure used to carry out the experiments.

**Table 5.6.16** Conversion and Product Molar Quantities for the Oxidative Dehydrogenation of Butane using 0.65% Pt/Al<sub>2</sub>O<sub>3</sub> as a function of Catalyst Mass.

Catalyst Mass (mg)	Time (mins)	Moles Bypass (x10 <sup>-7</sup> )	Moles Reacted (x10 <sup>-7</sup> )	Conv. (%)	CO <sub>2</sub> /Pr (x10 <sup>-7</sup> )	CO (x10 <sup>-7</sup> )	Met. (x10 <sup>-7</sup> )	Eth. (x10 <sup>-7</sup> )	Iso (x10 <sup>-7</sup> )	B-1 (x10 <sup>-7</sup> )	Trans B-2 (x10 <sup>-7</sup> )	Cis B-2 (x10 <sup>-7</sup> )	Diene (x10 <sup>-7</sup> )
375	0	46.93	22.31	47.5	3.09	0.96	0.49	0.22	0	0.62	1.15	1.01	0
375	42	46.93	11.63	24.8	4.13	0.18	0	0	0	0.08	0.31	0.31	0
375	97	46.93	11.25	24.0	4.24	0.16	0	0	0	0.04	0.17	0.15	0
375	132	46.93	12.23	26.1	4.05	0.17	0	0	0	0.03	0.18	0.17	0
375	172	46.93	12.85	27.4	4.22	0.13	0	0	0	0.02	0.15	0.13	0
752	0	46.93	10.92	23.3	4.56	0.32	0	0	0	0.15	0.43	0.39	0
752	75	46.93	11.49	24.5	4.16	0	0	0	0	0.06	0.26	0.21	0
752	115	46.93	10.73	22.9	4.16	0	0	0	0	0.04	0.23	0.21	0
752	152	46.93	10.79	23.0	4.28	0	0	0	0	0.03	0.20	0.15	0

**Table 5.6.17** Product Selectivity for the Oxidative Dehydrogenation of Butane using 0.65% Pt/Al<sub>2</sub>O<sub>3</sub> as a function of Catalyst Mass.

Catalyst Mass (mg)	Time (mins)	CO <sub>2</sub> /Pr Sel. (%)	CO Sel. (%)	Met. Sel. (%)	Eth. Sel. (%)	Iso Sel. (%)	B-1 Sel. (%)	Trans B-2 Sel. (%)	Cis B-2 Sel. (%)	Diene Sel. (%)	Dehydro. Sel. (%)
375	0	3.5	1.1	0.5	0.5	0	2.8	5.2	4.5	0	12.5
375	42	8.9	0.4	0	0	0	0.7	2.7	2.7	0	6.1
375	97	9.4	0.4	0	0	0	0.4	1.5	1.3	0	3.2
375	132	8.3	0.3	0	0	0	0.2	1.5	1.4	0	3.1
375	172	8.2	0.2	0	0	0	0.2	1.2	1.0	0	2.4
752	0	10.4	0.7	0	0	0	1.4	3.9	3.6	0	8.9
752	75	9.0	0	0	0	0	0.5	2.3	1.8	0	4.6
752	115	9.7	0	0	0	0	0.3	2.1	2.0	0	4.4
752	152	9.9	0	0	0	0	0.3	1.8	1.4	0	3.5

**Table 5.6.18** Product Yields for the Oxidative Dehydrogenation of Butane using 0.65% Pt/Al<sub>2</sub>O<sub>3</sub> as a function of Catalyst Mass.

Catalyst Mass (mg)	Time (mins)	CO <sub>2</sub> /Pr Yield (%)	CO Yield (%)	Met. Yield (%)	Eth. Yield (%)	Iso Yield (%)	B-1 Yield (%)	Trans B-2 Yield (%)	Cis B-2 Yield (%)	Diene Yield (%)	Dehydro. Yield (%)
375	0	1.66	0.52	0.24	0.24	0	1.33	2.47	2.14	0	5.94
375	42	2.21	0.10	0	0	0	0.17	0.67	0.67	0	1.51
375	97	2.26	0.10	0	0	0	0.10	0.36	0.31	0	0.77
375	132	2.17	0.08	0	0	0	0.05	0.39	0.36	0	0.81
375	172	2.25	0.05	0	0	0	0.05	0.33	0.27	0	0.66
752	0	2.42	0.16	0	0	0	0.33	0.91	0.84	0	2.07
752	75	2.20	0	0	0	0	0.12	0.56	0.44	0	1.13
752	115	2.22	0	0	0	0	0.07	0.48	0.46	0	1.01
752	152	2.28	0	0	0	0	0.07	0.41	0.32	0	0.80

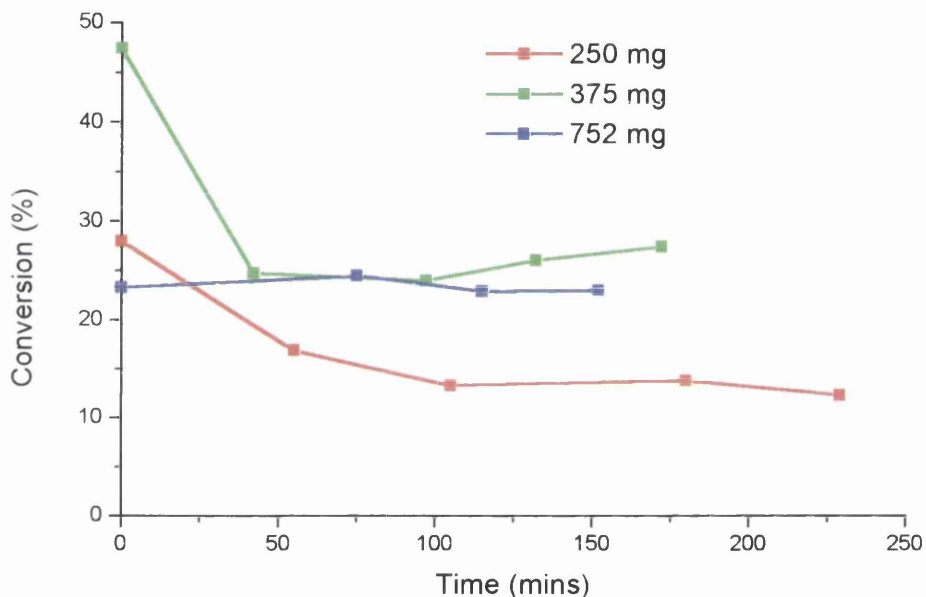


**Fig. 5.6.47** Conversion as a function of Time during the Oxidative Dehydrogenation of Butane at various Catalyst Masses using 0.65% Pt/Al<sub>2</sub>O<sub>3</sub>.

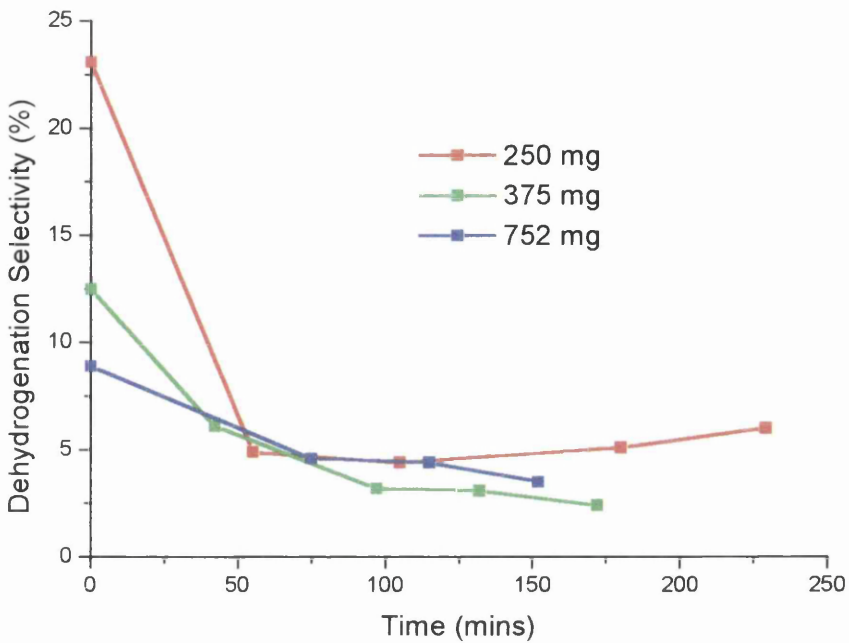


**Fig. 5.6.48** Dehydrogenation Selectivity as a function of Time during the Oxidative Dehydrogenation of Butane at various Catalyst Masses using 0.65% Pt/Al<sub>2</sub>O<sub>3</sub>.

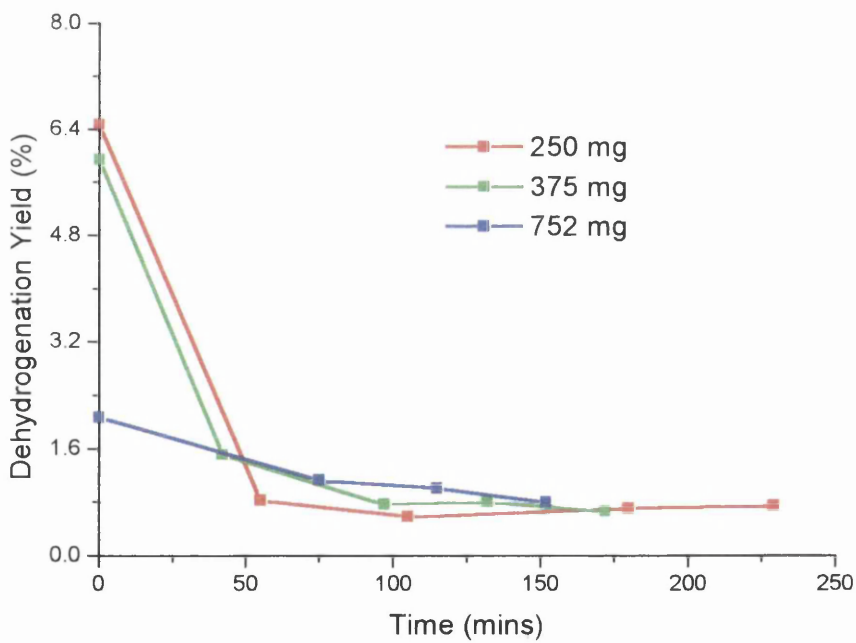


**Fig. 5.6.49** Dehydrogenation Yield as a function of Time during the Oxidative Dehydrogenation of Butane at various Catalyst Masses using 0.65% Pt/Al<sub>2</sub>O<sub>3</sub>.

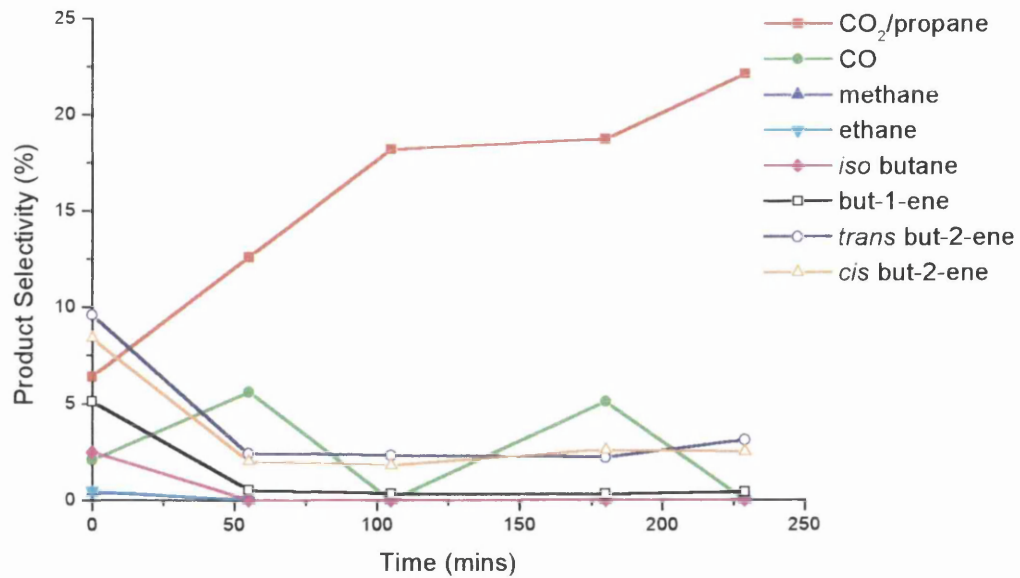


**Fig. 5.6.50** Product Selectivity as a function of Time during the Oxidative Dehydrogenation of Butane using 250mg of 0.65% Pt/Al<sub>2</sub>O<sub>3</sub>.

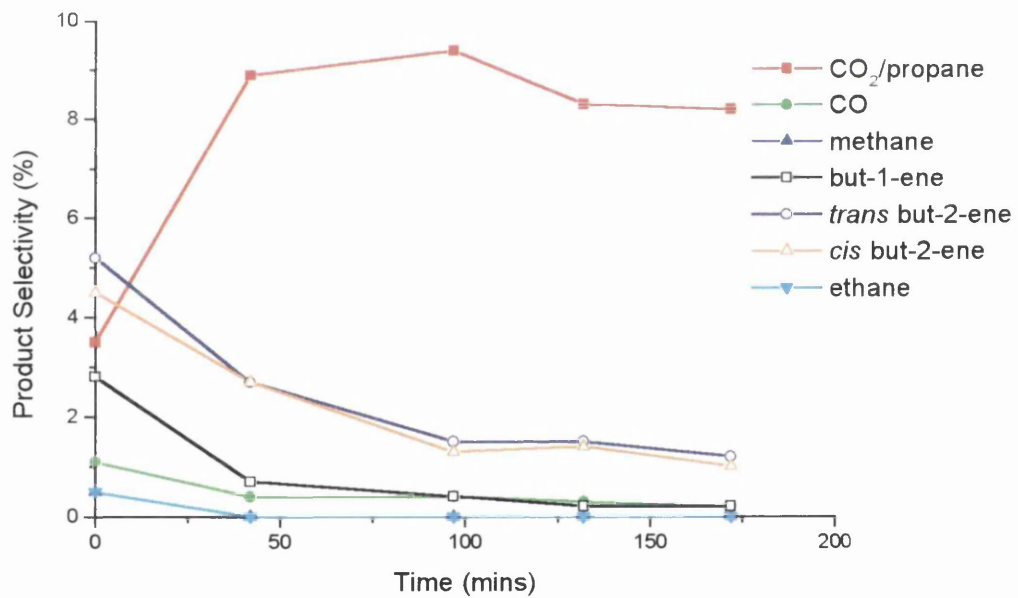


**Fig. 5.6.51** Product Selectivity as a function of Time during the Oxidative Dehydrogenation of Butane using 375mg of 0.65% Pt/Al<sub>2</sub>O<sub>3</sub>.

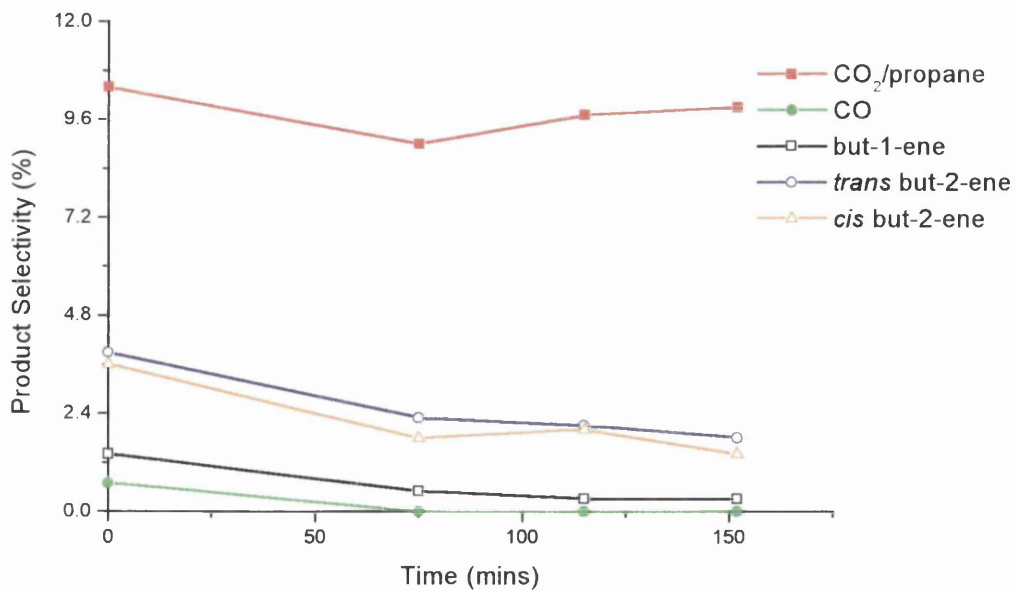


**Fig. 5.6.52** Product Selectivity as a function of Time during the Oxidative Dehydrogenation of Butane using 752mg of 0.65% Pt/ $\text{Al}_2\text{O}_3$ .

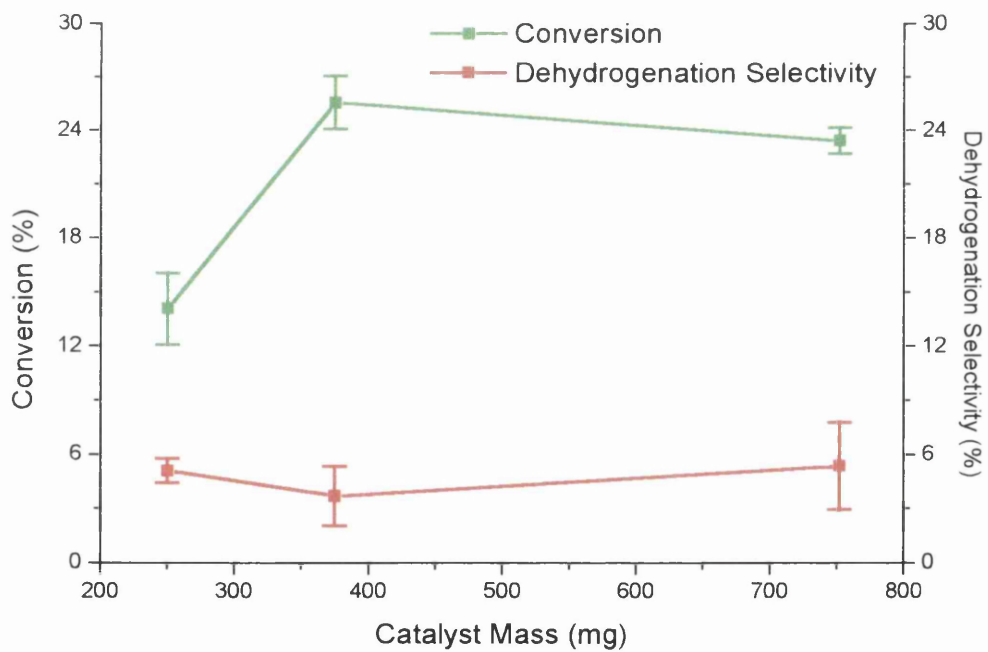


**Fig. 5.6.53** Conversion and Dehydrogenation Selectivity as a function of Catalyst Mass during the Oxidative Dehydrogenation of Butane using 0.65% Pt/ $\text{Al}_2\text{O}_3$  at 400°C.

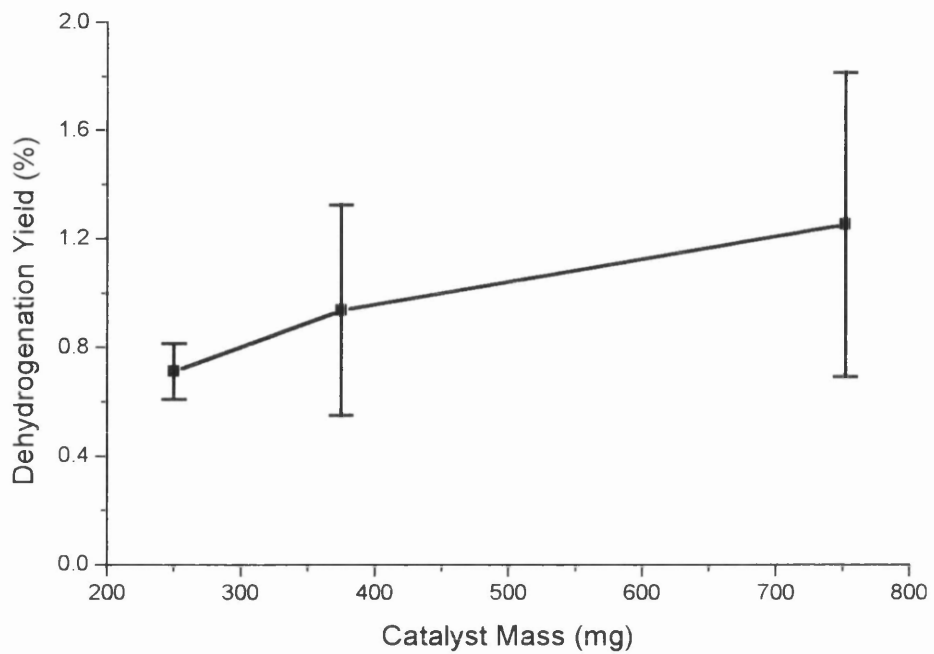


**Fig. 5.6.54** Dehydrogenation Yield as a function of Catalyst Mass during the Oxidative Dehydrogenation of Butane using 0.65% Pt/Al<sub>2</sub>O<sub>3</sub> at 400°C.

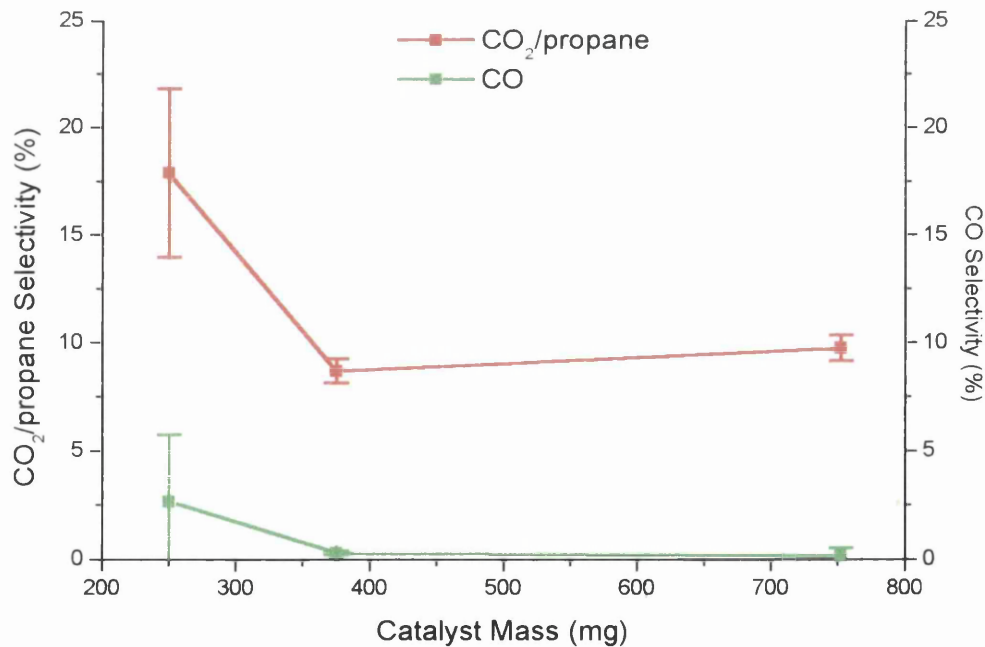


**Fig. 5.6.55** CO<sub>2</sub> and CO Product Selectivity during the Oxidative Dehydrogenation of Butane using 0.65% Pt/Al<sub>2</sub>O<sub>3</sub> at 400°C.

### 5.6.7 The Oxidative Dehydrogenation of Butane as a function of Hydrocarbon:Oxygen Ratio under Continuous-flow conditions using 0.65% Pt/Al<sub>2</sub>O<sub>3</sub>

Tables 5.6.19, 5.6.20 and 5.6.21 contain the conversion and product molar quantities, the product selectivity and the product yield values respectively for the oxidative dehydrogenation of butane using 0.65% Pt/Al<sub>2</sub>O<sub>3</sub> as a function of hydrocarbon:oxygen ratio. Figures 5.6.56 - 5.6.67 graphically represent these results with respect to the conversion, individual product selectivity, dehydrogenation selectivity and dehydrogenation yield as a function of time and catalyst mass. Section 4.1.3 describes the procedure used to carry out the experiments.

**Table 5.6.19** Conversion and Product Molar Quantities for the Oxidative Dehydrogenation of Butane as a function of Hydrocarbon/Oxygen ratio using 0.65% Pt/Al<sub>2</sub>O<sub>3</sub>.

H <sub>C</sub> :O <sub>2</sub> Ratio	Time (mins)	Moles Bypass ( $\times 10^{-7}$ )	Moles Reacted ( $\times 10^{-7}$ )	Conv. (%)	CO <sub>2</sub> /Pr ( $\times 10^{-7}$ )	CO ( $\times 10^{-7}$ )	Met. ( $\times 10^{-7}$ )	Eth. ( $\times 10^{-7}$ )	Iso. ( $\times 10^{-7}$ )	B-1 ( $\times 10^{-7}$ )	Trans-B-2 ( $\times 10^{-7}$ )	Cis-B-2 ( $\times 10^{-7}$ )	Diene ( $\times 10^{-7}$ )
25:1	0	35.80	6.50	18.2	0.26	0.18	0.23	0.07	0.12	0.78	1.28	1.02	0
25:1	51	35.80	0.80	2.2	0.14	0	0	0	0	0.06	0.14	0.11	0
25:1	92	35.80	0.50	1.4	0.20	0	0	0	0	0.05	0.11	0.07	0
25:1	132	35.80	1.10	3.1	0.15	0	0	0	0	0.04	0.09	0.07	0
25:1	202	35.80	1.30	3.6	0.22	0	0	0	0	0.04	0.08	0.05	0
13.3:1	0	35.56	7.49	21.1	0.22	0.36	0	0.04	0.08	0.49	1.01	0.81	0
13.3:1	47	35.56	3.36	9.4	0.27	0	0	0	0	0.01	0.14	0.11	0
13.3:1	126	35.56	1.58	4.4	0.29	0	0	0	0	0	0.11	0.11	0
13.3:1	196	35.56	1.21	3.4	0.33	0	0	0	0	0	0.10	0.07	0
13.3:1	226	35.56	0.78	2.2	0.39	0	0	0	0	0	0.09	0.05	0
4:1	0	36.59	5.53	15.1	1.18	0.25	0.28	0	0	0.07	0.23	0.19	0
4:1	54	36.59	2.57	7.0	1.28	0.10	0	0	0	0	0.07	0.07	0
4:1	142	36.59	3.81	10.4	1.37	0	0	0	0	0	0.07	0	0
4:1	192	36.59	3.66	10.0	1.53	0	0	0	0	0	0.06	0.06	0
4:1	242	36.59	1.74	4.8	1.53	0	0	0	0	0	0.07	0.04	0
1:1	0	32.08	15.08	47.0	2.58	0.59	0.16	0.09	0.19	0.35	0.48	0.39	0
1:1	49	32.08	13.73	42.8	2.86	0	0	0	0	0.05	0.12	0.10	0
1:1	98	32.08	14.73	45.9	2.72	0	0	0	0	0.04	0.08	0.04	0
1:1	153	32.08	13.00	40.5	3.08	0	0	0	0	0.04	0.06	0.05	0
1:1	212	32.08	11.98	37.3	3.79	0	0	0	0	0.01	0.11	0.08	0
1:2	0	25.47	11.35	44.6	3.05	1.19	0.73	0.34	0	0.45	0.76	0.64	0
1:2	64	25.47	10.61	41.6	4.48	0.14	0	0	0	0.02	0.08	0.09	0
1:2	112	25.47	10.90	42.8	3.49	0.16	0	0	0	0.02	0.08	0.07	0
1:2	207	25.47	11.53	45.3	4.08	0.15	0	0	0	0.02	0.05	0.07	0
1:2	262	25.47	10.89	42.8	4.61	0.12	0	0	0	0.03	0.09	0.08	0

**Table 5.6.20** Product Selectivity for the Oxidative Dehydrogenation of Butane as a function of Hydrocarbon/Oxygen ratio using 0.65% Pt/Al<sub>2</sub>O<sub>3</sub>.

H <sub>C</sub> :O <sub>2</sub> Ratio	Time (mins)	CO <sub>2</sub> /Pr Sel. (%)	CO Sel. (%)	Met. Sel. (%)	Eth. Sel. (%)	Iso Sel. (%)	B-1 Sel. (%)	Trans B-2 Sel. (%)	Cis B-2 Sel. (%)	Diene Sel. (%)	Dehydro. Sel. (%)
25:1	0	1.0	0.7	0.9	0.5	1.8	12.0	19.7	15.7	0	47.4
25:1	51	4.4	0	0	0	0	7.5	17.5	13.8	0	38.8
25:1	92	10.0	0	0	0	0	10.0	22.0	14.0	0	46.0
25:1	132	3.4	0	0	0	0	3.6	8.2	6.4	0	18.2
25:1	202	4.2	0	0	0	0	3.1	6.2	3.8	0	13.0
13.3:1	0	0.7	1.2	0	0.3	1.1	6.5	13.5	10.8	0	30.8
13.3:1	47	2.0	0	0	0	0	0.3	4.2	3.3	0	7.8
13.3:1	126	4.6	0	0	0	0	0	7.0	7.0	0	14.0
13.3:1	196	6.8	0	0	0	0	0	8.3	5.8	0	14.1
13.3:1	226	12.5	0	0	0	0	0	11.5	6.4	0	17.9
4:1	0	5.3	1.1	1.3	0	0	1.3	4.2	3.4	0	8.9
4:1	54	12.4	1.0	0	0	0	0	2.7	2.7	0	5.4
4:1	142	9.0	0	0	0	0	0	1.8	0	0	1.8
4:1	192	10.4	0	0	0	0	0	1.6	1.6	0	3.2
4:1	242	22.0	0	0	0	0	0	4.0	2.3	0	6.3
1:1	0	4.3	1.0	0.3	0.3	1.2	2.3	3.2	2.6	0	8.1
1:1	49	5.2	0	0	0	0	0.4	0.9	0.7	0	2.0
1:1	98	4.6	0	0	0	0	0.3	0.5	0.3	0	1.1
1:1	153	5.9	0	0	0	0	0.3	0.5	0.4	0	1.2
1:1	212	7.9	0	0	0	0	0.1	0.9	0.7	0	1.7
1:2	0	6.7	2.6	1.6	1.6	0	4.0	6.7	5.6	0	16.3
1:2	64	10.6	0.3	0	0	0	0.2	0.8	0.8	0	1.8
1:2	112	8.0	0.4	0	0	0	0.2	0.7	0.6	0	1.5
1:2	207	8.8	0.3	0	0	0	0.2	0.4	0.6	0	1.2
1:2	262	10.6	0.3	0	0	0	0.3	0.8	0.7	0	1.8

**Table 5.6.21** Product Yields for the Oxidative Dehydrogenation of Butane as a function of Hydrocarbon/Oxygen ratio using 0.65% Pt/Al<sub>2</sub>O<sub>3</sub>.

H <sub>C</sub> :O <sub>2</sub> Ratio	Time (mins)	CO <sub>2</sub> /Pr Yield (%)	CO Yield (%)	Met. Yield (%)	Eth. Yield (%)	Iso Yield (%)	B-1 Yield (%)	Trans B-2 Yield (%)	Cis B-2 Yield (%)	Diene Yield (%)	Dehydro. Yield (%)
25:1	0	0.18	0.13	0.16	0.09	0.33	2.18	3.58	2.86	0	8.63
25:1	51	0.10	0	0	0	0	0.16	0.38	0.30	0	0.85
25:1	92	0.14	0	0	0	0	0.14	0.31	0.20	0	0.64
25:1	132	0.10	0	0	0	0	0.11	0.25	0.20	0	0.56
25:1	202	0.15	0	0	0	0	0.11	0.22	0.14	0	0.47
13.3:1	0	0.15	0.25	0	0.06	0.23	1.37	2.85	2.28	0	6.50
13.3:1	47	0.19	0	0	0	0	0.03	0.39	0.31	0	0.73
13.3:1	126	0.20	0	0	0	0	0	0.31	0.31	0	0.62
13.3:1	196	0.23	0	0	0	0	0	0.28	0.20	0	0.48
13.3:1	226	0.28	0	0	0	0	0	0.25	0.14	0	0.39
4:1	0	0.80	0.17	0.20	0	0	0.20	0.63	0.51	0	1.34
4:1	54	0.87	0.07	0	0	0	0	0.19	0.19	0	0.38
4:1	142	0.94	0	0	0	0	0	0.19	0	0	0.19
4:1	192	1.04	0	0	0	0	0	0.16	0.16	0	0.32
4:1	242	1.06	0	0	0	0	0	0.19	0.11	0	0.30
1:1	0	2.02	0.47	0.14	0.14	0.56	1.08	1.50	1.22	0	3.81
1:1	49	2.22	0	0	0	0	0.17	0.38	0.30	0	0.86
1:1	98	2.11	0	0	0	0	0.14	0.23	0.14	0	0.50
1:1	153	2.39	0	0	0	0	0.12	0.20	0.16	0	0.49
1:1	212	2.95	0	0	0	0	0.04	0.34	0.26	0	0.63
1:2	0	2.99	1.16	0.71	0.71	0	1.78	2.99	2.50	0	7.27
1:2	64	4.41	0.12	0	0	0	0.08	0.33	0.33	0	0.75
1:2	112	3.42	0.17	0	0	0	0.08	0.30	0.26	0	0.64
1:2	207	3.99	0.14	0	0	0	0.09	0.18	0.27	0	0.54
1:2	262	4.54	0.13	0	0	0	0.13	0.34	0.30	0	0.77

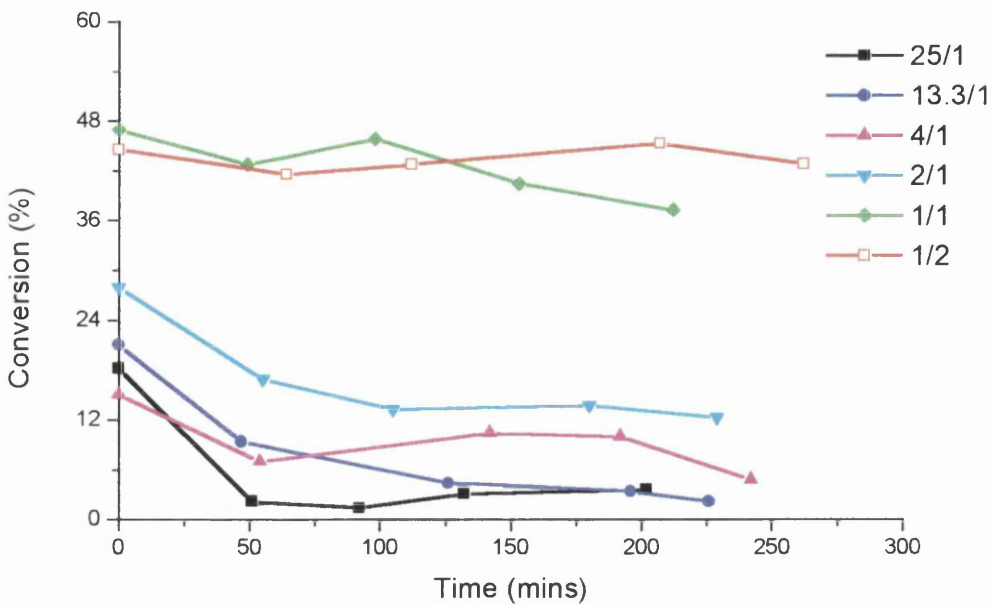


**Fig. 5.6.56** Conversion as a function of Time during the Straight Dehydrogenation of Butane at various Hydrocarbon:Oxygen Ratios using 0.65% Pt/Al<sub>2</sub>O<sub>3</sub>.

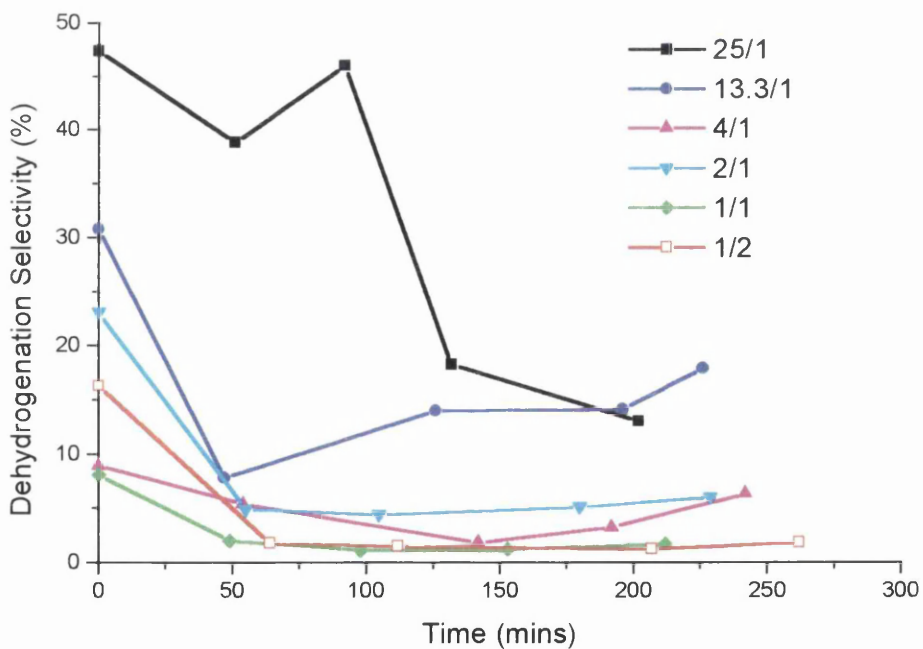


**Fig. 5.6.57** Dehydrogenation Selectivity as a function of Time during the Oxidative Dehydrogenation of Butane at various H<sub>c</sub>:O<sub>2</sub> Ratios using 0.65% Pt/Al<sub>2</sub>O<sub>3</sub>.

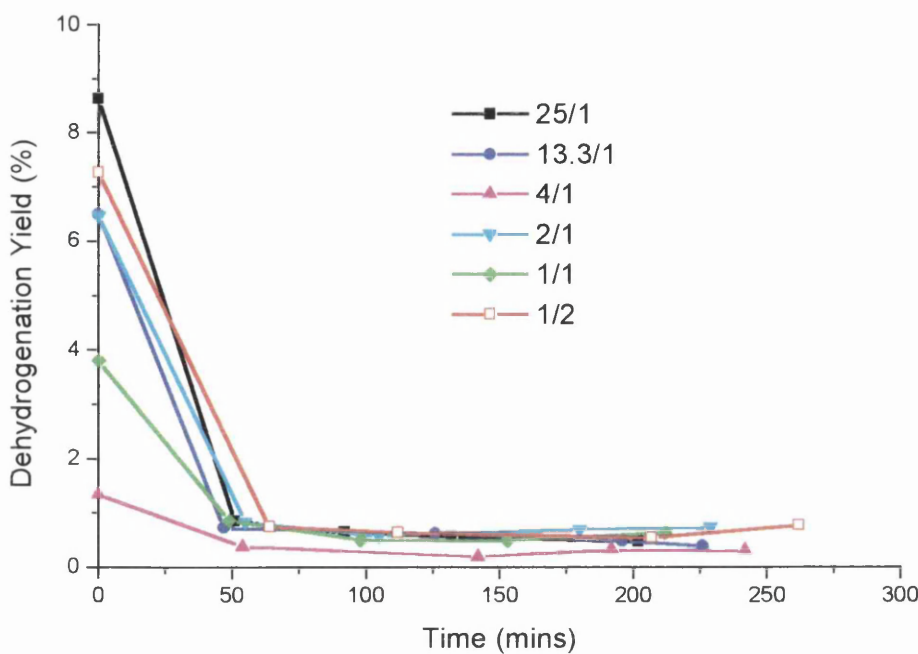


**Fig. 5.6.58** Dehydrogenation Yield as a function of Time during the Oxidative Dehydrogenation of Butane at various H<sub>c</sub>:O<sub>2</sub> Ratios using 0.65% Pt/Al<sub>2</sub>O<sub>3</sub>.

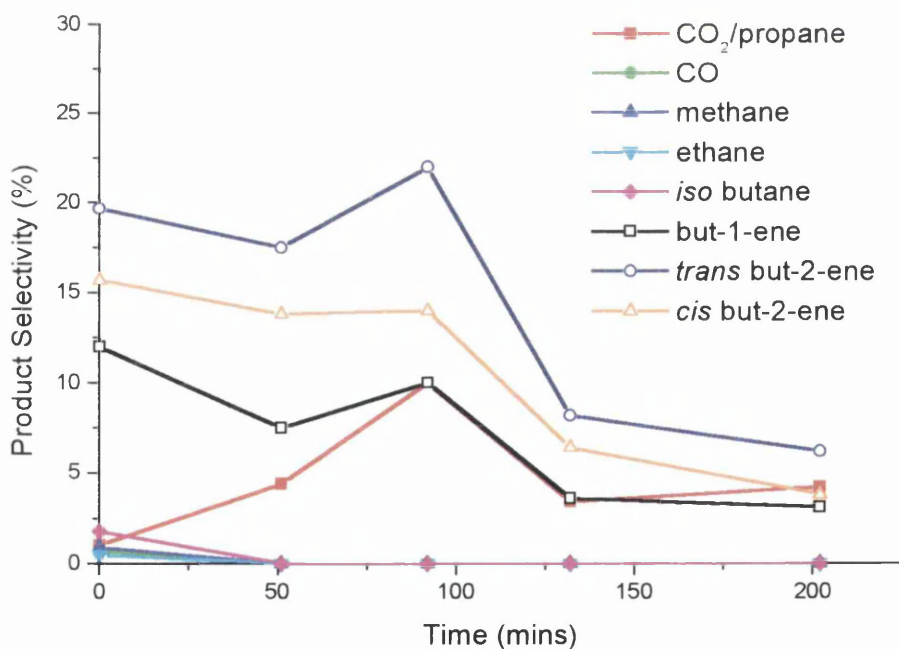


**Fig. 5.6.59** Product Selectivity as a function of Time during the Oxidative Dehydrogenation of Butane 0.65% Pt/Al<sub>2</sub>O<sub>3</sub> with H<sub>c</sub>:O<sub>2</sub> = 25:1.

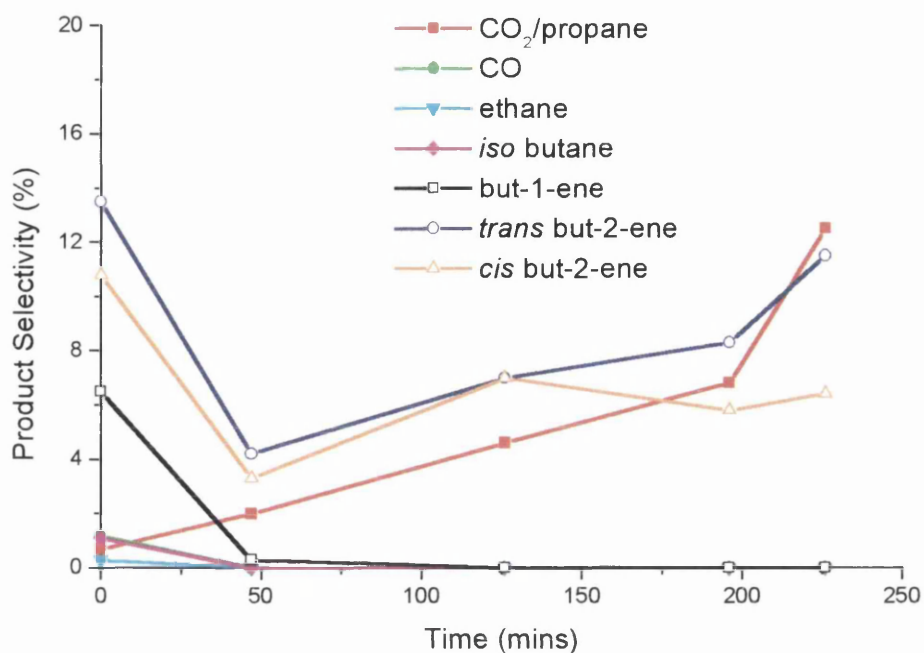


**Fig. 5.6.60** Product Selectivity as a function of Time during the Oxidative Dehydrogenation of Butane 0.65% Pt/Al<sub>2</sub>O<sub>3</sub> with H<sub>c</sub>:O<sub>2</sub> = 13.3:1.

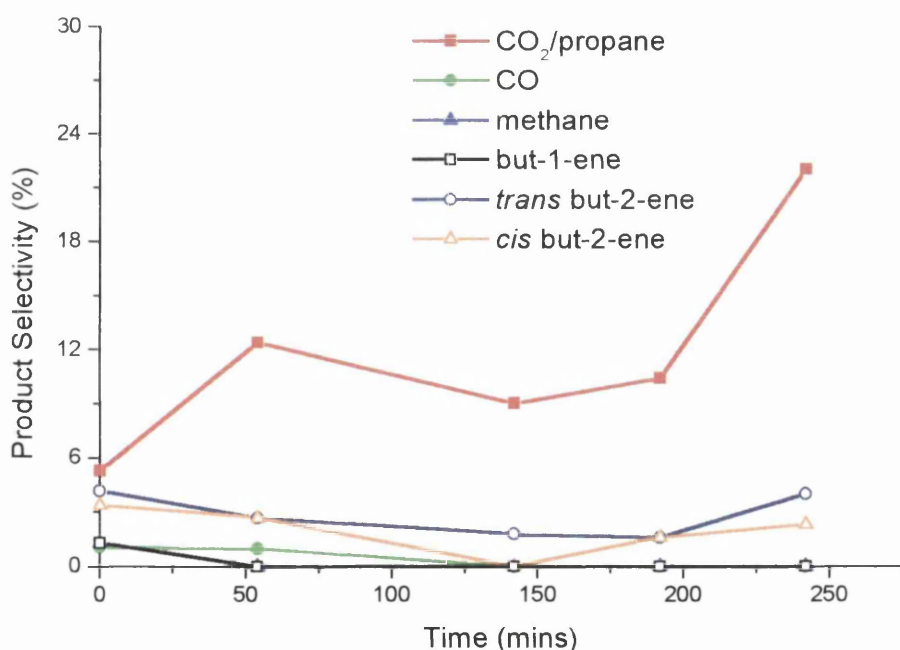


**Fig. 5.6.61** Product Selectivity as a function of Time during the Oxidative Dehydrogenation of Butane 0.65% Pt/Al<sub>2</sub>O<sub>3</sub> with H<sub>c</sub>:O<sub>2</sub> = 4:1.

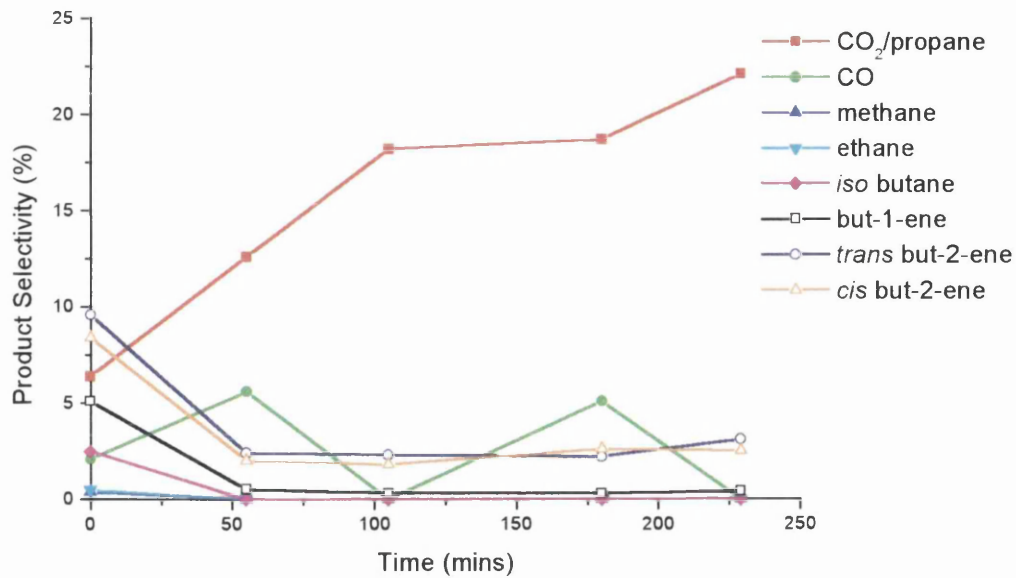


**Fig. 5.6.62** Product Selectivity as a function of Time during the Oxidative Dehydrogenation of Butane 0.65% Pt/Al<sub>2</sub>O<sub>3</sub> with H<sub>c</sub>:O<sub>2</sub> = 2:1.

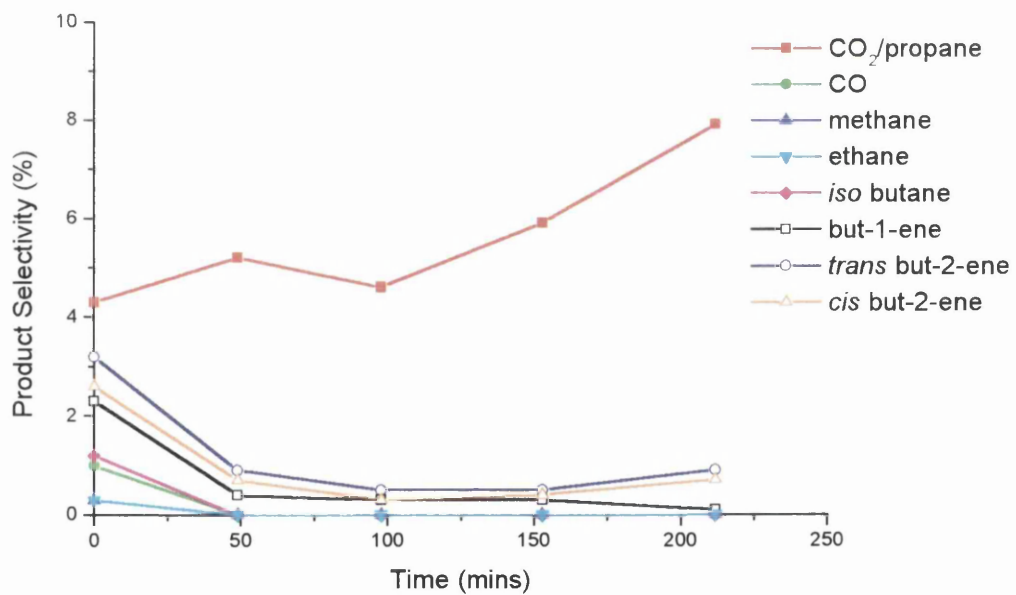


**Fig. 5.6.63** Product Selectivity as a function of Time during the Oxidative Dehydrogenation of Butane 0.65% Pt/Al<sub>2</sub>O<sub>3</sub> with H<sub>c</sub>:O<sub>2</sub> = 1:1.

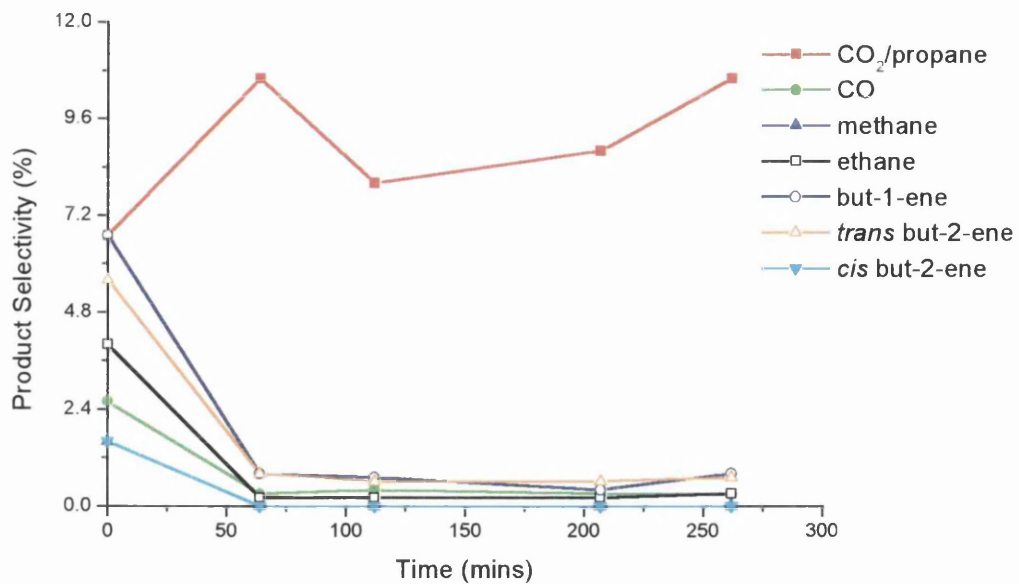


**Fig. 5.6.64** Product Selectivity as a function of Time during the Oxidative Dehydrogenation of Butane 0.65% Pt/ $\text{Al}_2\text{O}_3$  with  $\text{H}_2:\text{O}_2 = 1:2$ .

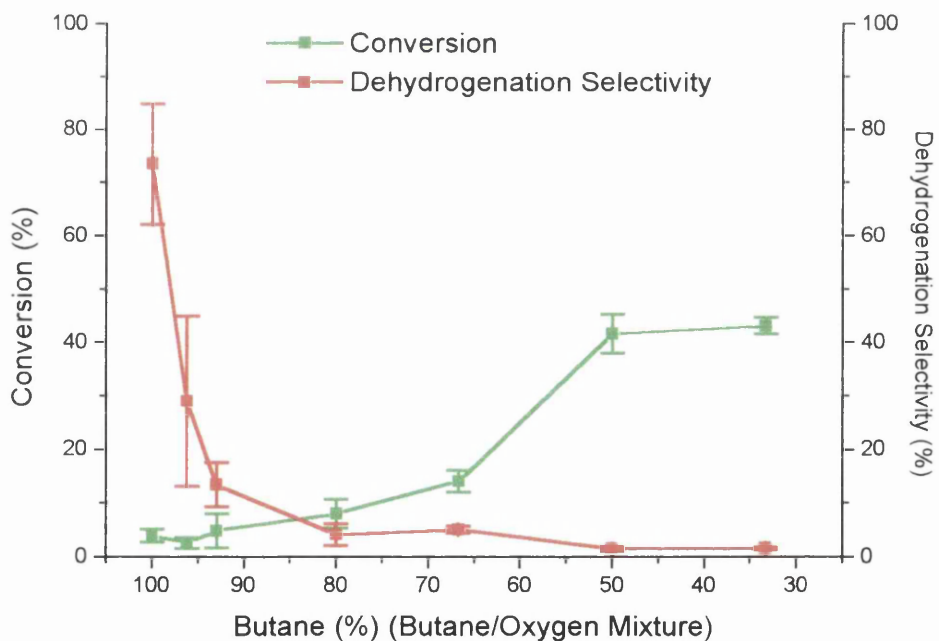


**Fig. 5.6.65** Conversion and Dehydrogenation Selectivity as a function of Hydrocarbon:Oxygen Ratio during the Oxidative Dehydrogenation of Butane using 0.65% Pt/ $\text{Al}_2\text{O}_3$  at 400°C.

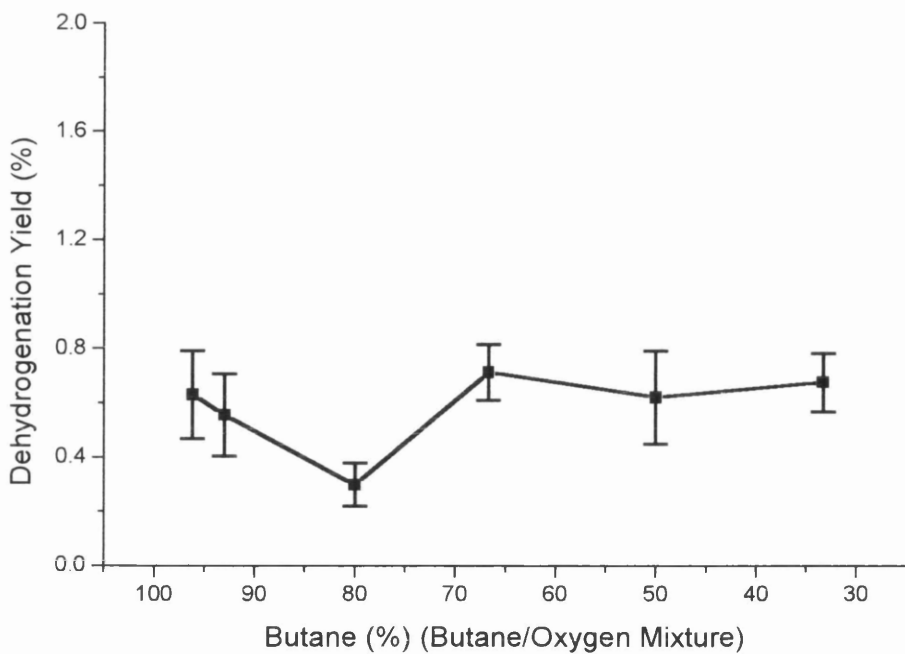


**Fig. 5.6.66** Dehydrogenation Yield as a function of Hydrocarbon:Oxygen Ratio during the Oxidative Dehydrogenation of Butane using 0.65% Pt/Al<sub>2</sub>O<sub>3</sub> at 400°C.

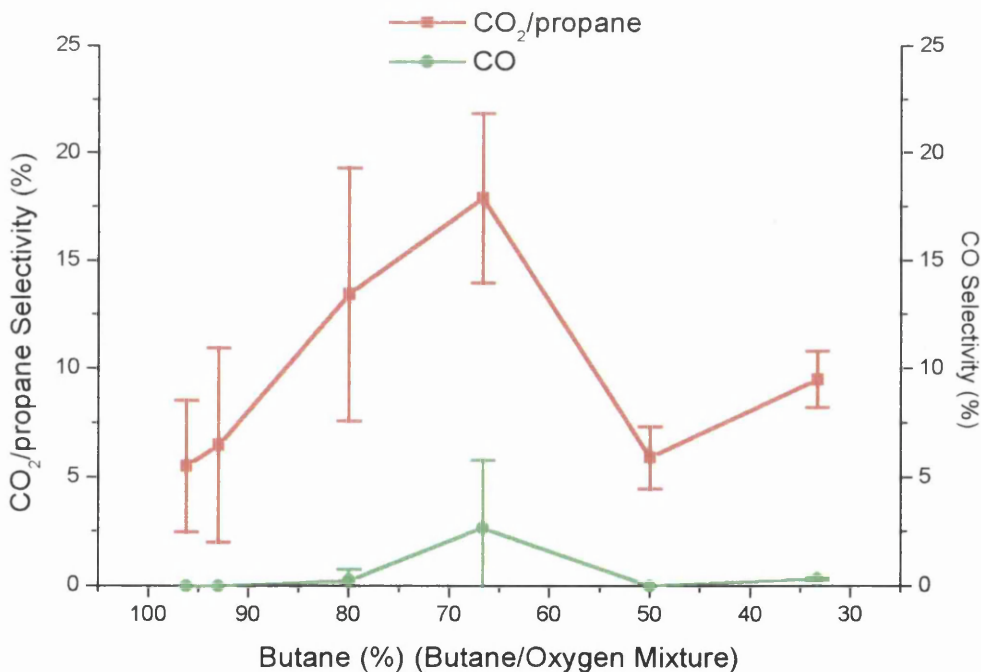


**Fig. 5.6.67** CO<sub>2</sub> and CO Product Selectivity during the Oxidative Dehydrogenation of Butane using 0.65% Pt/Al<sub>2</sub>O<sub>3</sub> at 400°C.

### **5.6.8 Summary of the Testing Reactions of the 0.65% Pt/Al<sub>2</sub>O<sub>3</sub> Catalyst under Continuous-flow conditions**

Comparison of figure 5.6.8 and 5.6.18 highlights the difference between the straight and oxidative dehydrogenation process towards the conversion of butane in an attempt to produce C<sub>4</sub> olefin species. In a similar way to the 0.5% Pt/Al<sub>2</sub>O<sub>3</sub>, the 0.65% catalyst is more active towards the oxidative dehydrogenation relative to the straight dehydrogenation, in terms of conversion, even down to temperatures as low as 200°C. This, as discussed previously, is due to the continuous regeneration of the metal surface by the oxygen in the feed-gas, resulting in the formation of CO<sub>2</sub>. In the absence of oxygen, previous work by Webb and Kennedy indicates that the metal surface has a substantial covering of a carbonaceous overlayer [86, 96]. It is also apparent that the homogeneous reactions start to become more influential at the lower temperatures in the case of oxidative dehydrogenation compared to those taking place during the straight dehydrogenation. This results from the activating power of the oxygen towards the alkane molecules by initiating radical type reactions [58]. Finally, it can also be observed that there is a slight increase in the conversion of butane in the case of the straight dehydrogenation using the 0.65% catalyst compared to that of the 0.5% catalyst at temperatures from 400-500°C from ~2% to ~7% (figures 5.5.9 and 5.6.8 respectively). This is attributed to the increased metal surface area of the 0.65% catalyst compared to the 0.5% substrate. The difference in the metal surface areas were highlighted in section 5.2.2.

The most dramatic difference between the two catalysts is observed on inspection of the selectivity towards dehydrogenation products. Figure 5.6.8 shows that selectivity of up to ~75% towards the dehydrogenation products is achieved at temperatures of 400-500°C in the case of straight dehydrogenation. On comparison with the empty vessel (figure 5.3.2) it can be concluded that this is an entirely catalytic effect. Chen *et al* only detected “trace” amounts of dehydrogenation products at 450°C [18].

The opposite effect is shown to be the case for the oxidative reaction process. It can be seen that dehydrogenation selectivity of up to 25-30% is obtained for the homogeneous reaction where no catalyst is present (figure 5.3.3) falling to ~5% on addition of the 0.65% Pt/Al<sub>2</sub>O<sub>3</sub> catalyst (figure 5.6.18). It is therefore apparent, as with

the previous catalyst, that when oxygen is used in the feed-gas, the surface is ‘cleaned’ of the carbonaceous residue necessary for the formation of dehydrogenated species, forming CO<sub>2</sub> in the process. This conditioning of the metal surface and subsequent increase in dehydrogenation selectivity is studied in more detail in the pulse-flow section below (section 5.7).

When the catalyst surface is ‘clean’ with respect to the carbonaceous species, such as in the oxidative case and initially in the straight dehydrogenation case, other processes take place. As with the previous catalyst, hydrogenolysis to form methane and ethane takes place while there is hydrogen available on the metal surface left behind from the reduction procedure [27], as well as isomerisation to form *iso*-butane. These processes also occur, to a greater extent, as homogeneous reactions when the temperature is high enough. Figures 5.6.4 - 5.6.7 illustrate these results for the catalytic straight dehydrogenation.

On comparison with the empty reactor (figure 5.3.2 in section 5.3.1), it is clear that the majority of these processes which occur can be attributed to homogeneous reactions which take place in the gas phase. It should, however, be pointed out that there is a small degree of hydrogenolysis and isomerisation taking place at 400-500°C which is catalytic and forms mainly methane and *iso*-butane respectively (figures 5.6.5 and 5.6.6). These observations could be as a result of the acidic nature of the alumina support, as discussed in section 5.4.1 [73].

Similar processes to those shown above also take place in the oxidative dehydrogenation as seen on the 0.5% catalyst. All the products formed from these reactions can be seen on figures 5.6.13 - 5.6.17. Again, CO<sub>2</sub> is the major product formed at temperatures up to 500°C as a result of combustion of the incident butane and decreases at 600°C as cracking and isomerisation reactions forming methane, ethane and *iso*-butane begin to take place (figure 5.6.17).

The deactivation of the catalyst can also be observed. Figure 5.6.1 shows clearly that when temperatures of 500 and 600°C are used the catalyst activity decreases markedly from its initial value. As discussed previously, this happens when the active metal surface is covered with carbonaceous material and the pores of the support material become blocked, resulting in the hindered access of the reactant material to the active catalyst [46, 47]. The deposition of carbonaceous material is discussed and quantified in more detail in the pulse-flow study.

A study of the influence of linear velocity on the catalyst performance was also carried out as before with the 0.5% catalyst. Figure 5.6.28 displays the changes in conversion and dehydrogenation selectivity respectively as a function of linear velocity. It is shown that by increasing the linear velocity from 30 to 130 ml min<sup>-1</sup> the conversion of butane decreases slightly. Thus, reduced contact time leads to a decrease in conversion. This effect was also observed by Jackson *et al* when modelling an isothermal propane dehydrogenation reactor under similar conditions [45]. However, increasing the flow-rate also resulted in a substantial loss in selectivity towards the dehydrogenation products. This is the opposite effect to that observed for the 0.5% catalyst (figure 5.5.29). This can be explained in terms of figure 1.2.3 which shows the mechanism of propane dehydrogenation. It is clear from this figure that adsorption is required to form the alkyl species, which then loses a hydrogen atom before desorption as the olefin. Extended contact times are therefore necessary for this process to occur and by decreasing the contact time the chance of adsorption and transformation to the olefin is also decreased. This example illustrates the difference in surface chemistry of the 0.5% catalyst compared to the 0.65% catalyst. The larger particles of the 0.5% catalyst promote the break-up of the butane species after adsorption and therefore reduced contact times are beneficial to the dehydrogenation selectivity. In contrast, it is clear that the 0.65% catalyst is very selective towards olefins, even when the bed length is extended (section 5.6.5) and therefore increased contact times are favoured.

The outcome of the linear velocity study for the oxidative dehydrogenation was the same as previously seen using the 0.5% catalyst. Figure 5.6.36 illustrates the effect of contact time on the conversion and dehydrogenation selectivity during the oxidative dehydrogenation of butane using the 0.65% Pt/Al<sub>2</sub>O<sub>3</sub>. A small decrease in the dehydrogenation selectivity is observed indicating that this process favours extended contact times, although the magnitude of this effect is significantly attenuated compared to conventional dehydrogenation (figure 5.6.28). CO<sub>2</sub> production also decreases with reduced contact time (figure 5.6.38) indicating, again, that decomposition processes leading to the formation of oligomer species are responsible for the increased conversion observed. As discussed previously these oligomers were detected visually on the outlet side of the reactor and were found to be high molecular weight species containing aromatic moieties. Oligomer formation has been reported in the literature for similar systems[1]. The TPO data below (figure 5.6.68) for the

oxidative system also highlight that large amounts of retained species can be removed from the catalyst, by oxygen, after it has been used for an oxidative reaction. It is therefore possible that these two observations stem from similar processes.

An additional study was also carried out on the 0.65% catalyst where the depth of the catalyst bed was increased to see what effect this had on conversion and selectivity. In these reactions the WHSV with respect to butane and the GHSV were varied while the total linear space velocity was unchanged (see chapter 4). Figure 5.6.45 illustrates the results obtained for the straight dehydrogenation in terms of conversion and dehydrogenation selectivity. It can be seen that by changing the above parameters the conversion has increased very slightly (5% to ~10%) while maintaining the high level of selectivity towards the olefin species (75 to 80%). Such insensitivity to catalyst mass could occur if the system were at equilibrium and included on figure 5.6.45 is the equilibrium conversion value. It is seen that the measured conversion approaches the equilibrium value over the mass range studied strongly suggesting the system is at equilibrium under these conditions.

Analogous studies were also performed under oxidative conditions. Figure 5.6.53 illustrates how the conversion and dehydrogenation selectivity were affected by adding oxygen into the feed-gas. Although the dehydrogenation selectivity remains effectively fixed as the catalyst bed increases, there is an initial rise then leveling off of the conversion. This is thought to arise from diffusion limitations where the gas stream is too dilute in hydrocarbon with respect to the increasing number of active sites that result on increasing the catalyst mass from 250-750mg.

During the course of this study it was the intention to investigate the oxidative dehydrogenation of butane as a low temperature alternative in the formation of butenes. Work carried out on supported metal catalysts in fluidised bed reactors by Schmidt [5, 62] as well as surface science studies [77, 78, 79] have shown that the amount of oxygen on the surface of the metal can have a crucial impact on the selectivity observed. On the basis of this work it was decided that reactions would be performed where the hydrocarbon:oxygen ratio was varied to see how this affected the activity of the catalyst.

Figure 5.6.65 summarises the results gathered from this work in terms of conversion and dehydrogenation selectivity. It is clear from the figure that the increased presence of oxygen is having a detrimental effect on the production of

butenes. At a hydrocarbon:oxygen ratio of 24:1 (hydrocarbon rich conditions) the selectivity towards the olefin products is relatively high (~28%). When oxygen is added into the reactant gas flow, at constant WHSV with respect to butane, the selectivity towards the butenes drops dramatically to ~5%. On the positive side it can be seen that the conversion of butane is enhanced as the oxygen content is increased. The dehydrogenation yield, composed of the conversion and dehydrogenation selectivity, is steady at approximately 0.7% (figure 5.6.66) which indicates that as the conversion increases the dehydrogenation selectivity decreases. As mentioned earlier the decrease in dehydrogenation selectivity is due to surface ‘cleaning’ of the residual carbonaceous deposits by the oxygen to form CO<sub>2</sub> leaving a carbon free metal surface active for hydrocarbon combustion. The increase in selectivity towards this product illustrates this process. Again oligomer formation is visually observed on the exhaust side of the reactor tube when oxygen is present in the feed-gas, consistent with the presence of the oxygen inducing radical type chemistry as described in section 5.3.2.

### **5.6.9 Post-reaction Analysis of the 0.65% Pt/Al<sub>2</sub>O<sub>3</sub> Catalyst after Continuous-flow Experiments**

The post-reaction analysis of the 0.65% Pt/Al<sub>2</sub>O<sub>3</sub> catalyst was carried out, in a similar way to before with the 0.5% catalyst, in an attempt to see if any changes were made to the size and composition of the catalyst after being subject to straight and oxidative dehydrogenation reactions under continuous-flow. Again, two measurements were carried out. TPO was carried out in order to observe any changes to the catalyst surface in terms of carbon deposition while TEM was conducted to see if there was any change to the particle size through sintering of the metal crystallites.

Figure 5.6.68 illustrates the outcome of the TPO experiments and section 4.3.6 describes the method used to carry out these experiments. Similarly to the 0.5% catalyst both spectra show the presence of a peak centered at approximately 395°C. As explained previously, data obtained from the literature suggest that this results from carbonaceous material deposited on the alumina support material [41]. It was also suggested that carbonaceous material associated with the metal would be found at a lower temperature. However, this is not observed in this set of spectra possibly because the surface area of the metal is very much smaller than that of the support

material, thus it is conceivable that the resultant peak would be small in comparison to that associated with the support material. The peak observed at approximately 475°C in the oxidative dehydrogenation is not observed in the literature, but could be attributed to the oxidation of the oligomer products observed during these reactions.

Again, problems with the electron microscope has resulted in uninformative micrographs. Figure 5.6.69 and 5.6.70, in the same way as before, shows no sign of any metal particles. Again, it was hoped that changes in the particle size could be observed, especially with the oxidative dehydrogenation, where the large amounts of water that form almost certainly result in sintering. Unfortunately the micrographs are not able to confirm or deny this assumption.

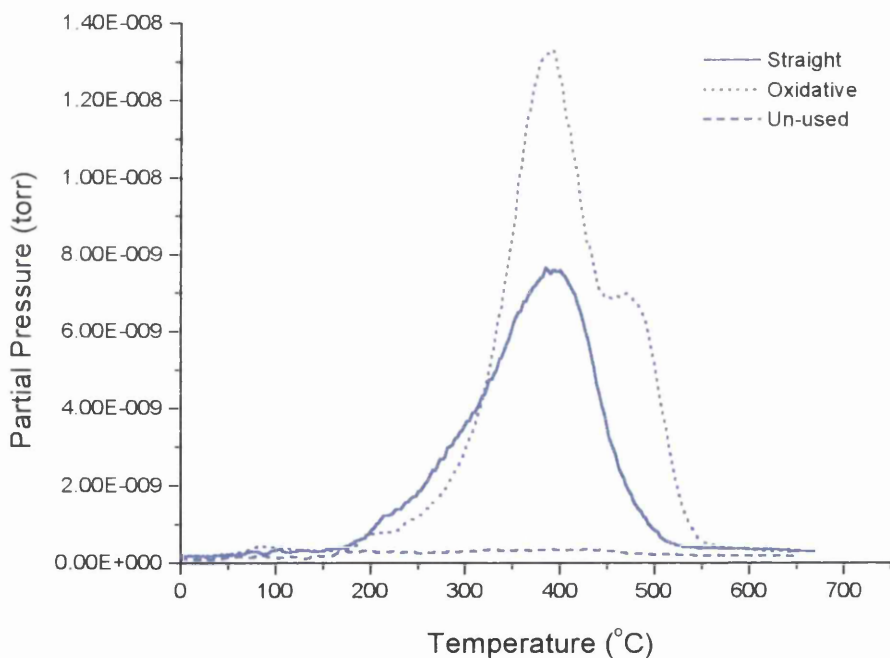


**Fig. 5.6.68** TPO of the 0.65% Pt/Al<sub>2</sub>O<sub>3</sub> Catalysts.

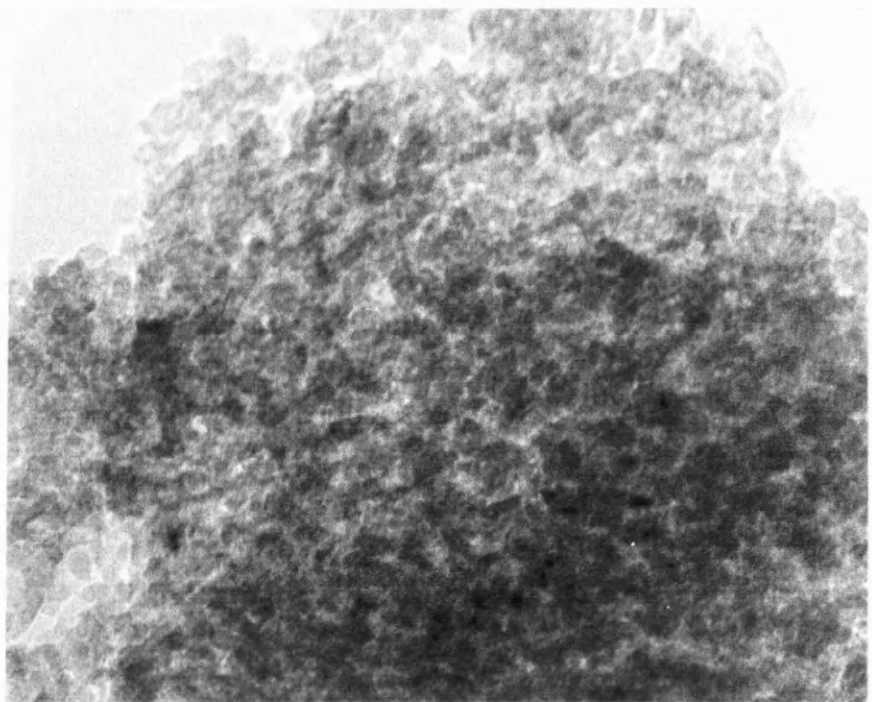


**Fig. 5.6.69** TEM Micrograph of the 0.65% Pt/Al<sub>2</sub>O<sub>3</sub> Catalyst after Straight Dehydrogenation.

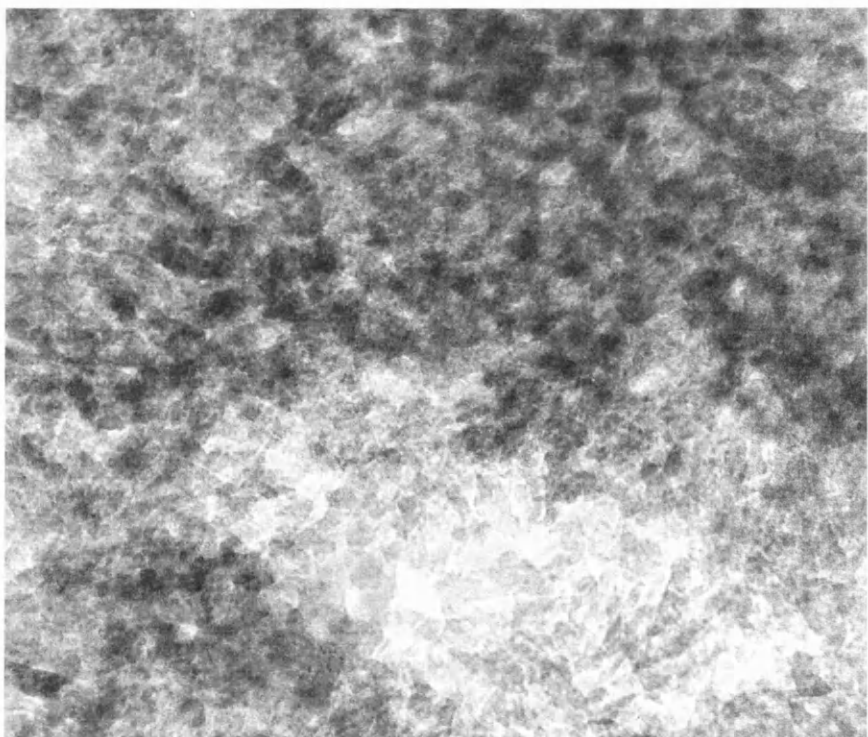


**Fig. 5.6.70** TEM Micrograph of the 0.65% Pt/Al<sub>2</sub>O<sub>3</sub> Catalyst after Oxidative Dehydrogenation.

## *5.7 The Straight and Oxidative Dehydrogenation of Butane using 0.65% Pt/Al<sub>2</sub>O<sub>3</sub>, under Pulse-flow Conditions*

The previous sections describe and explain the pattern of results obtained for the straight and oxidative dehydrogenation of butane under continuous-flow conditions using 0.5% and 0.65% Pt/Al<sub>2</sub>O<sub>3</sub> catalysts. These efforts were conducted in order to assess as closely as possible, given that the work was carried out within a university laboratory, how these processes would perform within an industrial plant. Continuous-flow enables steady state measurements to be made. However, it is during the early stages of the catalyst life while undergoing reaction that modifications to the catalytic surface are made as the process approaches steady state behavior. This was illustrated very clearly by Kennedy and Webb during a study of the hydrogenation of substituted acetylenes [86, 97, 98].

In order to gain access to the initial stages and gather evidence towards building up a clear picture of what changes take place to allow steady state to be reached, it is necessary to carry out pulse-flow measurements [86]. The controlled nature of pulse-flow methodology means that small specific amounts of the reactant gases can be passed through the catalyst bed. This allows the initial conditioning period, which occurs rapidly during continuous-flow and which determines the ultimate activity and selectivity of the catalyst, to be monitored in more detail. The advantage of this is that the exact number of reactant molecules having passed over the catalyst is known. Therefore, assuming that all the products can be accounted for, the retention of certain atoms to the catalyst surface can be calculated and correlated with the catalyst activity and selectivity. Kinetic studies can also be carried out using labeled compounds enabling mechanistic information to be gathered. Webb *et al* have used this type of reaction testing in many systems and it has provided important information towards the validation of the carbonaceous overlayer model.[27, 44] Figure 5.7.1 illustrates the areas under study when using these two different flow regimes.

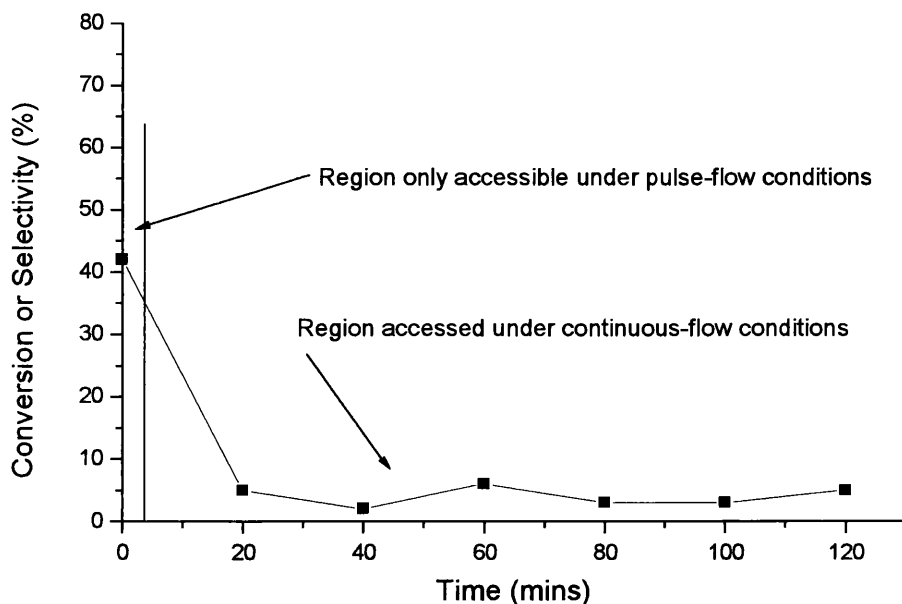


**Fig. 5.7.1** Diagram illustrating the Regions covered by Straight and Oxidative Dehydrogenation Techniques.

The following tables and figures display the results gained for the pulse-flow studies carried out on the 0.65% Pt/Al<sub>2</sub>O<sub>3</sub> at 400°C. This temperature was chosen as it represents the lowest temperature where the highest selectivity towards the olefin products was obtained. The 0.65wt% catalyst was selected as this gave favourable straight dehydrogenation results (section 5.6.1). For each reaction, tables containing the conversion and molar quantities of each product formed are presented, as well as product selectivities and yields. The carbon, hydrogen and oxygen mass balance data are also tabulated. The figures illustrate diagrammatically conversion, selectivity, dehydrogenation yield and the amount of carbon retained on the catalyst or lost to the system. Additionally, for the sequential experiments, the amount of CO<sub>2</sub> detected from each oxygen pulse is also plotted. Hydrogen and oxygen mass balances are potentially unreliable in the case of oxidative dehydrogenation because of water formation that cannot be quantified in the apparatus used. However, it is included for completeness and is useful for considering trends within a given experimental sequence.

Section 4.2 describes the procedures used for making up the reaction mixtures and methods and parameters used to carry out the experiments. In terms of the sequential experiments, pulses of oxygen and *n*-butane were passed over the catalyst

separately. The first pulse was oxygen, the second pulse *n*-butane the third oxygen. This cycle was continued until the end of the experiment and the products were analysed after each pulse.

**Table 5.7.1** Conversion and Product Molar Quantities for the Straight Dehydrogenation of Butane under Pulse-flow conditions using Un-reduced 0.65% Pt/Al<sub>2</sub>O<sub>3</sub>.

Temp. (°C)	Pulse No.	Moles Bypass (x10 <sup>-7</sup> )	Moles Reacted (x10 <sup>-7</sup> )	Conv. (%)	CO <sub>2</sub> /Pr (x10 <sup>-7</sup> )	CO (x10 <sup>-7</sup> )	Met. (x10 <sup>-7</sup> )	Eth. (x10 <sup>-7</sup> )	Iso (x10 <sup>-7</sup> )	B-1 (x10 <sup>-7</sup> )	Trans B-2 (x10 <sup>-7</sup> )	Cis B-2 (x10 <sup>-7</sup> )	Diene (x10 <sup>-7</sup> )
400	1	103.2	103.2	100.0	58.42	33.44	216.4	13.00	0	0	0	0	0
400	2	103.2	97.52	94.5	17.69	31.36	185.4	15.78	0	0.721	0.467	0.489	0
400	3	103.2	74.80	72.5	17.31	21.90	84.30	17.71	4.262	3.264	2.355	1.827	0
400	4	103.2	54.88	53.2	10.73	14.51	40.37	9.535	4.354	5.476	3.939	3.348	0
400	5	103.2	44.31	42.9	6.914	1.728	25.90	6.488	3.884	6.500	4.543	3.909	0
400	6	103.2	37.95	36.8	4.980	1.392	18.05	4.205	3.458	6.899	4.620	3.856	0

**Table 5.7.2** Product Selectivity for the Straight Dehydrogenation of Butane under Pulse-flow conditions using Un-reduced 0.65% Pt/Al<sub>2</sub>O<sub>3</sub>.

Temp. (°C)	Pulse No.	CO <sub>2</sub> /Pr Sel. (%)	CO Sel. (%)	Met. Sel. (%)	Eth. Sel. (%)	Iso Sel. (%)	B-1 Sel. (%)	Trans B-2 Sel. (%)	Cis B-2 Sel. (%)	Diene Sel. (%)	Dehydro. Sel. (%)
400	1	14.2	8.1	52.4	6.3	0	0	0	0	0	0
400	2	4.5	8.0	47.5	8.1	0	0.7	0.5	0.5	0	1.7
400	3	5.8	7.3	28.2	11.8	5.7	4.4	3.1	2.4	0	9.9
400	4	4.9	6.6	18.4	8.7	7.9	10.0	7.2	6.1	0	23.3
400	5	3.9	1.0	14.6	7.3	8.8	14.7	10.2	8.8	0	33.7
400	6	3.3	0.9	11.9	5.5	9.1	18.2	12.2	10.2	0	40.6

**Table 5.7.3** Product Yields for the Straight Dehydrogenation of Butane under Pulse-flow conditions using Un-reduced 0.65% Pt/Al<sub>2</sub>O<sub>3</sub>.

Temp. (°C)	Pulse No.	CO <sub>2</sub> /Pr Yield (%)	CO Yield (%)	Met. Yield (%)	Eth. Yield (%)	Iso Yield (%)	B-1 Yield (%)	Trans B-2 Yield (%)	Cis B-2 Yield (%)	Diene Yield (%)	Dehydro. Yield (%)
400	1	14.2	8.1	52.4	6.3	0	0	0	0	0	0
400	2	4.2	7.6	44.9	7.6	0	0.7	0.5	0.5	0	1.6
400	3	4.2	5.3	20.4	8.6	4.1	2.2	2.2	1.7	0	7.2
400	4	2.6	3.5	9.8	4.6	4.2	5.3	3.8	3.2	0	12.4
400	5	1.7	0.4	6.3	3.1	3.8	6.3	4.4	3.8	0	14.4
400	6	1.2	0.3	4.4	2.0	3.3	6.7	4.5	3.8	0	14.9

**Table 5.7.4** Mass Balance Data for the Straight Dehydrogenation of Butane under Pulse-flow conditions using Un-reduced 0.65% Pt/Al<sub>2</sub>O<sub>3</sub>.

Temp. (°C)	Pulse No.	C in (x10 <sup>19</sup> )	C out (x10 <sup>19</sup> )	C diff (x10 <sup>19</sup> )	O in	O out (x10 <sup>17</sup> )	O diff (x10 <sup>17</sup> )	H in (x10 <sup>19</sup> )	H out (x10 <sup>19</sup> )	H diff (x10 <sup>19</sup> )
400	1	2.486	2.013	0.473	0	90.50	-90.50	6.215	5.682	0.533
400	2	2.486	1.779	0.707	0	40.19	-40.19	6.215	5.459	0.756
400	3	2.486	1.923	0.563	0	34.04	-34.04	6.215	4.996	1.219
400	4	2.486	2.086	0.400	0	21.66	-21.66	6.215	5.264	0.951
400	5	2.486	2.158	0.328	0	9.368	-9.368	6.215	5.359	0.856
400	6	2.486	2.223	0.263	0	6.836	-6.836	6.215	5.465	0.750

**Table 5.7.5** Conversion and Product Molar Quantities for the Straight Dehydrogenation of Butane under Pulse-flow conditions using 0.65% Pt/Al<sub>2</sub>O<sub>3</sub>.

Temp. (°C)	Pulse No.	Moles Bypass (x10 <sup>-7</sup> )	Moles Reacted (x10 <sup>-7</sup> )	Conv. (%)	CO <sub>2</sub> /Pr (x10 <sup>-7</sup> )	CO (x10 <sup>-7</sup> )	Met. (x10 <sup>-7</sup> )	Eth. (x10 <sup>-7</sup> )	Iso (x10 <sup>-7</sup> )	B-1 (x10 <sup>-7</sup> )	Trans B-2 (x10 <sup>-7</sup> )	Cis B-2 (x10 <sup>-7</sup> )	Diene (x10 <sup>-7</sup> )
400	1	104.6	104.6	100	15.55	12.59	168.7	23.88	0	0	0	0	0
400	2	104.6	92.99	88.9	24.43	5.934	76.28	25.15	3.884	1.454	1.117	0.836	0
400	3	104.6	65.82	62.9	16.84	2.877	29.21	12.82	5.027	5.072	4.910	3.704	0
400	4	104.6	56.10	53.6	11.65	1.009	17.90	8.701	4.473	6.659	6.486	4.961	0
400	5	104.6	49.97	47.8	8.461	1.579	13.86	6.855	4.097	7.190	6.937	5.270	0
400	6	104.6	47.16	45.1	6.654	2.152	11.36	5.088	3.830	7.423	7.027	5.588	0
400	7	104.6	43.37	41.5	5.511	1.032	8.972	4.334	3.639	7.729	7.240	5.924	0

**Table 5.7.6** Product Selectivity for the Straight Dehydrogenation of Butane under Pulse-flow conditions using 0.65% Pt/Al<sub>2</sub>O<sub>3</sub>.

Temp. (°C)	Pulse No.	CO <sub>2</sub> /Pr Sel. (%)	CO Sel. (%)	Met. Sel. (%)	Eth. Sel. (%)	Iso Sel. (%)	B-1 Sel. (%)	Trans B-2 Sel. (%)	Cis B-2 Sel. (%)	Diene Sel. (%)	Dehydro. Sel. (%)
400	1	11.1	3.0	40.3	11.4	0	0	0	0	0	0
400	2	19.7	1.6	20.5	13.5	4.2	1.6	1.2	0.9	0	3.7
400	3	19.2	1.1	11.1	9.7	7.6	7.7	7.4	5.6	0	20.7
400	4	15.6	0.4	8.0	7.8	8.0	11.9	11.6	8.8	0	32.3
400	5	12.7	0.8	6.9	6.8	8.2	14.4	13.9	6.5	0	38.8
400	6	10.6	1.1	6.0	5.4	8.1	15.7	14.9	11.8	0	42.4
400	7	9.5	0.6	5.2	5.0	8.4	17.8	16.7	13.6	0	48.1

**Table 5.7.7** Product Yields for the Straight Dehydrogenation of Butane under Pulse-flow conditions using 0.65% Pt/Al<sub>2</sub>O<sub>3</sub>.

Temp. (°C)	Pulse No.	CO <sub>2</sub> /Pr Yield (%)	CO Yield (%)	Met. Yield (%)	Eth. Yield (%)	Iso Yield (%)	B-1 Yield (%)	Trans B-2 Yield (%)	Cis B-2 Yield (%)	Diene Yield (%)	Dehydro. Yield (%)
400	1	11.1	3.0	40.3	11.4	0	0	0	0	0	0
400	2	17.5	1.4	18.2	12.0	3.7	1.4	1.1	0.8	0	3.3
400	3	12.1	0.7	7.0	6.1	4.8	4.8	4.6	3.5	0	13.0
400	4	8.4	0.2	4.3	4.2	4.3	6.4	6.2	4.7	0	17.3
400	5	6.1	0.4	3.3	3.2	3.9	6.9	6.6	3.1	0	18.5
400	6	4.8	0.5	2.7	2.4	3.6	7.1	6.7	5.3	0	19.1
400	7	3.9	0.2	2.2	2.1	3.5	7.4	6.9	5.6	0	20.0

**Table 5.7.8** Mass Balance Data for the Straight Dehydrogenation of Butane under Pulse-flow conditions using 0.65% Pt/Al<sub>2</sub>O<sub>3</sub>.

Temp. (°C)	Pulse No.	C in (x10 <sup>19</sup> )	C out (x10 <sup>19</sup> )	C diff (x10 <sup>19</sup> )	O in	O out (x10 <sup>17</sup> )	O diff (x10 <sup>17</sup> )	H in (x10 <sup>19</sup> )	H out (x10 <sup>19</sup> )	H diff (x10 <sup>19</sup> )
400	1	2.520	1.660	0.880	0	7.582	-7.582	6.299	5.676	0.623
400	2	2.520	1.695	0.825	0	3.573	-3.573	6.299	4.414	1.885
400	3	2.520	2.037	0.483	0	1.732	-1.732	6.299	5.276	1.023
400	4	2.520	2.143	0.327	0	0.608	-0.608	6.299	5.373	0.926
400	5	2.520	2.210	0.310	0	0.951	-0.951	6.299	5.460	0.839
400	6	2.520	2.221	0.299	0	1.296	-1.296	6.299	5.433	0.866
400	7	2.520	2.278	0.242	0	0.622	-0.622	6.299	5.551	0.748

**Table 5.7.9** Conversion and Product Molar Quantities for the Oxidative Dehydrogenation of Butane under Pulse-flow conditions using 0.65% Pt/Al<sub>2</sub>O<sub>3</sub> (Co-Adsorption 2:1).

Temp. (°C)	Pulse No.	Moles Bypass (x10 <sup>-7</sup> )	Moles Reacted (x10 <sup>-7</sup> )	Conv. (%)	CO <sub>2</sub> /Pr (x10 <sup>-7</sup> )	CO (x10 <sup>-7</sup> )	Met. (x10 <sup>-7</sup> )	Eth. (x10 <sup>-7</sup> )	Iso (x10 <sup>-7</sup> )	B-1 (x10 <sup>-7</sup> )	Trans B-2 (x10 <sup>-7</sup> )	Cis B-2 (x10 <sup>-7</sup> )	Diene (x10 <sup>-7</sup> )
400	1	96.92	96.92	100	44.59	42.55	141.2	23.93	0	0	0	0	0
400	2	96.92	88.73	91.5	48.59	48.90	84.37	22.21	0.341	1.117	0.834	0.639	0
400	3	96.92	66.41	68.5	42.40	46.51	38.40	12.26	5.119	3.678	3.441	2.852	0
400	4	96.92	53.35	55.0	38.80	43.36	22.38	8.034	4.978	4.519	4.317	3.457	0
400	5	96.92	47.15	48.6	37.02	42.19	17.96	6.187	4.589	4.735	4.471	3.646	0
400	6	96.92	41.09	42.4	34.52	32.31	13.36	5.522	4.571	4.677	4.486	3.710	0

**Table 5.7.10** Product Selectivity for the Oxidative Dehydrogenation of Butane under Pulse-flow conditions using 0.65% Pt/Al<sub>2</sub>O<sub>3</sub> (Co-Adsorption 2:1).

Temp. (°C)	Pulse No.	CO <sub>2</sub> /Pr Sel. (%)	CO Sel. (%)	Met. Sel. (%)	Eth. Sel. (%)	Iso Sel. (%)	B-1 Sel. (%)	Trans B-2 Sel. (%)	Cis B-2 Sel. (%)	Diene Sel. (%)	Dehydro. Sel. (%)
400	1	11.5	11.0	36.4	12.3	0	0	0	0	0	0
400	2	13.7	13.8	23.8	12.5	0.4	1.2	0.9	0.7	0	2.8
400	3	16.0	17.5	14.4	9.2	7.7	5.5	5.2	4.3	0	15.0
400	4	18.2	20.3	10.5	7.5	9.3	8.5	8.1	6.5	0	23.1
400	5	19.6	22.4	9.5	6.6	9.7	10.0	9.5	7.7	0	27.2
400	6	21.0	19.6	8.1	6.7	11.1	11.4	10.9	9.0	0	31.3

**Table 5.7.11** Product Yields for the Oxidative Dehydrogenation of Butane under Pulse-flow conditions using 0.65% Pt/Al<sub>2</sub>O<sub>3</sub> (Co-Adsorption 2:1).

Temp. (°C)	Pulse No.	CO <sub>2</sub> /Pr Yield (%)	CO Yield (%)	Met. Yield (%)	Eth. Yield (%)	Iso Yield (%)	B-1 Yield (%)	Trans B-2 Yield (%)	Cis B-2 Yield (%)	Diene Yield (%)	Dehydro. Yield (%)
400	1	11.5	11.0	36.4	12.3	0	0	0	0	0	0
400	2	12.5	12.6	21.8	11.4	0.4	1.1	0.8	0.6	0	2.6
400	3	11.0	12.0	9.9	6.3	5.3	3.8	3.6	2.9	0	10.3
400	4	10.0	11.2	5.8	4.1	5.1	4.7	4.4	3.6	0	12.7
400	5	9.5	10.9	4.6	3.2	4.7	4.9	4.6	3.7	0	13.2
400	6	8.9	8.3	3.4	2.8	4.7	4.8	4.6	3.8	0	13.3

**Table 5.7.12** Mass Balance Data for the Oxidative Dehydrogenation of Butane under Pulse-flow conditions using 0.65% Pt/Al<sub>2</sub>O<sub>3</sub> (Co-Adsorption 2:1).

Temp. (°C)	Pulse No.	C in (x10 <sup>19</sup> )	C out (x10 <sup>19</sup> )	C diff (x10 <sup>19</sup> )	O in (x10 <sup>17</sup> )	O out (x10 <sup>17</sup> )	O diff (x10 <sup>17</sup> )	H in (x10 <sup>19</sup> )	H out (x10 <sup>19</sup> )	H diff (x10 <sup>19</sup> )
400	1	2.335	1.663	0.672	59.64	79.33	-19.69	5.836	4.266	1.570
400	2	2.335	1.630	0.705	59.64	87.97	-28.33	5.836	3.473	2.363
400	3	2.335	2.013	0.322	59.64	79.07	-19.43	5.836	3.994	1.842
400	4	2.335	2.192	0.143	59.64	72.84	-13.20	5.836	4.345	1.491
400	5	2.335	2.279	0.056	59.64	69.99	-10.35	5.836	4.549	1.287
400	6	2.335	2.314	0.021	59.64	61.03	-1.39	5.836	4.779	1.057

**Table 5.7.13** Conversion and Product Molar Quantities for the Oxidative Dehydrogenation of Butane under Pulse-flow conditions using 0.65% Pt/Al<sub>2</sub>O<sub>3</sub> (Co-Adsorption 19.4:1).

Temp. (°C)	Pulse No.	Moles Bypass (x10 <sup>-7</sup> )	Moles Reacted (x10 <sup>-7</sup> )	Conv. (%)	CO <sub>2</sub> /Pr (x10 <sup>-7</sup> )	CO (x10 <sup>-7</sup> )	Met. (x10 <sup>-7</sup> )	Eth. (x10 <sup>-7</sup> )	Iso (x10 <sup>-7</sup> )	B-1 (x10 <sup>-7</sup> )	Trans B-2 (x10 <sup>-7</sup> )	Cis B-2 (x10 <sup>-7</sup> )	Diene (x10 <sup>-7</sup> )
400	1	93.54	93.54	100.0	17.41	34.79	195.9	13.73	0	0	0	0	0
400	2	93.54	82.34	88.1	18.95	13.94	90.34	22.67	3.119	1.681	1.215	0.9236	0
400	3	93.54	58.20	62.3	16.81	15.48	35.95	12.88	4.951	5.243	4.306	3.481	0
400	4	93.54	46.76	50.0	10.90	7.105	20.73	8.824	4.553	6.525	5.511	4.403	0
400	5	93.54	40.55	43.4	9.193	12.48	16.14	6.568	4.179	7.027	6.025	4.805	0.4318
400	6	93.54	36.66	39.2	7.525	7.766	11.88	5.465	3.840	6.945	5.875	4.736	0.5571

**Table 5.7.14** Product Selectivity for the Oxidative Dehydrogenation of Butane under Pulse-flow conditions using 0.65% Pt/Al<sub>2</sub>O<sub>3</sub> (Co-Adsorption 19.4:1).

Temp. (°C)	Pulse No.	CO <sub>2</sub> /Pr Sel. (%)	CO Sel. (%)	Met. Sel. (%)	Eth. Sel. (%)	Iso Sel. (%)	B-1 Sel. (%)	Trans B-2 Sel. (%)	Cis B-2 Sel. (%)	Diene Sel. (%)	Dehydro. Sel. (%)
400	1	4.6	9.3	52.4	7.3	0	0	0	0	0	0
400	2	5.8	4.2	27.4	13.8	3.8	2.0	1.5	1.1	0	4.6
400	3	7.2	6.6	15.4	11.1	8.5	9.0	7.4	6.0	0	22.4
400	4	5.8	3.8	11.1	9.4	9.7	14.0	11.8	9.4	0	35.2
400	5	5.7	7.7	10.0	8.1	10.3	17.3	14.8	11.8	1.1	45.0
400	6	5.1	5.3	8.1	7.4	10.5	18.9	16.0	12.9	1.5	49.3

**Table 5.7.15** Product Yields for the Oxidative Dehydrogenation of Butane under Pulse-flow conditions using 0.65% Pt/Al<sub>2</sub>O<sub>3</sub> (Co-Adsorption 19.4:1).

Temp. (°C)	Pulse No.	CO <sub>2</sub> /Pr Yield (%)	CO Yield (%)	Met. Yield (%)	Eth. Yield (%)	Iso Yield (%)	B-1 Yield (%)	Trans B-2 Yield (%)	Cis B-2 Yield (%)	Diene Yield (%)	Dehydro. Yield (%)
400	1	4.6	9.3	52.4	7.3	0	0	0	0	0	0
400	2	5.1	3.7	24.1	12.2	3.3	1.8	1.3	1.0	0	4.0
400	3	4.5	4.1	9.6	6.9	5.3	5.6	4.6	3.7	0	14.0
400	4	2.9	1.9	5.6	4.7	4.8	7.0	5.9	4.7	0	17.6
400	5	2.5	3.3	4.3	3.5	4.5	7.5	6.4	5.1	0.5	19.5
400	6	2.0	2.1	3.2	2.9	4.1	7.4	6.3	5.0	0.6	19.3

**Table 5.7.16** Mass Balance Data for the Oxidative Dehydrogenation of Butane under Pulse-flow conditions using 0.65% Pt/Al<sub>2</sub>O<sub>3</sub> (Co-Adsorption 19.4:1).

Temp. (°C)	Pulse No.	C in (x10 <sup>19</sup> )	C out (x10 <sup>19</sup> )	C diff (x10 <sup>19</sup> )	O in (x10 <sup>17</sup> )	O out (x10 <sup>17</sup> )	O diff (x10 <sup>17</sup> )	H in (x10 <sup>19</sup> )	H out (x10 <sup>19</sup> )	H diff (x10 <sup>19</sup> )
400	1	2.253	1.659	0.594	5.810	41.92	-36.11	5.633	5.215	0.418
400	2	2.253	1.450	0.803	5.810	31.22	-25.41	5.633	4.036	1.597
400	3	2.253	1.848	0.405	5.810	29.57	-23.76	5.633	4.380	1.253
400	4	2.253	1.837	0.416	5.810	17.41	-11.60	5.633	4.696	0.937
400	5	2.253	2.122	0.131	5.810	18.59	-12.78	5.633	4.939	0.694
400	6	2.253	2.126	0.127	5.810	13.74	-7.930	5.633	5.001	0.632

**Table 5.7.17** Conversion and Product Molar Quantities for the Oxidative Dehydrogenation of Butane under Pulse-flow conditions using 0.65% Pt/Al<sub>2</sub>O<sub>3</sub> (Sequential Dosing 2:1).

Temp. (°C)	Pulse No.	Moles Bypass (x10 <sup>-7</sup> )	Moles Reacted (x10 <sup>-7</sup> )	Conv. (%)	CO <sub>2</sub> /Pr (x10 <sup>-7</sup> )	CO (x10 <sup>-7</sup> )	Met. (x10 <sup>-7</sup> )	Eth. (x10 <sup>-7</sup> )	Iso (x10 <sup>-7</sup> )	B-1 (x10 <sup>-7</sup> )	Trans B-2 (x10 <sup>-7</sup> )	Cis B-2 (x10 <sup>-7</sup> )	Diene (x10 <sup>-7</sup> )
400	1	104.6	104.3	99.7	30.70	30.04	175.3	18.83	0	0	0	0	0
400	2	104.6	99.72	95.3	18.24	15.99	133.9	21.52	2.014	0.760	0.410	0.322	0
400	3	104.6	78.08	74.6	19.04	14.11	131.5	18.34	3.191	1.002	0.900	0.701	0
400	4	104.6	78.45	75.0	19.41	12.96	64.69	16.24	5.090	3.688	2.441	2.019	0
400	5	104.6	71.82	68.7	17.24	5.106	52.68	14.47	5.050	4.360	2.971	2.467	0
400	6	104.6	51.78	49.5	8.803	5.229	12.21	6.813	4.271	6.542	4.758	3.934	0

**Table 5.7.18** Product Selectivity for the Oxidative Dehydrogenation of Butane under Pulse-flow conditions using 0.65% Pt/Al<sub>2</sub>O<sub>3</sub> (Sequential Dosing 2:1).

Temp. (°C)	Pulse No.	CO <sub>2</sub> /Pr Sel. (%)	CO Sel. (%)	Met. Sel. (%)	Eth. Sel. (%)	Iso Sel. (%)	B-1 Sel. (%)	Trans B-2 Sel. (%)	Cis B-2 Sel. (%)	Diene Sel. (%)	Dehydro. Sel. (%)
400	1	22.1	7.2	42.0	9.0	0	0	0	0	0	0
400	2	13.7	4.0	33.6	10.8	2.0	0.8	0.4	0.3	0	1.5
400	3	18.3	4.5	42.1	11.7	4.1	1.3	1.2	0.9	0	3.4
400	4	18.6	4.1	20.6	10.4	6.5	4.7	3.1	2.6	0	10.4
400	5	18.0	1.8	18.3	10.1	7.0	6.1	4.1	3.4	0	13.6
400	6	12.8	2.5	5.9	5.6	8.2	12.6	9.2	7.6	0	29.2

**Table 5.7.19** Product Yields for the Oxidative Dehydrogenation of Butane under Pulse-flow conditions using 0.65% Pt/Al<sub>2</sub>O<sub>3</sub> (Sequential Dosing 2:1).

Temp. (°C)	Pulse No.	CO <sub>2</sub> /Pr Yield (%)	CO Yield (%)	Met. Yield (%)	Eth. Yield (%)	Iso Yield (%)	B-1 Yield (%)	Trans B-2 Yield (%)	Cis B-2 Yield (%)	Diene Yield (%)	Dehydro. Yield (%)
400	1	22.0	7.2	41.9	9.0	0	0	0	0	0	0
400	2	13.0	3.8	32.0	10.3	1.9	0.8	0.4	0.3	0	1.4
400	3	13.6	3.4	31.4	8.7	3.0	1.0	0.9	0.7	0	2.5
400	4	14.0	3.1	15.4	7.8	4.9	3.5	2.3	2.0	0	7.8
400	5	12.4	1.2	12.6	6.9	4.8	4.2	2.8	2.3	0	9.3
400	6	6.3	1.2	2.9	2.8	4.0	6.2	4.6	3.8	0	14.4

**Table 5.7.20** Mass Balance Data for the Oxidative Dehydrogenation of Butane under Pulse-flow conditions using 0.65% Pt/Al<sub>2</sub>O<sub>3</sub> (Sequential Dosing 2:1).

Temp. (°C)	Pulse No.	C in (x10 <sup>19</sup> )	C out (x10 <sup>19</sup> )	C diff (x10 <sup>19</sup> )	O in (x10 <sup>17</sup> )	O out (x10 <sup>17</sup> )	O diff (x10 <sup>17</sup> )	H in (x10 <sup>19</sup> )	H out (x10 <sup>19</sup> )	H diff (x10 <sup>19</sup> )
400	1	2.520	2.217	0.303	74.25	68.09	6.160	6.299	6.398	-0.099
400	2	2.520	1.899	0.621	74.25	48.18	26.07	6.299	5.368	0.931
400	3	2.520	2.483	0.037	74.25	47.90	26.35	6.299	6.662	-0.363
400	4	2.520	2.167	0.353	74.25	50.76	23.49	6.299	5.451	0.848
400	5	2.520	1.981	0.539	74.25	44.02	30.23	6.299	5.372	0.927
400	6	2.520	2.088	0.432	0	3.149	-3.149	6.299	5.136	1.163

**Table 5.7.21** Conversion and Product Molar Quantities for the Oxidative Dehydrogenation of Butane under Pulse-flow conditions using 0.65% Pt/Al<sub>2</sub>O<sub>3</sub> (Sequential Dosing 20:1).

Temp. (°C)	Pulse No.	Moles Bypass (x10 <sup>-7</sup> )	Moles Reacted (x10 <sup>-7</sup> )	Conv. (%)	CO <sub>2</sub> /Pr (x10 <sup>-7</sup> )	CO (x10 <sup>-7</sup> )	Met. (x10 <sup>-7</sup> )	Eth. (x10 <sup>-7</sup> )	Iso (x10 <sup>-7</sup> )	B-1 (x10 <sup>-7</sup> )	Trans B-2 (x10 <sup>-7</sup> )	Cis B-2 (x10 <sup>-7</sup> )	Diene (x10 <sup>-7</sup> )
400	1	104.6	103.7	99.1	26.52	18.80	186.3	15.06	0	0	0	0	0
400	2	104.6	89.87	85.9	15.99	13.34	126.9	16.68	2.423	1.005	1.140	0.869	0
400	3	104.6	73.34	70.1	18.32	19.39	62.51	16.06	4.406	3.286	3.205	2.510	0
400	4	104.6	57.24	54.7	14.86	12.54	35.58	10.89	4.641	3.378	3.926	2.997	0
400	5	104.6	52.15	49.8	11.36	5.118	24.21	8.226	4.480	5.544	5.436	4.662	0
400	6	104.6	47.77	45.7	9.865	7.362	19.65	6.533	4.114	5.736	5.647	4.609	0

**Table 5.7.22** Product Selectivity for the Oxidative Dehydrogenation of Butane under Pulse-flow conditions using 0.65% Pt/Al<sub>2</sub>O<sub>3</sub> (Sequential Dosing 20:1).

Temp. (°C)	Pulse No.	CO <sub>2</sub> /Pr Sel. (%)	CO Sel. (%)	Met. Sel. (%)	Eth. Sel. (%)	Iso Sel. (%)	B-1 Sel. (%)	Trans B-2 Sel. (%)	Cis B-2 Sel. (%)	Diene Sel. (%)	Dehydro. Sel. (%)
400	1	19.2	4.5	44.9	7.3	0	0	0	0	0	0
400	2	13.3	3.7	35.3	9.3	2.7	1.1	1.3	1.0	0	3.4
400	3	18.7	6.6	21.3	10.9	6.0	4.5	4.4	3.4	0	12.3
400	4	19.5	5.5	15.5	9.5	8.1	5.9	6.8	5.2	0	17.9
400	5	16.3	2.4	11.6	7.9	8.6	10.6	10.4	8.9	0	29.9
400	6	15.5	3.8	10.3	6.8	8.6	12.0	11.8	9.6	0	33.4

**Table 5.7.23** Product Yields for the Oxidative Dehydrogenation of Butane under Pulse-flow conditions using 0.65% Pt/Al<sub>2</sub>O<sub>3</sub> (Sequential Dosing 20:1).

Temp. (°C)	Pulse No.	CO <sub>2</sub> /Pr Yield (%)	CO Yield (%)	Met. Yield (%)	Eth. Yield (%)	Iso Yield (%)	B-1 Yield (%)	Trans B-2 Yield (%)	Cis B-2 Yield (%)	Diene Yield (%)	Dehydro. Yield (%)
400	1	19.0	4.4	44.5	7.2	0	0	0	0	0	0
400	2	11.4	3.2	30.3	8.0	2.3	0.9	1.1	0.8	0	2.9
400	3	13.1	4.6	14.9	7.6	4.2	3.2	3.1	2.4	0	8.6
400	4	10.7	3.0	8.5	5.2	4.4	3.2	3.7	2.8	0	9.8
400	5	8.1	1.2	5.8	3.9	4.3	5.3	5.2	4.4	0	14.9
400	6	7.1	1.7	4.7	3.1	3.9	5.5	5.4	4.4	0	15.3

**Table 5.7.24** Mass Balance Data for the Oxidative Dehydrogenation of Butane under Pulse-flow conditions using 0.65% Pt/Al<sub>2</sub>O<sub>3</sub> (Sequential Dosing 20:1).

Temp. (°C)	Pulse No.	C in (x10 <sup>19</sup> )	C out (x10 <sup>19</sup> )	C diff (x10 <sup>19</sup> )	O in (x10 <sup>17</sup> )	O out (x10 <sup>17</sup> )	O diff (x10 <sup>17</sup> )	H in (x10 <sup>19</sup> )	H out (x10 <sup>19</sup> )	H diff (x10 <sup>19</sup> )
400	1	2.520	1.931	0.589	2.626	13.10	-10.48	6.299	6.364	-0.065
400	2	2.520	1.830	0.690	2.626	10.77	-8.144	6.299	5.608	0.691
400	3	2.520	2.044	0.476	2.626	13.79	-11.16	6.299	5.550	0.749
400	4	2.520	2.195	0.325	2.626	9.728	-7.102	6.299	5.594	0.705
400	5	2.520	2.226	0.294	2.626	4.033	-1.407	6.299	5.591	0.708
400	6	2.520	2.273	0.247	2.626	5.206	-2.580	6.299	5.625	0.674

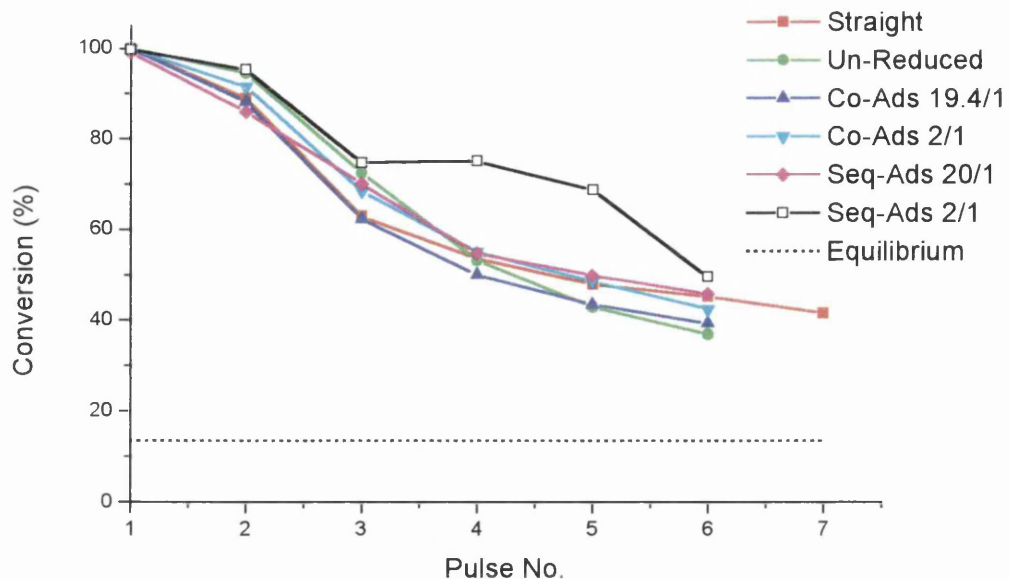


**Fig. 5.7.1** Conversion as a function of Pulse Number During the Straight and Oxidative Dehydrogenation of Butane using 0.65% Pt/Al<sub>2</sub>O<sub>3</sub> at 400°C.

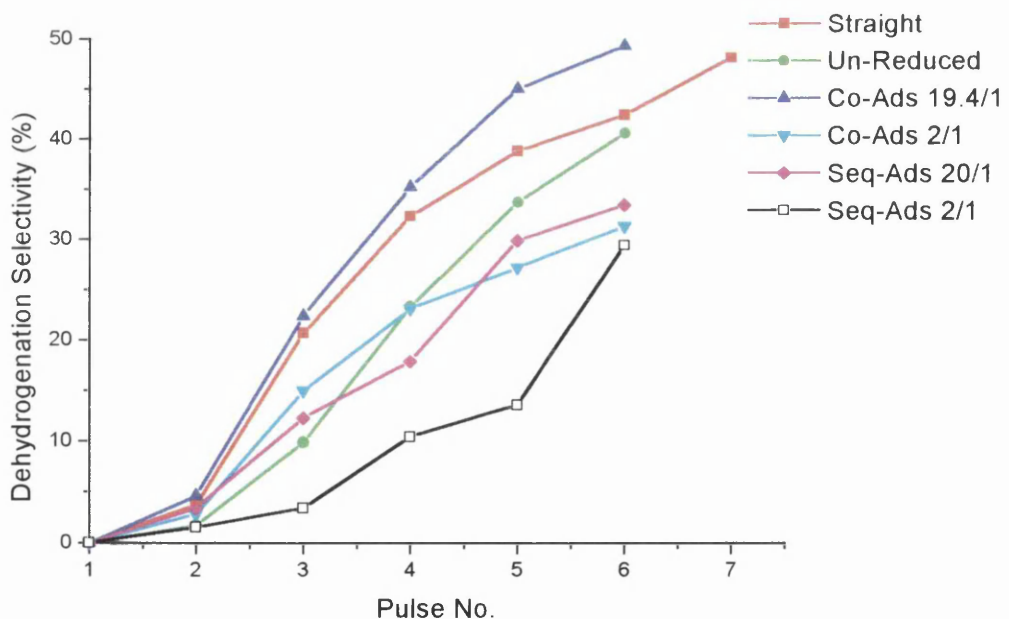


**Fig. 5.7.2** Dehydrogenation Selectivity as a function of Pulse Number During the Straight and Oxidative Dehydrogenation of Butane using 0.65% Pt/Al<sub>2</sub>O<sub>3</sub> at 400°C.

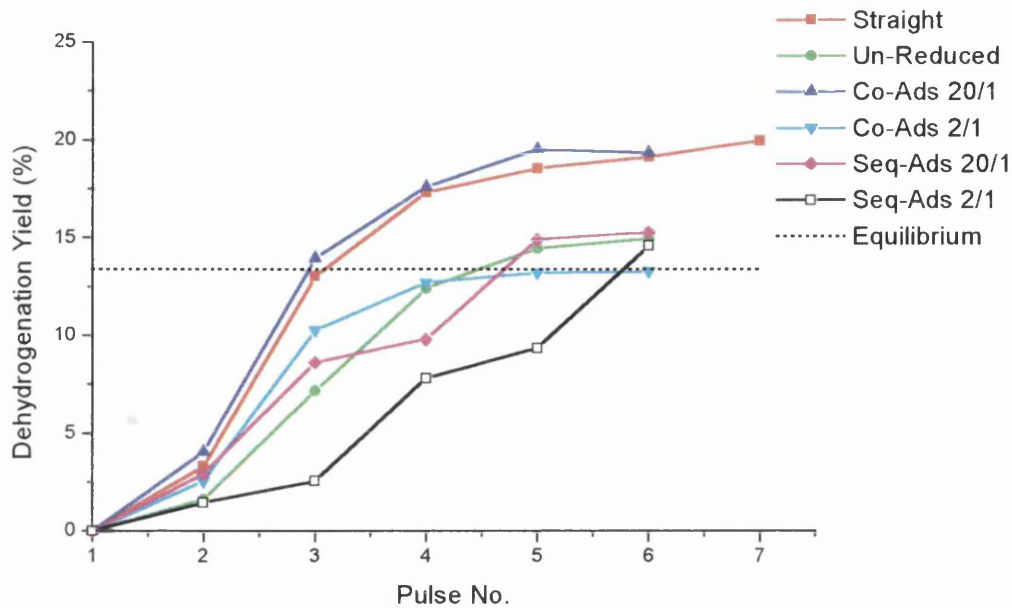


**Fig. 5.7.3** Dehydrogenation Yield as a function of Pulse Number During the Straight and Oxidative Dehydrogenation of Butane using 0.65% Pt/Al<sub>2</sub>O<sub>3</sub> at 400°C.

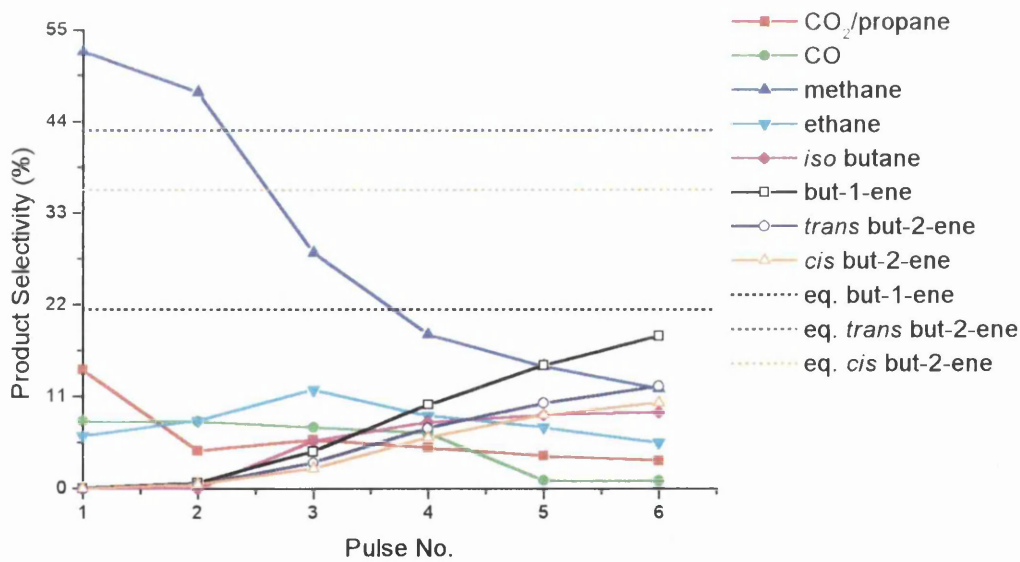


**Fig. 5.7.4** Product Selectivity as a function of Pulse Number During the Straight Dehydrogenation of Butane using Un-reduced 0.65% Pt/Al<sub>2</sub>O<sub>3</sub> at 400°C.

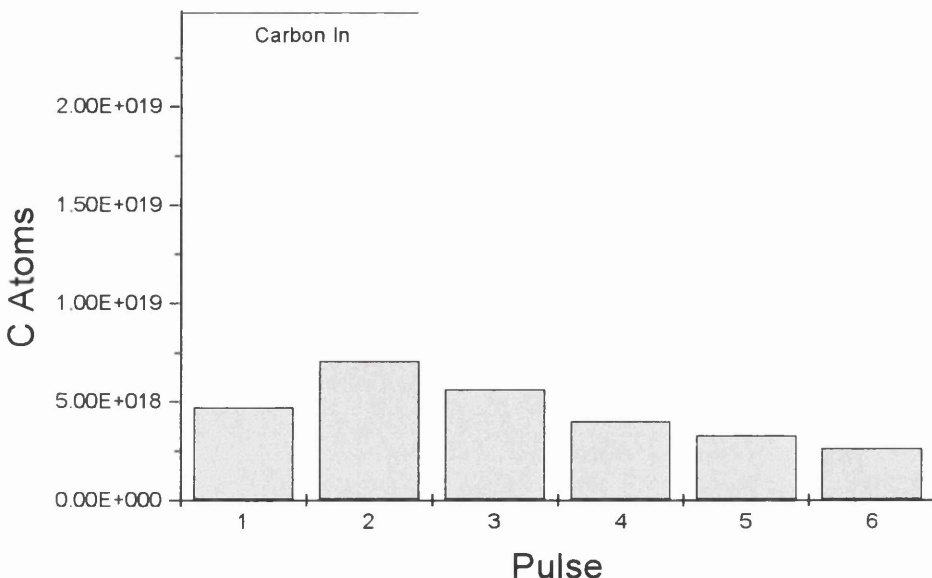


**Fig. 5.7.5** Carbon Retention as a function of Pulse Number During the Straight Dehydrogenation of Butane using Un-reduced 0.65% Pt/Al<sub>2</sub>O<sub>3</sub> at 400°C.

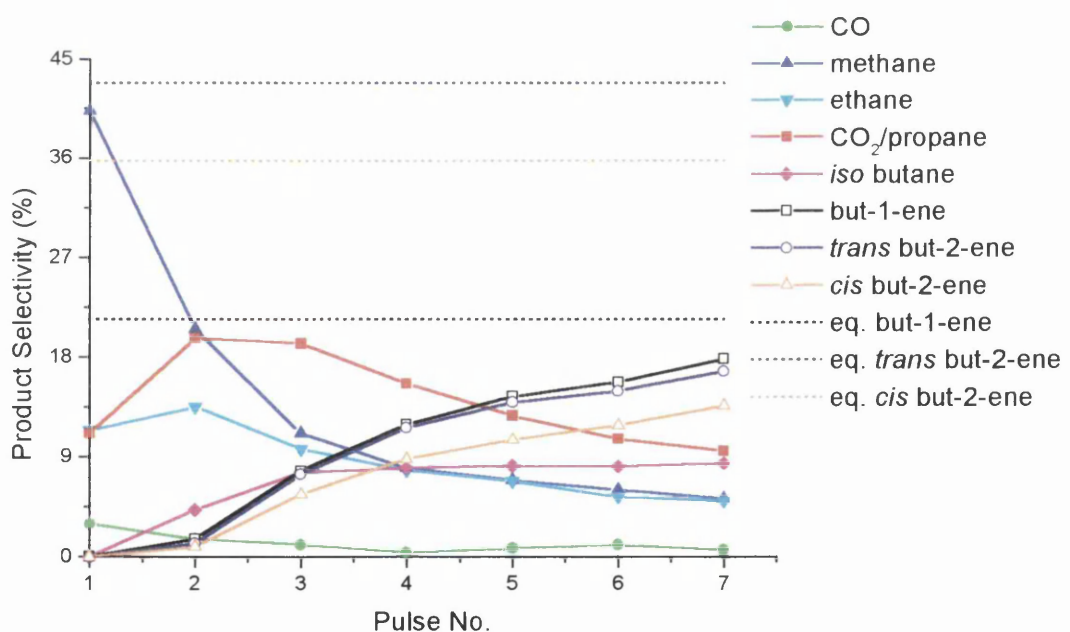


**Fig. 5.7.6** Product Selectivity as a function of Pulse Number During the Straight Dehydrogenation of Butane using 0.65% Pt/Al<sub>2</sub>O<sub>3</sub> at 400°C.

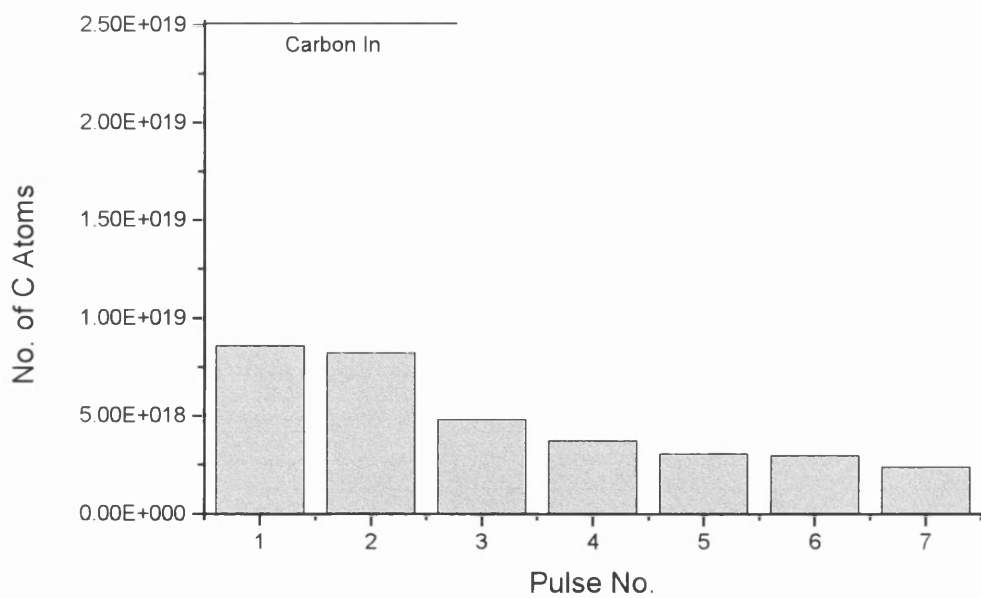


**Fig. 5.7.7** Carbon Retention as a function of Pulse Number During the Straight Dehydrogenation of Butane using 0.65% Pt/Al<sub>2</sub>O<sub>3</sub> at 400°C.

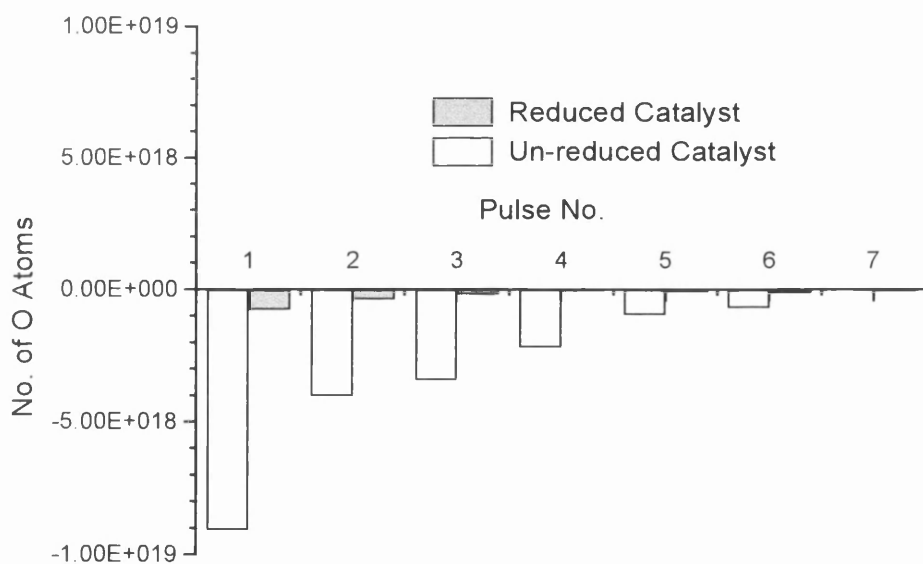


**Fig. 5.7.8** Oxygen Retention as a function of Pulse Number During the Straight Dehydrogenation of Butane using Reduced and Un-reduced 0.65% Pt/Al<sub>2</sub>O<sub>3</sub> at 400°C.

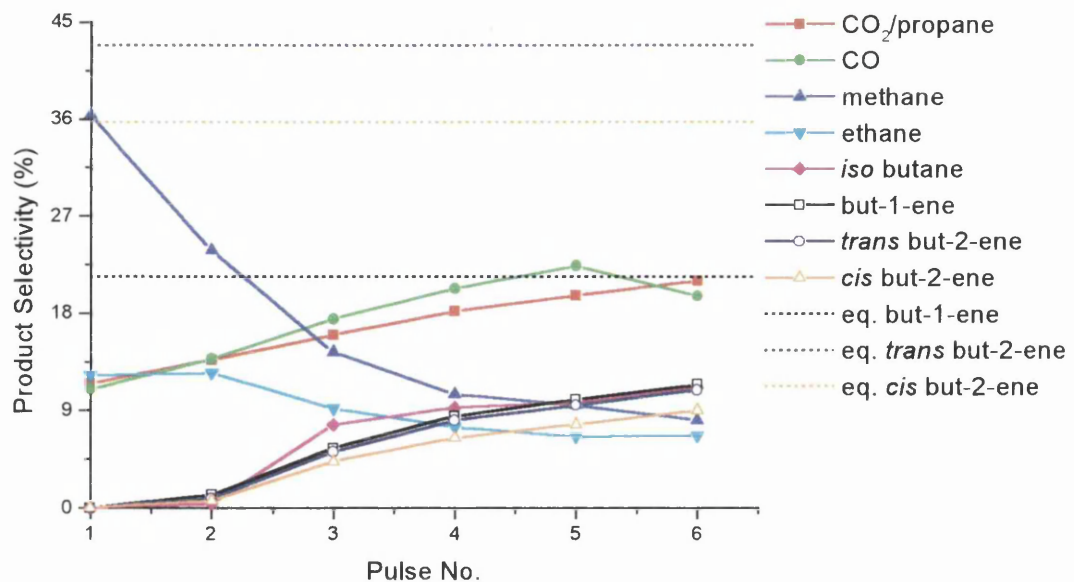


**Fig. 5.7.9** Product Selectivity as a function of Pulse Number During the Oxidative Dehydrogenation of Butane using 0.65% Pt/ $\text{Al}_2\text{O}_3$  at 400°C (Co-adsorption 2/1).

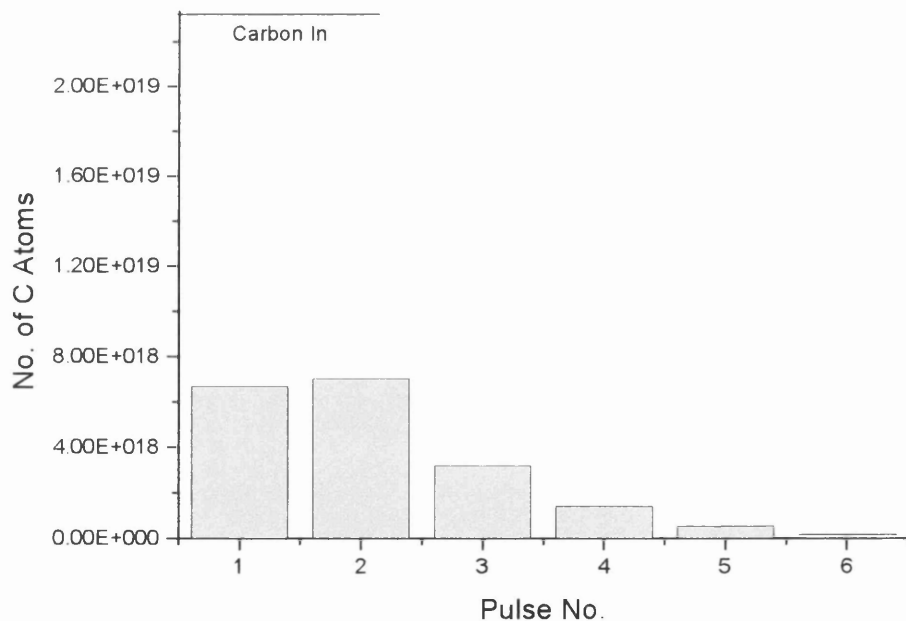


**Fig. 5.7.10** Carbon Retention as a function of Pulse Number During the Oxidative Dehydrogenation of Butane using 0.65% Pt/ $\text{Al}_2\text{O}_3$  at 400°C (Co-adsorption 2/1).

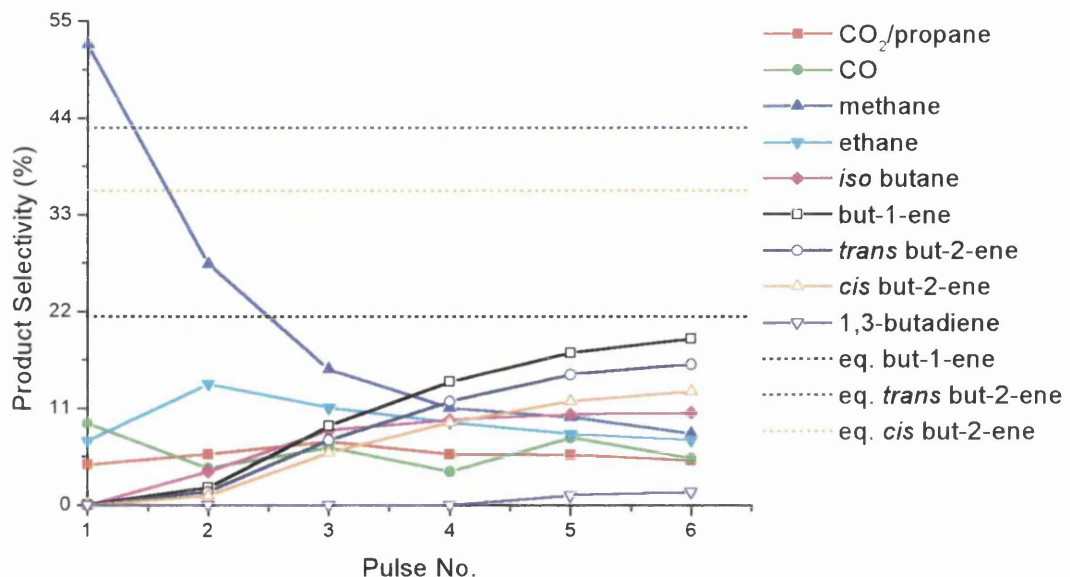


**Fig. 5.7.11** Product Selectivity as a function of Pulse Number During the Oxidative Dehydrogenation of Butane using 0.65% Pt/Al<sub>2</sub>O<sub>3</sub> at 400°C (Co-adsorption 19.4/1).

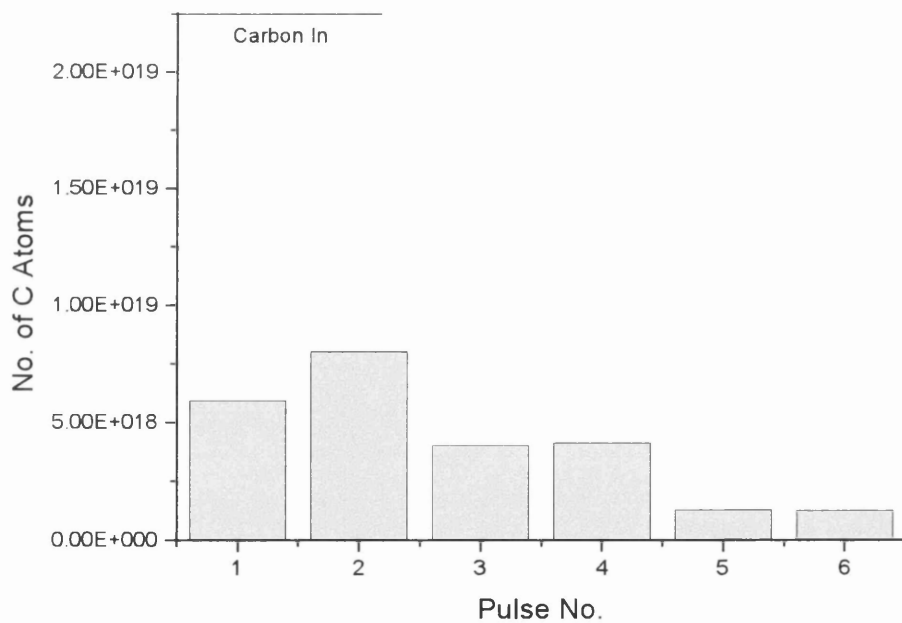


**Fig. 5.7.12** Carbon Retention as a function of Pulse Number During the Oxidative Dehydrogenation of Butane using 0.65% Pt/Al<sub>2</sub>O<sub>3</sub> at 400°C (Co-adsorption 19.4/1).

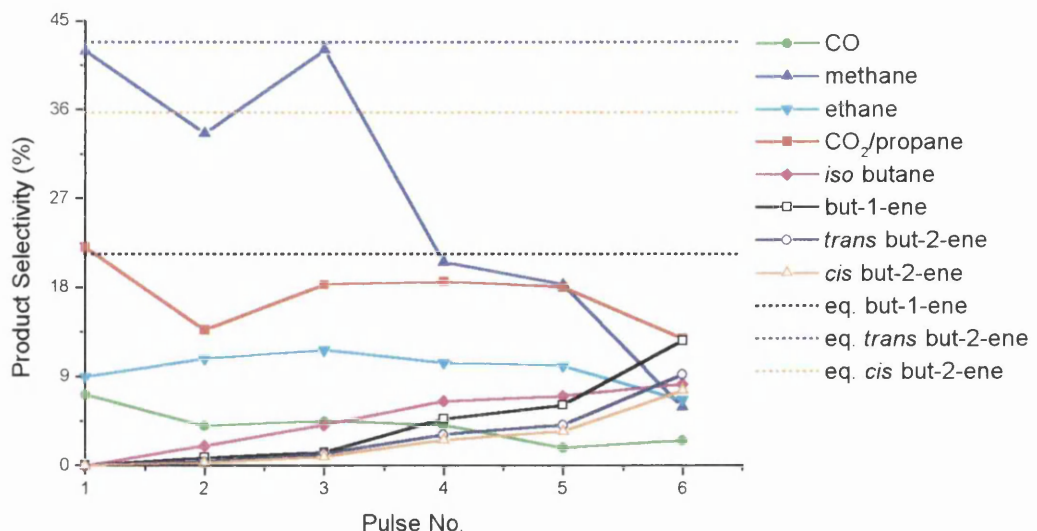


**Fig. 5.7.13** Product Selectivity as a function of Pulse Number During the Oxidative Dehydrogenation of Butane using 0.65% Pt/ $\text{Al}_2\text{O}_3$  at 400°C (Seq.-adsorption 2/1).

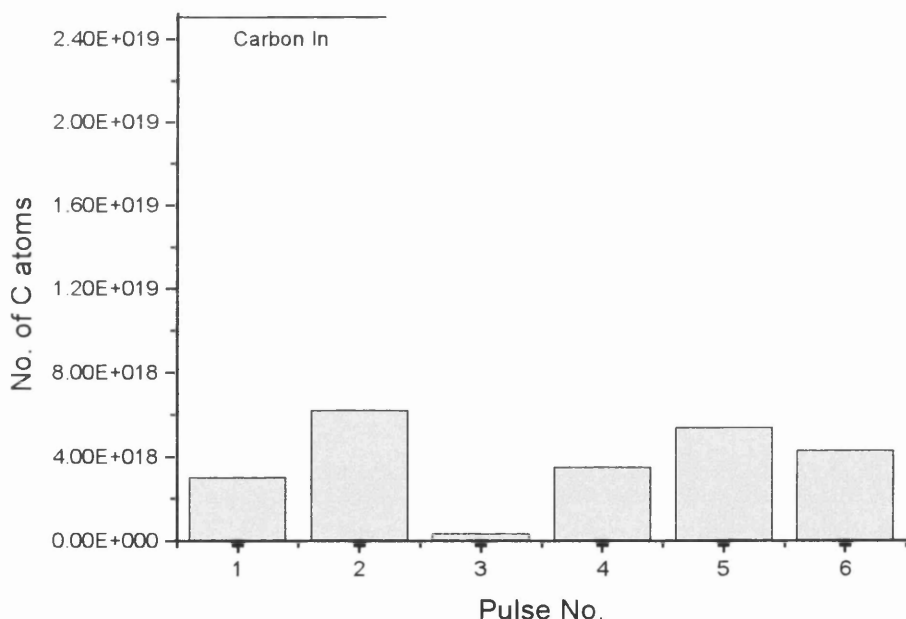


**Fig. 5.7.14** Carbon Retention as a function of Pulse Number During the Oxidative Dehydrogenation of Butane using 0.65% Pt/ $\text{Al}_2\text{O}_3$  at 400°C (Seq.-adsorption 2/1).

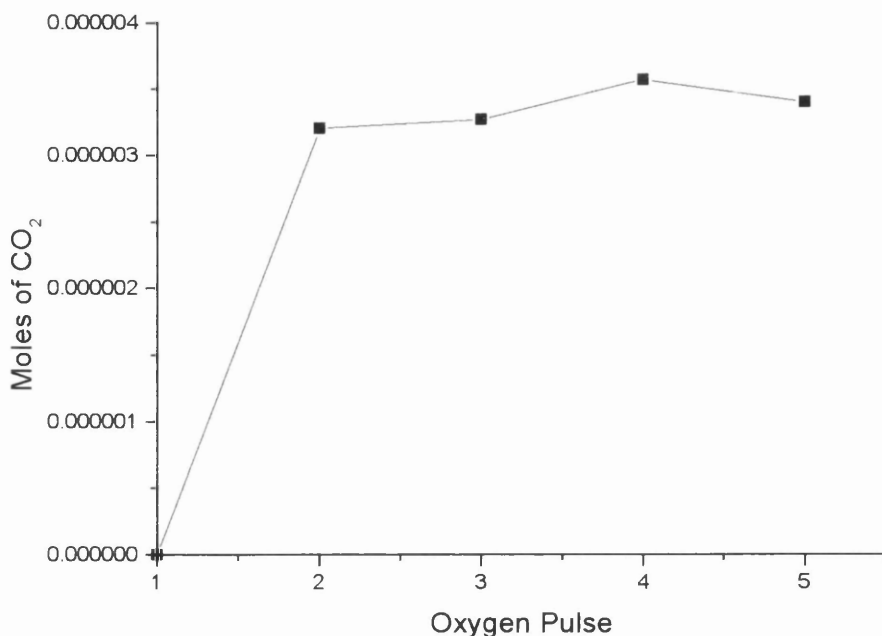


**Fig. 5.7.15** Intermittent Carbon Dioxide formed During the Oxidative Dehydrogenation of Butane using 0.65% Pt/Al<sub>2</sub>O<sub>3</sub> at 400°C (Seq.-adsorption 2/1).

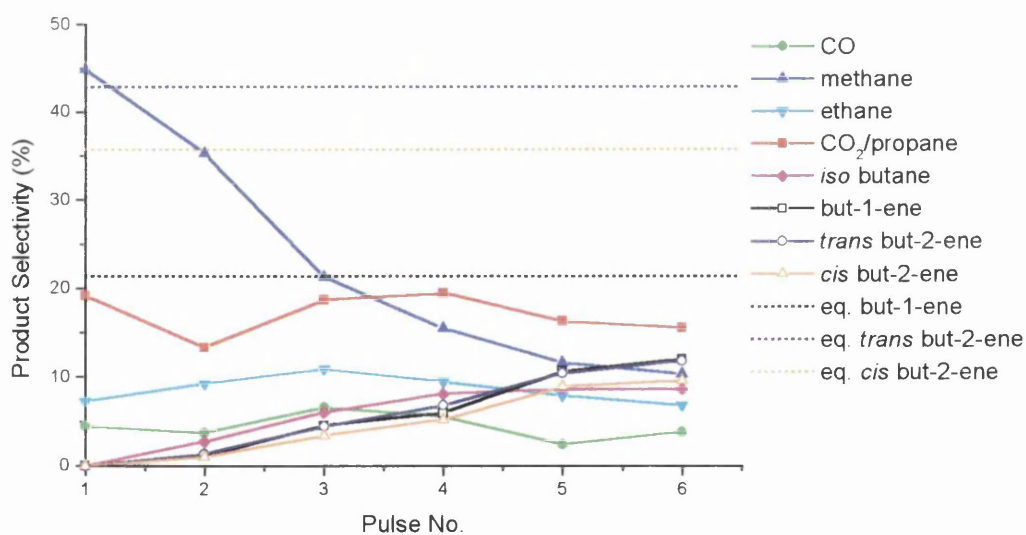


**Fig. 5.7.16** Product Selectivity as a function of Pulse Number During the Oxidative Dehydrogenation of Butane using 0.65% Pt/Al<sub>2</sub>O<sub>3</sub> at 400°C (Seq.-adsorption 20/1).

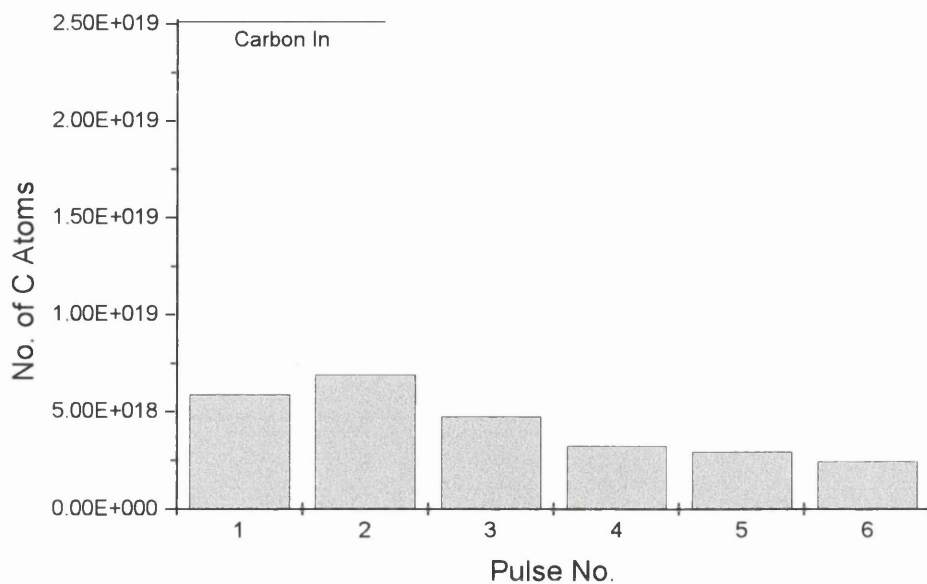


**Fig. 5.7.17** Carbon Retention as a function of Pulse Number During the Oxidative Dehydrogenation of Butane using 0.65% Pt/Al<sub>2</sub>O<sub>3</sub> at 400°C (Seq.-adsorption 20/1).

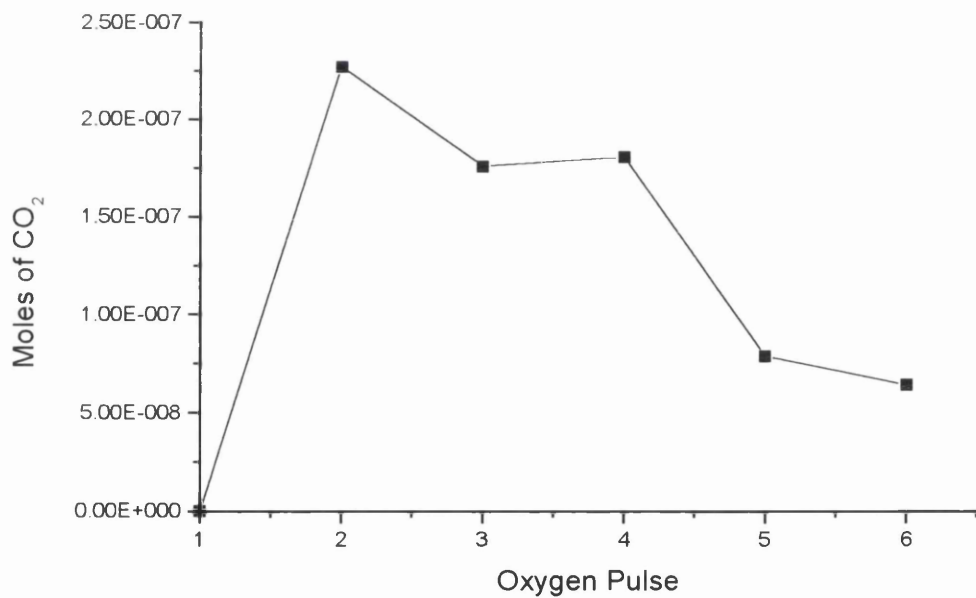


**Fig. 5.7.18** Intermittent Carbon Dioxide formed During the Oxidative Dehydrogenation of Butane using 0.65% Pt/Al<sub>2</sub>O<sub>3</sub> at 400°C (Seq.-adsorption 20/1).

Initial consideration of the results above for the pulse-flow testing of butane dehydrogenation with and without the presence of oxygen show very little difference between the various reactions. However, there is a subtle pattern evolving from the results, providing information that can be used to identify the processes shaping the overall reaction chemistry of the system.

Figure 5.7.1 displays the conversion obtained for each of the reactions. It is shown that for each of the studies carried out the conversion starts off at 100% falling to 40% as deactivation and the reactions consisting of the break-up of the hydrocarbon molecules, forming lower alkanes and C<sub>1</sub> oxygenates, and isomerisation to *iso*-butane begin to diminish, which would potentially leave dehydrogenation as the only process taking place. This also explains why the conversion observed during the experiment is higher than that predicted by equilibrium, which assumes that only dehydrogenation processes are taking place.

The only potential difference that can be observed across all the reactions is that the conversion for the sequential dosing, with a hydrocarbon:oxygen ratio of 2:1, is slightly higher than the others. It is thought that this could be due to the removal of the carbonaceous material by the excess amounts of oxygen available through combustion processes [78]. Figure 5.7.15 illustrates the carbon dioxide formed from the intermittent oxygen pulses. It is shown that there is a constant amount of CO<sub>2</sub> produced with each pulse of oxygen. This potentially has the effect of stripping off the carbonaceous material, leaving bare metal surface, which as shown in the first pulse, results in the breakdown of the butane backbone. With respect to the amount of carbon dioxide formed intermittently and carbon retained, it can be calculated that approximately 52% of the carbon retained is removed on each pulse. This effect can not be observed when only small amounts of oxygen are used. For example figure 5.7.18 shows that the intermittent CO<sub>2</sub> produced, when the hydrocarbon:oxygen ratio is 20:1, is less by between 1 - 2 orders of magnitude compared to that for the case of the 2:1 experiment. This is because the amount of carbon deposited is much greater due to the higher hydrocarbon content while the quantity of oxygen is less and so the amount of carbonaceous material removed is much less than with the previous example *i.e.* the reaction is oxygen limited. This reaction is behaving very similar, in terms of selectivity and conversion, to the straight dehydrogenation reaction.

These processes and trends can be seen more clearly by looking at the dehydrogenation yield (figure 5.7.3), which takes account of the dehydrogenation selectivity with respect to conversion. The highest yields are produced when the oxygen content is lowest, in the straight dehydrogenation reaction and the co-adsorption case where the hydrocarbon:oxygen ratio is 19.4:1 (both achieve approximately 20%). This can be explained by comparing figures 5.7.6 and 5.7.7. Figure 5.7.6 shows the product selectivity for all of the products detected during the straight dehydrogenation of *n*-butane at 400°C under pulse-flow conditions, while figure 5.7.7 illustrates the amount of carbon retained during the same experiment. It is clearly evident from these figures that a correlation exists between the amount of carbon deposited on the catalyst surface with the chemistry that takes place. To be more specific, it can be observed that the formation of olefin products increases as carbonaceous material builds up on the catalyst surface. Initially, cracking processes forming lower alkanes such as methane, C<sub>2</sub> and possibly C<sub>3</sub>'s, as well as carbon laydown takes place as long as the surface is bare. It has already been shown that the homogeneous formation of these lower alkanes does not measurably occur until 500°C (figure 5.3.2) and therefore in this case they are catalytic (heterogeneous) in origin. It can thus be concluded that the interaction of carbonaceous material with the catalyst surface provides a more suitable platform on which dehydrogenation reactions take place in contrast to the bare metal which is more suited to the unwanted cracking reactions. The removal of this surface layer by oxygen, as described above, is therefore detrimental to the production of olefins.

If the reaction was allowed to continue under non-transient conditions the yield would eventually decrease, as the conversion decreases with the deactivation of the catalyst (caused primarily by pore blocking), to that observed in the continuous-flow experiments. This pore blocking prevents the reactant alkane molecules reaching the active sites and dehydrogenating to olefin products. Figure 5.7.19 illustrates this effect in the form of a schematic diagram, where the metal particles are shown as green dots, the thin black line represents the outline of the alumina support and the thick black line represents the carbonaceous material blocking the pores of the support material. This could have been confirmed by post reaction pore distribution and volume measurements. However, due to time constraints and equipment breakdown problems these measurements were not carried out.

The lowest dehydrogenation yields are observed when the oxygen content is highest. The two extreme cases where the hydrocarbon:oxygen ratio is 2:1 illustrates this (co-adsorption and sequential adsorption on figure 5.7.3). The maximum yield obtained in these two reactions is approximately 13%, compared to 20% in the straight and co-adsorbed with 20:1 hydrocarbon:oxygen cases, where the oxygen concentration is minimal. This is due, not to a decrease in conversion, but to a reduction in the selectivity towards the dehydrogenation products and can be backed up by figure 5.7.2, which highlights the trends in dehydrogenation selectivity, and shows clearly that the selectivity towards olefin products is at its lowest when large amounts of oxygen are present. The shape of the curve in the case of the co-adsorption with hydrocarbon:oxygen ration of 2:1 is very similar to that of the low oxygen content reactions (*e.g.* straight dehydrogenation on figure 5.7.3). The only difference being that the plateau occurs at lower yield. This happens because the high oxygen content prevents the carbonaceous overlayer forming to the same extent as with the straight dehydrogenation (as explained above) and the low content oxygen reactions, therefore the amount of dehydrogenation taking place is less, with a subsequent increase in the production of C<sub>1</sub> oxygenates (see product selectivity figures 5.7.9 and 5.7.13).

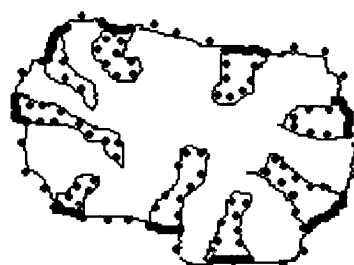


**Fig. 5.7.19** Schematic Illustration of Pore Blocking.

It is also noticeable that the highest yield value for each reaction is higher than the theoretical equilibrium value (figure 5.7.3). As stated previously, the reason for this is that the thermodynamics were calculated assuming that all the reactions taking place are dehydrogenation to C<sub>4</sub> olefin products, when in fact pyrolysis, isomerisation and carbon deposition processes are also occurring (*e.g.* figure 5.7.6).

The conditioning process is also illustrated by the carbon mass balance data. Figure 5.7.7 shows, for straight dehydrogenation, that large amounts of carbon are

retained over the first couple of pulses which decreases with subsequent pulses. The layer of carbonaceous material deposited amounts to approximately 8.6 carbon atoms for every surface platinum atom. With reference to figure 5.7.6 this observation correlates well with the increase in dehydrogenation selectivity and combined together is interpreted that a carbonaceous overlayer is forming during the initial stages of the reaction due to which dehydrogenation reactions take place. The data from the mass balances of hydrogen and oxygen have been included in the tables. However, due to the formation of water, which was not detected or quantified by instrumental means as mentioned above, these numbers cannot be used to represent operation of the chemical system as a whole. Nevertheless, it is interesting to make the comparison between the straight dehydrogenation using reduced and un-reduced catalysts, in terms of oxygen retention. Figure 5.7.8 shows that large amounts of oxygen were removed from the surface of the platinum over the first few pulses in the case of the un-reduced catalyst relative to the reduced catalyst. This result provides a clear illustration of the effect of reducing the catalyst before use. This also suggests the possibility of *in situ* reduction in the butane stream.

Differences between the conversion and dehydrogenation selectivity can also be seen with these two examples as the pseudo steady state is approached. Figure 5.7.1 shows that the ultimate conversion is slightly less for the un-reduced case compared to the reduced. This is also observed for the dehydrogenation selectivity where it is also shown that the time taken for dehydrogenation process to take effect is longer (figure 5.7.2). The reason for the latter observation is that before the carbonaceous overlayer forms, the oxygen covering the surface of the platinum is being removed and is done so by the hydrocarbon molecules forming combustion products as shown on figure 5.7.4. The decrease in CO/CO<sub>2</sub> reveal the consumption of surface oxygen. Figure 5.7.3 shows the resulting increase in dehydrogenation yield as the selectivity increases upon formation of the carbonaceous overlayer. These observations imply that the activation process is not required.

A possible explanation for the slight reduction in conversion and selectivity and therefore the overall yield between the un-reduced, and indeed all the oxidative reactions, and the straight dehydrogenation using the reduced catalyst (figure 5.7.3) is that when oxygen is present water is formed. This could have the effect of promoting a sintering process, which would result in agglomeration of the platinum particles with a

subsequent loss of surface area [15]. If this did in fact take place, then not only would the activity of the catalyst be limited but also the degree of dehydrogenation selectivity would be less, as the surface area on which to form a carbonaceous overlayer would be reduced. This argument could also be extended to explain some of the effects observed in the continuous-flow experiments where large amounts of water are also formed and where the overall dehydrogenation selectivity is significantly lower. Unfortunately the post-reaction electron microscopy measurements were unable to determine metal crystallite dimensions.

*Chapter 6*

Conclusion

The initial aim of this project was to investigate the feasibility of oxidative dehydrogenation (ODH) of *n*-butane in the presence of molecular oxygen, catalysed by platinum alumina catalysts, as a low temperature alternative to alkene formation. Throughout the study it rapidly became apparent that this route to the production of alkene species was not suitable under the conditions attainable with the conventional plug flow reactor used during the work. As a result, the focus of the study turned to addressing the reasons why ODH did not take place compared to straight dehydrogenation (SDH) carried out under almost identical conditions, with the only difference being the absence of oxygen. Several issues have been examined, notably the effect of changing the relative concentration of oxygen, the differences between the two Pt/Al<sub>2</sub>O<sub>3</sub> catalysts, with the greatest emphasis placed on the particle size, the effect of changing the linear velocity of the reactant gas flow, and the effect of carbonaceous deposits on the activity and selectivity of the catalysts. In addition, the potential correlation of the pulse-flow methodology with the continuous-flow studies has been undertaken to glean information about the reaction under study, in particular during the initial stages of reaction.

Continuous-flow experiments were carried out as the standard reaction testing method mimicking conditions encountered in an industrial scenario, providing data such as the steady state conversion and dehydrogenation selectivity. Pulse-flow was also carried out and provided very useful information towards determining the processes which took place preventing a high yield of butene products in the case of ODH. Plots highlighting trends in carbon deposition, conversion and dehydrogenation yield were also obtained using this method.

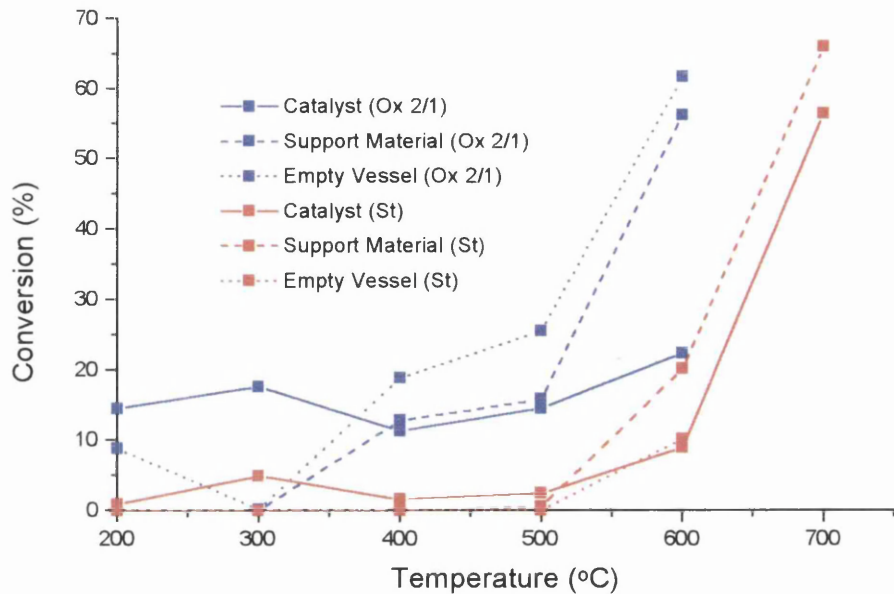


**Fig. 6.1** Comparison of SD and ODH as a Function of Temperature for the 0.5% Pt/Al<sub>2</sub>O<sub>3</sub> Catalyst.

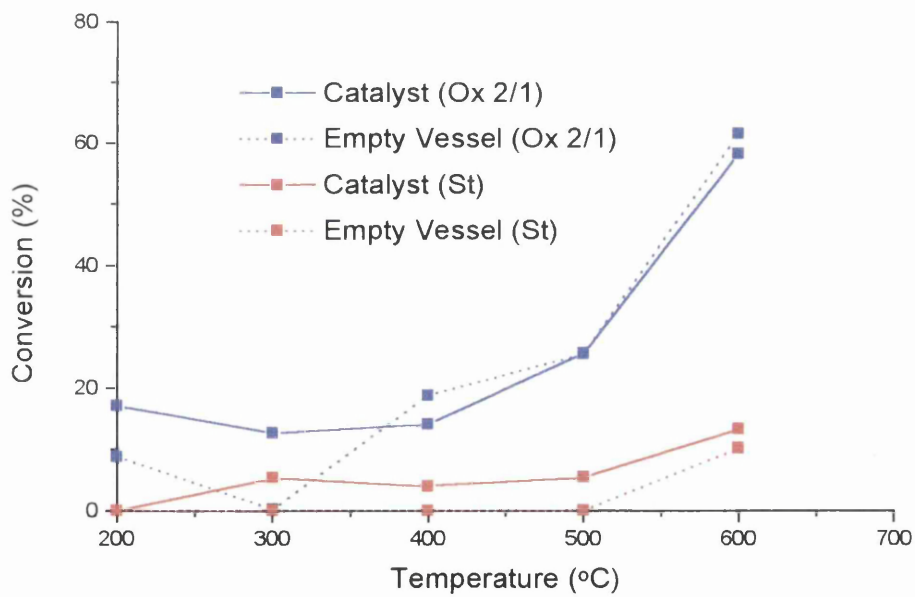


**Fig. 6.2** Comparison of SD and ODH as a Function of Temperature for the 0.65% Pt/Al<sub>2</sub>O<sub>3</sub> Catalyst.

From consideration of the results, it is immediately clear why the use of ODH is favourable to the activity of the system. Figures 6.1 and 6.2 show both catalysts to exhibit a rapid increase in activity in the SDH reactions at temperatures between 500°C and 700°C, due to the introduction of the homogeneous reactions at these temperatures (refer to section 5.1 for the thermodynamic explanation) and the activation of the acid sites on the alumina supports [73], which favour cracking and isomerisation reactions (refer to figures 5.5.8 and 5.6.7). When oxygen is added to the system it is clear that the homogeneous reactions begin to take place at temperatures approximately 100°C lower than in the SDH, forming similar products with the addition of CO and CO<sub>2</sub> (figures 5.5.18 and 5.6.17). These observations were also seen by Burch and Crabb during their studies of VMgO catalysts [58]. It was explained that the oxygen activates radical reaction mechanisms as described in section 5.3.

Figures 6.1 and 6.2 also show improved activity, of the ODH compared to the SDH, below 500°C down to temperatures as low as 200°C, which is mostly catalytic in origin (compare figure 5.3.6 with figures 5.5.21 and 5.6.20). These observations are due to catalytic combustion reactions taking place, for which platinum based catalysts are well known to be active. Similar observations were made by Forazatti *et al* [10] when investigating the use of an annular reactor system for propane dehydrogenation, again, attributing the observations to a platinum metal surface. It was suggested from their results that inter-phase diffusion control was limiting the production of CO<sub>2</sub> as shown by an almost flat temperature dependence between 200°C and 500°C. The same conclusion is made here.

The final point to take from figures 6.1 and 6.2 is the difference in activity between the SDH at temperatures between 300°C and 500°C for the two catalysts. Virtually no steady state conversion is measured for the 0.5% catalyst over this temperature range, with the exception of a small measurement at 300°C, while the 0.65% substrate maintains approximately 8% conversion over the same range. With the 0.5% catalyst the surface becomes heavily poisoned by carbonaceous deposits resulting in rapid deactivation (refer to figures 5.5.1 and 5.5.5) and minimal activity, whereas large amounts of dehydrogenation products are formed, relative to conversion, when using the 0.65% Pt/Al<sub>2</sub>O<sub>3</sub>. Comparison with table 5.1.3 shows that even the 0.65% catalyst, at 8% conversion, is well below the equilibrium value highlighting that there is also a degree of deactivation with this catalyst. Deactivation,

as a result of coking, is well known for platinum based catalysts, resulting in restricted access to the active metal through direct deposition and as a result of pore blocking [46, 47]. These effects were described extensively in section 1.4.1.

The difference between the two catalysts towards dehydrogenation production is highlighted clearly on figures 6.3 and 6.4. It can be seen that very high selectivity towards SDH takes place on the 0.65% catalyst, which is completely catalytic (compare the empty vessel with the catalyst result), compared to the 0.5% case, which displays some selectivity but not to the same extent. It is proposed that the reason for this difference is due to the physical nature of the catalyst itself, in particular the relative platinum crystallite size. As discussed in section 5.2.2 the crystallites in the 0.5% catalyst are larger than those in the 0.65% catalyst (estimated from CO chemisorption results). It has been reported previously in the literature that cracking reactions, leading to coke and therefore deactivation, is structure sensitive and requires the presence of larger particles [1, 37, 38, 40], whereas dehydrogenation reactions require only one active centre on which to take place [14]. It is therefore concluded in this case that the larger particles of the 0.5% catalyst are more subject to cracking reactions resulting in rapid deactivation, relative to the smaller particles of the 0.65% catalyst which are more resistant to the cracking reactions and therefore favour dehydrogenation, although some carbonaceous deposits do form on the latter. The effect of these is discussed below with the pulse-flow results.

Figures 6.3 and 6.4 also imply that ODH reactions occur with a relatively high selectivity towards olefins in the absence of the active platinum metal. Figure 6.3 shows that the dehydrogenation selectivity for both the empty vessel and the alumina support material associated with the 0.5% catalyst behave almost identically. It is therefore concluded that the reactions responsible for these observations are purely homogeneous, occurring via radical mechanisms activated by gas-phase H-atom abstraction, as shown for propane by Burch and Crabb [58]. Again, these observations have been seen by numerous authors on similar systems, also with the conclusion that the reactions are homogeneous in origin [58, 10, 63, 64]. The two figures also illustrate clearly how the addition of platinum to the system results in a dramatic decrease in selectivity to the dehydrogenation products.

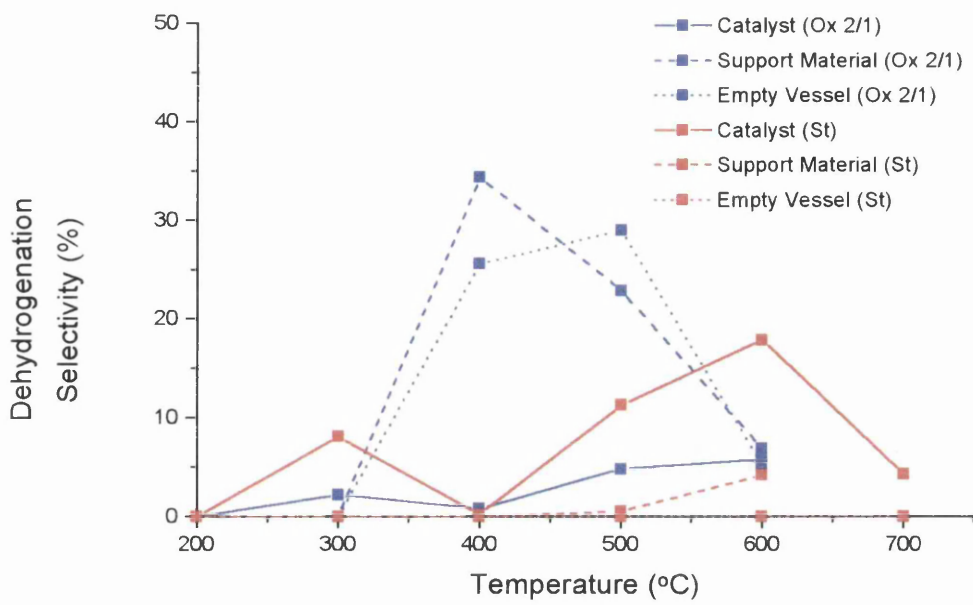


**Fig. 6.3** Comparison of SD and ODH as a Function of Temperature for the 0.5% Pt/Al<sub>2</sub>O<sub>3</sub> Catalyst.

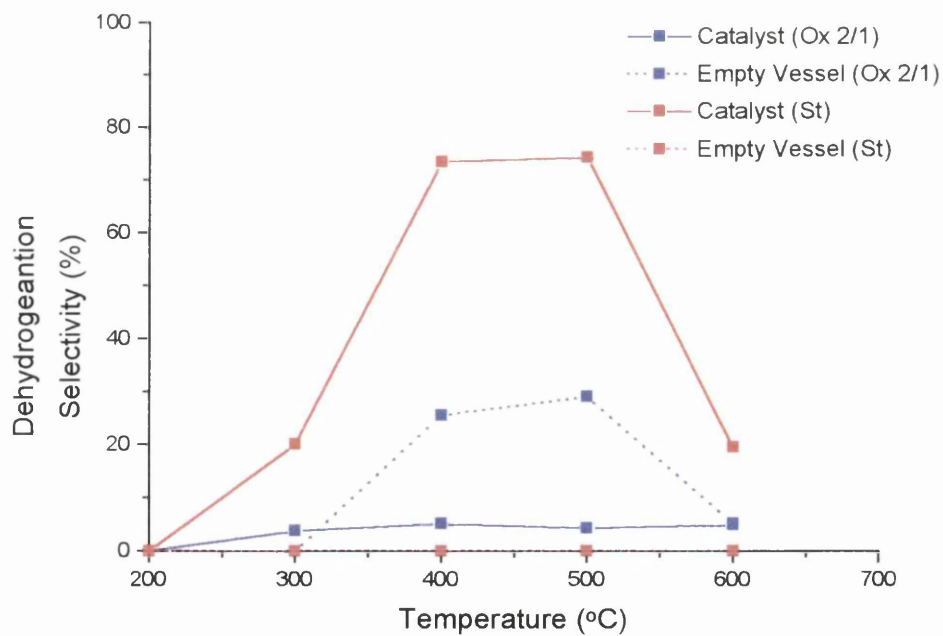


**Fig. 6.4** Comparison of SD and ODH as a Function of Temperature for the 0.65% Pt/Al<sub>2</sub>O<sub>3</sub> Catalyst.

This latter effect was studied in greater detail using pulse-flow techniques. As explained earlier, pulse-flow allows access to the processes taking place during the approach to steady-state. During these experiments, again, the effect of SDH was compared to that of ODH for the 0.65% Pt/Al<sub>2</sub>O<sub>3</sub> catalyst at 400°C, the optimum temperature for olefin formation below the temperature at which homogenous reactions become important. Oxygen rich and oxygen lean mixtures were used and sequential pulsing as well as co-adsorption experiments were carried out to see what effects changing the reaction parameters induced on the conversion and selectivity of the catalyst to the various reactions taking place. Pulse-flow methodology has proved to be a very important technique in the past for these types of study [86, 44, 27].

The results of the SDH show, as expected, a decrease in conversion towards the value at steady-state with increasing pulse number (figure 5.7.1). At the same time the dehydrogenation selectivity increased, again approaching the steady state value (figure 5.7.2). These results were correlated against the carbon mass balance data, where it is evident that the increase in olefin selectivity is coincident with the deposition of carbonaceous material (figure 5.7.7), plateauing as carbon retention comes towards an end. Under steady-state conditions the coke deposition is uncontrollable and result in the rapid loss in activity. However, under these non-steady state conditions this does not happen and thus allows important conclusions to be made. The increase in selectivity and decrease in conversion with carbon deposition has been observed previously [31, 44, 18]. The conclusion made here to account for these results is based on an electronic effect theory similar to that observed with the alloy based catalysts [28, 29, 30, 31]. In those studies the presence of the promoter reduced the adsorptivity of the metal surface resulting in a reduced heat of adsorption of the alkane molecule. As a result reactions such as cracking and isomerisation, which require strong adsorption, were suppressed, resulting in an observed increase in the selectivity towards olefin products. In this case there is no secondary metal promoter, however, there is the formation of carbonaceous deposits on the metal surface. Work carried out by Somorjai [39] suggested that carbonaceous deposits can form three dimensional structures and leave areas of isolated metal catalyst where transformations can occur. The deposited carbonaceous material inflicting an electronic effect resulting in the bare metal areas having reduced adsorptivity towards reactant species, as measured by various chemisorption studies. This was also suggested by Jackson *et al*

[45] and Barbier *et al* [41] and could possibly be used as an explanation of the results collected by Liwu *et al*, depending on interpretation [28].

It is therefore concluded in this study that the deposited carbonaceous material gives rise to an electronic effect which reduces the strength of adsorption of the *n*-butane starting material with the outcome that only dehydrogenation takes place and the reactions requiring strong adsorption, cracking and isomerisation, which would result in loss of dehydrogenation selectivity, are suppressed. Other explanations exist which also fit the data, assuming the formation of three dimensional structures. It is possible that the carbonaceous deposits block the sites required by the unfavourable cracking and isomerisation reactions, leaving the dehydrogenation sites un-blocked and available for reaction. This too would lead to a reduction in conversion and an increase in dehydrogenation selectivity. Again, this explanation has been used in the literature to explain similar results [41]. It is also feasible that the dehydrogenation reactions take place on the top of a layer of carbonaceous material through which hydrogen transfer can take place (donation or abstraction). This theory has been the subject of many studies both in hydrogenation and dehydrogenation investigations [44, 86].

First inspection of the other plots on figures 5.7.1 and 5.7.2 show little relative difference between the various reaction conditions used. However, closer inspection does yield information that can be used in an attempt to explain why the results of the ODH in the presence of the active metal are poor. Figure 5.7.3, which combines the effects of conversion and selectivity forming dehydrogenation yield data, illustrates the problems clearly. A separation in the plots is evident. Those with very little oxygen, such as the straight and co-adsorbed with *n*-butane:oxygen ratio of 20:1, show the highest yield values, while the others which are richer in oxygen content (except the sequentially adsorbed with *n*-butane:ratio of 20:1) display lower yield values. Given that the production of CO<sub>2</sub> and CO is higher in the latter cases, it is concluded that the presence of oxygen strips away the carbonaceous material deposited on the metal, which as established above, is crucial to the adsorptive properties of the metal, leading to the formation of less dehydrogenation products. The combustion and subsequent removal of surface carbonaceous material has been described in the literature and is known to take place on Pt/Al<sub>2</sub>O<sub>3</sub> systems [76]. It should also be noted that very little distinction can be made between the carbon retention plots of the various reactions. As an explanation, it could be possible that most of the retained coke is deposited on the

support material (C:Pt ratio of 8.2:1), as discussed previously for the alloy catalysts [42], and that the specific material removed from the metal constitutes only a small fraction of that removed from the overall catalyst (52% carbon removal at high oxygen content).

A final conclusion that could be used, together with the others, to explain the loss of dehydrogenation selectivity in the ODH reactions compared to the SDH reactions is based on sintering. It has been shown in the literature that water promotes sintering of platinum crystallites [15]. During the combustion reactions which take place, large amounts of water also form, which could be seen condensing in the glass line exiting the reactor. Therefore, it is possible that water-promoted sintering occurs when oxygen is present resulting in the growth of the platinum particles and a change in the associated chemistry, favouring the un-wanted cracking reactions, as discussed in detail above. Good TEM results would have enabled confirmation of this suggestion.

The effect of oxygen can thus be summarised and attributed to a combination of the following three theories, which all lead to reduced activity towards dehydrogenation:

- 1.) Oxygen in the feed-gas results in the thermodynamically more favourable combustion reactions, which are known to be catalysed by platinum;
- 2.) Oxygen in the feed-gas results in the stripping off of the carbonaceous deposits or the prevention of their formation, which are known to be crucial to the reduction in adsorptivity of the metal and the promotion of dehydrogenation reactions; and
- 3.) Oxygen in the feed-gas leads to water promoted growth of the platinum crystallites and the subsequent change in surface chemistry associated with this growth.

These conclusions have been drawn on the basis of the pulse-flow evidence but relate also to the continuous-flow system and account for the reduced dehydrogenation selectivity in the ODH systems.

In an attempt to investigate the observations made by Schmidt in the monolith and fluidised bed work [62, 5] and in the surface science literature [77, 78, 79], in which it was concluded that the concentration of oxygen in the system is crucial to the reaction specificity, it was also decided to carry out reactions where the *n*-butane:oxygen ratio was varied. Figure 6.5 presents the results of this study. It was hoped that at high butane:oxygen ratios (small oxygen concentrations), ‘hot oxygen’

could be formed, resulting in the desired high selectivity and conversions. However, figure 6.5 shows this not to be the case. Again, it is clear that increasing the oxygen concentration only led to increased conversion and decreased dehydrogenation selectivity as a result of increased combustion reactions (shown on figure 5.6.67). Also increased oligomer formation at the very highest oxygen contents is seen, the products of which were not completely identified, but were accounted for visually (see section 5.5.5) and the formation of which explain the reduction in CO<sub>2</sub> formed below 66% hydrocarbon, as shown on the above mentioned figure. The crucial issue here is reagent contact time. It is thought, as a result of the long contact times of the reactants in the present study (in the order of 10<sup>-1</sup>s), that ‘hot oxygen’, which is short-lived *i.e.* 10<sup>-5</sup>s [77], is effectively quenched during the reaction conditions and cannot contribute to the surface chemistry under the conditions used here. As a result we do not see the benefits displayed by Schmidt and co-workers who, with the help of monoliths and fluidised bed type reactors can easily access these shorter contact times over which the reagents can access active oxygen (O<sup>•</sup>s).

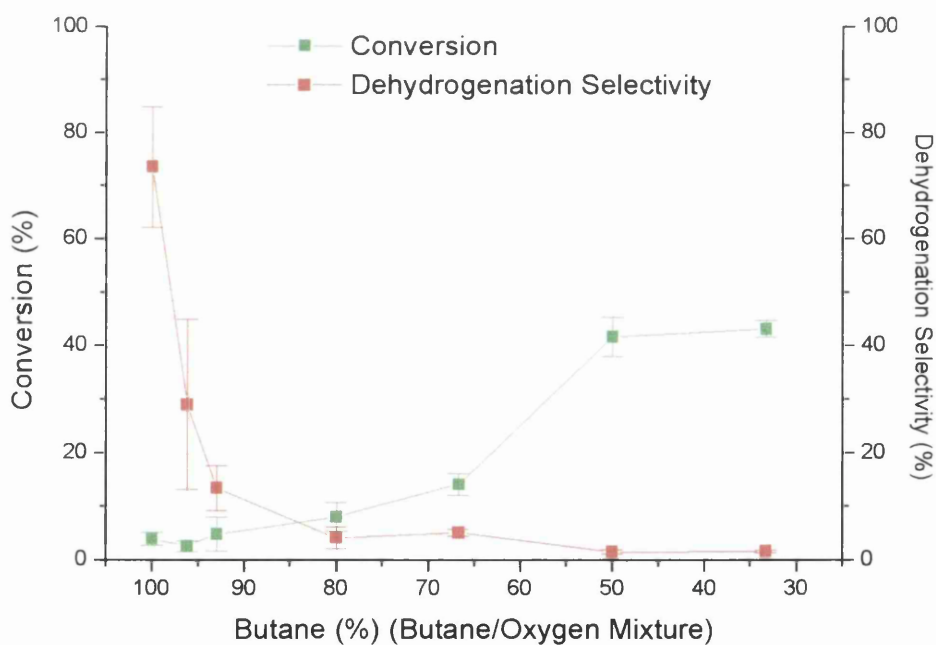


**Fig. 6.5** Conversion and Dehydrogenation Selectivity as a function of *n*-butane:oxygen ratio for the 0.65% Pt/Al<sub>2</sub>O<sub>3</sub> at 400°C.

These latter points relate to the final set of data produced which were collected during an attempt at varying the space velocity through the reactor and therefore contact time of the reactants with the catalyst surface. Again, this was a parameter chosen by Schmidt during his work with monoliths and fluidised beds. During the course of those particular studies an optimum contact time was achieved between reactant gases and catalyst surface. It was found that by increasing the flow-rate the conversion became less but the destructive cracking reactions were also reduced and an increase in the non-destructive dehydrogenation reactions was observed, and an increase in dehydrogenation yield was therefore obtained. By decreasing the contact time, dehydrogenation took place and then rapid diffusion of the product molecules through the catalyst bed took place before secondary un-wanted reaction could occur. In order to achieve these conditions it was necessary to work at high temperatures ( $1000^{\circ}\text{C}$ ) where equilibrium limitations are insignificant. The use of a reactor and catalyst bed allowing high flow-rates was also required, hence the use of monoliths and fluidised beds. Experimentally, we could not access such high space velocities with our apparatus.

The results of our attempt at a similar study are shown on figures 5.5.29, 5.5.37, 5.6.28 and 5.6.36 (conversion) for the 0.5 and 0.65% catalysts and straight and oxidative dehydrogenation reactions respectively. Having considered the conditions at which the reactions were carried out, *i.e.*  $500^{\circ}\text{C}$  and  $400^{\circ}\text{C}$  for the 0.5 and 0.65% catalysts respectively, where the conversion was already very low, increasing the flow-rate resulted in only a few percent of conversion, at which the resultant range of products were difficult to detect. There are two main problems in our reactions. Firstly, as explained above, the temperature was too low and therefore conversion was too low before the contact times were decreased. Secondly, the pore structure of the catalysts meant that decreasing the contact time was highly limited to the diffusion of the reactant molecules through the catalysts. It is possible that figure 5.5.29 illustrates this. Increasing the flow-rate from  $30\text{ml min}^{-1}$  to  $50\text{ml min}^{-1}$  resulted in a decrease in conversion, as expected. Further increases did not result in any further changes in either the conversion or the dehydrogenation selectivity (figure 5.5.30), which increased upon changing the flow-rate from  $30\text{ml min}^{-1}$  to  $50\text{ml min}^{-1}$ , as the unwanted isomerisation and cracking reactions were minimised, leveling off up to a flow-rate of  $130\text{ml min}^{-1}$ . This final observation could result from diffusion limitations.

Nevertheless, it is possible that a distinction can be made between the two catalysts from the results obtained from the flow-rate study. The chemistry observed on the small particles of the 0.65% catalyst is olefin favoured and so, given the mechanism described in figure 1.2.3, requires long contact times where the butane can adsorb, convert to the olefin and then desorb. In the case of the 0.5% catalyst the particles are bigger leading to unwanted reactions such as cracking and isomerisation, in addition to dehydrogenation. By reducing the contact time in this case the selectivity towards the unwanted reaction products can be reduced while the dehydrogenation selectivity can be increased. This is very different to the observations made by Schmidt, where a decrease in contact time was also responsible for high olefin yields [5, 62]. However, those studies were carried out at very high temperatures ( $1000^{\circ}\text{C}$ ) where destruction of the olefin would almost certainly occur if the residence time within the reactor was too high. Although surface reactions were claimed in this study, it is very difficult to contemplate this under the experimental conditions used.

A number of studies have been carried out mainly to investigate the feasibility of oxidative dehydrogenation as a serious challenger to normal catalytic dehydrogenation, justifiably based on a variety of very useful studies carried out by other groups in this particular field. The following closing remarks and opinions are made with respect to the results obtained and the literature gathered throughout this work.

- Catalytic straight (without the presence of oxygen) dehydrogenation is an endothermic process and therefore thermodynamically limited. As a result high temperatures are required in order to obtain economically efficient yields. At these high temperatures ( $>500^{\circ}\text{C}$ ) unfavourable processes such as isomerisation, cracking and deactivation resulting from carbon deposition, reduce the selectivity of the system towards olefin products.
- Oxidative dehydrogenation on the other hand, is exothermic due to the formation of water. There is thus the potential to produce olefins at lower temperatures provided that a selective catalyst is found on which the transformations can take place.

- The ideas for this work were based on a combination of supported metal catalysts work carried out by Schmidt and recent surface science studies that indicate a range of chemistry depending on the nature of adsorbed oxygen. Pioneering studies by Schmidt *et al* have shown that selectivity of up to 65% at conversion levels of 100% can be achieved by optimising parameters such as temperature, contact time and hydrocarbon:oxygen ratio. Very low contact times were used and obtained using monolith supports and fluidised bed type reactors. In this work it was claimed that all processes taking place were surface reactions and that no homogeneous gas phase reactions were measured at the temperatures used (1000°C). The suggested mechanism for the dehydrogenation process was claimed to be initiated by hydrogen abstraction of a hydrogen atom from the reacting alkane molecule by a surface oxygen atom, forming surface alkyl and hydroxyl species.
- The surface science work showed that it was possible to tune the specificity of the system by manipulation of oxygen concentration in terms of activation of the alkane species. The formation of ‘hot oxygen’ (short lived, meta-stable species) with translational energy was required in order to observe this effect. However, this work was only demonstrated for the very pure environment of UHV where the number and type of incident molecules is contained and could be very tightly controlled.
- Continuous-flow measurements have shown that high selectivity towards olefin production can be achieved at relatively low temperature (400°C) for straight dehydrogenation. However, due to the equilibrium restriction and deactivation the resultant conversion was modest. Nevertheless, these processes were found to be catalytic in origin. On addition of oxygen to the system the conversion increases and the dehydrogenation selectivity decreases dramatically. It is also observed that the thermodynamically more favourable combustion reactions forming CO<sub>2</sub> and CO dominate the range of products detected.
- Relatively high olefin yield was observed for non-catalytic oxidative dehydrogenation at temperatures in the region 400-500°C as a result of gas phase

radical reactions. Similar observations have been made by other groups when using similar systems, of which makes Schmidt's conclusions, with regard to a lack of homogeneous reactions, very difficult to comprehend. It is more likely that the observation of high conversion is due to the high temperature within the reactor and that the formation of olefin products instead of cracking products is probably more due to the high space velocity (low contact times) of the gases through the reactor bed, with the catalyst allowing light-off temperatures to be achieved. Comparably low contact times could not be achieved in our packed bed reactor due to diffusion limitations resulting from the pore structure of the alumina support material.

- Pulse-flow studies were carried out and allowed the processes involved in the conditioning period of the catalyst to be observed. A clear correlation between carbon deposition and increased dehydrogenation selectivity was obtained. Three possible explanations could be put forward to explain this correlation. Firstly, the presence of the carbonaceous material on the metal surface could induce an electronic effect which reduces the adsorptivity of any remaining exposed metal surface. Secondly, the deposited carbonaceous material could selectively block the sites leading to unfavourable products, and thirdly, the carbonaceous material could provide a hydrogen transfer medium on which the dehydrogenation transformations readily take place. Based on the results obtained from the pulse-flow results and various work carried out in the literature, the first explanation seems to be the most plausible with respect to the experimental conditions used. The bare metal surface was found to be more suited for the unfavourable cracking and isomerisation reactions.
- As a result of these findings and the observations made during the continuous-flow experiments it is concluded that the inhibiting influence of oxygen is due to its 'cleaning' of the surface of the carbonaceous material necessary for dehydrogenation in addition to the combustion processes which also take place. It has also been revealed that surface science comparisons are inappropriate for these systems and that in a real catalyst system many processes are taking place and many crystal faces are present. Also the sheer amount of reactant species interacting with

the catalyst are orders of magnitude higher than would ever be exposed to a single crystal surface. As a result of these differences, temperature gradients and mass transport issues exist in real working catalysts that would not be present in metal single crystal work.

This work has attempted to examine the fundamental issues relevant to operating an oxidative dehydrogenation process on supported metal catalysts. Under the experimental conditions examined, it is concluded that oxidative dehydrogenation is not a suitable low temperature alternative to straight dehydrogenation using supported metal catalysts in a packed-bed reactor.

## *References*

1. F. Buonomo, D. Sanfilippo, F. Trifiro, in: G. Ertl, H. Knozinger, J. Weitkamp (Eds.), *Handbook of Heterogeneous Catalysis*, Vol. 4, Wiley-VCH, Germany, 1997, P. 2140.
2. S. Carra, L. Forni, *Catal. Rev.-Sci. Eng.* 5 (1971) 159.
3. S. R. Vatcha, *Oxidative Dehydrogenation and Alternative Dehydrogenation Processes*, Catalytica Studies Division, California, 1993.
4. P. R. Pujado, B. V. Vora, *Energy Progress* 4 (1984) 186.
5. S. S. Bharadwaj, L. D. Schmidt, *J. Catal.* 155 (1995) 403-413.
6. J. M. McNamara, *Platinum Metal Rev.* 44 (2000) 71-73.
7. R. H. H. Smits, PhD Thesis, University of Twente, (1994).
8. A. Sarkany, G. Stefler, J. W. Hightower, *Appl. Catal. A* 127 (1995) 77-92.
9. K. Weissermel, H.-J. Arpe, *Industrial Organic Chemistry*, Wiley-VCH, Germany, 1997, P. 59-89.
10. A. Beretta, L. Piovesan, P. Forzatti, *J. Catal.* 184 (1999) 455-468.
11. J. G. Stark, H. G. Wallace, *Chemistry Data Book*, John Murray Ltd., London, 1982, p. 55.
12. O. A. Barrias, A. Holmen, E. A. Blekkan, *Stud. Surf. Sci. Catal.* 88 (1994) 519.
13. V. Ponec, G. C. Bond, *Stud. Surf. Sci. Catal.* 95 (1995) 280-291.
14. P. Biloen, F. M. Dautzenberg, W. M. H. Sachtler, *J. Catal.* 50 (1977) 77-86.
15. P. Forzatti, L. Lietti, *Catal. Today* 52 (1999) 165-181.
16. F. H. Ribeiro, A. L. Bonivardi, C. Kim, G. A. Somorjai, *J. Catal.* 150 (1994) 186-198.
17. P. Biloen, J. N. Helle, H. Verbeek, F. M. Dautzenberg, W. M. H. Sachtler, *J. Catal.* 63 (1980) 112-118.
18. H-W. Chen, C-H. Chou, C. T. Hong, *J. Chin. Chem. Soc.* 43 (1996) 379-386.
19. O. A. Barrias, A. Holmen, E. A. Blekkan, *J. Catal.* 158 (1996) 1-12.
20. L. C. Lok, N. A. Gaidai, S. B. Kogan, S. L. Kiperman, *Proceedings of the Fifth International Symposium on Heterogeneous Catalysis*, Sofia, 1 (1987).
21. K. L. Lyu, N. A. Gaidai, S. L. Kiperman, H. S. Thoang, N. M. Podkletnova, S. B. Kogan, *Kinet. Catal.* 32 (1991) 61-66.
22. L. C. Loc, N. A. Gaidai, S. L. Kiperman, H. S. Thoang, *Kinet. Catal.* 34 (1993) 505-509.

23. L. C. Loc, N. A. Gaidai, S. L. Kiperman, H. S. Thoang, N. M. Podkletnova, S. B. Kogan, V. Y. Georgievskii, *Kinet. Catal.* 34 (1993) 677-680.
24. L. C. Loc, N. A. Gaidai, S. L. Kiperman, H. S. Thoang, N. M. Podkletnova, V. Y. Georgievskii, *Kinet. Catal.* 36 (1995) 564-570.
25. L. C. Loc, N. A. Gaidai, S. L. Kiperman, H. S. Thoang, *Kinet. Catal.* 37 (1996) 851-857.
26. D. Casanave, K. Fiaty, J. A. Dalmon, M. Forissier, *Reaction Kinetics and the Development Catalytic Processes* (1999) 367.
27. S. D. Jackson, J. Grenfell, I. M. Matheson, G. Webb, *Reaction Kinetics and the Development Catalytic Processes* (1999) 149.
28. J. Jifei, S. Jianya, X. Zhusheng, G. Xin, Z. Tao, L. Liwu, *Chin. J. Catal.* 18 (1997) 17.
29. L. V. Babenkova, S. Szabo, I. N. Naidina, Y. G. Kulievskaia, *Models in Chemistry* 131 (1994) 113-120.
30. B. D. Chandler, L. I. Rubinstien, L. H. Pignolet, *J. Mol. Catal. A* 133 (1998) 267-282.
31. E. L. Jablonski, A. A. Castro, O. A. Scelza, S. R. de Miguel, *Appl. Catal. A* 183 (1999) 189-198.
32. J. R. Rostrup-Nielsen, *Catal. Today* 37 (1997) 225-232.
33. B. V. Vora, P. R. Pujado, R. F. Anderson, *Energy Progress* 6 (1986) 171.
34. K. K. Kearby, in: P.H. Emmet (Ed.), *Cataysis, Fundamental Principles*, Chapter 10, vol. 3, Reinhold, New York, p. 453.
35. R. J. Rennard, J. Freel, *J. Catal.* 98 (1986) 235-244.
36. J. R. Rostrup-Nielsen, D. L. Trimm, *J. Catal.* 48 (1977) 155-165.
37. D. L. Trimm, *Catal. Rev. Sci. Eng.* 16 (1977) 155-189.
38. B. J. Cooper, D. L. Trimm, in: B. Delmon, G. F. Froment (Eds.), *Proceedings of the Second International Symposium on Catalyst Deactivation*, 1980, p. 63.
39. S. M. Davis, F. Zaera, G. A. Somorjai, *J. Catal.* 77 (1982) 439-459.
40. G. C. Bond, *Appl. Catal. A* 149 (1997) 3-25.
41. J. Barbier, P. Marecot, N. Martin, L. Elassal, R. Maurel, in: B. Delmon, G. F. Froment (Eds.), *Proceedings of the Second International Symposium on Catalyst Deactivation*, 1980, p. 53.
42. C. A. Querini, S. C. Fung, *Catal. Today* 37 (1997) 277-283.

43. M. Larsson, M. Hulten, E. A. Blekkan, B. Andersson, *J. Catal.* 164 (1996) 44-53.
44. G. Webb, I. M. Matheson, S. D. Jackson, J. Grenfell, *Stud. Surf. Sci. Catal.* 88 (1994) 297.
45. E. H. Stitt, S. D. Jackson, F. King, *Reaction Kinetics and the Development of Catalytic Processes* (1999) 291.
46. F. M. Mandani, R. Hughes, *Stud. Surf. Sci. Catal.* 88 (1994) 507.
47. G. F. Froment, in: B. Delmon, G. F. Froment (Eds.), *Proceedings of the Second International Symposium on Catalyst Deactivation*, 1980, p. 1.
48. Z. C. Zhang, B. C. Beard, *Appl. Catal. A* 188 (1999) 229-240.
49. J. P. Bourdonville, G. Martino, in: B. Delmon, G. F. Froment (Eds.), *Proceedings of the Second International Symposium on Catalyst Deactivation*, 1980, p. 159.
50. J. W. Geus, P. B. Wells, *Appl. Catal.* 18 (1985) 231-242.
51. S. D. Jackson, P. Leeming, G. Webb, *J. Catal.* 160 (1996) 235-243.
52. M-V. Mathieu, M. Primet, *Appl. Catal.* 9 (1984) 361-370.
53. P. Marecot, A. Fakche, B. Kellali, G. Mabilon, M. Prignet, J. Barbier, *Appl. Catal. B* 3 (1994) 283-294.
54. D. O. Simeone, T. Kennelly, N. L. Brungard, R. J. Farrauto, *Appl. Catal.* 70 (1991) 87-100.
55. F. A. Cotton, G. Wilkinson, *Advanced Inorganic Chemistry*, Wiley Interscience, 5<sup>th</sup> Edition, New York, 1988, p. 665.
56. M. A. Chaar, D. Patel, M. C. Kung, H. H. Kung, *J. Catal.* 105 (1987) 483-498.
57. H. H. Kung, M. A. Chaar, US Pat. 4 777 319 (1988).
58. R. Burch, E. M. Crabb, *Appl. Catal.* 100 (1993) 111-130.
59. E. A. Mamedov, V. C. Corberan, *Appl. Catal.* 127 (1995) 1-40.
60. B. Delmon, P. Ruiz, S. R. G. Carrazan, S. Korili, M. A. Vincente Rodriguez, Z. Sobalik, *Stud. Surf. Sci. Catal.* 100 (1996) 1-25.
61. C. Batiot, B. K. Hodnett, *Appl. Catal.* 137 (1996) 179-191.
62. M. Huff, L. D. Schmidt, *J. Catal.* 149 (1994) 127-141.
63. A. Beretta, P. Forzatti, E. Ranzi, *J. Catal.* 184 (1999) 469-478.
64. R. Lodeng, O. A. Lindvag, S. Kvistle, H. R. Nielsen, A. Holmen, *Appl. Catal.* 187 (1999) 25-31.

65. F. J. Maldonado-Hodar, L. M. Madeira, M. F. Portela, *Appl. Catal. A* 178 (1999) 49-60.
66. S. E. Golunski, J. W. Hayes, *E Pat.* 0 937 697 A2 (1999).
67. S. M. Davis, F. Zaera, G. A. Somorjai, *J. Am. Chem. Soc.* 104 (1982) 7453-7461.
68. G. C. Bond, R. H. Cunningham, *J. Catal.* 166 (1997) 172-185.
69. J. Houzvicka, S. Hansildaar, J. G. Nienhuis, V. Ponec, *Appl. Catal. A* 176 (1999) 83-89.
70. S. D. Jackson, G. J. Kelly, G. Webb, *J. Catal.* 176 (1998) 225-234.
71. C. H. Lin, B-Z. Wan, *J. Chin. I. Ch. E.* 24 (1993) 71.
72. B. C. Gates, J. R. Katzer, G. C. A. Schuit, *Chemistry of Catalytic Processes*, McGraw-Hill Co., New York, 1979, P. 266-288.
73. C. Morterra, G. Magnacca, *Catal. Today* 27 (1996) 497-532.
74. Z. X. Cheng, V. Ponec, *J. Catal.* 148 (1994) 607-616.
75. D. I. Iordanoglou, L. D. Schmidt, *J. Catal.* 176 (1998) 503-512.
76. C. Li, C. L. Minh, T. C. Brown, *J. Catal.* 178 (1998) 275-283.
77. M. W. Roberts, *Chem. Soc. Revs.* 6 (1996) 437.
78. X-C. Guo, R. J. Madix, *Faraday Discuss.* 105 (1996) 139-149.
79. A. F. Carley, A. Chambers, P. R. Davies, G. G. Mariotti, R. Kurian, M. W. Roberts, *Faraday Discuss.* 105 (1996) 225-235.
80. H. F. Coward, G. W. Jones, *Limits of Flammability of Gases and Vapours*, US Bureau of Mines, Bulletin 503, Washington D.C. (1952).
81. J. G. Eon, R. Olier, J. C. Volta, *J. Catal.* 145 (1994) 318-326.
82. C. P. Hubbard, K. Otto, H. S. Gandhi, K. Y. S. Ng, *J. Catal.* 139 (1993) 268-276.
83. M. Boudart, in: G. Ertl, H. Knozinger, J. Weitkamp (Eds.), *Handbook of Heterogeneous Catalysis*, Vol. 1, Wiley-VCH, Germany, 1997, P. 1-12.
84. R. E. Walpole, *Introduction to Statistics*, 3<sup>rd</sup> Edition, Collier Macmillan, London, 1982.
85. P. Millington, PhD Thesis, University of Reading, (1995).
86. D. R. Kennedy, PhD Thesis, University of Glasgow, (1997).
87. E. Allen, PhD Thesis, University of Glasgow, (1995).

88. Handbook of Chemistry and Physics, 46<sup>th</sup> Edition, The Chemical Rubber Co., 1966, p. D-51.
89. A. Frennet, P. B. Wells, *Appl. Catal.* 18 (1985) 243-257.
90. C. H. Bartholomew, *Catalysis* 11 (1994) 93.
91. C. De La Cruz, N. Sheppard, *Spectrochimica Acta* 50A (1994) 271-285.
92. D. M. Haaland, *Surf. Sci.* 185 (1987) 1-14.
93. C. N. Banwell, E. M. McCash, *Fundamentals of Molecular Spectroscopy*, McGraw-Hill Co., London, 1997, p. 67.
94. E. I. Altman, R. J. Gorte, *J. Catal.* 110 (1988) 191-196.
95. I. M. Matheson, PhD Thesis, University of Glasgow, (1995).
96. G. Webb, S. J. Thomson, *J. Chem. Soc. Chem. Comm.* (1976) 526.
97. D. Lennon, D. R. Kennedy, G. Webb, S. D. Jackson, in: B. Delmon, G. F. Froment (Eds.), *Proceedings of the Eighth International Symposium on Catalyst Deactivation*, 1999, p. 341.
98. D. R. Kennedy, B. Cullen, D. Lennon, G. Webb, P. R. Dennison, S. D. Jackson, *Reaction Kinetics and the Development Catalytic Processes* 122 (1999) 125.
99. C. N. Satterfield, *Heterogeneous Catalysis in Practice*, McGraw-Hill Co., London, 1980, p. 268-277.
100. S. D. Jackson, J. Grenfell, I. M. Matheson, G. Webb, *Abs. Amer. Chem. Soc.* 2 (1995) 104.

## *Future Work*

## **Future Work**

- Post pulse-flow and continuous-flow, *in situ* CO infrared and TPD studies to investigate the availability of any bare metal surface and to observe any difference between fresh and used catalyst in an attempt to confirm the change in electronic nature of the metal surface after deposition of carbonaceous material.
- Post reaction pore volume measurements to investigate any changes in pore structure and pore blockage due to the deposition of carbonaceous material.
- Re-investigate particle size changes after straight and oxidative dehydrogenation reactions using TEM in an attempt to observe the metal sintering though to occur in the oxidative case due to the formation of water. The formation of larger particles would have a profound effect on the surface chemistry.

